Buckling and Post-Buckling Analysis of Cracked Plates by The Boundary Element Method

Purbolaksono, Judha

POST - BUCKLING.

Buckling and ~~Large Deformation~~ Analysis of Cracked Plates by The Boundary Element Method

By

Judha Purbolaksono

Thesis submitted for the degree of Doctor of Philosophy
of the University of London

Department of Engineering
Queen Mary
University of London

2003

Abstract

This thesis presents boundary element formulations for buckling and nonlinear buckling analysis of plates. Dual boundary element formulations are also presented for linear and nonlinear buckling, and large deformation analysis of crack behaviour in plates.

Reissner plate theory is adopted to represent shear deformable plate bending, and two dimensional plane stress is used to model the membrane behaviour of plate. By taking into account the nonlinear interaction between forces and rotations in the equilibrium equation, the nonlinear formulation is formed by coupling equations of shear deformable plate bending and two dimensional elasticity.

The boundary element formulation for plate buckling is developed. Plate buckling equations are written as a standard eigenvalue problem. Buckling coefficients and buckling modes are obtained using this formulation. Initially, the boundary is discretised into quadratic isoparametric elements, and the domain is discretised using constants cells. Next, the dual reciprocity method is utilized to transform the domain integral into equivalent boundary integrals. Examples are presented for plate buckling problems with different geometry, loading and boundary conditions. The results obtained are shown to be in good agreement with analytical and finite element results.

The Dual Boundary Element Method (DBEM) for buckling analysis of plate is also developed. The plate buckling equations are also presented as a standard eigenvalue problem, which would allow direct evaluation of critical load factor and buckling modes for cracked plates.

Geometrically nonlinear boundary element formulation is developed to analyse large deformation and nonlinear buckling of plates. Different load incremental approaches and solution procedures are presented. Nonlinear terms are evaluated using a radial basis function. Large deformation analysis for Fracture Mechanics problems is also presented. Five stress intensity factors are calculated, i.e. three for plate bending and two for membrane. Crack Opening Displacement (COD) is used to compute the stress intensity factors. The nonlinear buckling of thin plate is also presented. Two models of imperfection are introduced in the formulation, i.e. a small uniform transverse loads and distributed transverse loads based on eigenvectors. A simple numerical algorithm is presented to analyse the problems. Finally, nonlinear buckling analysis of cracked plate is presented. Numerical examples of nonlinear buckling and large deformation problems are presented. The BEM results presented are shown to be in good agreements with analytical and other numerical results.

And with Him are the keys of the unseen; none knows them except Him.
And He knows what is on the land and in the sea;
Not a leaf falls but that He knows it.
There is not a grain in the darkness of the earth nor anything fresh or dry,
but that it is written in a clear record.

English translation of the meaning
of the Holy Qur'an
Surah 6: Al-An'am, verse 59

Dedicated to:

my parents, my wife and my daughter

Acknowledgements

All praises and thanks be to Allah Almighty, the Most Gracious, the Most Merciful.

I would like to express my sincere appreciation and gratitude to my supervisor, Professor Ferri M.H. Aliabadi for his invaluable advice, support, friendship and great encouragement throughout the duration of this work.

I would like to acknowledge to Queen Mary Research Council, University of London for financial support.

I also wish to thank Dr. T. Dirgantara for all fruitfull and useful disscussions, Dr. Ichsan Setya Putra for advices and supports, Mr. Moehammad Dwimunali for helps and supports, and Mr. D. Widagdo, Mr. E. Pineda, Mr. P.M. Baiz, Mr. C. Dipisa, Mr. Supriyono and Mr. A.S. Darmawan, colleagues and staff at Department of Engineering, Queen Mary, University of London, all my friends in UK particularly 'Al-Ikhlas'- Indonesian Muslim Circle in London for their friendship, helps and advices.

Special thanks and gratitude for my wife, Berliria Hardhiani Purwoadi, for her love, support, patience, and understanding throughout the completion of this work.

Thanks are also due to my mother and father, my sister, my mother and father-in-law, and my families for their prayer they do.

Contents

List of Figures

List of Tables

List of Notations

a	length of plate
$A(z), B(z)$	linear combination of the modified Bessel functions
B	$\left(= Eh/\left(1-\nu^2\right)\right)$ tension stiffness
$\mathbf{b}$	domain load vectors
b	width of plate
C	$\left(= \left[D(1-\nu)\lambda^2\right]/2\right)$ shear stiffness
c	half crack length
c_{ij}	jump terms
D	$\left(= Eh^3/\left[12\left(1-\nu^2\right)\right]\right)$ bending stiffness
E	modulus of elasticity
e_1, e_2, e_3	unit vectors parallel to x_1, x_2, and x_3- axes
$f(r)$	$(=1+r)$ radial basis function,
f_b	body force used in dual reciprocity technique
f_1, f_2, f_3	body forces in the x_1-, x_2- and x_3- directions
$\mathbf{G}$	boundary element influence matrix
$\mathbf{G}_3^p$	domain coefficient matrix
$\mathbf{G}_{eq}^p$	domain coefficient matrix
$\mathbf{H}$	boundary element influence matrix
h	plate thickness

I	identity matrix
$I_0(z), I_1(z)$	modified Bessel functions of the first kind
$J(\xi)$	Jacobian of transformation
K	buckling coefficient
K_I, K_{II}, K_{III}	stress intensity factors for mode I, II and III
K_1, K_2, K_3	stress resultant intensity factors for mode I, II and III
K_{nl}	normalized critical load
$K_0(z), K_1(z)$	modified Bessel functions of the second kind
	x_1- and x_2- directions
K_{1b}	stress intensity factors of plate bending for mode 1
K_{1bn}	normalized stress intensity factors of plate bending for mode 1
K_{1m}	stress intensity factors of membrane for mode 1
K_{1mn}	normalized stress intensity factors of membrane for mode 1
L_{ik}	Navier differential operator
$M_{\alpha\beta}$	bending stress resultants
$\hat{M}^i_{m\alpha\beta}$	bending stress resultant particular solutions
	for plate bending problems
N_i	special shape functions for crack tip element
$N_{\alpha\beta}$	membrane stress resultants
$\hat{N}^\gamma_{m\alpha\beta}$	membrane stress resultant particular solutions
	for two-dimensional plane stress problems
n_1, n_2	outward unit normal vectors at the boundary in
	x_1- and x_2- directions
P^*_{ij}, P^*_{ijk}	plate bending traction fundamental solutions
p_1, p_2, p_3	generalised bending and shear tractions
$\hat{p}^i_{mk}$	traction particular solutions for plate bending problems
$\mathbf{p}$	bending and shear traction vectors
Q	normalized load for large deformation
Q_α	shear stress resultants
$\hat{Q}^i_{m\beta}$	shear stress resultant particular solutions
	for plate bending problems

q	transverse load
q_0	initial imperfection
R	radius of a hole
r	absolute distance between the source and the field points
r, θ	polar coordinates
T	critical compression load
$T^*_{\theta\alpha}, T^*_{\alpha\beta\gamma}$	2-D plane stress traction fundamental solutions
t_1, t_2	generalised membrane tractions
t_1, t_2, t_3	tractions in global coordinate system, used in multi-region BEM formulation
$\hat{t}^{\alpha}_{m\beta}$	traction particular solutions for two-dimensional plane stress problems
$\mathbf{t}$	membrane traction vectors
$U^*_{\theta\alpha}, U^*_{\alpha\beta\gamma}$	2-D plane stress displacement fundamental solutions
u_1, u_2	generalised in-plane displacements
u, v, w	translational displacements
$\hat{u}^{\alpha}_{m\beta}$	displacement particular solutions for two-dimensional plane stress problems
$\mathbf{u}$	in-plane displacement vectors
$V^*_{i,\beta}, Q^*_{i\beta}$	kernels for transformation of domain integrals `to boundary integral
W^*_{ij}, W^*_{ijk}	plate bending displacement fundamental solutions
W	strain energy density
$\hat{w}^{i}_{mk}$	displacement particular solutions for plate bending problems
w_1, w_2, w_3	generalised rotations and out-of-plane displacements
$\mathbf{w}$	rotations and out-of-plane displacement vectors
$\mathbf{x}, \mathbf{X}$	field points, where $\mathbf{x} \in \mathbf{\Gamma}$, $\mathbf{X} \in \mathbf{\Omega}$
$\mathbf{x}', \mathbf{X}'$	source points, where $\mathbf{x}' \in \mathbf{\Gamma}$, $\mathbf{X}' \in \mathbf{\Omega}$
x_1, x_2, x_3	Cartesian coordinates

z	$(=\lambda r)$
Z	normalized deflection
Γ	boundary of the plate
δ	Dirac delta function
$\delta_{\alpha\beta}$	Kronecker delta function
$\varepsilon_{ij}, \gamma_{ij}$	normal and shear strains
θ_t	crack extension direction
λ	$\left(=\sqrt{10}/h\right)$ shear factor, eigenvalues, critical load factor
ν	Poisson's ratio
ξ', ξ	source point and field point in local coordinate
Φ^m	shape functions
Ω	domain of the plate
σ_{ij}	normal and shear stresses

Chapter 1

Introduction

1.1 General

Since the early 1940s researchers have been concerned with development of methods for studying the behaviour of buckling and failure of plate structures. The buckling investigation on compression members is particularly important in engineering structures. Buckling phenomenon of structure members in compression has been investigated by researchers analytically, experimentally and numerically. Analytical solutions of plate buckling based on the classical plate theory can be found in [90] [23]. In recent years, numerical methods have been widely used to investigate the problem [54][72][83]. Review of experimental of works on buckling can be found in [93].

Similarly, geometrically nonlinear behaviour of thin walled structures is an important problem in engineering. Bending of rectangular plates with large deflection was presented by Levy [50][51] using a solution of von Karman's equation in term of trigonometric series. An approximation of the analysis of large deflections of plates was introduced by Berger[17] which has since become known as the Berger equation.

There are two basic theories of plates. The first theory is known as the classical theory and it was first proposed by Kirchhoff [47] in 1850. The Kirchhoff theory neglected the shear deformation through the plate thickness. The other theory is known as the shear deformable plate theory and it was first proposed by Reissner [71] in 1947. The shear deformation and the transverse normal stresses are taken

into account in this theory. Reissner [71] modelled the plate structure as a two-dimensional structure with an assumed stress variation through the plate thickness.

In dealing with stress concentration problems such as, stresses at an edge of a hole when the hole diameter became so small as to be of the order of magnitude of the plate thickness, the classical theory is known to provide inaccurate results. In this respect, Reissner [71] showed that results obtained by the Kirchhoff's theory of thin plates was not in agreement with the experimental results. Moreover, when the Kirchhoff theory is applied to crack problems, it leads to difficulties when combined bending and membrane stress fields are required. On the other hand, the shear deformable theory is known to overcome the problems associated with the application of the classical theory. The other important feature of shear deformable plate theories is that they can be used to analyse both thin and thick plates.

1.2 Review for Buckling and Geometrically Nonlinear Analysis of Plates

In general, there are three popular numerical methods used in practical problems, the Finite Different Method (FDM), the Finite Element Method (FEM), and the Boundary Element Method (BEM).

The direct solution of the differential form of the governing differential equation is used in the FDM formulation. Review of the FDM applications to the classical and shear deformable plate theories can be found in [38, 89]. The FEM can also be used to solve the integral representation of the differential equation [104]. The application of the Finite Element Method in the classical Kirchhoff and in shear deformable plate theories are presented by Zienkiewicz and Taylor [105]. Fracture mechanics of plate bending based on shear deformable plate theories has been solved successfully by FEM. Boduroglu and Erdogan [26], Sosa and Eischen[76], Sosa and Herrmann[77] presented stress intensity factor solutions for several crack geometries of the Reissner plates.

The FDM and FEM are called domain methods as the discretisation of the problem domain is required. On the other hand the boundary element method [20] is known as a boundary type method. The most important feature of boundary

elements is that only boundary discretisations is required. Accurate value of interior stresses and displacements can be achieved since the BEM provides a continuous modelling of the interior without discretisation of the domain.

Based on the classical theory of plates, the implementation of BEM to plate theory are performed. Plates with smooth boundary analysis based on the Kirchhoff theory was introduced by Forbes and Robinson [33]. Later, Bézine [16] and Stern [79] studied plate problems with corner points and different types of boundary conditions. In the Kirchhoff theory, additional integral equations for the normal slope are obtained from the derivatives of out-of-plane deflection. Further development of the method for plates with relatively complex geometries, loading and supports is performed by Hartmann and Zormantel [37]. Other applications of the plate bending formulation can be found from the works of Stern [80], Stern and Lin [81], Abdel-Akher and Hartley [1][2], and Karami *et al.* [45].

The application of the BEM to Reissner plate analysis was first presented by Vander Weeën [94, 95] in 1982. In Weeën's work, the boundary integral equations are derived from the Betti's theorem and fundamental solutions are derived using the Hörmander's method. Following his formulation, Karam and Telles [44] reported that Reissner's plate model can be used to analyse both thin and thick plates. They also developed the formulation to account for infinite regions. A similar formulation to that of Vander Weeën's work [94] is presented by Barcellos and Silva [15] to study Mindlin plate model. The difference between their formulation and the Reissner formulation is in the shear factor constant. Westphal and Barcellos [101] discussed the importance of the neglected terms in the fundamental solution derived by Vander Weeën [94], that the terms have no effect on the results. Later, other fundamental solutions for the Reissner plate is derived by El-Zafrany, Debbih and Fadhil [29] using the Hankel integral transformation. The results were shown to be same as that of Vander Weeën's results [94]. In [30], a modified form of the fundamental solutions were derived, by separating parts of the kernel representing the effect of transverse shear, to allow analysis of thin and thick plates. Recent advances in plate bending analysis with the boundary element method can be found in the book edited by Aliabadi [9].

More recently, the boundary element method (BEM), has provided a powerful

solution to the field of plate buckling. Syngellakis and Elzein [82] extended the boundary element solution of the plate buckling based on Kirchhoff theory to accommodate any combination of loadings and support conditions. Nerantzaki and Katsidelakis [58], developed a BEM-based method for plate buckling analysis of plates with variable thickness. Lin, Duffield and Shih [52], developed a more general boundary element formulation for wide variety of boundary conditions and arbitrary planar shapes to investigate the stability of elastic plate. The boundary element method for buckling analysis of shear deformable plates was developed by Purbolaksono and Aliabadi [64]. Elastic buckling analysis of plates using boundary element can also be found in [24][85].

During the last decade, the Dual Boundary Element Method (DBEM) has been established as a robust numerical method for fracture mechanics problems. Based on displacement and traction integral equations, DBEM has been applied to many fracture mechanics problems e.g. elastostatics, thermoelastic, elastoplastic, stiffened panel, concrete cracking, composite materials and dynamics, as reviewed by Aliabadi [7][8]. The application of the dual boundary element method to analyse Reissner plate bending problems was reported by Ahmadi-Brooghani and Wearing [4].

Buckling analysis of cracked panels is investigated by only few researchers analytically and numerically. Stahl and Keer [78] studied stability of simply supported rectangular cracked plates using an analytical approach. Vafai and Estekanchi [92] investigated the buckling behaviour of edge cracked plate subjected to axial loads. Liu [54] presented the buckling analysis of rectangular Mindlin plates having cracks using differential quadrature element method. A new boundary integral equation is presented by Purbolaksono and Aliabadi [65] to analyse buckling problems of cracked plates.

The application of the boundary element method to nonlinear large deformation is relatively new with only a few publications dealing with the topic. Tanaka [84] presented a coupled boundary and inner domain integral equations in terms of stress and displacement functions based on von Karman's equation. Kamiya and Sawaki [43] investigated the large deflection of elastic plates based on the Berger equation. Ye and Lin [102] analysed the finite deflection of thin plates by the boundary element method. One of the other works can be found in [12] by Atluri and Pipkins. Based

on the general nonlinear differential equations of finite deflection of the plate, an integral equation formulation for the geometrically nonlinear analysis of the Reissner type plate was proposed by Lei, Huang and Wang [49]. Later, Sun, He and Qin [66] derived the exact boundary equation for the analysis of the nonlinear Reissner plate based on a variational principle.

The boundary element method has also been applied to analyse nonlinear problems in the plate stability. Contributions to the nonlinear buckling analysis of thin plates by BEM were made Manolis and Beskos [55], Kamiya, Sawaki and Nakamura [42], Costa and Brebbia [24], Kawabe [46], Qin and Huang [67], and Tanaka, Matsumoto and Zheng [86]. The review of the application of BEM to the stability analysis of thin plate can be found in Liu [53] and Syngellakis [83].

This thesis presents the formulation of boundary integral equations for the buckling analysis of shear deformable plates for the first time. The formulation is formed by coupling boundary element formulations of shear deformable plate and two dimensional plane stress. Plate buckling equations are presented as a standard eigenvalue problem.

The formulation for plate buckling problem is next extended to analyse plate buckling problem of cracked plates by the dual boundary element method. The critical load factor and buckling modes of cracked plate buckling are obtained. The dual reciprocity method is utilized to deal with the domain integrals that appear in the formulation.

Geometrically nonlinear boundary element formulation is also developed to analyse large deformation and nonlinear buckling of plates. Different load incremental approaches and solution procedures are presented. Nonlinear terms that appear in the domain integrals are evaluated using an approximation function. Large deformation formulation to analyse Fracture Mechanics problems is also developed. Five stress intensity factors are obtained, i.e. three for plate bending and two for membrane. The nonlinear buckling formulation of thin plates is also presented with introducing two models of imperfection; i.e. a small uniform transverse loads and distributed transverse loads based on eigenvectors. A simple numerical algorithm is presented to analyse the problems. Finally, the formulation is extended to nonlinear buckling problem of cracked plates.

1.3 Overview of the Present Work

The aim of this thesis is to investigate and develop boundary element methods for buckling and geometrically nonlinear analysis of shear deformable plates.

Chapter 2 describes some basic concepts of the shear deformable theory for elastic plates, two-dimensional plane stress, and geometrically nonlinear plates. A brief review of linear elastic fracture mechanics related to two-dimensional plane stress and plate bending problems, buckling of thin plates and eigenvalue problems are also presented.

Chapter 3 presents the boundary integral equations for shear deformable plates and two-dimensional plane stress problems. The quadratic isoparametric elements are used to discretise the boundary integral equations. The treatment for the evaluation of the singular integrals is described. Transformation of domain integrals to boundary integrals using the dual reciprocity technique is presented. The traction boundary integrals that will be used to form the dual boundary integral equations are also presented.

Chapter 4 presents the boundary integral equations for buckling analysis of shear deformable plates. Plate buckling equations are presented as a standard eigenvalue problem. The formulation is formed by coupling boundary element formulations of a shear deformable plate and two dimensional plane stress elasticity. The domain integrals which appear in this formulation are treated by two different methods: initially the integrals are discretised using constant cells, and next, they are transformed into equivalent boundary integrals using the dual reciprocity method. The eigenvalue problem of plate buckling yields a critical load factor and buckling modes. To demonstrate the accuracy of the proposed method, several examples with different geometry, loadings and boundary conditions are presented.

Chapter 5 presents the dual boundary integral equations for the buckling analysis of the Reissner shear deformable cracked plates. The boundary integral equation is presented as an eigenvalue problem. The domain integrals which appear in this formulation are transferred to boundary integrals using the dual reciprocity method. The plate buckling equations are presented as a standard eigenvalue problem, which would allow for direct evaluation of the critical load factor and buckling modes.

Several examples with different geometries, loadings and boundary conditions are presented to demonstrate the accuracy of the proposed method.

Chapter 6 presents the boundary integral equations for geometrically nonlinear shear deformable plates. In the large deformation analysis, initially the domain is discretised using constant cells. An approximation function is used to calculate the derivatives of the nonlinear terms in the domain integral. Next, meshless domain using the dual reciprocity technique is presented [98]. The nonlinear buckling of a thin plate is also presented in this chapter. Two models of imperfection are introduced in the formulation, i.e. a small uniform transverse load and distributed transverse load evaluated based on eigenvectors. Next, large deformation analysis of cracked plates is presented. The analysis is performed using the dual boundary element method (DBEM). Five stress intensity factors are obtained, i.e. three SIFs from plate bending problem and two SIFs from membrane problem. Several examples are presented and comparisons are made with analytical results, the other numerical results and the published results.

Finally, **Chapter 7** presents conclusions and future works.

1.4 Author's Published Works

The following sections present the submitted papers corresponding to present work.

1.4.1 International journal

1. Purbolaksono, J. and Aliabadi, M.H., *Buckling Analysis of Shear Deformable Plates by Boundary Element Method,* submitted for publication

2. Purbolaksono, J. and Aliabadi, M.H., *Dual Boundary Element Analysis of Cracked Plates under Buckling Loads,* submitted for publication

3. Purbolaksono, J. and Aliabadi, M.H., *Large Deformation of Shear Deformable Plates by The Boundary Element Method,* submitted for publication

1.4.2 Conference proceedings

1. Purbolaksono, J. and Aliabadi, M.H., *Shear Deformable Plates Buckling by the Boundary Element Method*, 4th International Conference Boundary Elements Techniques, University of Granada, Granada (Spain), pp 359-364, July 2003

2. Purbolaksono, J. and Aliabadi, M.H., *Buckling of Cracked Plates,* 3rd International Conference Fracture and Damage Mechanics, Paderborn (Germany), pp 153-158, September 2003

Chapter 2

Basic Concepts

2.1 Introduction

In this chapter, basic concepts for elastostatic analysis of shear deformable plates and two-dimensional plane stress for linear and geometrically nonlinear problems are presented. The fundamental concepts of fracture mechanics and a brief review of the buckling of thin plates and general algebraic eigenvalue problem are also reviewed.

The theory of elastic plates and two-dimensional plane stress are presented by Reissner [71], Mindlin [56] and Timoshenko and Goodier [88], while the fundamental concept of fracture mechanics can be found in Sih [74], Broek [22], Anderson [11] and Aliabadi and Rooke [6].

Indicial notation is used throughout the thesis. Greek indices will vary from 1 to 2 and Roman indices from 1 to 3. The partial derivative of (...) with respect to the coordinate x_β is expressed by comma subscript, such as $(...)_{,\beta} = \partial_\beta(...) = \dfrac{\partial}{\partial x_\beta}(...)$, and $(...)_{,n}$ stands for the derivative of (...) with respect to the outward normal n.

2.2 Governing Equations of Linear Elastic Plates

The elastic behaviour of shear deformable plate bending and two dimensional plane stress theories can be considered separately. Consider an arbitrary plate of thickness h as shown in Figure 2-1. The $x_1 - x_2$ plane is assumed to be located at the middle surface $x_3 = 0$, where $-h/2 \leqslant x_3 \leqslant +h/2$. The generalised displacements for bending and shear are denoted as w_i and for in-plane as u_α, with the sign convention

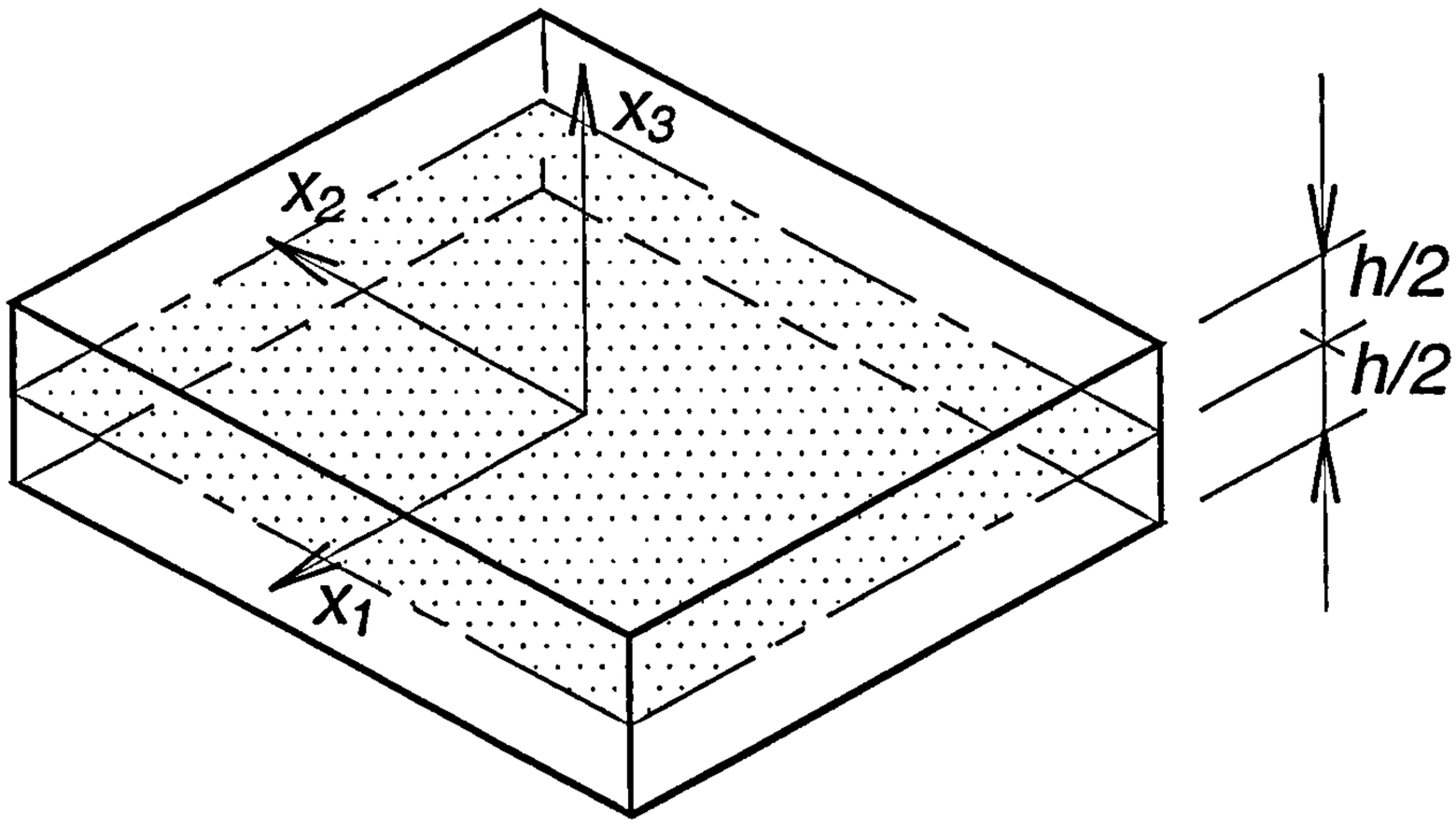

Figure 2-1: Plate geometry.

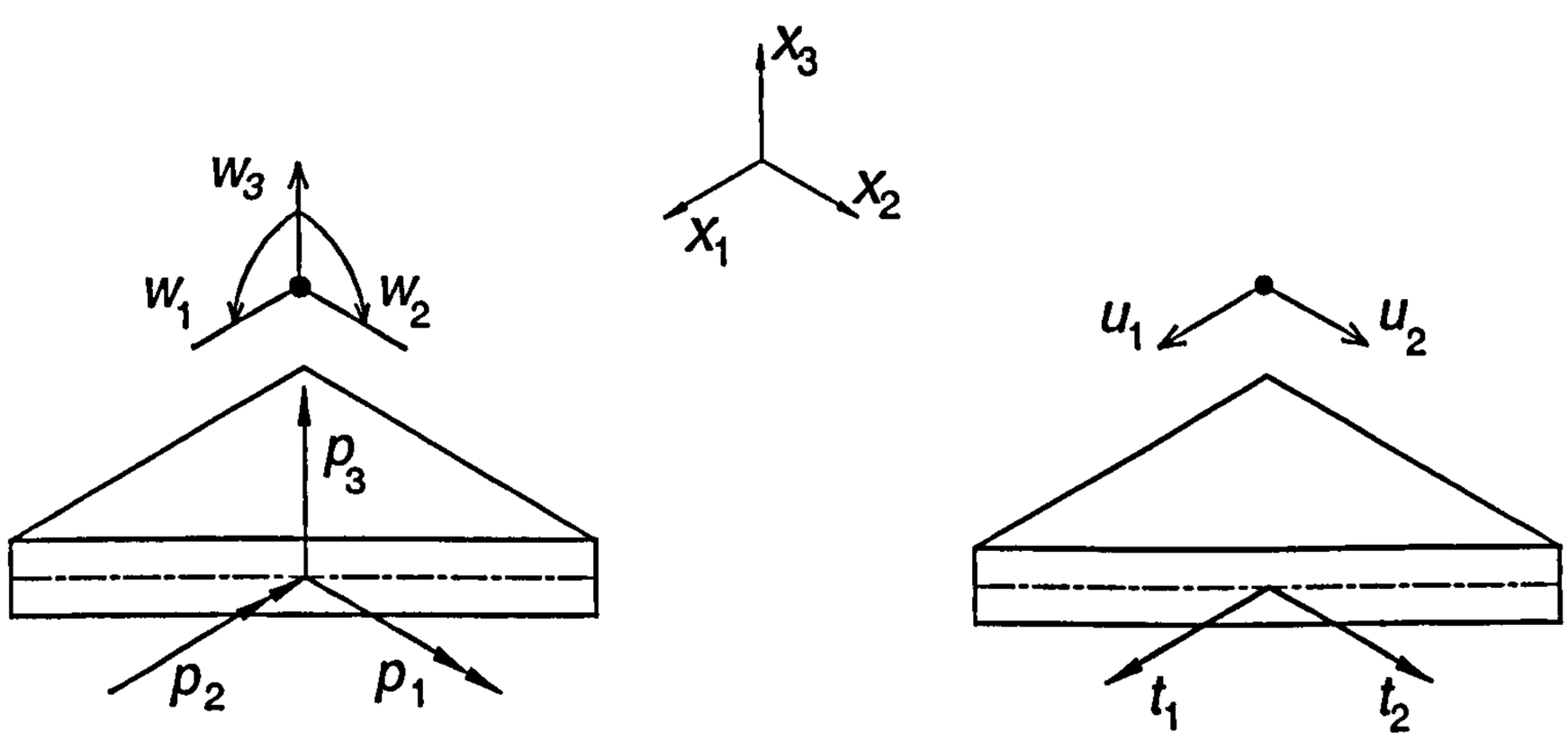

Figure 2-2: Definition for generalized displacement and traction terms.

as shown in Figure 2-2. Detailed definition of the generalised displacements can be found in [71].

2.2.1 Stress resultants and stress couples

The bending stress resultants $M_{\alpha\beta}$, and the shearing stress resultants Q_α can be defined as:

$$M_{\alpha\beta} = \int_{-h/2}^{+h/2} x_3 \sigma_{\alpha\beta} dx_3$$

$$Q_\alpha = \int_{-h/2}^{+h/2} \sigma_{\alpha 3} dx_3 \tag{2.1}$$

where $\sigma_{\alpha\beta}$ are the three-dimensional components of stresses through the plate thickness and $\sigma_{\alpha 3}$ are the components of the transverse shear stresses.

The membrane stress resultants $N_{\alpha\beta}$ are defined as:

$$N_{\alpha\beta} = \int_{-h/2}^{+h/2} \sigma_{\alpha\beta} dx_3 \tag{2.2}$$

Based on the two-dimensional theory of elasticity, stresses $\sigma_{\alpha\beta}$ due to membrane forces are assumed to be uniformly distributed over the thickness, and as proposed by Reissner [71] for shear deformable plate bending, the stresses due to bending and twisting moments $\sigma_{\alpha\beta}$ vary linearly and the transverse shear stresses $\sigma_{\alpha 3}$ vary parabolically over the thickness. Hence, the stress components can be expressed via the following relationships:

$$\sigma_{\alpha\beta} = \frac{1}{h} N_{\alpha\beta} + \frac{12 x_3}{h^3} M_{\alpha\beta} \tag{2.3}$$

and

$$\sigma_{\alpha 3} = \frac{3}{2h} \left[1 - \left(\frac{2x_3}{h} \right)^2 \right] Q_\alpha \tag{2.4}$$

The generalised bending and shear tractions at a boundary point can be defined as:

$$p_\alpha = p_\alpha^{linear} = M_{\alpha\beta} n_\beta \qquad \text{and} \qquad p_3^{linear} = Q_\alpha n_\alpha \tag{2.5}$$

and membrane tractions

$$t_\alpha^{linear} = N_{\alpha\beta}^{linear} n_\beta \tag{2.6}$$

where n_β are components of the outward normal vector to the plate boundary.

2.2.2 Strain-displacement relationships

The transverse shear strains $\gamma_{\alpha 3}$ of the element can be written as

$$\gamma_{\alpha 3} = \psi_\alpha = w_\alpha + w_{3,\alpha} \tag{2.7}$$

the curvature relationships or the flexural strain $\kappa_{\alpha\beta}$ as

$$\kappa_{\alpha\beta} = 2\chi_{\alpha\beta} = w_{\alpha,\beta} + w_{\beta,\alpha} \tag{2.8}$$

and the in-plane strains $\epsilon_{\alpha\beta}^{linear}$ of the element as

$$\epsilon_{\alpha\beta}^{linear} = \frac{1}{2}\left(u_{\alpha,\beta} + u_{\beta,\alpha}\right) \tag{2.9}$$

2.2.3 Equilibrium equations

The notation $(.)_{12}^{+}$ is used to denote $(.)_{12} + \frac{\partial(.)_{12}}{\partial x_1}dx_1$; the notation $(.)_{21}^{+}$ is used to denote $(.)_{21} + \frac{\partial(.)_{21}}{\partial x_2}dx_2$, etc (see Figure 2-3). After taking the equilibrium of moments and forces, ignoring the higher order terms, the linear elastic equilibrium equations of shear deformable plates can be written as follows:

$$\frac{\partial M_{11}}{\partial x_1} + \frac{\partial M_{21}}{\partial x_2} - Q_1 = 0 \tag{2.10}$$

$$\frac{\partial M_{12}}{\partial x_1} + \frac{\partial M_{22}}{\partial x_2} - Q_2 = 0 \tag{2.11}$$

$$\frac{\partial Q_1}{\partial x_1} + \frac{\partial Q_2}{\partial x_2} + q = 0 \tag{2.12}$$

$$\frac{\partial N_{11}}{\partial x_1} + \frac{\partial N_{21}}{\partial x_2} = 0 \tag{2.13}$$

$$\frac{\partial N_{12}}{\partial x_1} + \frac{\partial N_{22}}{\partial x_2} = 0 \tag{2.14}$$

The equilibrium equations can be formed by considering the equilibrium of a typical plate element having dimensions of $dx_1 \times dx_2 \times h$ and under uniform load q (per unit area), which is regarded to be positive when it is applied in x_i directions (see Figure 2-3). These equations are derived in a similar manner to the section 2.3 and can be written in indicial notation as follows:

$$M_{\alpha\beta,\beta} - Q_\alpha = 0; \tag{2.15}$$

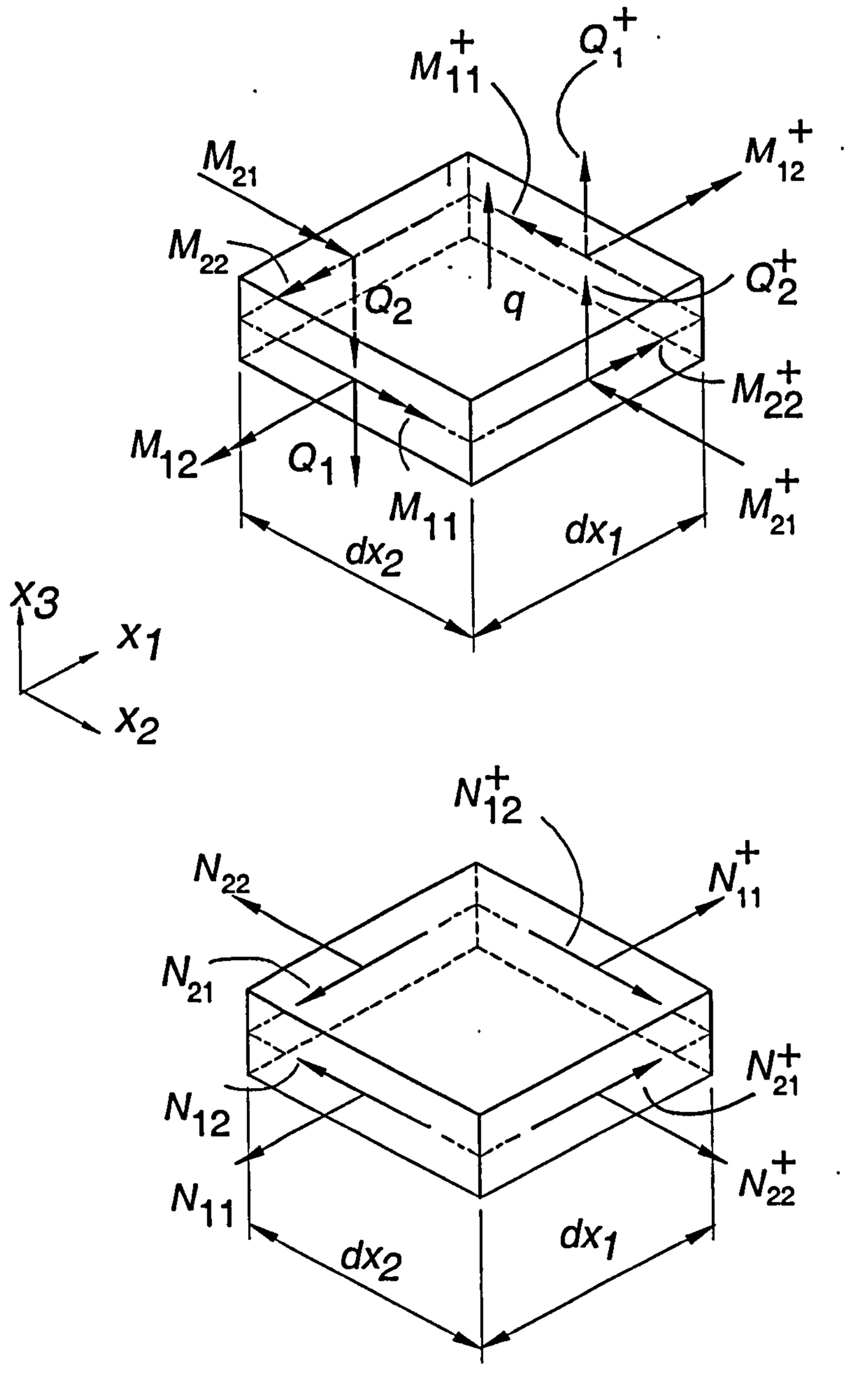

Figure 2-3: Stress resultant equilibrium in a linear plate element.

$$Q_{\alpha,\alpha} + q = 0; \tag{2.16}$$

and

$$N^{linear}_{\alpha\beta,\beta} = 0 \tag{2.17}$$

2.2.4 Stress resultant-strain relationships

The stress resultant-strain relationships for plate bending are derived by Reissner [71] as follows:

$$M_{\alpha\beta} = D\frac{1-\nu}{2}\left(2\chi_{\alpha\beta} + \frac{2\nu}{1-\nu}\chi_{\gamma\gamma}\delta_{\alpha\beta}\right);$$

$$Q_\alpha = C\psi_\alpha \tag{2.18}$$

and based on Hooke's law for two-dimensional plane stress, membrane stress resultant-strain relationships can be written as follows:

$$N^{linear}_{\alpha\beta} = B\frac{1-\nu}{2}\left(2\varepsilon_{\alpha\beta} + \frac{2\nu}{1-\nu}\varepsilon_{\gamma\gamma}\delta_{\alpha\beta}\right) \tag{2.19}$$

Equations (2.18 – 2.19) represent the generalised Hooke's law. Equations (2.18) and (2.19) together with equations (2.7 – 2.9) represent the stress resultant-displacement relationships as follows:

$$\begin{aligned} M_{\alpha\beta} &= D\frac{1-\nu}{2}\left(w_{\alpha,\beta} + w_{\beta,\alpha} + \frac{2\nu}{1-\nu}w_{\gamma,\gamma}\delta_{\alpha\beta}\right); \\ Q_\alpha &= C(w_\alpha + w_{3,\alpha}) \end{aligned} \tag{2.20}$$

and

$$N^{linear}_{\alpha\beta} = B\frac{1-\nu}{2}\left(u_{\alpha,\beta} + u_{\beta,\alpha} + \frac{2\nu}{1-\nu}u_{\gamma,\gamma}\delta_{\alpha\beta}\right) \tag{2.21}$$

where $B(= Eh/\left(1-\nu^2\right))$ is known as the tension stiffness; $D(= Eh^3/\left[12\left(1-\nu^2\right)\right])$ is the bending stiffness of the plate; $C(=\left[D\left(1-\nu\right)\lambda^2\right]/2)$ is the shear stiffness; and $\delta_{\alpha\beta}$ is the Kronecker delta function, which has property

$$\delta_{\alpha\beta} = \begin{cases} 1 \text{ if } \alpha = \beta \\ 0 \text{ if} \alpha \neq \beta \end{cases} \tag{2.22}$$

2.2.5 Equilibrium equations in terms of displacements

The equilibrium equations could be rewritten in terms of the displacements. By substituting (2.20 – 2.21) into (2.15 – 2.17), the equilibrium equations in terms of displacements are obtained as follows:

$$D\nabla^2 w_1 + \frac{D}{2}(1+\nu)\frac{\partial}{\partial x_2}\left(-\frac{\partial w_1}{\partial x_2} + \frac{\partial w_2}{\partial x_1}\right) - Cw_1 - C\frac{\partial w_3}{\partial x_1} = 0 \tag{2.23}$$

$$\frac{D}{2}(1+\nu)\frac{\partial}{\partial x_1}\left(\frac{\partial w_1}{\partial x_2} - \frac{\partial w_2}{\partial x_1}\right) + D\nabla^2 w_2 - Cw_2 - C\frac{\partial w_3}{\partial x_2} = 0 \tag{2.24}$$

$$C\nabla^2 w_3 + C\frac{\partial w_1}{\partial x_1} + C\frac{\partial w_2}{\partial x_2} + q = 0 \tag{2.25}$$

and

$$B\nabla^2 u_1 + \frac{B}{2}(1+\nu)\frac{\partial}{\partial x_2}\left(-\frac{\partial u_1}{\partial x_2} + \frac{\partial u_2}{\partial x_1}\right) = 0 \tag{2.26}$$

$$\frac{B}{2}(1+\nu)\frac{\partial}{\partial x_1}\left(\frac{\partial u_1}{\partial x_2} - \frac{\partial u_2}{\partial x_1}\right) + B\nabla^2 u_2 = 0 \tag{2.27}$$

2.3 Governing Equations of Geometrically Nonlinear Plates

2.3.1 Strain-displacement relationships

The transverse shear strains and the flexural strain of the element are the same with the ones for linear plates. But the strain-displacement relationships of in-plane strains and displacements are now coupled with bending strains and displacements. The in-plane strains of the element are written as follows

$$\varepsilon_{\alpha\beta} = \varepsilon_{\alpha\beta}^{linear} + \varepsilon_{\alpha\beta}^{nonlinear} \tag{2.28}$$

where

$$\varepsilon_{\alpha\beta}^{nonlinear} = \frac{1}{2} w_{3,\alpha} w_{3,\beta} \tag{2.29}$$

and $\varepsilon_{\alpha\beta}^{linear}$ is defined as in equation (2.9).

The generalized membrane tractions can be defined as

$$t_\alpha = t_\alpha^{linear} + t_\alpha^{nonlinear} \tag{2.30}$$

where

$$t_\alpha^{nonlinear} = N_{\alpha\beta}^{nonlinear} n_\beta \tag{2.31}$$

and t_α^{linear} is defined as in equation 2.6.

2.3.2 Equilibrium equations

To derive the nonlinear equations for shear deformable plates, the nonlinear interactions between forces and rotations must be taken into account. Therefore the equations representing equilibrium of forces and moments must be derived for the plate element in the deformed state. In the derivation of the equilibrium equations, the sketches of force and moment intensities are separated as shown in Figure 2-4.

The rotations β_1 and β_2 in Figure 2-4 represent the angle between a coordinate and the corresponding tangent on the middle surface of the plate element at its upper corner. The force and moment intensities and rotations vary across the element.

After taking the equilibrium of moments and forces, simplifying and ignoring the higher order terms, the nonlinear equilibrium equations of shear deformable plate can be written as follows:

$$\frac{\partial M_{11}}{\partial x_1} + \frac{\partial M_{12}}{\partial x_2} - Q_1 = 0 \tag{2.32}$$

$$\frac{\partial M_{22}}{\partial x_2} + \frac{\partial M_{21}}{\partial x_1} - Q_2 = 0 \tag{2.33}$$

$$\frac{\partial Q_1}{\partial x_1} + \frac{\partial Q_2}{\partial x_2} + N_{11}\frac{\partial^2 w}{\partial x_1^2} + N_{12}\frac{\partial^2 w}{\partial x_1 \partial x_2} + N_{22}\frac{\partial^2 w}{\partial x_2^2} + N_{21}\frac{\partial^2 w}{\partial x_1 \partial x_2} + q = 0 \tag{2.34}$$

$$\frac{\partial N_{11}}{\partial x_1} + \frac{\partial N_{12}}{\partial x_2} = 0 \tag{2.35}$$

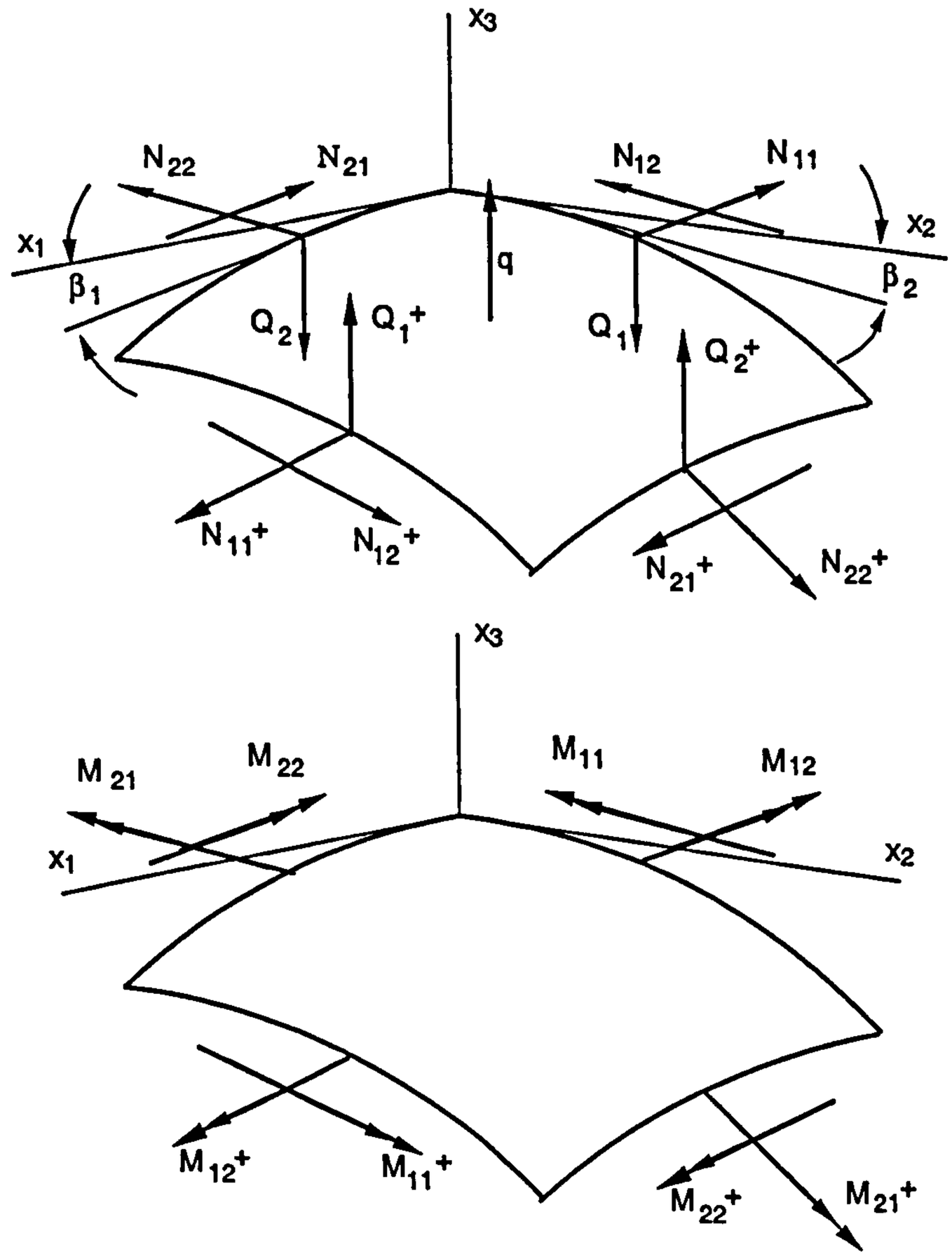

Figure 2-4: Stress resultant equilibrium in geometrically nonlinear plate element.

$$\frac{\partial N_{22}}{\partial x_2} + \frac{\partial N_{21}}{\partial x_1} = 0 \tag{2.36}$$

The above equations can be written in a compact form using indicial notation as below:

$$M_{\alpha\beta,\beta} - Q_\alpha = 0 \tag{2.37}$$

$$Q_{\alpha,\alpha} + (N_{\alpha\beta} w_{3,\beta})_{,\alpha} + q = 0 \tag{2.38}$$

$$N_{\alpha\beta,\beta} = 0 \tag{2.39}$$

where,

$$M_{\alpha\beta} = \frac{1-\upsilon}{2} D(w_{\alpha,\beta} + w_{\beta,\alpha} + \frac{2\upsilon}{1-\upsilon} w_{\gamma,\gamma}\delta_{\alpha\beta}) \tag{2.40}$$

$$Q_\alpha = C(w_\alpha + w_{3,\alpha}) \tag{2.41}$$

$$N_{\alpha\beta} = N_{\alpha\beta}^{linear} + N_{\alpha\beta}^{nonlinear} \tag{2.42}$$

$$N_{\alpha\beta}^{linear} = \frac{1-\upsilon}{2} B(u_{\alpha,\beta} + u_{\beta,\alpha} + \frac{2\upsilon}{1-\upsilon} u_{\gamma,\gamma}\delta_{\alpha\beta}) \tag{2.43}$$

$$N_{\alpha\beta}^{nonlinear} = \frac{1-\upsilon}{2} B(w_{3,\beta} w_{3,\alpha} + \frac{\upsilon}{1-\upsilon} w_{3,\gamma} w_{3,\gamma}\delta_{\alpha\beta}) \tag{2.44}$$

in which the tension stiffness B, the bending stiffness of the plate D, the shear stiffness C, and the Kronecker delta function $\delta_{\alpha\beta}$ are the same as the ones defined in section 2.2.

2.3.3 Equilibrium equations in terms of displacements

By substituting (2.40 – 2.44) into (2.37 – 2.39), the equilibrium equations in terms of displacements are obtained as follows:

$$D\nabla^2 w_1 + \frac{D}{2}(1+\nu)\frac{\partial}{\partial x_2}\left(-\frac{\partial w_1}{\partial x_2} + \frac{\partial w_2}{\partial x_1}\right) - Cw_1 - C\frac{\partial w_3}{\partial x_1} = 0 \qquad (2.45)$$

$$\frac{D}{2}(1+\nu)\frac{\partial}{\partial x_1}\left(\frac{\partial w_1}{\partial x_2} - \frac{\partial w_2}{\partial x_1}\right) + D\nabla^2 w_2 - Cw_2 - C\frac{\partial w_3}{\partial x_2} = 0 \qquad (2.46)$$

$$C\left[\nabla^2 w_3 + \frac{\partial w_1}{\partial x_1} + \frac{\partial w_2}{\partial x_2}\right] + B\ \left[\frac{\partial^2 w}{\partial x_1^2}\left(\frac{\partial u_1}{\partial x_1} + \nu\frac{\partial u_2}{\partial x_2}\right)\right] +$$

$$B\ \left[\frac{\partial^2 w}{\partial x_2^2}\left(\frac{\partial u_2}{\partial x_2} + \nu\frac{\partial u_1}{\partial x_1}\right)\right]\ + B\left[(1-\nu)\frac{\partial^2 w}{\partial x_1 \partial x_2}\left(\frac{\partial u_2}{\partial x_2} + \frac{\partial u_1}{\partial x_1}\right)\right]\ + q = 0 \qquad (2.47)$$

and

$$B\nabla^2 u_1 + \frac{B}{2}(1+\nu)\frac{\partial}{\partial x_2}\left(-\frac{\partial u_1}{\partial x_2} + \frac{\partial u_2}{\partial x_1}\right) +$$

$$\frac{B}{2}\frac{\partial}{\partial x_1}\left(\frac{\partial w_3}{\partial x_1}\frac{\partial w_3}{\partial x_1} - \nu\frac{\partial w_3}{\partial x_2}\frac{\partial w_3}{\partial x_2}\right) + \frac{(1-\nu)}{2}B\frac{\partial}{\partial x_2}\left(\frac{\partial w_3}{\partial x_1}\frac{\partial w_3}{\partial x2}\right) = 0 \qquad (2.48)$$

$$\frac{B}{2}(1+\nu)\frac{\partial}{\partial x_1}\left(\frac{\partial u_1}{\partial x_2} - \frac{\partial u_2}{\partial x_1}\right) + B\nabla^2 u_2 +$$

$$\frac{B}{2}\frac{\partial}{\partial x_2}\left(\frac{\partial w_3}{\partial x_2}\frac{\partial w_3}{\partial x_2} - \nu\frac{\partial w_3}{\partial x_1}\frac{\partial w_3}{\partial x_1}\right) + \frac{(1-\nu)}{2}B\frac{\partial}{\partial x_1}\left(\frac{\partial w_3}{\partial x_1}\frac{\partial w_3}{\partial x2}\right) = 0 \qquad (2.49)$$

2.4 Boundary conditions

There are three possible boundary conditions considered in this work, i.e. clamped, simply supported and free boundary. These boundary conditions can be summarised

as follows:

Clamped boundary condition

$$w_t = 0, \quad w_n = 0, \quad w_3 = 0, \quad u_t = 0, \quad \text{and} \quad u_n = 0 \tag{2.50}$$

Simply supported boundary condition

$$w_t = 0, \quad w_3 = 0, \quad M_n = 0, \quad \text{and} \quad u_1 = 0 \quad \text{or} \quad u_2 = 0 \tag{2.51}$$

Free boundary condition

$$M_t = 0, \quad M_n = 0, \quad p_3 = 0, \quad N_t = 0, \quad \text{and} \quad N_n = 0 \tag{2.52}$$

2.5 Basic Concepts of Fracture Mechanics

Since the pioneering investigation in 1920 by Griffith [36], followed by Irwin [40] in 1948, and through rapid developments during 1960s and 1970s Fracture Mechanics has become the primary approach for analysing, predicting and preventing failures in structures. Although a relatively new scientific discipline, fracture mechanics considerations are nowadays a requirement for engineering design, particularly in aircraft structures.

The linear elastic assumptions are commonly used for most of the studies on fracture mechanics. The theory is well known as the Linear Elastic Fracture Mechanics (LEFM). One of the most important parameters used in LEFM analysis is the stress intensity factor (SIF). Crack growth, life prediction and residual strength of engineering structures are determined using the stress intensity factors. Therefore, accurate evaluation of stress intensity factors is important.

For crack analysis of plates, five stress intensity factors are obtained, two SIFs due to membrane loads (as shown in Figure 2-5(a) and (b)) and three SIFs due to bending moments and shear loads (as shown in Figure 2-5(c), (d) and (e)).

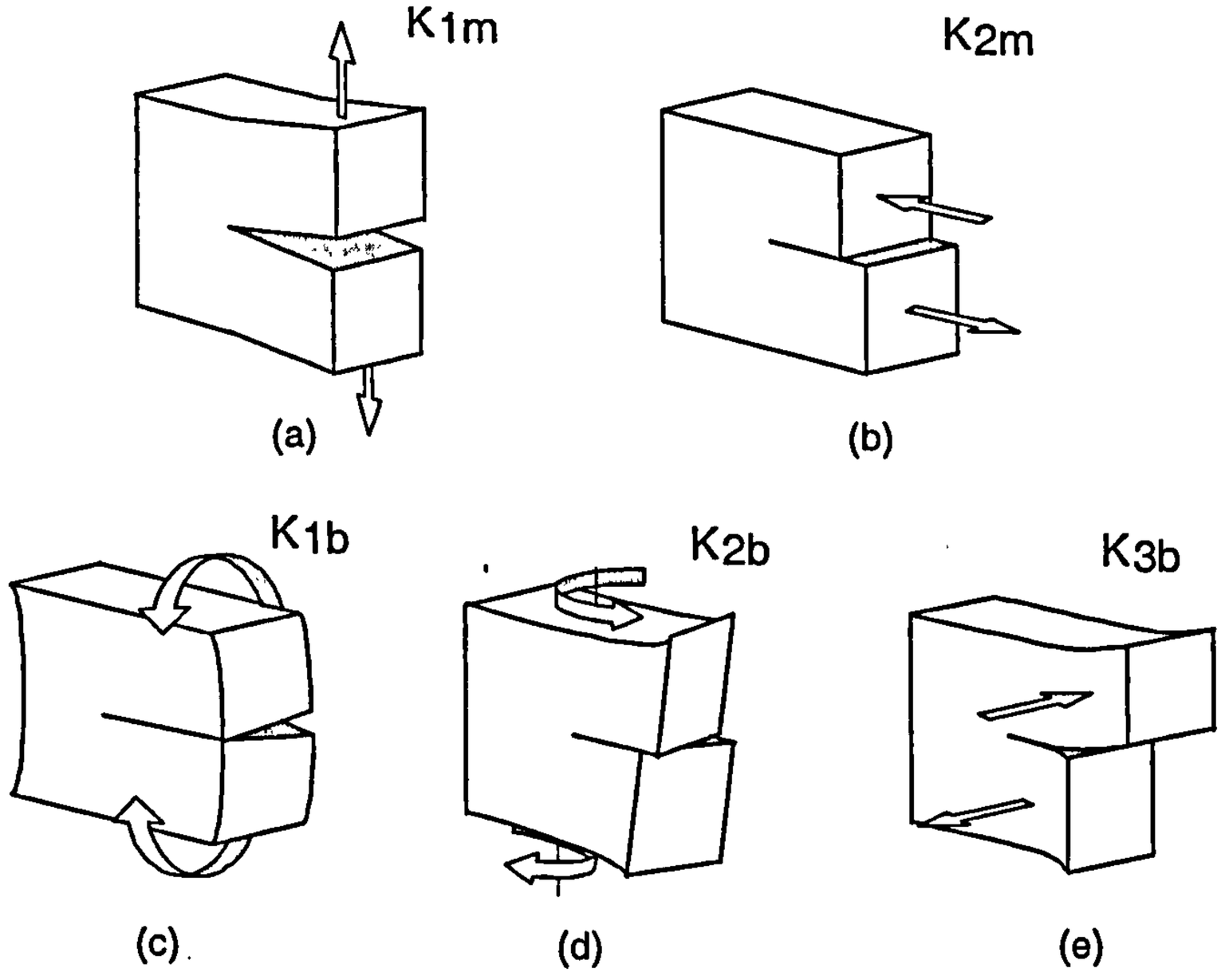

Figure 2-5: Crack modes.

The stress resultant intensity factors are denoted as K_1, K_2 and K_3 respectively. Subscript m is added for stress intensity factors and stress resultant intensity factors due to membrane loads, and subscript b is added for stress resultant intensity factors due to bending and shear loads.

2.5.1 Crack tip elastic fields

Using the local polar coordinate system shown in Figure 2-6, the elastic fields in the vicinity of a crack tip are given by Sih [74] as:

$$\begin{aligned} M_{11} &= \frac{K_{1b}}{\sqrt{2\pi r}} \cos\frac{\theta}{2}\left(1-\sin\frac{\theta}{2}\sin\frac{3\theta}{2}\right) \\ &\quad -\frac{K_{2b}}{\sqrt{2\pi r}} \sin\frac{\theta}{2}\left(2+\cos\frac{\theta}{2}\cos\frac{3\theta}{2}\right)+O(1) \end{aligned} \tag{2.53}$$

$$M_{22} = \frac{K_{1b}}{\sqrt{2\pi r}} \cos\frac{\theta}{2}\left(1+\sin\frac{\theta}{2}\sin\frac{3\theta}{2}\right)+$$

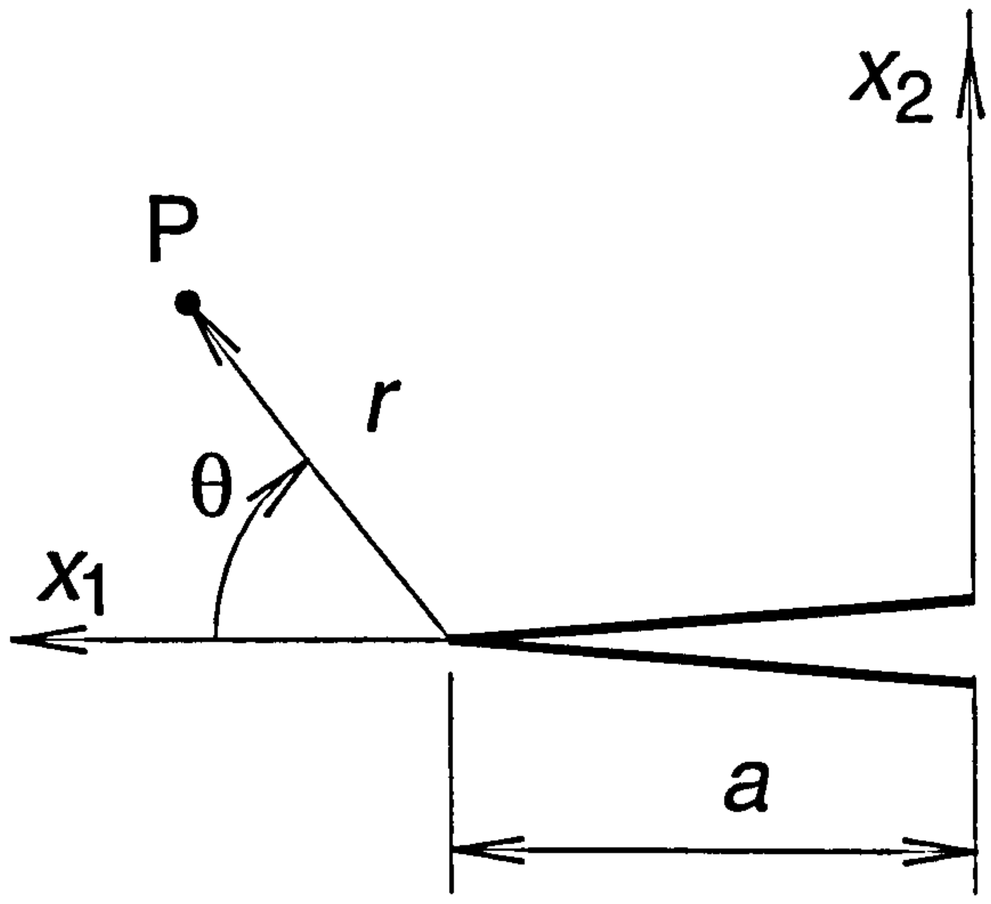

Figure 2-6: Crack tip.

$$\frac{K_{2b}}{\sqrt{2\pi r}} \sin\frac{\theta}{2} \cos\frac{\theta}{2} \cos\frac{3\theta}{2} + O(1) \tag{2.54}$$

$$\begin{aligned} M_{12} &= \frac{K_{1b}}{\sqrt{2\pi r}} \sin\frac{\theta}{2} \cos\frac{\theta}{2} \cos\frac{3\theta}{2} + \\ &\quad \frac{K_{2b}}{\sqrt{2\pi r}} \cos\frac{\theta}{2} \left(1 - \sin\frac{\theta}{2} \sin\frac{3\theta}{2}\right) + O(1) \end{aligned} \tag{2.55}$$

$$Q_1 = -\frac{K_{3b}}{\sqrt{2\pi r}} \sin\frac{\theta}{2} + O(1) \tag{2.56}$$

$$Q_2 = \frac{K_{3b}}{\sqrt{2\pi r}} \cos\frac{\theta}{2} + O(1) \tag{2.57}$$

$$\begin{aligned} N_{11} &= \frac{K_{1m}}{\sqrt{2\pi r}} \cos\frac{\theta}{2} \left(1 - \sin\frac{\theta}{2} \sin\frac{3\theta}{2}\right) \\ &\quad -\frac{K_{2m}}{\sqrt{2\pi r}} \sin\frac{\theta}{2} \left(2 + \cos\frac{\theta}{2} \cos\frac{3\theta}{2}\right) + O(1) \end{aligned} \tag{2.58}$$

$$\begin{aligned} N_{22} &= \frac{K_{1m}}{\sqrt{2\pi r}} \cos\frac{\theta}{2} \left(1 + \sin\frac{\theta}{2} \sin\frac{3\theta}{2}\right) \\ &\quad +\frac{K_{2m}}{\sqrt{2\pi r}} \sin\frac{\theta}{2} \cos\frac{\theta}{2} \cos\frac{3\theta}{2} + O(1) \end{aligned} \tag{2.59}$$

$$N_{12} = \frac{K_{1m}}{\sqrt{2\pi r}} \sin\frac{\theta}{2}\cos\frac{\theta}{2}\cos\frac{3\theta}{2} + \frac{K_{2m}}{\sqrt{2\pi r}}\cos\frac{\theta}{2}\left(1-\sin\frac{\theta}{2}\sin\frac{3\theta}{2}\right)+O(1) \tag{2.60}$$

for stress resultants, and

$$w_1 = \frac{1+\nu}{E}\left(\frac{12}{h^3}\right)\sqrt{\frac{r}{2\pi}}\left[K_{1b}\cos\frac{\theta}{2}\left(\frac{3-\nu}{1+\nu}-\cos\theta\right) + K_{2b}\sin\frac{\theta}{2}\left(\frac{5+\nu}{1+\nu}-\cos\theta\right)\right]+O(r) \tag{2.61}$$

$$w_2 = \frac{1+\nu}{E}\left(\frac{12}{h^3}\right)\sqrt{\frac{r}{2\pi}}\left[K_{1b}\sin\frac{\theta}{2}\left(\frac{3-\nu}{1+\nu}-\cos\theta\right) + K_{2b}\cos\frac{\theta}{2}\left(\frac{1-3\nu}{1+\nu}-\cos\theta\right)\right]+O(r) \tag{2.62}$$

$$w_3 = \frac{24(1+\nu)}{5Eh}\sqrt{\frac{r}{2\pi}}K_{3b}\sin\frac{\theta}{2}+O(r) \tag{2.63}$$

$$u_1 = \frac{2(1+\nu)}{Eh}\sqrt{\frac{r}{2\pi}}\left[K_{1m}\cos\frac{\theta}{2}\left(\frac{1-\nu}{1+\nu}+\sin^2\frac{\theta}{2}\right) + K_{2m}\sin\frac{\theta}{2}\left(\frac{2}{1+\nu}+\cos^2\frac{\theta}{2}\right)\right]+O(r) \tag{2.64}$$

$$u_2 = \frac{2(1+\nu)}{Eh}\sqrt{\frac{r}{2\pi}}\left[K_{1m}\sin\frac{\theta}{2}\left(\frac{2}{1+\nu}-\cos^2\frac{\theta}{2}\right) + K_{2m}\cos\frac{\theta}{2}\left(\frac{\nu-1}{1+\nu}+\sin^2\frac{\theta}{2}\right)\right]+O(r) \tag{2.65}$$

for displacements[96], where (r,θ) are the polar coordinates measured from the crack tip, K_{1m} and K_{2m} are mode I and mode II membrane stress resultant intensity factors respectively, K_{1b}, K_{2b}, and K_{3b} are two bending and shear stress resultant intensity factors respectively.

2.5.2 Stress intensity factors evaluation

Stress resultant intensity factors can be explicitly derived from equations (2.53 – 2.60). Substituting $\theta = 0$ in equations (2.53 – 2.60), the stress resultant intensity

factors can be expressed as:

$$K_{1b} = \lim_{r \to 0} M_{22} \sqrt{2\pi r}\,(r, 0) \tag{2.66}$$

$$K_{2b} = \lim_{r \to 0} M_{12} \sqrt{2\pi r}\,(r, 0) \tag{2.67}$$

$$K_{3b} = \lim_{r \to 0} Q_2 \sqrt{2\pi r}\,(r, 0) \tag{2.68}$$

$$K_{1m} = \lim_{r \to 0} N_{22} \sqrt{2\pi r}\,(r, 0) \tag{2.69}$$

and

$$K_{2m} = \lim_{r \to 0} N_{12} \sqrt{2\pi r}\,(r, 0) \tag{2.70}$$

By omitting the $O(r)$ terms in equations (2.61 − 2.65) for small r and substituting θ with $\pm\pi$, the displacements on the crack surfaces near the tip are obtained as:

$$\begin{Bmatrix} \Delta w_2 \\ \Delta w_1 \\ \Delta w_3 \\ \Delta u_2 \\ \Delta u_1 \end{Bmatrix} = \begin{Bmatrix} w_2 \\ w_1 \\ w_3 \\ u_2 \\ u_1 \end{Bmatrix}_{\theta=180^0} - \begin{Bmatrix} w_2 \\ w_1 \\ w_3 \\ u_2 \\ u_1 \end{Bmatrix}_{\theta=-180^0} \tag{2.71}$$

$$= \begin{bmatrix} \frac{48}{Eh^3}\sqrt{\frac{2r}{\pi}} & 0 & 0 & 0 & 0 \\ 0 & \frac{48}{Eh^3}\sqrt{\frac{2r}{\pi}} & 0 & 0 & 0 \\ 0 & 0 & \frac{24(1+\nu)}{5Eh}\sqrt{\frac{2r}{\pi}} & 0 & 0 \\ 0 & 0 & 0 & \frac{8}{Eh}\sqrt{\frac{r}{2\pi}} & 0 \\ 0 & 0 & 0 & 0 & \frac{8}{Eh}\sqrt{\frac{r}{2\pi}} \end{bmatrix} \begin{Bmatrix} K_{1b} \\ K_{2b} \\ K_{3b} \\ K_{1m} \\ K_{2m} \end{Bmatrix}$$

Then the stress intensity factors can be written in terms of displacements on the crack surfaces, as

$$\{K\} = \frac{1}{\sqrt{r}} [\mathbf{Fc}] \{w\} \tag{2.72}$$

where

$$\{K\} = \begin{Bmatrix} K_{1b} \\ K_{2b} \\ K_{3b} \\ K_{1m} \\ K_{2m} \end{Bmatrix}, \qquad \{w\} = \begin{Bmatrix} \Delta w_2 \\ \Delta w_1 \\ \Delta w_3 \\ \Delta u_2 \\ \Delta u_1 \end{Bmatrix} \tag{2.73}$$

and

$$[\mathbf{Fc}] = \begin{bmatrix} \frac{Eh^3}{48}\sqrt{\frac{\pi}{2}} & 0 & 0 & 0 & 0 \\ 0 & \frac{Eh^3}{48}\sqrt{\frac{\pi}{2}} & 0 & 0 & 0 \\ 0 & 0 & \frac{5Eh}{24(1+\nu)}\sqrt{\frac{\pi}{2}} & 0 & 0 \\ 0 & 0 & 0 & \frac{Eh}{8}\sqrt{2\pi} & 0 \\ 0 & 0 & 0 & 0 & \frac{Eh}{8}\sqrt{2\pi} \end{bmatrix} \tag{2.74}$$

2.6 Buckling of Thin Plates

The theoretical buckling stress of a flat panel is the stress at which a stability condition of equilibrium configurations occurs between the straight and the slightly bent form [34]. It marks the region in which a continued application of load results in accelerated growth of deflections perpendicular to the plane of the plate. This important phenomenon describes that buckling initiates the physical processes which lead to the eventual failure of the plate.

The need for approximate methods to analyse buckling problems arises from the fact that exact solutions can be found for only a limited number of problems. Timoshenko [90], Sokolnikoff [75], and Bleich [19] discussed extensively the different methods of buckling analysis and their applications to wide range of problems.

2.6.1 Calculation of critical loads

The critical values of the forces acting in the mid-plane of a plate can be obtained by assuming that from the beginning the plate has some initial curvature or lateral loading. Those values of forces at which deflections are growing indefinitely are commonly called as the *critical values* [90]. Recently, it has been shown that eigenvalue

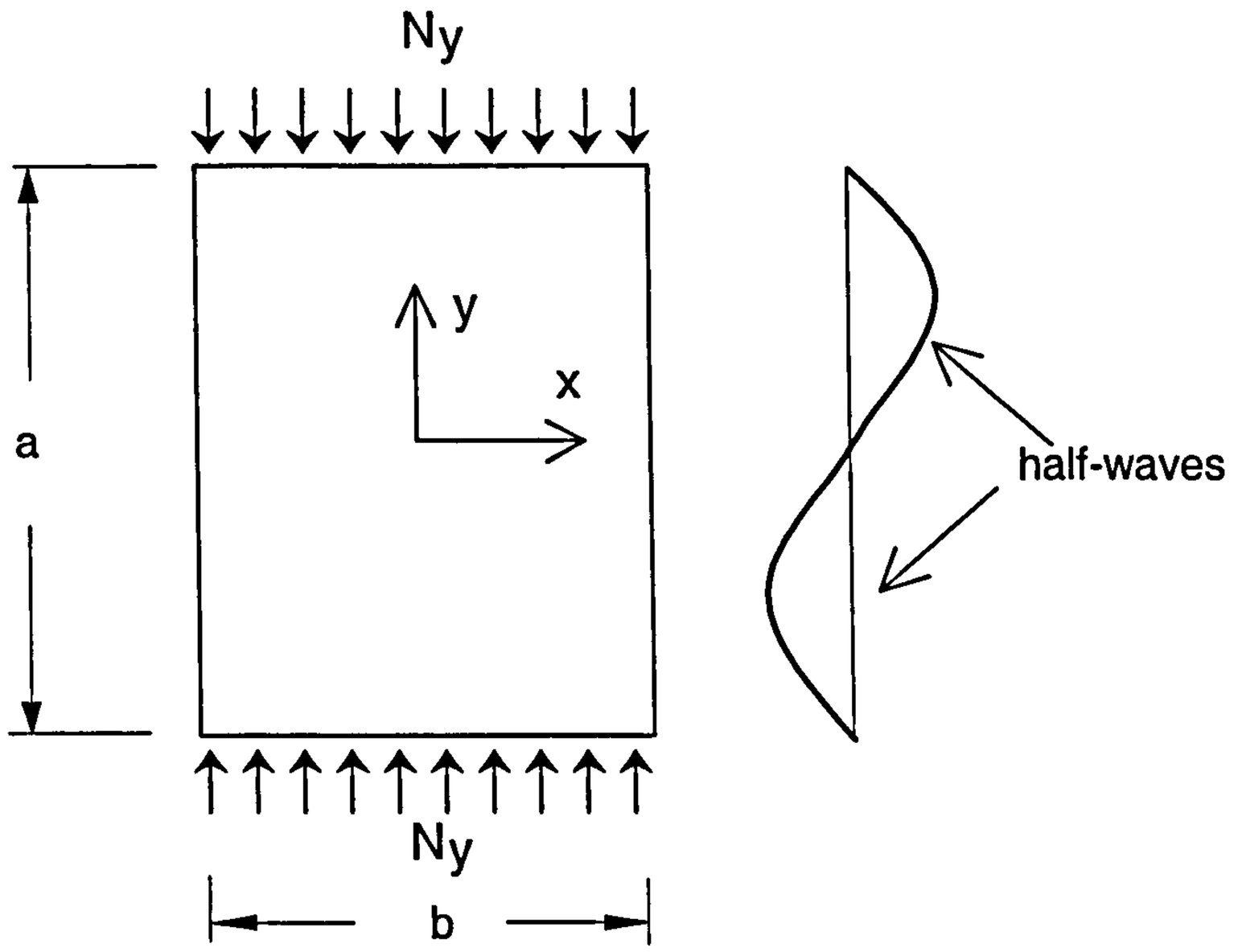

Figure 2-7: Simple buckling model.

formulations can be introduced to obtain the critical values for the linear buckling of thin plates [23].

For the illustrated simple model of a plate shown in Figure 2-7, the critical values of the buckling load can be represented in the form:

$$(N_y)_{critical} = k\frac{\pi^2 D}{b^2} \tag{2.75}$$

where k is buckling coefficient, b is the width of the plate and D is the bending stiffness of the plate. The magnitude of k depends on the aspect ratio a/b of plate. Different aspect ratios are also providing different number of half-waves when the plate buckles [90].

2.7 Eigenvalue Problem

Algebraic eigenvalue formulation has been used to analyse a wide variety of problems. In this thesis, eigenvalue formulation is used to obtain the buckling coefficients of plates. The general algebraic eigenvalue problem is given by

$$(A - \lambda I)X = 0 \tag{2.76}$$

where I is the identity matrix, A is an arbitrary square matrix $n \times n$, X is the unknown vector and λ is the eigenvalue. A non-trivial solution to this system of linear homogeneous equations exists if and only if the determinant is equal zero.

$$\det(A - \lambda I) = \begin{vmatrix} a_{11} - \lambda & a_{12} & \cdots & a_{1n} \\ a_{21} & a_{22} - \lambda & \cdots & a_{2n} \\ \vdots & \vdots & \vdots & \vdots \\ a_{n1} & a_{n2} & \cdots & a_{nn} - \lambda \end{vmatrix} = 0 \tag{2.77}$$

The above equation is called as the characteristic polynomial equation. Its roots are called the eigenvalues and the corresponding vectors eigenvectors.

2.8 Summary

In this chapter, the basic concepts for the elastostatic theories of shear deformable plates and the two-dimensional plane stress were reviewed. Some basic fundamental concepts of fracture mechanics, buckling of thin plates and general algebraic eigenvalue were also reviewed .

Chapter 3

The Boundary Element Method for Shear Deformable Plates

3.1 Introduction

The Boundary Element Method (BEM) has developed into a powerful numerical method for the solution of linear elastic problems. Although its development for plates has not been as rapid as for the two- and three-dimensional problems, recent applications to more complex problems, such as cracked plates [28], stiffened panels [99], geometrically nonlinear [49] and buckling analysis [82] have been encouraging.

Based on the classical Kirchhoff plate theory , Forbes and Robinson [33] presented a BEM formulation for plates with smooth boundaries. Later, Bézine [16] and Stern [79] studied plate problems with corner points and different types of boundary conditions. In the Kirchhoff theory, the additional integral equations for the normal slope are obtained from the derivatives of out-of-plane deflection. Further development of the method for plates with relatively complex geometries, loadings and supports is performed by Hartmann and Zormantel [37]. Other applications of the plate bending formulation can be found in the works of Syngellakis [83], Stern [80], Stern and Lin [81], Abdel-Akher and Hartley [1][2], and Karami *et al.* [45].

The application of the BEM for Reissner plate analysis was first presented by Vander Weeën [94, 95] in 1982. In Vander Weeën's work, the boundary integral equations are derived from the Betti's theorem and the fundamental solutions are

derived using the Hörmander's method. Following his formulation, Karam and Telles [44] reported that the Reissner's plate model can be used to analyse both thin and thick plates. They also developed the formulation to account for infinite regions. A similar formulation to that of Vander Weeën's work is presented by Barcellos and Silva [15] to study Mindlin plate model. The difference between their formulation and the Reissner formulation is in the shear factor constant. Westphal and Barcellos [101] discussed the importance of the neglected terms in the fundamental solution derived by Vander Weeën [94], and demonstrated that the terms have no effect on the results. Later, other fundamental solutions for the Reissner plate were derived by El-Zafrany, Debbih and Fadhil [29] using the Hankel integral transformation. The results were shown to be the same as that of Vander Weeën's results [94]. Rashed and Aliabadi [70] presented fundamental solution for thick foundation plates. In [30], a modified form of the fundamental solutions were derived, by separating parts of the kernel representing the effect of transverse shear, to allow analysis of thin and thick plates. Recent advances in plate bending analysis with the boundary element method can be found in the book edited by Aliabadi [9].

The need for numerical tools to model cracks in structures has led researchers to development of methods which are efficient and can provide accurate results. One such method is the dual boundary element method [63]. The dual boundary element method is formed by using both displacement and traction integral equations. The method has been successfully applied to solve many applications of fracture mechanics problems [7][8].

In this chapter, the derivation of boundary integral equations for the analysis of linear elastic shear deformable plate bending and two dimensional plane stress elasticity are presented. The boundary is discretised into quadratic isoparametric elements. The domain integrals which appear in this formulation are transformed to boundary integrals using the dual reciprocity technique [98]. The traction integral equations of shear deformable plates bending and two-dimensional plane stress are also presented [28][68]. The integrals are used to form the dual boundary element formulation to analyse crack problems.

3.2 The Integral Representations

The equilibrium equations of shear deformable plate in equations (2.10 – 2.14) can be rewritten as follows [98]:

$$D\nabla^2 w_1 + \frac{D}{2}(1+\nu)\frac{\partial}{\partial x_2}\left(-\frac{\partial w_1}{\partial x_2} + \frac{\partial w_2}{\partial x_1}\right) - Cw_1 - C\frac{\partial w_3}{\partial x_1} = 0 \qquad (3.1)$$

$$\frac{D}{2}(1+\nu)\frac{\partial}{\partial x_1}\left(\frac{\partial w_1}{\partial x_2} - \frac{\partial w_2}{\partial x_1}\right) + D\nabla^2 w_2 - Cw_2 - C\frac{\partial w_3}{\partial x_2} = 0 \qquad (3.2)$$

$$C\nabla^2 w_3 + C\frac{\partial w_1}{\partial x_1} + C\frac{\partial w_2}{\partial x_2} + q = 0 \qquad (3.3)$$

$$B\nabla^2 u_1 + \frac{B}{2}(1+\nu)\frac{\partial}{\partial x_2}\left(-\frac{\partial u_1}{\partial x_2} + \frac{\partial u_2}{\partial x_1}\right) = 0 \qquad (3.4)$$

$$\frac{B}{2}(1+\nu)\frac{\partial}{\partial x_1}\left(\frac{\partial u_1}{\partial x_2} - \frac{\partial u_2}{\partial x_1}\right) + B\nabla^2 u_2 = 0 \qquad (3.5)$$

Equations (3.1 – 3.5) can be rewritten as follows [98]:

$$L^b_{ik} w_k + f^b_i = 0 \qquad (3.6)$$

and

$$L^m_{\alpha\beta} u_\beta = 0 \qquad (3.7)$$

where L^b_{ik} is the Navier differential operator for shear deformable plate bending problems

$$L^b_{\alpha\beta} = \frac{D(1-\nu)}{2}\left[\left(\nabla^2 - \lambda^2\right)\delta_{\alpha\beta} + \frac{(1+\nu)}{(1-\nu)}\frac{\partial}{\partial x_\alpha}\frac{\partial}{\partial x_\beta}\right] \qquad (3.8)$$

$$L^b_{\alpha 3} = -\frac{(1-\nu)D}{2}\lambda^2\frac{\partial}{\partial x_\alpha} \qquad (3.9)$$

$$L^b_{3\alpha} = -L^b_{\alpha 3} \qquad (3.10)$$

$$L^b_{33} = \frac{(1-\nu)D}{2}\lambda^2\nabla^2 \qquad (3.11)$$

with $f^b_\alpha = 0$ and $f^b_3 = q$, $\lambda\left(=\sqrt{10}/h\right)$ is shear factor, while $L^m_{\alpha\beta}$ is the Navier differential operator for two-dimensional plane stress problems

$$L^m_{\alpha\beta} = B\nabla^2\delta_{\alpha\beta} + \frac{B(1+\nu)}{2}\frac{\partial}{\partial x_\alpha}\frac{\partial}{\partial x_\beta}(1-2\delta_{\alpha\beta}) \tag{3.12}$$

By considering the integral representations of the governing equations (2.15 – 2.17), the integral equations for plate bending problems can be derived from the following integral identities [69]:

$$\int_\Omega [(M_{\alpha\beta,\beta} - Q_\alpha)\, W^*_\alpha + (Q_{\alpha,\alpha} + q)\, W^*_3]\, d\Omega = 0 \tag{3.13}$$

and

$$\int_\Omega (N^{linear}_{\alpha\beta,\beta})\, U^*_\alpha d\Omega = 0 \tag{3.14}$$

where U^*_α and $W^*_i (i = \alpha, 3)$ are weighting functions. Equation (3.13) is an integral representation related to the governing equations for bending and transverse shear stress resultants, while equation (3.14) is an integral representation related to the governing equations for membrane stress resultants.

3.2.1 Rotations and out-of-plane displacement integral representations

Using the weighted residual method [21], the integral representations related to the governing equations for bending and transverse shear stress resultants can be derived [69]. Integrating equation (3.13) by parts and applying the Green's identity [1], gives:

$$\int_\Gamma M_{\alpha\beta} n_\beta W^*_\alpha d\Gamma - \int_\Omega M_{\alpha\beta} W^*_{\alpha,\beta} d\Omega - \int_\Omega Q_\alpha W^*_\alpha d\Omega$$

$$+ \int_\Gamma Q_\alpha n_\alpha W^*_3 d\Gamma - \int_\Omega Q_\alpha W^*_{3,\alpha} d\Omega + \int_\Omega q W^*_3 d\Omega = 0 \tag{3.15}$$

[1] The Green's identity between two functions P and $u_{,\alpha}$ can be written as follows[35]:

$$\int_\Omega P\dot{u}_{,\alpha} d\Omega = \int_\Gamma P u n_\alpha d\Gamma - \int_\Omega P_{,\alpha} u d\Omega$$

then, by substituting the relationships for p_j^{linear} in equation (2.5), equation (3.15) can be written as follows:

$$\int_\Gamma p_j^{linear} W_j^* d\Gamma - \int_\Omega M_{\alpha\beta} W^*_{\alpha,\beta} d\Omega - \int_\Omega Q_\alpha (W^*_\alpha + W^*_{3,\alpha}) d\Omega$$

$$+ \int_\Omega q W_3^* d\Omega = 0 \tag{3.16}$$

where $(j = \alpha, 3)$. Replacing the bending and shear stress resultants ($M_{\alpha\beta}$ and Q_α) with the generalised displacements and their derivatives using equation (2.18), equation (3.16) can be written as

$$\int_\Gamma p_j^{linear} W_j^* d\Gamma - \int_\Omega W^*_{\alpha,\beta} \left\{ \frac{D(1-\nu)}{2} \left(w_{\alpha,\beta} + w_{\beta,\alpha} + \frac{2\nu}{(1-\nu)} \delta_{\alpha\beta} w_{\gamma,\gamma} \right) \right\} d\Omega$$

$$- \int_\Omega C(w_\alpha + w_{3,\alpha})(W^*_\alpha + W^*_{3,\alpha}) d\Omega + \int_\Omega q W_3^* d\Omega = 0 \tag{3.17}$$

then Green's identity can be applied to the integral $M_{\alpha\beta}$ and rearranging the third integral of equation (3.17), gives:

$$\int_\Gamma p_j^{linear} W_j^* d\Gamma - \int_\Gamma W^*_{\alpha,\beta} \left\{ \frac{D(1-\nu)}{2} \left(w_\alpha n_\beta + w_\beta n_\alpha + \frac{2\nu}{(1-\nu)} \delta_{\alpha\beta} w_\gamma n_\gamma \right) \right\} d\Gamma$$

$$+ \int_\Omega \frac{D(1-\nu)}{2} \left(w_\alpha W^*_{\alpha,\beta\beta} + w_\beta W^*_{\alpha,\beta\alpha} + \frac{2\nu}{(1-\nu)} w_\gamma W^*_{\alpha,\beta\gamma} \delta_{\alpha\beta} \right) d\Omega$$

$$- \int_\Omega Q^*_\alpha (w_\alpha + w_{3,\alpha}) d\Omega + \int_\Omega q W_3^* d\Omega = 0 \tag{3.18}$$

Making use of the relationships $w_\beta = w_\alpha \delta_{\alpha\beta}$; $w_\gamma = w_\alpha \delta_{\alpha\gamma}$; $n_\alpha = n_\beta \delta_{\alpha\beta}$ and $n_\gamma = n_\beta \delta_{\beta\gamma}$, the Green's identity, and together with equations (2.5) and (2.18), the equation (3.18) will become:

$$\int_\Gamma (W_j^* p_j^{linear} - P_j^* w_j) d\Gamma$$

$$+ \int_\Omega [(M^*_{\alpha\beta,\beta} - Q^*_\alpha) w_\alpha + Q^*_{\alpha,\alpha} w_3] d\Omega + \int_\Omega W_3^* q d\Omega = 0 \tag{3.19}$$

The $(\cdot)^*$ state can be chosen arbitrary. If the state is defined for concentrated generalised loads: two bending moments $(i = \alpha = 1, 2)$ and one concentrated shear

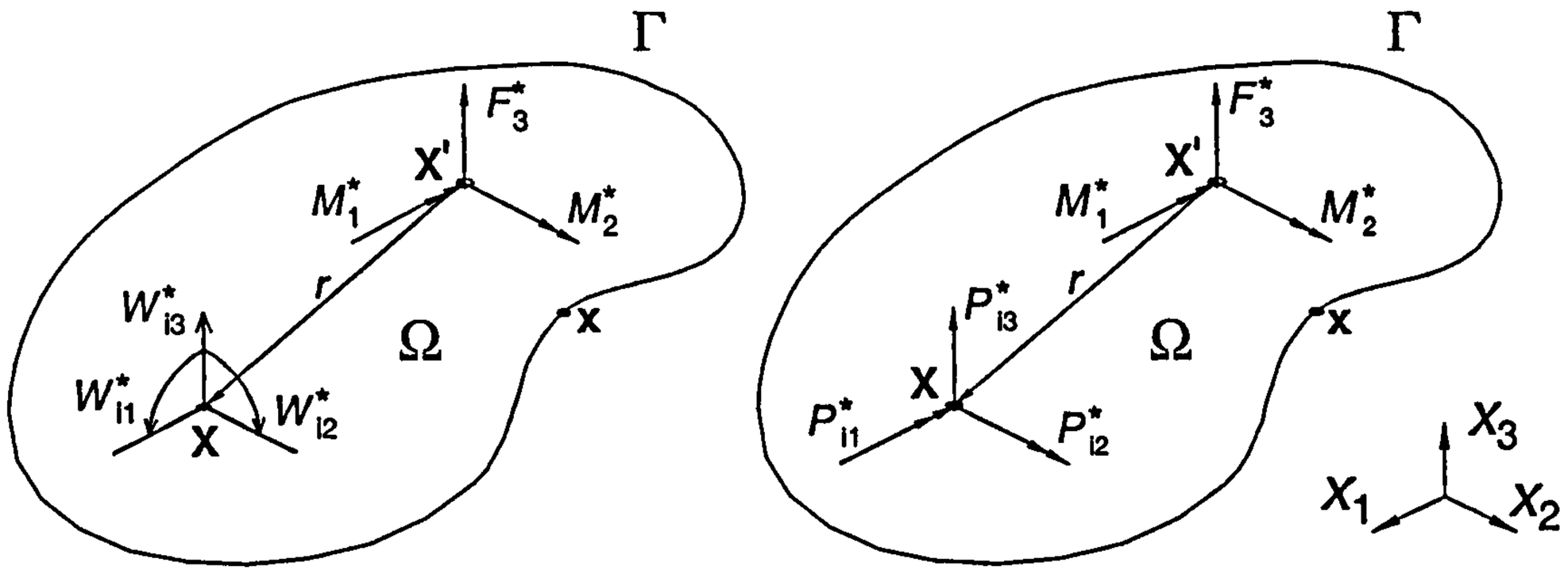

Figure 3-1: Fundamental state due to bending moments and shear forces.

force ($i = 3$) at an arbitrary source point $\mathbf{X}' \in \Omega$ as shown in Figure 3-1, then equation (3.19) can be rewritten after introducing the direction of the load i as follows:

$$\int_\Gamma \left[W_{ij}^* \left(\mathbf{X}', \mathbf{x}\right) p_j^{linear} \left(\mathbf{x}\right) - P_{ij}^* \left(\mathbf{X}', \mathbf{x}\right) w_j \left(\mathbf{x}\right) \right] d\Gamma \left(\mathbf{x}\right) + \int_\Omega W_{i3}^* \left(\mathbf{X}', \mathbf{X}\right) q d\Omega \left(\mathbf{X}\right)$$

$$+ \frac{2\nu}{1-\nu} u_\gamma \left(\mathbf{X}\right) W_{i3,\gamma}^* \left(\mathbf{X}', \mathbf{X}\right) \delta_{\alpha\beta} \Big] d\Omega \left(\mathbf{X}\right)$$

$$+ \int_\Omega \left[M_{i\alpha\beta,\beta}^*(\mathbf{X}', \mathbf{X}) - Q_{i\alpha}^*(\mathbf{X}', \mathbf{X}) \right] w_\alpha(\mathbf{X}) d\Omega(\mathbf{X})$$

$$+ \int_\Omega Q_{i\alpha,\alpha}^*(\mathbf{X}', \mathbf{X}) w_3(\mathbf{X}) d\Omega(\mathbf{X}) = 0 \tag{3.20}$$

where $\mathbf{x} \in \Gamma$ and $\mathbf{X} \in \Omega$ are field points. By choosing the $(\cdot)^*$ state to represent the fundamental state such as:

$$M_{i\alpha\beta,\beta}^*(\mathbf{X}', \mathbf{X}) - Q_{i\alpha}^*(\mathbf{X}', \mathbf{X}) + \delta(\mathbf{X}', \mathbf{X}) \delta_{i\alpha} = 0$$

$$Q_{i\alpha,\alpha}^*(\mathbf{X}', \mathbf{X}) + \delta(\mathbf{X}', \mathbf{X}) \delta_{i3} = 0 \tag{3.21}$$

where $\delta(\mathbf{X}', \mathbf{X})$ is the Dirac delta, and making use of the following property:

$$\int_\Omega \delta(\mathbf{X}', \mathbf{X}) w_i(\mathbf{X}) d\Omega = w_i(\mathbf{X}') \tag{3.22}$$

Equation (3.20) can now be written for an internal source point $\mathbf{X}'$ as:

$$w_i(\mathbf{X}') + \int_\Gamma P^*_{ij}(\mathbf{X}', \mathbf{x}) w_j(\mathbf{x})\, d\Gamma(\mathbf{x}) = \int_\Gamma W^*_{ij}(\mathbf{X}', \mathbf{x}) p_j^{linear}(\mathbf{x})\, d\Gamma(\mathbf{x})$$

$$+ \int_\Omega W^*_{i3}(\mathbf{X}', \mathbf{X}) q(\mathbf{X}) d\Omega(\mathbf{X}) \tag{3.23}$$

where $W^*_{ij}(\mathbf{X}', \mathbf{x})$ and $P^*_{ij}(\mathbf{X}', \mathbf{x})$ are the fundamental solutions for rotations and out-of-plane displacements and bending and shear tractions respectively. It represents the displacement or the tractions at the point $\mathbf{x}$ or $\mathbf{X}$ in the direction j due to unit load applied at $\mathbf{X}'$ at the direction i. The kernels W^*_{ij} and P^*_{ij} are given in Appendix A.

3.2.2 In-plane displacements integral representations

The integral representations related to governing equations for membrane stress resultants can be solved in a similar way. Separating the term in the bracket in equation (3.14) then integrating by parts and applying Green's identity, gives:

$$\int_\Gamma N^{linear}_{\alpha\beta} n_\beta U^*_\alpha d\Gamma - \int_\Omega N^{linear}_{\alpha\beta} U^*_{\alpha,\beta} d\Omega = 0 \tag{3.24}$$

Utilizing and substituting equation (2.19) into (3.24), gives:

$$\int_\Gamma t^{linear}_\alpha U^*_\alpha d\Gamma - \int_\Omega B \frac{1-\nu}{2} \left(u_{\alpha,\beta} + u_{\beta,\alpha} + \frac{2\nu}{1-\nu} u_{\gamma,\gamma} \delta_{\alpha\beta} \right) U^*_{\alpha,\beta} d\Omega = 0 \tag{3.25}$$

Integrating by parts the second integral of equation (3.25), gives:

$$\int_\Gamma t^{linear}_\alpha U^*_\alpha d\Gamma - \int_\Gamma B \frac{1-\nu}{2} \left(u_\alpha n_\beta + u_\beta n_\alpha + \frac{2\nu}{1-\nu} u_\gamma n_\gamma \delta_{\alpha\beta} \right) U^*_{\alpha,\beta} d\Gamma$$

$$+ \int_\Omega B \frac{1-\nu}{2} \left(u_\alpha U^*_{\alpha,\beta\beta} + u_\beta U^*_{\alpha,\beta\alpha} + \frac{2\nu}{1-\nu} \delta_{\alpha\beta} u_\gamma U^*_{\alpha,\beta\gamma} \right) d\Omega = 0 \tag{3.26}$$

Making use of the relationships $u_\beta = u_\alpha \delta_{\alpha\beta}$; $u_\gamma = u_\alpha \delta_{\alpha\gamma}$; $n_\alpha = n_\beta \delta_{\alpha\beta}$ and $n_\gamma = n_\beta \delta_{\beta\gamma}$, and for $N^{linear}_{\alpha\beta}$ in equation (2.19), and the Green's identity, the equation

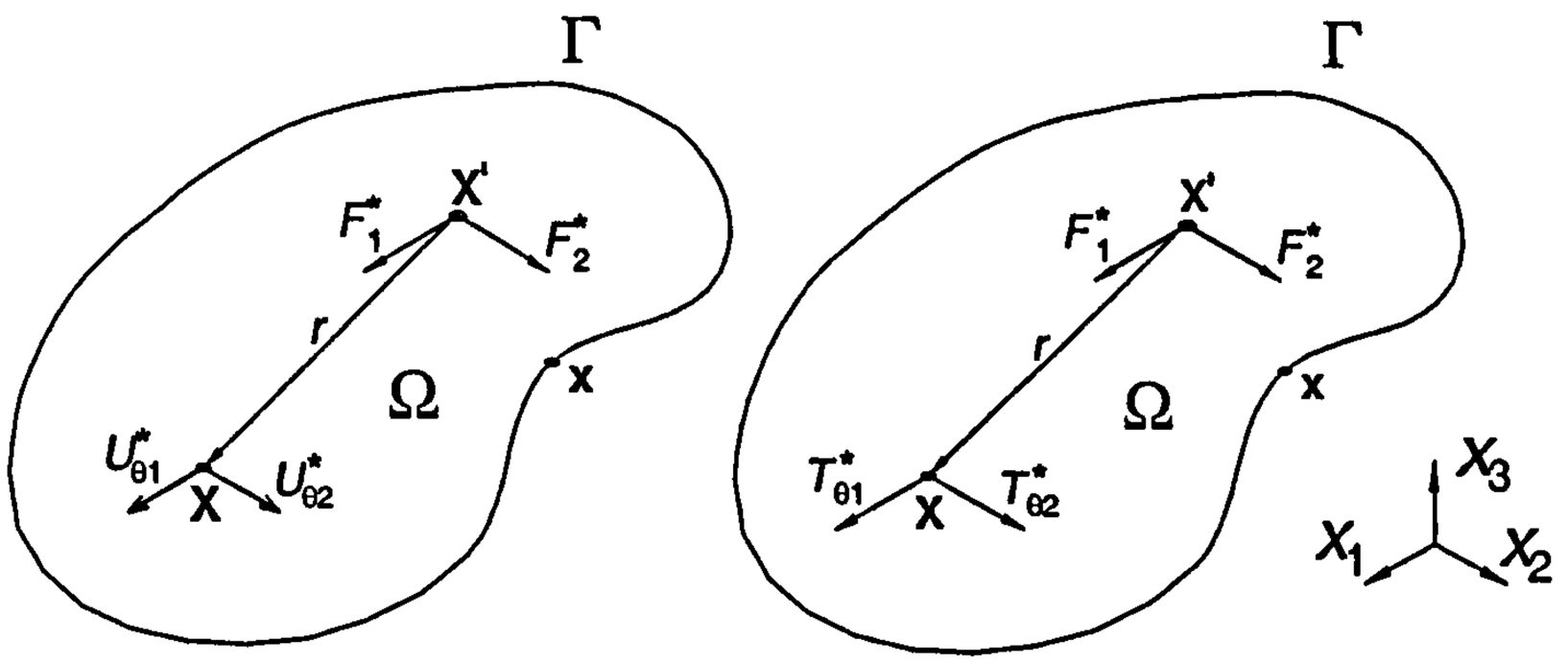

Figure 3-2: Fundamental state due to membrane stresses.

(3.26) can be written as

$$\int_\Gamma t_\alpha^{linear} U_\alpha^* d\Gamma - \int_\Gamma u_\alpha T_\alpha^* d\Gamma + \int_\Omega u_\alpha N_{\alpha\beta,\beta}^* d\Omega = 0 \tag{3.27}$$

The $(\cdot)^*$ state (as shown in Figure 3-2) are defined for concentrated generalised loads: two concentrated membrane forces ($\theta = 1, 2$) at an arbitrary point $\mathbf{X}' \in \Omega$. Thus, equation (3.27) can be rewritten after introducing the direction of the load θ as follows:

$$\int_\Gamma U_{\theta\alpha}^* (\mathbf{X}', \mathbf{x})\, t_\alpha^{linear} (\mathbf{x})\, d\Gamma (\mathbf{x}) - \int_\Gamma T_{\theta\alpha}^* (\mathbf{X}', \mathbf{x})\, u_\alpha (\mathbf{x})\, d\Gamma (\mathbf{x})$$

$$+ \int_\Omega N_{\theta\alpha\beta,\beta}^* (\mathbf{X}', \mathbf{X})\, u_\alpha (\mathbf{x})\, d\Omega (\mathbf{X}) = 0 \tag{3.28}$$

By choosing the $(\cdot)^*$ state to represent the fundamental state such as:

$$N_{\theta\alpha\beta,\beta}^* (\mathbf{X}', \mathbf{X}) + \delta(\mathbf{X}', \mathbf{X}) \delta_{\theta\alpha} = 0 \tag{3.29}$$

and making use of the Dirac delta property (3.22), equation (3.28) can be written for an internal source point $\mathbf{X}'$ as:

$$u_\theta (\mathbf{X}') + \int_\Gamma T_{\theta\alpha}^* (\mathbf{X}', \mathbf{x})\, u_\alpha (\mathbf{x})\, d\Gamma (\mathbf{x})$$

$$= \int_\Gamma U_{\theta\alpha}^* (\mathbf{X}', \mathbf{x})\, t_\alpha^{linear} (\mathbf{x})\, d\Gamma (\mathbf{x}) \tag{3.30}$$

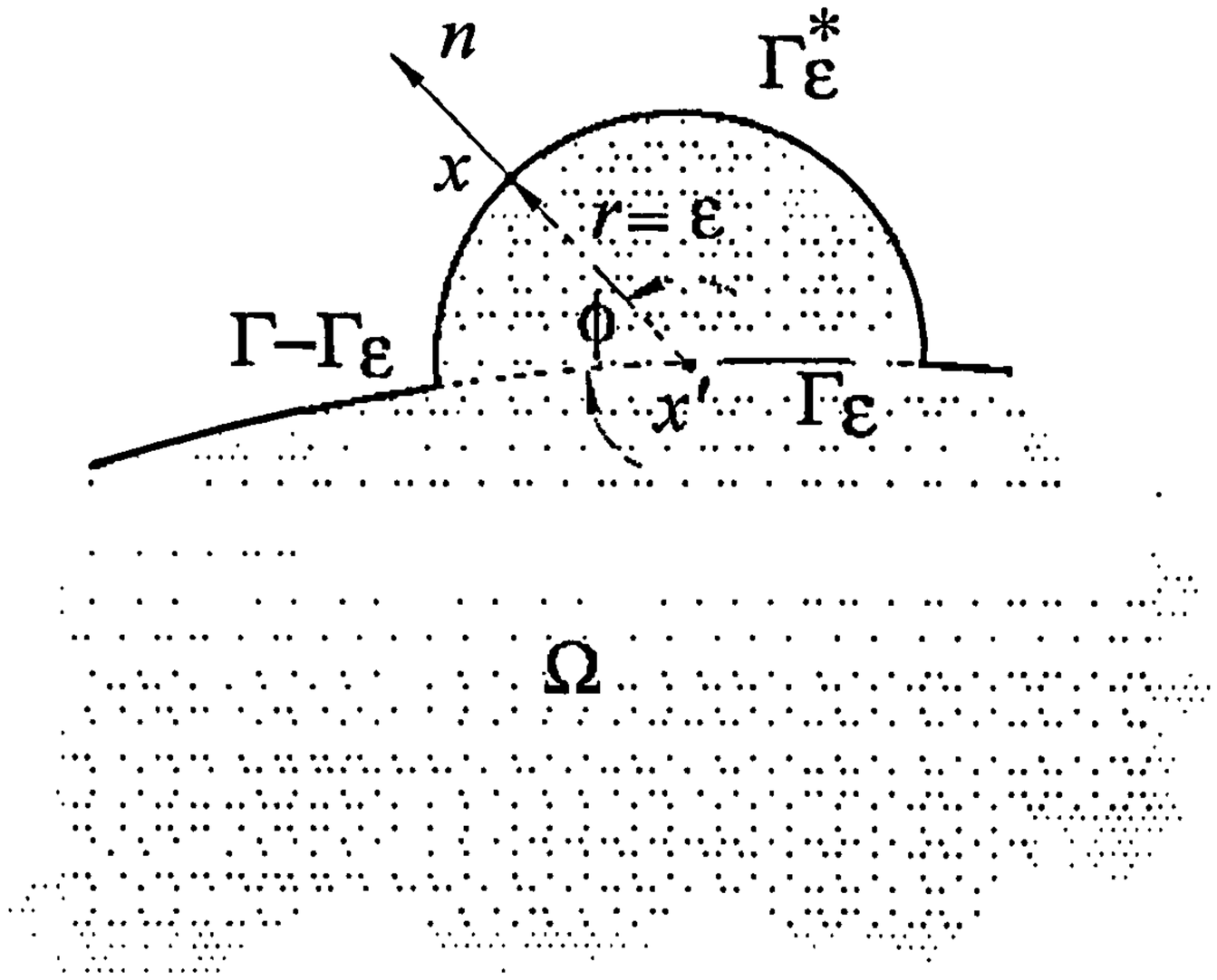

Figure 3-3: Semi-circular region around the source point x' on the boundary.

where $U^*_{\theta\alpha}(\mathbf{X}',\mathbf{x})$ and $T^*_{\theta\alpha}(\mathbf{X}',\mathbf{x})$ are the fundamental solutions for in-plane displacements and membrane tractions respectively. It represents displacements or tractions at the field point $\mathbf{x}$ or $\mathbf{X}$ in the direction α due to unit load applied at the source point $\mathbf{X}'$ in the direction θ. The Kelvin fundamental solutions $U^*_{\theta\alpha}$ and $T^*_{\theta\alpha}$ are given in Appendix A.

3.3 Boundary Integral Equations

If the point $\mathbf{X}'$ is taken to the boundary, that is $\mathbf{X}' \rightarrow \mathbf{x}' \in \Gamma$, the distance r tends to zero and, in the limit, the fundamental solutions will contain singularities. In analysing the limit, a semi-circular domain with boundary Γ^*_ε and radius ε centered at the source point $\mathbf{x}'$ is introduced, as shown in Figure 3-3.

Equation (3.23) can be written as follows :

$$w_i(\mathbf{x}')+\lim_{\varepsilon\to 0}\int_{\Gamma-\Gamma_\varepsilon+\Gamma^*_\varepsilon} P^*_{ij}(\mathbf{x}',\mathbf{x})w_j(\mathbf{x})\,d\Gamma(\mathbf{x}) = \lim_{\varepsilon\to 0}\int_{\Gamma-\Gamma_\varepsilon+\Gamma^*_\varepsilon} W^*_{ij}(\mathbf{x}',\mathbf{x})p^{linear}_j(\mathbf{x})\,d\Gamma(\mathbf{x})$$

$$+\int_\Omega W^*_{i3}(\mathbf{X}',\mathbf{X})q(\mathbf{X})d\Omega(\mathbf{X}) \qquad (3.31)$$

and equation (3.30) can be written as

$$u_\theta(\mathbf{x}') + \lim_{\varepsilon\to 0}\int_{\Gamma-\Gamma_\varepsilon+\Gamma_\varepsilon^*} T^*_{\theta\alpha}(\mathbf{x}',\mathbf{x})\,u_\alpha(\mathbf{x})\,d\Gamma(\mathbf{x})$$

$$= \lim_{\varepsilon\to 0}\int_{\Gamma-\Gamma_\varepsilon+\Gamma_\varepsilon^*} U^*_{\theta\alpha}(\mathbf{x}',\mathbf{x})\,t_\alpha^{linear}(\mathbf{x})\,d\Gamma(\mathbf{x}) \tag{3.32}$$

Taking into account all the limits and the jump terms, the boundary integral equations are obtained as follows:

$$c_{ij}(\mathbf{x}')w_j(\mathbf{x}') + \int_\Gamma \quad P^*_{ij}(\mathbf{x}',\mathbf{x})w_j(\mathbf{x})\,d\Gamma(\mathbf{x}) = \int_\Gamma W^*_{ij}(\mathbf{x}',\mathbf{x})p_j^{linear}(\mathbf{x})\,d\Gamma(\mathbf{x})$$

$$+\int_\Omega W^*_{i3}(\mathbf{x}',\mathbf{X})q(\mathbf{X})d\Omega(\mathbf{X}) \tag{3.33}$$

and

$$c_{\theta\alpha}(\mathbf{x}')\,u_\alpha(\mathbf{x}') + \int_\Gamma T^*_{\theta\alpha}(\mathbf{x}',\mathbf{x})u_\alpha(\mathbf{x})d\Gamma(\mathbf{x})$$

$$= \int_\Gamma U^*_{\theta\alpha}(\mathbf{x}',\mathbf{x})t_\alpha^{linear}(\mathbf{x})d\Gamma(\mathbf{x}) \tag{3.34}$$

where $\mathbf{x}', \mathbf{x} \in \Gamma$ are source and field points respectively, $c_{ij}(\mathbf{x}')$ and $c_{\theta\alpha}(\mathbf{x}')$ are the jump terms. The value of $c_{ij}(\mathbf{x}')$ and $c_{\theta\alpha}(\mathbf{x}')$ are equal to $\frac{1}{2}\delta_{ij}$ and $\frac{1}{2}\delta_{\theta\alpha}$ respectively when $\mathbf{x}'$ is located on a smooth boundary.

Equations (3.33 – 3.34) represent five boundary integral equations, the first two in (3.33) ($i = \alpha = 1,2$) are for rotations, the third ($i = 3$) is for the out-of-plane displacement and two in (3.34) ($\alpha = 1,2$) for in-plane displacements.

By applying the divergence theorem, the last domain integral in (3.33) can be transferred to boundary integral, in the case of a uniform load (q = constant) to give:

$$\int_\Omega W^*_{i3}(\mathbf{x}',\mathbf{X})q(\mathbf{X})d\Omega(\mathbf{X}) = q\int_\Gamma V^*_{i,\alpha}(\mathbf{x}',\mathbf{x})n_\alpha(\mathbf{x})d\Gamma(\mathbf{x}) \tag{3.35}$$

where V_i^* are the particular solutions of the equation $V^*_{i,\theta\theta} = W^*_{i3}$. The expressions for $V^*_{i,\beta}$ are:

$$\begin{aligned} V^*_{\alpha,\beta} &= \frac{r^2}{128\pi D}[(4\ln z - 5)\delta_{\alpha\beta} + 2(4\ln z - 3)r_{,\alpha}r_{,\beta}] \\ V^*_{3,\beta} &= \frac{-rr_{,\beta}}{128\pi D(1-\nu)\lambda^2}[32(2\ln z - 1) - z^2(1-\nu)(4\ln z - 5)] \end{aligned} \tag{3.36}$$

If q is not uniform, then this term cannot be taken out of the integral. The transformation of domain integrals for other distribution cases of q can be carried out by using the dual reciprocity technique, as explained in section 3.5.

3.4 Numerical Implementation

3.4.1 Discretisation

The geometry and the function along the boundary is discretised using quadratic isoparametric boundary elements, while for the domain, constant cell elements are used. To avoid difficulties with discontinuity of the tractions at corners, semi-discontinuous elements are used. Shape functions for continuous and semi-discontinuous elements are illustrated as in Figure 3-4.

Assuming that q is uniform, equation (3.23) can be rewritten in a discretised forms as:

$$c_{ij}(\mathbf{x}')w_j(\mathbf{x}') + \sum_{n=1}^{N_e}\sum_{m=1}^{3} w_j^{nm}\int_{\xi=-1}^{\xi=+1} P_{ij}^*(\mathbf{x}',\mathbf{x})\Phi^m(\xi)J_n(\xi)d\xi$$

$$= \sum_{n=1}^{N_e}\sum_{m=1}^{3} p_j^{nm\ linear}\int_{\xi=-1}^{\xi=+1} W_{ij}^*(\mathbf{x}',\mathbf{x})\Phi^m(\xi)J_n(\xi)d\xi$$

$$+q\sum_{n=1}^{N_e}\int_{\xi=-1}^{\xi=+1} V_{i,\alpha}^*(\mathbf{x}',\mathbf{x})n_\alpha(\xi)J_n(\xi)d\xi \qquad (3.37)$$

and equation (3.30) can be written as

$$c_{\theta\alpha}(\mathbf{x}')\,u_\alpha(\mathbf{x}') + \sum_{n=1}^{N_e}\sum_{m=1}^{3} u_\alpha^{nm}\int_{\xi=-1}^{\xi=+1} T_{\theta\alpha}^*(\mathbf{x}',\mathbf{x})\Phi^m(\xi)J_n(\xi)d\xi$$

$$= \sum_{n=1}^{N_e}\sum_{m=1}^{3} t_\alpha^{nm\ linear}\int_{\xi=-1}^{\xi=+1} U_{\theta\alpha}^*(\mathbf{x}',\mathbf{x})\Phi^m(\xi)J_n(\xi)d\xi \qquad (3.38)$$

where N_e is a number of boundary elements, Φ^m are the quadratic shape functions. For a continuous quadratic element, they are defined as:

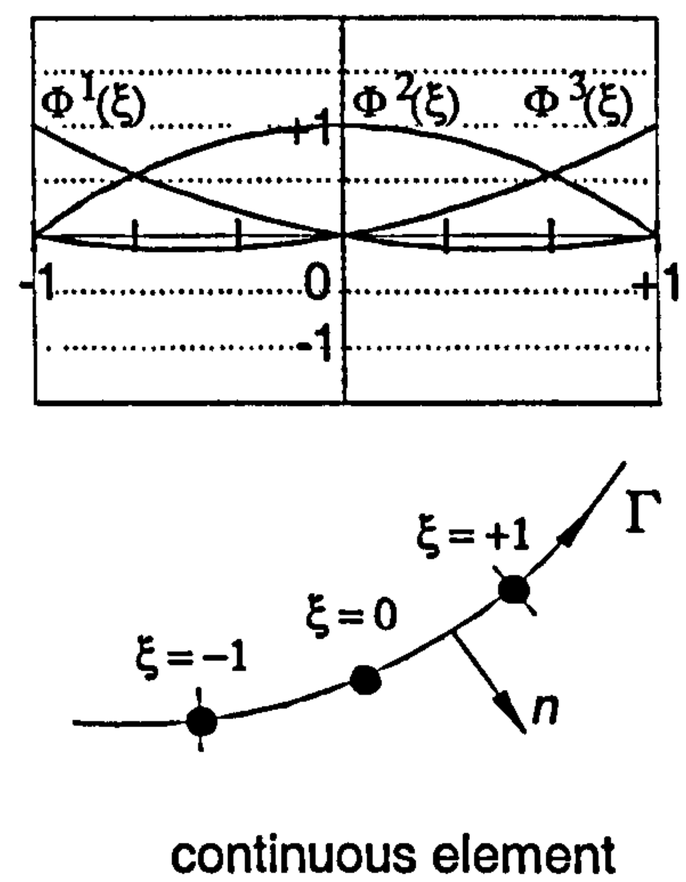

continuous element

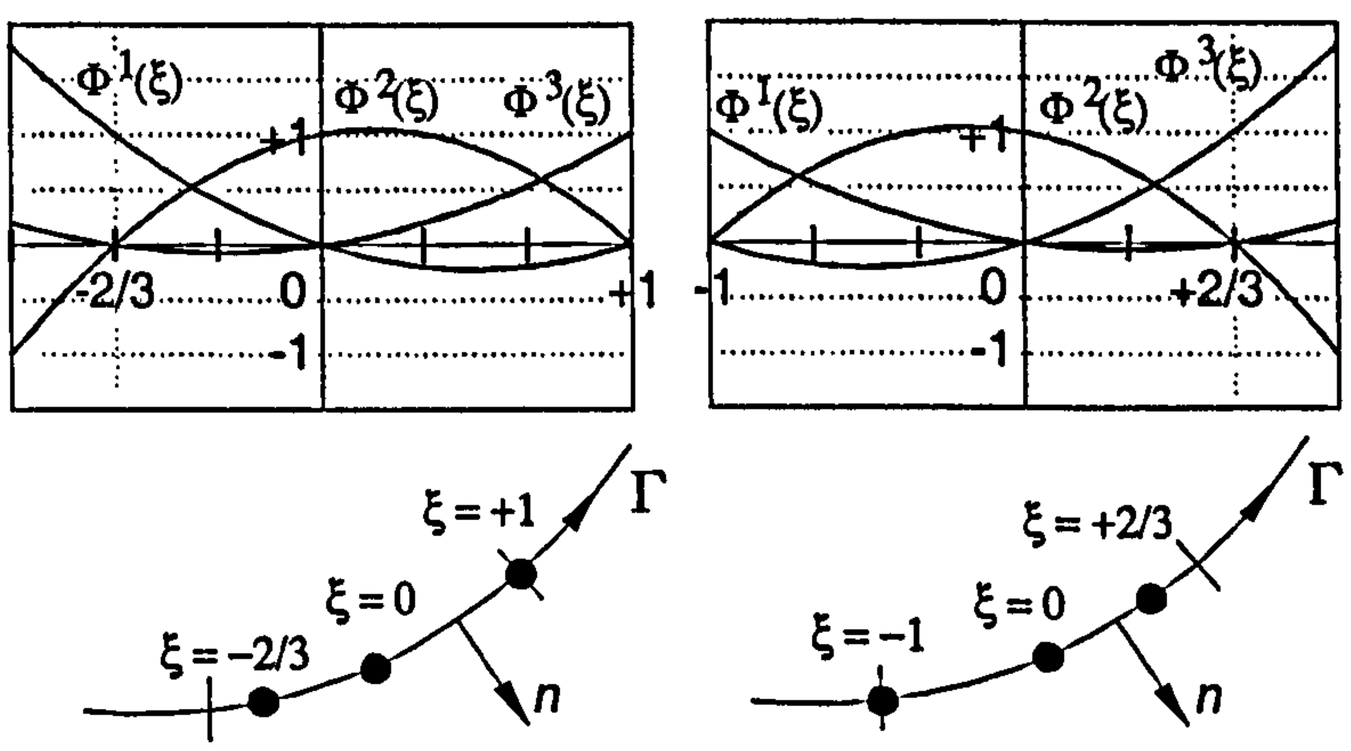

semi-discontinuous element

Figure 3-4: Shape functions for continuous and semi-discontinuous elements.

$$\begin{aligned} \Phi_C^1(\xi) &= \frac{1}{2}\xi(\xi-1) \\ \Phi_C^2(\xi) &= (1-\xi)(1+\xi) \\ \Phi_C^3(\xi) &= \frac{1}{2}\xi(\xi+1) \end{aligned} \tag{3.39}$$

and for a semi-discontinuous element, with nodes placed at $\xi = -\frac{2}{3}, 0, +1$, as:

$$\Phi_{S1}^1(\xi) = \frac{9}{10}\xi(\xi-1)$$

$$\begin{aligned} \Phi^2_{S1}(\xi) &= -\frac{3}{2}(\xi-1)(\xi+\frac{2}{3}) \\ \Phi^3_{S1}(\xi) &= \frac{6}{10}\xi(\xi+\frac{2}{3}) \end{aligned} \tag{3.40}$$

and for an element with nodes are placed at $\xi = -1, 0, +\frac{2}{3}$, as:

$$\begin{aligned} \Phi^1_{S3}(\xi) &= \frac{6}{10}\xi(\xi-\frac{2}{3}) \\ \Phi^2_{S3}(\xi) &= -\frac{3}{2}(\xi+1)(\xi-\frac{2}{3}) \\ \Phi^3_{S3}(\xi) &= \frac{9}{10}\xi(\xi+1) \end{aligned} \tag{3.41}$$

The internal node position in semi-discontinuous element is chosen arbitrarily at $-\frac{2}{3}$ or $+\frac{2}{3}$, not very close to the element end point to avoid near singularity problems.

The Jacobian of transformation for boundary elements is defined as:

$$J_n(\xi) = \sqrt{\frac{\partial x_\theta(\xi)}{\partial \xi}\frac{\partial x_\theta(\xi)}{\partial \xi}} \tag{3.42}$$

where $\frac{\partial x_\theta(\xi)}{\partial \xi}$ is the derivative of the global coordinates x_θ with respect to the local coordinate ξ, and the normal as:

$$n_\alpha(\xi) = \frac{1}{J(\xi)}\frac{\partial x_\beta(\xi)}{\partial \xi}\omega_{\alpha\beta 3} \tag{3.43}$$

where $\omega_{\alpha\beta 3}$ is the permutation tensor and is defined by the following set of rules:

$\omega_{\alpha\beta 3} = +1$, if $\alpha, \beta, 3$ is a clockwise cyclic sequence

$\omega_{\alpha\beta 3} = 0$, if $\alpha, \beta, 3$ is an acyclic sequence

$\omega_{\alpha\beta 3} = -1$, if $\alpha, \beta, 3$ is an anti clockwise cyclic sequence

For every collocation node, equations (3.37 – 3.38) will give the following linear system of equation in a matrix form:

$$\begin{bmatrix} \mathbf{H}^p & \mathbf{0} \\ \mathbf{0} & \mathbf{H}^s \end{bmatrix}_{5\times5} \begin{Bmatrix} \mathbf{w} \\ \mathbf{u} \end{Bmatrix}_{5\times1} = \begin{bmatrix} \mathbf{G}^p & \mathbf{0} \\ \mathbf{0} & \mathbf{G}^s \end{bmatrix}_{5\times5} \begin{Bmatrix} \mathbf{p} \\ \mathbf{t} \end{Bmatrix}_{5\times1} + \begin{Bmatrix} \mathbf{b} \\ \mathbf{0} \end{Bmatrix}_{5\times1} \tag{3.44}$$

where $\mathbf{w} = \{w_1, w_2, w_3\}^\intercal$, $\mathbf{u} = \{u_1, u_2\}^\intercal$, $\mathbf{p} = \{p_1, p_2, p_3\}^\intercal$, and $\mathbf{t} = \{t_1, t_2\}^\intercal$ are displacement and traction vectors for plate bending and plane stress formulations

respectively, $\mathbf{b} = \{0, 0, q\}^{\intercal}$ is domain load vectors, $\mathbf{H}^p$, $\mathbf{H}^s$, $\mathbf{G}^p$ and $\mathbf{G}^s$ are boundary element influence matrices for plate bending and plane stress formulations respectively. The matrices $\mathbf{H}^p$, $\mathbf{H}^s$, $\mathbf{G}^p$ and $\mathbf{G}^s$ then form plate bending influence matrices. After performing all of the collocation process, equations (3.37 – 3.38) can be written as

$$\begin{aligned} & [H]_{5Nbn \times 5Nbn} \{w\}_{5Nbn \times 1} \\ = \; & [G]_{5Nbn \times 15Nbe} \{p\}_{15Nbe \times 1} + \{Q\}_{5Nbn \times 1} \end{aligned} \tag{3.45}$$

where $[H]$ and $[G]$ are the well-known boundary element influence matrices [21], $\{w\}$ and $\{u\}$ are the boundary displacement vectors, $\{p\}$ and $\{t\}$ are the boundary traction vectors, and $\{Q\}$ is the domain load vector. Nbn and Nbe are number of boundary nodes and boundary elements respectively.

After imposing boundary conditions, equation (3.45) can be written as:

$$[A]_{5Nbn \times 5Nbn} \{x\}_{5Nbn} = \{f\}_{5Nbn} \tag{3.46}$$

where $[A]$ is the system matrix, $\{x\}$ is the unknown vector and $\{f\}$ is the vector of prescribed boundary values.

3.4.2 Treatment of singularities

Several different orders of singularities in integrands appear in the boundary integral equations. These singular integrals are treated separately based on their order of singularity. The standard Gauss quadrature formulae is used to evaluate numerically all of the regular integrals. The influence matrix $[G]$ and the load vector matrix $\{Q\}$ contain weakly singular integrals, which are treated using a nonlinear coordinate transformation as in Telles [87]. However, for better numerical accuracy, as was shown by Okada *et al.* [59], a suitable number of element sub divisions must be used with the non-linear transformation. In this thesis four element sub divisions are used.

Strongly singular integrals in the influence matrix $[H]$ are computed indirectly by considering the generalised rigid body movements. This can be achieved as follows:

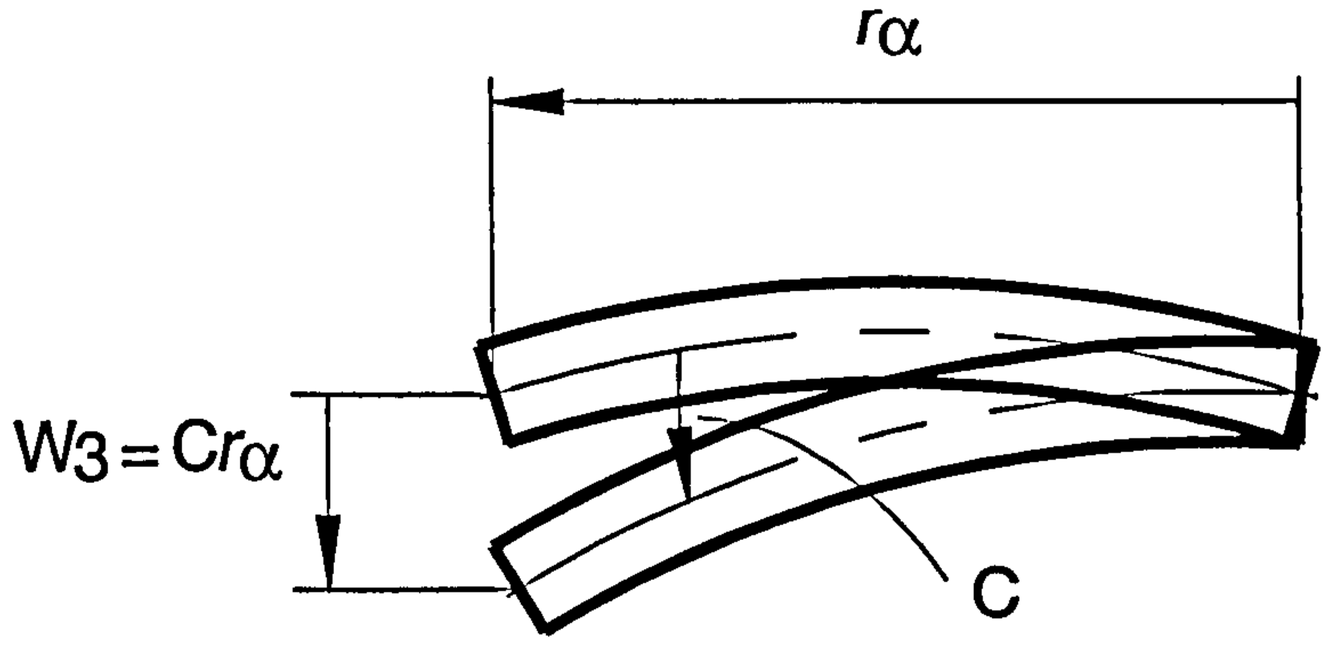

Figure 3-5: Rigid body rotations.

If a traction-free problem is considered, five independent cases may be observed, that is, two rigid body rotations:

- $u_1 = 0$, $u_2 = 0$, $w_1 = C$ and $w_2 = 0$, then $w_3 = -Cr_1$,
- $u_1 = 0$, $u_2 = 0$, $w_2 = C$ and $w_1 = 0$, then $w_3 = -Cr_2$

as shown in Figure 3-5 and a rigid body out-of-plane translation:

- $u_1 = 0$, $u_2 = 0$, $w_3 = C$, $w_1 = 0$, and $w_2 = 0$

for the rotations and out-of-plane displacement integral equations, and two rigid body conditions for in-plane translations

- $u_1 = C$, $u_2 = 0$, $w_1 = 0$, $w_2 = 0$, and $w_3 = 0$
- $u_2 = C$, $u_1 = 0$, $w_1 = 0$, $w_2 = 0$, and $w_3 = 0$

for the in-plane displacements integral equations. The term C is an arbitrary constant, and r_α denotes components of vector r in x_α coordinates.

By applying the above cases to the system of equations in (3.45), the following expressions can be written:

$$\begin{aligned} H^{i\alpha}(\mathbf{x}') &= -\int_\Gamma [P^*_{i\alpha}(\mathbf{x}',\mathbf{x}) + (-r_\alpha) P^*_{i3}(\mathbf{x}',\mathbf{x})] d\Gamma(\mathbf{x}) \\ H^{i3}(\mathbf{x}') &= -\int_\Gamma P^*_{i3}(\mathbf{x}',\mathbf{x}) d\Gamma(\mathbf{x}) \\ H^{(3+\theta)(3+\alpha)}(\mathbf{x}') &= -\int_\Gamma T^*_{\theta\alpha}(\mathbf{x}',\mathbf{x}) d\Gamma(\mathbf{x}) \end{aligned} \tag{3.47}$$

where $H^{i\alpha}(\mathbf{x}')$, $H^{i3}(\mathbf{x}')$ and $H^{(3+\theta)(3+\alpha)}(\mathbf{x}')$ include the diagonal sub-matrix and the jump term c_{ij} in the influence matrix $[H]$. All terms in the integrals in equation (3.47) were already computed except the second term in the first integral. Fortunately, in the second term of the first integral, the distance r_α cancels the weak singularity in $P^*_{\alpha 3}$ and the strong singularity in P^*_{33} in the singular element under consideration.

3.5 Transformation of Domain Integrals

The domain integrals which appear in the boundary integral equations derived in sections 3.2 and 3.3 can be transformed to boundary integrals with the use of the dual reciprocity technique [61]. Recently Wen, Aliabadi and Young [97] used the formulations developed by Dirgantara and Aliabadi [27] and transformed the domain integrals into boundary integrals. The plate can be discretised into quadratic isoparametric boundary elements.

The integral equations (3.23) and (3.33) can be recalled as follows :

$$w_i(\mathbf{X}') + \int_\Gamma P^*_{ij}(\mathbf{X}', \mathbf{x}) w_j(\mathbf{x})\, d\Gamma(\mathbf{x}) = \int_\Gamma W^*_{ij}(\mathbf{X}', \mathbf{x}) p_j^{linear}(\mathbf{x})\, d\Gamma(\mathbf{x})$$

$$+ \int_\Omega W^*_{i3}(\mathbf{X}', \mathbf{X}) q(\mathbf{X}) d\Omega(\mathbf{X}) \tag{3.48}$$

and

$$c_{ij}(\mathbf{x}') w_j(\mathbf{x}') + \int_\Gamma P^*_{ij}(\mathbf{x}', \mathbf{x}) w_j(\mathbf{x})\, d\Gamma(\mathbf{x}) = \int_\Gamma W^*_{ij}(\mathbf{x}', \mathbf{x}) p_j^{linear}(\mathbf{x})\, d\Gamma(\mathbf{x})$$

$$+ \int_\Omega W^*_{i3}(\mathbf{x}', \mathbf{X}) q(\mathbf{X}) d\Omega(\mathbf{X}) \tag{3.49}$$

The equations (3.48) and (3.49) contain a domain integral as follows:

$$I^D = \int_\Omega W^*_{i3} q\, d\Omega, \tag{3.50}$$

Assume that the term q are the body forces, therefore it can be approximated by

$$q = \sum_{m=1}^{M} f^m(r)\phi^m \tag{3.51}$$

where $f(r)$ is a radial basis function, see Appendix B, the ϕ_j^m are a set of unknown coefficients, $r = \sqrt{(x_1 - x_1^m)^2 + (x_2 - x_2^m)^2}$, M is the total number of the selected points.

The ϕ_j^m are coefficients which are determined by values at the selected points M as follows

$$\phi = \mathbf{F}^{-1} q \tag{3.52}$$

where F matrix is obtained by collocation of the selected points M.

From the particular solutions $\hat{w}_{mj}$, which satisfy the differential equation, i.e.

$$L_{\alpha j}\hat{w}_{mj} = 0 \tag{3.53}$$

and

$$L_{3j}\hat{w}_{mj} = F_m(r) \tag{3.54}$$

where L_{ij} is the Navier differential operator for shear deformable plate bending problems, see section 3.2.

Then, equation (3.50) can be transformed to be:

$$I^D = \sum_{m=1}^{M} \left[c_{ik}(\mathbf{x}')\hat{w}_{mk}^3(\mathbf{x}') - \int_\Gamma W_{ik}^*(\mathbf{x}', \mathbf{x})\hat{p}_{mk}^3(\mathbf{x})\, d\Gamma(\mathbf{x}) \right.$$

$$\left. + \int_\Gamma P_{ik}^*(\mathbf{x}', \mathbf{x})\hat{w}_{mk}^3(\mathbf{x})\, d\Gamma(\mathbf{x}) \right] (\mathbf{F}^{-1} q)_m \tag{3.55}$$

where the particular solution $\hat{w}_{mk}^3$ and $\hat{p}_{mk}^3$ for radial basis function $F_m(r) = 1 + r$ were derived in [97] and are given in the Appendix B.

3.6 Internal Stress Resultants

The stress resultants at domain point X' can be evaluated from equations (3.23) and (3.50) by using relationships in equations (2.20) and (2.21), obtained as:

$$M_{\alpha\beta}\left(\mathrm{X}'\right) = \int_{\Gamma} W^{*}_{\alpha\beta k}(\mathrm{X}',\mathrm{x}) p_k^{linear}(\mathrm{x}) d\Gamma(\mathrm{x}) - \int_{\Gamma} P^{*}_{\alpha\beta k}(\mathrm{X}',\mathrm{x}) w_k(\mathrm{x}) d\Gamma(\mathrm{x})$$

$$+ \int_{\Omega} W^{*}_{\alpha\beta 3}(\mathrm{X}',\mathrm{X}) q d\Omega(\mathrm{X}) \; ; \tag{3.56}$$

$$Q_{\beta}\left(\mathrm{X}'\right) = \int_{\Gamma} W^{*}_{3\beta k}(\mathrm{X}',\mathrm{x}) p_k^{linear}(\mathrm{x}) d\Gamma(\mathrm{x}) - \int_{\Gamma} P^{*}_{3\beta k}(\mathrm{X}',\mathrm{x}) w_k(\mathrm{x}) d\Gamma(\mathrm{x})$$

$$+ \int_{\Omega} W^{*}_{3\beta 3}(\mathrm{X}',\mathrm{X}) q d\Omega(\mathrm{X}) \tag{3.57}$$

and

$$N_{\alpha\beta}\left(\mathrm{X}'\right) = \int_{\Gamma} U^{*}_{\alpha\beta\gamma}(\mathrm{X}',\mathrm{x}) t_{\gamma}^{linear}(\mathrm{x}) d\Gamma(\mathrm{x}) - \int_{\Gamma} T^{*}_{\alpha\beta\gamma}(\mathrm{X}',\mathrm{x}) u_{\gamma}(\mathrm{x}) d\Gamma(\mathrm{x}) \tag{3.58}$$

In the case of a uniform load, the domain integral $\int_{\Omega} W^{*}_{i\beta 3}(\mathrm{X}',\mathrm{X}) q(\mathrm{X}) d\Omega(\mathrm{X})$ in (3.56 − 3.57) can be transferred to boundary integral, by applying the divergence theorem, to give:

$$\int_{\Omega} W^{*}_{i\beta 3}(\mathrm{X}',\mathrm{X}) q(\mathrm{X}) d\Omega(\mathrm{X}) = q \int_{\Gamma} Q^{*}_{i\beta}(\mathrm{X}',\mathrm{x}) d\Gamma(\mathrm{x}) \tag{3.59}$$

The kernels $W^{*}_{i\beta k}$, $P^{*}_{i\beta k}$ and $Q^{*}_{i\beta}$ are linear combinations of the first derivatives of W^{*}_{ij}, P^{*}_{ij} and $V^{*}_{i,\beta}$ where the kernels $U^{*}_{\alpha\beta\gamma}$ and $T^{*}_{\alpha\beta\gamma}$ are linear combinations of the first derivatives of $U^{*}_{\alpha\beta}$ and $T^{*}_{\alpha\beta}$. The kernels W^{*}_{ijk}, P^{*}_{ijk}, $Q^{*}_{i\beta}$, $U^{*}_{\alpha\beta\gamma}$ and $T^{*}_{\alpha\beta\gamma}$ are given in Appendix A

3.7 Traction Integral Equations

The traction integral equations are obtained by taking X' to the boundary leading to hypersingular integral representation of the shear deformable plate bending problems. The integrals in (3.56 - 3.58) can now be written as

$$\frac{1}{2}M_{\alpha\beta}(\mathbf{x}') = \int_\Gamma W^*_{\alpha\beta k}(\mathbf{x}',\mathbf{x})p_k^{linear}(\mathbf{x})d\Gamma(\mathbf{x}) - \int_\Gamma P^*_{\alpha\beta k}(\mathbf{x}',\mathbf{x})w_k(\mathbf{x})d\Gamma(\mathbf{x}) + \int_\Omega W^*_{\alpha\beta 3}(\mathbf{x}',\mathbf{X})qd\Omega(\mathbf{X}) \tag{3.60}$$

$$\frac{1}{2}Q_\beta(\mathbf{x}') = \int_\Gamma W^*_{3\beta k}(\mathbf{x}',\mathbf{x})p_k^{linear}(\mathbf{x})d\Gamma(\mathbf{x}) - \int_\Gamma P^*_{3\beta k}(\mathbf{x}',\mathbf{x})w_k(\mathbf{x})d\Gamma(\mathbf{x}) + \int_\Omega W^*_{3\beta 3}(\mathbf{x}',\mathbf{X})qd\Omega(\mathbf{X}) \tag{3.61}$$

and the integrals in equation (3.24) become hypersingular integral representations of the two-dimensional plane stress elasticity problems,

$$\frac{1}{2}N_{\alpha\beta}(\mathbf{x}') + \int_\Gamma T^*_{\alpha\beta\gamma}(\mathbf{x}',\mathbf{x})u_\gamma(\mathbf{x})d\Gamma(\mathbf{x}) = \int_\Gamma U^*_{\alpha\beta\gamma}(\mathbf{x}',\mathbf{x})t_\gamma(\mathbf{x})d\Gamma(\mathbf{x}) \tag{3.62}$$

The traction integral equations correspond to the integral equations in (3.60 – 3.62) are

$$\frac{1}{2}p_\alpha^{linear}(\mathbf{x}') + n_\beta(\mathbf{x}')\int_\Gamma P^*_{\alpha\beta\gamma}(\mathbf{x}',\mathbf{x})w_\gamma(\mathbf{x})d\Gamma(\mathbf{x}) + n_\beta(\mathbf{x}')\int_\Gamma P^*_{\alpha\beta 3}(\mathbf{x}',\mathbf{x})w_3(\mathbf{x})d\Gamma(\mathbf{x})$$

$$= n_\beta(\mathbf{x}')\int_\Gamma W^*_{\alpha\beta\gamma}(\mathbf{x}',\mathbf{x})p_\gamma^{linear}(\mathbf{x})d\Gamma(\mathbf{x}) + n_\beta(\mathbf{x}')\int_\Gamma W^*_{\alpha\beta 3}(\mathbf{x}',\mathbf{x})p_3^{linear}(\mathbf{x})d\Gamma(\mathbf{x})$$

$$+n_\beta(\mathbf{x}')\int_\Omega W^*_{\alpha\beta 3}(\mathbf{x}',\mathbf{X})qd\Omega(\mathbf{X}) \tag{3.63}$$

$$\frac{1}{2}p_3^{linear}(\mathbf{x}') + n_\beta(\mathbf{x}')\int_\Gamma P^*_{3\beta\gamma}(\mathbf{x}',\mathbf{x})u_\gamma(\mathbf{x})d\Gamma(\mathbf{x}) + n_\beta(\mathbf{x}')\int_\Gamma P^*_{3\beta 3}(\mathbf{x}',\mathbf{x})u_3(\mathbf{x})d\Gamma(\mathbf{x})$$

$$= n_\beta(\mathbf{x}')\int_\Gamma W^*_{3\beta\gamma}(\mathbf{x}',\mathbf{x})p_\gamma^{linear}(\mathbf{x})d\Gamma(\mathbf{x}) + n_\beta(\mathbf{x}')\int_\Gamma W^*_{3\beta 3}(\mathbf{x}',\mathbf{x})p_3^{linear}(\mathbf{x})d\Gamma(\mathbf{x})$$

$$+n_\beta(\mathbf{x}')\int_\Omega W^*_{3\beta 3}(\mathbf{x}',\mathbf{X})qd\Omega(\mathbf{X}) \tag{3.64}$$

and

$$\frac{1}{2}t_\alpha(\mathbf{x}') + n_\beta(\mathbf{x}')\int_\Gamma T^*_{\alpha\beta\gamma}(\mathbf{x}',\mathbf{x})u_\gamma(\mathbf{x})d\Gamma(\mathbf{x}) +$$

$$= n_\beta(\mathbf{x}')\int_\Gamma U^*_{\alpha\beta\gamma}(\mathbf{x}',\mathbf{x})t_\gamma^{linear}(\mathbf{x})d\Gamma(\mathbf{x}) \tag{3.65}$$

Equations (3.63 – 3.65) represent five integral equations in terms of boundary tractions, and can be used together with the five displacement integral equations (3.33 – 3.34) to form the dual boundary integral formulation. The treatment of singularities for the traction boundary integrals is described in Appendix C. Domain integrals which appear in the traction integral equations are transferred to the boundary by employing the dual reciprocity technique as described in sections 3.5.

3.8 Summary

Boundary element formulations for the linear elastic shear deformable plate bending and two dimensional plane stress were reviewed in this chapter. The singular integrals which appear in the formulation are treated individually based on the order of singularity. The weakly singular boundary integrals were treated using the non-linear coordinate transformation, while the strongly singular integrals were computed indirectly using generalised rigid body movement. The domain integrals due to the transverse loads q can be transferred to boundary integral, either of the case of uniform loads (q = constant) or distributed loads using the dual reciprocity technique. The traction integral equations of shear deformable plates bending and two-dimensional plane stress are used to form the dual boundary element formulation to analyse crack problems.

Chapter 4

Buckling of Elastic Plates

4.1 Introduction

Buckling analysis of compression panels are particularly important in aerospace structures. Phenomenon of the plate buckling has been investigated analytically and experimentally since the first experimental observation almost 150 years ago [93]. Analytical solutions of plate buckling based on the classical plate theory can be found in [90] and [23]. Numerical method such as the Finite Element Method (FEM) has been used by many researchers to investigate the problems [72][32][14]. Liu [54], applied the differential quadrature element method based on the Mindlin plate theory to the buckling analysis of discontinuous rectangular plates.

More recently, the boundary element method (BEM), has been applied to the field of plate buckling. Syngellakis and Elzein [82], extended the boundary element solution of the plate buckling based on Kirchhoff theory to accommodate any combination of loadings and support conditions. Nerantzaki and Katsidelakis [58], developed a BEM-based method for buckling of plates with variable thickness. Lin, Duffield and Shih [52], developed a more general boundary element formulation for wide variety of boundary conditions and arbitrary planar shapes to investigate the stability of elastic plate. Other works on elastic buckling analysis of plate using boundary element can also be found in [24][85].

In this chapter, the derivation of boundary integral equations for the buckling analysis of shear deformable plate are developed. Plate buckling equations are

written as a standard eigenvalue problem. The formulation is formed by coupling boundary element formulations of shear deformable plate and two dimensional plane stress elasticity. The domain integrals which appear in this formulation are treated in two different ways: initially the integrals are evaluated using constant cells, and next, they are transformed into equivalent boundary integrals using the dual reciprocity method (DRM). The eigenvalue problem of plate buckling yields a critical load factor and buckling modes. Examples with different geometry, loading and boundary conditions are presented to demonstrate the accuracy of the formulation.

4.2 Boundary Integral Equations

Here, the in-plane stress resultants in the domain due to external loads on the boundary is considered to be unknown. Therefore, determination of in-plane stress resultants in the domain is the first step in the solution of plate buckling. Next, the plate buckling equations are derived from the plate bending equations. Critical load factors are introduced into the equations as multiplication factors of body forces or transverse loads.

4.2.1 In-plane Stress Resultants

In the absence of body forces, the boundary integral representation of in-plane displacement is given by

$$C_{\theta\alpha}(\mathbf{x}')u_\alpha(\mathbf{x}') + \int_\Gamma T^*_{\theta\alpha}(\mathbf{x}',\mathbf{x})u_\alpha(\mathbf{x})d\Gamma(\mathbf{x}) = \int_\Gamma U^*_{\theta\alpha}(\mathbf{x}',\mathbf{x})t^{linear}_\alpha(\mathbf{x})d\Gamma(\mathbf{x}) \qquad (4.1)$$

where $C_{\theta\alpha}(\mathbf{x}')$ are jump terms. The value of $C_{\theta\alpha}(\mathbf{x}')$ is equal to $\frac{1}{2}\delta_{\theta\alpha}$ when $\mathbf{x}'$ is located on a smooth boundary.

The boundary integral of in-plane displacements in the domain can be expressed as

$$u_\alpha(\mathbf{X}') + \int_\Gamma T^*_{\theta\alpha}(\mathbf{X}',\mathbf{x})u_\alpha(\mathbf{x})d\Gamma(\mathbf{x}) = \int_\Gamma U^*_{\theta\alpha}(\mathbf{X}',\mathbf{x})t^{linear}_\alpha(\mathbf{x})d\Gamma(\mathbf{x}) \qquad (4.2)$$

The in-plane stress resultants at domain point X' are written as

$$N_{\alpha\beta}^{linear}(\mathrm{X}') = \int_{\Gamma} U_{\Delta\alpha\beta}^{*}(\mathrm{X}',\mathrm{x}) t_{\Delta}^{linear}(\mathrm{x}) d\Gamma(\mathrm{x}) - \int_{\Gamma} T_{\Delta\alpha\beta}^{*}(\mathrm{X}',\mathrm{x}) u_{\Delta}(\mathrm{x}) d\Gamma(\mathrm{x}) \quad (4.3)$$

The fundamental solutions $T_{\theta\alpha}^{*}$, $U_{\theta\alpha}^{*}$, $U_{\Delta\alpha\beta}^{*}$ and $T_{\Delta\alpha\beta}^{*}$ are the same as those described in the section 3.4 and are listed in Appendix A.

4.2.2 Plate Buckling Problem

The plate bending equation is transformed into an equivalent plate buckling formulation by introducing critical load factor λ as follows:

$$\begin{aligned} & C_{ij}(\mathrm{x}')w_i(\mathrm{x}') + \int_{\Gamma} P_{ij}^{*}(\mathrm{x}',\mathrm{x}) w_j(\mathrm{x}) d\Gamma(\mathrm{x}) \\ = & \int_{\Gamma} W_{ij}^{*}(\mathrm{x}',\mathrm{x}) p_j^{linear}(\mathrm{x}) d\Gamma(\mathrm{x}) + \lambda \int_{\Omega} W_{i3}^{*}(\mathrm{x}',\mathrm{X}) q(\mathrm{X}) d\Omega(X) \\ & + \lambda \int_{\Omega} W_{i3}^{*}(\mathrm{x}',\mathrm{X}) (N_{\alpha\beta}^{linear} w_{3,\beta})_{,\alpha}(\mathrm{X}) d\Omega(\mathrm{X}) \end{aligned} \quad (4.4)$$

where p_j^{linear} are described in equation (2.5). The terms $C_{ij}(\mathrm{x}')$ are equal to $\frac{1}{2}\delta_{ij}$ when x' is located on a smooth boundary.

Expanding the last integral in equation (4.4), gives:

$$\begin{aligned} & C_{ij}w_i(\mathrm{x}') + \int_{\Gamma} P_{ij}^{*}(\mathrm{x}',\mathrm{x}) w_j(\mathrm{x}) d\Gamma(\mathrm{x}) \\ = & \int_{\Gamma} W_{ij}^{*}(\mathrm{x}',\mathrm{x}) p_j^{linear}(\mathrm{x}) d\Gamma(\mathrm{x}) + \lambda \int_{\Omega} W_{i3}^{*}(\mathrm{x}',\mathrm{X}) q(\mathrm{X}) d\Omega(\mathrm{X}) \\ & + \lambda \int_{\Omega} W_{i3}^{*}(\mathrm{x}',\mathrm{X}) (N_{\alpha\beta,\alpha}^{linear} w_{3,\beta} + N_{\alpha\beta}^{linear} w_{3,\beta\alpha})(\mathrm{X}) d\Omega(\mathrm{X}) \end{aligned} \quad (4.5)$$

The deflection equation w_3 at the domain points X' is required as an additional equation to arrange an eigenvalue equation, as follows:

$$w_3(\mathrm{X}') = \int_{\Gamma} W_{3j}^{*}(\mathrm{X}',\mathrm{x}) p_j^{linear}(\mathrm{x}) d\Gamma(\mathrm{x}) - \int_{\Gamma} P_{3j}^{*}(\mathrm{X}',\mathrm{x}) w_j(\mathrm{x}) d\Gamma(\mathrm{x})$$

$$+\lambda \int_{\Omega} W^*_{33}(\mathbf{X}', \mathbf{X}) q(\mathbf{X}) d\Omega(\mathbf{X})$$
$$+\lambda \int_{\Omega} W^*_{33}(\mathbf{X}', \mathbf{X}) (N^{linear}_{\alpha\beta,\alpha} w_{3,\beta} + N^{linear}_{\alpha\beta} w_{3,\beta\alpha})(\mathbf{X}) d\Omega(\mathbf{X}) \quad (4.6)$$

To arrange an eigenvalue equation, the derivatives of $w_{3,\beta}(\mathbf{X})$ and $w_{3,\alpha\beta}(\mathbf{X})$ have to be expressed in terms of $w_3(\mathbf{X})$, see section 4.2.3.

Equation (4.5) can be written as

$$\begin{aligned} & C_{ij} w_i(\mathbf{x}') + \int_{\Gamma} P^*_{ij}(\mathbf{x}', \mathbf{x}) w_j(\mathbf{x}) d\Gamma(\mathbf{x}) \\ = & \int_{\Gamma} W^*_{ij}(\mathbf{x}', \mathbf{x}) p^{linear}_j(\mathbf{x}) d\Gamma(\mathbf{x}) \\ & +\lambda \int_{\Omega} W^*_{i3}(\mathbf{x}', \mathbf{X}) q(\mathbf{X}) d\Omega(\mathbf{X}) \\ & +\lambda \int_{\Omega} W^*_{i3}(\mathbf{x}', \mathbf{X}) (N^{linear}_{\alpha\beta,\alpha} \mathbf{f}(r)_{,\beta} \mathbf{F}^{-1} w_3)(\mathbf{X}) d\Omega(\mathbf{X}) \\ & +\lambda \int_{\Omega} W^*_{i3}(\mathbf{x}', \mathbf{X}) (N^{linear}_{\alpha\beta} \mathbf{f}(r)_{,\alpha} \mathbf{F}^{-1} \mathbf{f}(r)_{,\beta} \mathbf{F}^{-1} w_3)(\mathbf{X}) d\Omega(\mathbf{X}) \end{aligned} \quad (4.7)$$

The equation (4.6) can also be written as

$$\begin{aligned} w_3(\mathbf{X}') = & \int_{\Gamma} W^*_{3j}(\mathbf{X}', \mathbf{x}) p^{linear}_j(\mathbf{x}) d\Gamma(\mathbf{x}) \\ & - \int_{\Gamma} P^*_{3j}(\mathbf{X}', \mathbf{x}) w_j(\mathbf{x}) d\Gamma(\mathbf{x}) \\ & +\lambda \int_{\Omega} W^*_{33}(\mathbf{X}', X) q(\mathbf{X}) d\Omega(X) \\ & +\lambda \int_{\Omega} W^*_{33}(\mathbf{X}', \mathbf{X}) (N^{linear}_{\alpha\beta,\alpha} \mathbf{f}(r)_{,\beta} \mathbf{F}^{-1} w_3)(\mathbf{X}) d\Omega(\mathbf{X}) \\ & +\lambda \int_{\Omega} W^*_{33}(\mathbf{X}', \mathbf{X}) (N^{linear}_{\alpha\beta} \mathbf{f}(r)_{,\alpha} \mathbf{F}^{-1} \mathbf{f}(r)_{,\beta} \mathbf{F}^{-1} w_3)\ (\mathbf{X})\ d\Omega(\mathbf{X}) \end{aligned} \quad (4.8)$$

Equation (4.7) can be expressed as

$$\begin{aligned} & C_{ij} w_i(\mathbf{x}') + \int_{\Gamma} P^*_{ij}(\mathbf{x}', \mathbf{x}) w_j(\mathbf{x}) d\Gamma(\mathbf{x}) \\ = & \int_{\Gamma} W^*_{ij}(\mathbf{x}', \mathbf{x}) p^{linear}_j(\mathbf{x}) d\Gamma(\mathbf{x}) + \lambda \int_{\Omega} W^*_{i3}(\mathbf{x}', \mathbf{X}) f_b(\mathbf{X}) d\Omega(\mathbf{X}) \end{aligned} \quad (4.9)$$

where

$$f_b = q + N^{linear}_{\alpha\beta,\alpha}\mathbf{f}(r)_{,\beta}\mathbf{F}^{-1}\mathbf{w}_3 + N^{linear}_{\alpha\beta}\mathbf{f}(r)_{,\alpha}\mathbf{F}^{-1}\mathbf{f}(r)_{,\beta}\mathbf{F}^{-1}\mathbf{w}_3 \tag{4.10}$$

Thus, equation (4.8) can also be written as

$$\begin{aligned} w_3(\mathbf{X}') &= \int_\Gamma W^*_{3j}(\mathbf{X}',\mathbf{x})p^{linear}_j(\mathbf{x})d\Gamma(\mathbf{x}) \\ &\quad - \int_\Gamma P^*_{3j}(\mathbf{X}',\mathbf{x})w_j(\mathbf{x})d\Gamma(\mathbf{x}) \\ &\quad + \lambda\int_\Omega W^*_{33}(\mathbf{X}',\mathbf{X})f_b(\mathbf{X})d\Omega(\mathbf{X}) \end{aligned} \tag{4.11}$$

The kernel solutions P^*_{ij} and W^*_{ij} are the same those described in section 3.4.

4.2.3 Evaluation of the Derivative Terms

The $w_{3,\beta}(\mathbf{X})$ and $w_{3,\alpha\beta}(\mathbf{X})$ terms are approximated by a radial basis function $f(r)$ as follows;

$$w_3(x_1,x_2) = \sum_{m=1}^{M} f^m(r)\Psi^m \tag{4.12}$$

where the a radial basis function is chosen $f(r) = \sqrt{c^2 + r^2}$ and c^2 =2, and M is the total number of selected points.

$$r = \sqrt{(x_1 - x_1^m)^2 + (x_2 - x_2^m)^2} \tag{4.13}$$

The Ψ^m are coefficients which are determined by values at the selected points M as follows

$$\Psi = \mathbf{F}^{-1}\mathbf{w}_3 \tag{4.14}$$

Therefore, the first derivative of deflection $w_{3,\beta}$ is expressed as

$$w_{3,\beta}(x_1,x_2) = \mathbf{f}(r)_{,\beta}(\mathbf{F}^{-1}\mathbf{w}_3) \tag{4.15}$$

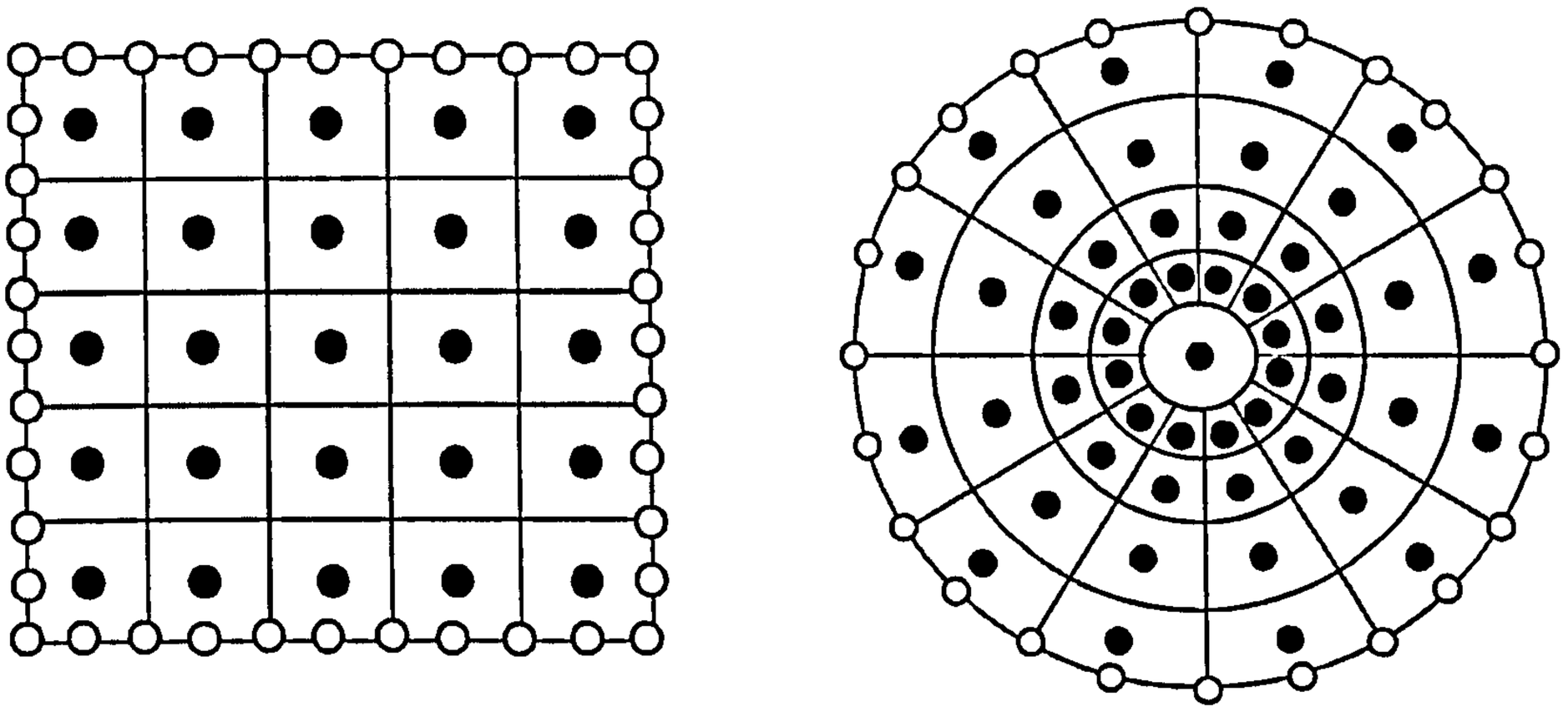

Figure 4-1: Models with cell elements.

The second derivative of deflection $w_{3,\alpha\beta}$ can be derived in a similar way as above

$$\Psi = \mathbf{F}^{-1}\mathbf{w}_{3,\beta} \tag{4.16}$$

Therefore,

$$w_{3,\alpha\beta}(x_1, x_2) = \mathbf{f}(r)_{,\alpha}(\mathbf{F}^{-1}\mathbf{w}_{3,\beta}) \tag{4.17}$$

Substituting equation (4.15) into equation (4.17), gives:

$$w_{3,\alpha\beta}(x_1, x_2) = \mathbf{f}(r)_{,\alpha}\mathbf{F}^{-1}(\mathbf{f}(r)_{,\beta}\mathbf{F}^{-1}\mathbf{w}_3) \tag{4.18}$$

Similar to the above expressions, the derivative of in-plane stress resultants $N^{linear}_{\alpha\beta,\alpha}$ can be expressed as

$$N^{linear}_{\alpha\beta,\alpha}(x_1, x_2) = \mathbf{f}(r)_{,\alpha}\mathbf{F}^{-1}N^{linear}_{\alpha\beta} \tag{4.19}$$

4.3 Numerical Implementation

As described in Chapter 3, quadratic isoparametric boundary elements are used to discretise along the boundary, while for the domain, the constant cell elements (as shown in Figure 4-1) are used to describe the geometry.

Equation (4.9) can be rewritten in a discretised forms as

$$
\begin{aligned}
& C_{ij}w_i(x') + \sum_{n=1}^{N_e}\sum_{\alpha=1}^{3} w_j^{n\alpha} \int_{\xi=-1}^{\xi=1} P_{ij}^*(x',x)M^{\alpha}(\xi)J_n(\xi)d\xi \\
= & \sum_{k=1}^{N_e}\sum_{\alpha=1}^{3} p_j^{n\alpha\ linear} \int_{\xi=-1}^{\xi=1} W_{ij}^*(x',x)M^{\alpha}(\xi)J_n(\xi)d\xi \\
& +\lambda \sum_{n=1}^{N_c} f_b^k \int_{\eta=-1}^{\eta=1}\int_{\xi=-1}^{\xi=1} W_{i3}^*(x',X)J_k(\xi,\eta)d\xi d\eta
\end{aligned} \tag{4.20}
$$

where N_e and N_c are number of boundary elements and internal cells respectively; $J_n(\xi)$ is the Jacobian of transformation for boundary elements (see Chapter 3). Φ^{α} are the quadratic shape functions, and defined as follows:

$$
\begin{aligned}
\Phi^1(\xi) &= \frac{1}{2}\xi(\xi-1) \\
\Phi^2(\xi) &= (1-\xi)(1+\xi) \\
\Phi^3(\xi) &= \frac{1}{2}\xi(\xi+1)
\end{aligned} \tag{4.21}
$$

The Jacobian of transformation $J_k(\xi,\eta)$ for cell elements is defined as:

$$
J_k(\xi,\eta) = \sqrt{(N_{31}^2 + N_{32}^2 + N_{33}^2)} \tag{4.22}
$$

where N_{ij} is a minor of

$$
\begin{bmatrix}
\dfrac{\partial x_1(\xi,\eta)}{\partial \xi} & \dfrac{\partial x_2(\xi,\eta)}{\partial \xi} & \dfrac{\partial x_3(\xi,\eta)}{\partial \xi} \\
\dfrac{\partial x_1(\eta)}{\partial \eta} & \dfrac{\partial x_2(\xi,\eta)}{\partial \eta} & \dfrac{\partial x_2(\xi,\eta)}{\partial \eta} \\
1 & 1 & 1
\end{bmatrix} \tag{4.23}
$$

There is a weak singular term in the domain integral in equation (4.9). When the integral is computed numerically using cell discretisation, the weak singular kernel is treated using a triangle to square transformation technique as explained in Aliabadi [6].

In this case, equation (4.9) can be expressed in matrix form as

$$\mathbf{H}^p\mathbf{w} - \mathbf{G}^p\mathbf{p} = \lambda\mathbf{G}_3^p\mathbf{f}_b \tag{4.24}$$

where $\mathbf{H}^p$and $\mathbf{G}^p$ are boundary element influence matrices for plate bending, while $\mathbf{G}_3^p$ is the domain coefficient matrix.

4.4 Transformation of The Domain Integral

In the boundary integral equation (4.9), there is a domain integral which can be written as follows:

$$I^p = \int_\Omega W_{i3}^* f_b d\Omega \tag{4.25}$$

The dual reciprocity method for shear deformable plate developed by Wen, Aliabadi and Young [98] can be used to evaluate the equation (4.25). Assume that the term f_b are the body forces, therefore they can be approximated by

$$f_b = \sum_{m=1}^{M} f(r)^m \phi_j^m \tag{4.26}$$

where $f(r)$ is a radial basis function, see Appendix B, the ϕ_j^m are a set of unknown coefficients, r is denoted as the equation (4.13), M is the total number of the selected points.

The ϕ_j^m are coefficients which are determined by values at the selected points M as follows

$$\phi = \mathbf{F}^{-1} f_b \tag{4.27}$$

The boundary integral equation (4.9) can be rewritten as

$$\begin{aligned} & C_{ij}(\mathbf{x}')\hat{w}_{mj}(\mathbf{x}') + \int_\Gamma P_{ij}^*(\mathbf{x}', \mathbf{x})\hat{w}_{mj}(\mathbf{x}) d\Gamma(\mathbf{x}) \\ = & \int_\Gamma W_{ij}^*(\mathbf{x}', \mathbf{x})\hat{p}_{mj}(\mathbf{x}) d\Gamma(\mathbf{x}) + \int_\Omega W_{i3}^*(\mathbf{x}', \mathbf{X}) F_m(r) d\Omega(\mathbf{X}) \end{aligned} \tag{4.28}$$

where $r = |\mathbf{X} - \mathbf{x}'|$ and $F_m(r)$ is radial basis function.. The domain integral in equation (4.25) can now be expressed in terms of boundary integrals as

$$\begin{aligned} &\int_{\Omega} W^*_{i3}(\mathbf{x}', \mathbf{X}) f_b(\mathbf{X}) d\Omega(\mathbf{X}) \\ = &\sum_{m=1}^{M} \phi_j^m [C_{ij}(\mathbf{x}') \hat{w}_{mj}(\mathbf{x}') + \int_{\Gamma} P^*_{ij}(\mathbf{x}', \mathbf{x}) \hat{w}_{mj}(\mathbf{x}) d\Gamma(x) \\ &- \int_{\Gamma} W^*_{ij}(\mathbf{x}', \mathbf{x}) \hat{p}_{mj}(\mathbf{x}) d\Gamma(\mathbf{x})] \end{aligned} \tag{4.29}$$

The boundary integral equation (4.9) can be written in a discretised form as

$$\begin{aligned} &C_{ij} w_i(\mathbf{x}') + \sum_{n=1}^{N_e} \sum_{m=1}^{3} w_j^{nm} \int_{\xi=-1}^{\xi=1} P^*_{ij}(\mathbf{x}', \mathbf{x}) \Phi^m(\xi) J_n(\xi) d\xi \\ = &\sum_{k=1}^{N_e} \sum_{m=1}^{3} p_j^{nm} \int_{\xi=-1}^{\xi=1} W^*_{ij}(\mathbf{x}', \mathbf{x}) \Phi^m(\xi) J_n(\xi) d\xi + \lambda\, I^p \end{aligned} \tag{4.30}$$

Equation (4.30) can be expressed in matrix form as

$$\mathbf{H}^p \mathbf{w} - \mathbf{G}^p \mathbf{p} = \lambda (\mathbf{H}^p \hat{\mathbf{w}} - \mathbf{G}^p \hat{\mathbf{p}}) \mathbf{F}^{-1} \mathbf{f}_b \tag{4.31}$$

where $\hat{\mathbf{w}}$ and $\hat{\mathbf{p}}$ are matrices of nodal values of particular solutions on the boundary, while $\mathbf{H}^p$and $\mathbf{G}^p$ are the same as in the section 4.3.

4.5 Numerical Procedure

In this section, the numerical procedure for calculating the critical load factor is presented. The first step is to solve the boundary integral equation of in-plane problem and calculate the stress resultants at the domain points. The second step is to solve boundary integral equation of buckling problem.

4.5.1 Determination of the in-plane stresses

After discretising and introducing boundary conditions into equation (4.1), the resulting system of algebraic equations can be arranged as

$$[\mathbf{C}]\{\mathbf{u}\} + [\mathbf{H}^s]\{\mathbf{u}\} = [\mathbf{G}^s]\{\mathbf{t}\} \tag{4.32}$$

where coefficient matrices $\mathbf{H}^s$ and $\mathbf{G}^s$ are obtained from the integral of the product of fundamental solutions, shape functions and the jacobian. (see Chapter 3).

The known and unknown quantities in equation (4.32) can be rearranged as a set of linear algebraic equation:

$$[\mathbf{A}]\{\mathbf{X}\} = \{\mathbf{F}\} \tag{4.33}$$

where matrix $\mathbf{X}$ contains the unknown vectors of $\mathbf{u}$ and $\mathbf{t}$. The vector $\mathbf{F}$ is obtained by multiplying the related matrices of $\mathbf{H}^s$ or $\mathbf{G}^s$ by the known vectors of $\mathbf{u}$ or $\mathbf{t}$.

Once equation (4.33) has been solved, in-plane stresses N_{11}, N_{12}, and N_{22} in the domain (equation 4.3) can be calculated. The stresses are required to solve the plate buckling problem.

4.5.2 Solving the plate buckling problem

Similar to the in-plane stresses procedure, after applying boundary conditions to the equation (4.9), the resulting system of algebraic equation can be written as:

$$[\mathbf{C}]\{\mathbf{w}\} + [\mathbf{H}^p]\{\mathbf{w}\} = [\mathbf{G}^p]\{\mathbf{p}\} + \lambda[\mathbf{G}^p_{eq}]\{\mathbf{f}_b\} \tag{4.34}$$

in which $\mathbf{G}^p_{eq} = \mathbf{G}^p_3$ for domain cell discretisation, and $\mathbf{G}^p_{eq} = (\mathbf{H}^p\hat{\mathbf{w}} - \mathbf{G}^p\hat{\mathbf{p}})\mathbf{F}^{-1}$ for the dual reciprocity method. The $q(\mathbf{X})$ quantities in the equations (4.7) and (4.8) are set to zero. The term $f_b(\mathbf{X})$ (equation 4.10) can be expressed in term of $w_3(\mathbf{X})$, as follows

$$f_b(\mathbf{X}) = \mathbf{f}_{bw}(X)w_3(\mathbf{X}) \tag{4.35}$$

where $\mathbf{f}_{bw} = N^{linear}_{\alpha\beta,\alpha}\mathbf{f}(r)_{,\beta}\mathbf{F}^{-1} + N^{linear}_{\alpha\beta}\mathbf{f}(r)_{,\alpha}\mathbf{f}(r)_{,\beta}\mathbf{F}^{-1}$

Equation (4.34) can be arranged in a similar manner as equation (4.33), and give

$$[\mathbf{B}]_{3N\times 3N}\{\mathbf{Y}\}_{3N} = \lambda[\mathbf{K}]_{3N\times L}\{\mathbf{w}_3\}_L \tag{4.36}$$

$$\mathbf{K} = \mathbf{G}^{p}_{eq}\mathbf{f}_{bw} \tag{4.37}$$

where the matrix **B** contains the coefficient matrices $\mathbf{H}^p$ and $\mathbf{G}^p$. N and L are the number of boundary elements and domain points, respectively.

The equation (4.11) also can be written in matrix form as follows:

$$[\mathrm{I}]\{\mathrm{w}_3\}_L = [\mathrm{BB}]_{L\times 3N}\{\mathrm{Y}\}_{3N} + \lambda[\mathrm{KK}]_{L\times L}\{\mathrm{w}_3\}_L \tag{4.38}$$

where matrix [I] is an identity matrix. The matrix [**BB**] contains coefficient matrices related to the fundamental solutions of W^*_{3j} and P^*_{3j}. The matrix [**KK**] are obtained by multiplication of coefficient matrix related to the fundamental solution W^*_{33} and matrix $\mathbf{f}_{bw}$.

The equation (4.36) can be rearranged in term of unknown vector $\{\mathbf{Y}\}_{3N}$,

$$\{\mathrm{Y}\}_{3N} = \lambda[\mathrm{B}]^{-1}_{3N\times 3N}[\mathrm{K}]_{3N\times L}\{\mathrm{w}_3\}_L \tag{4.39}$$

where matrix $\mathbf{B}^{-1}$ is the inverse matrix of **B**.

The substitution of the equation (4.39) into the equation (4.38) yields:

$$\begin{aligned}[\mathrm{I}]\{\mathrm{w}_3\}_L &= \lambda[\mathrm{BB}]_{L\times 3N}[\mathrm{B}]^{-1}_{3N\times 3N}[\mathrm{K}]_{3N\times L}\{\mathrm{w}_3\}_L \\ &\quad +\lambda[\mathrm{KK}]_{L\times L}\{\mathrm{w}_3\}_L\end{aligned} \tag{4.40}$$

Then,

$$\begin{aligned}[\mathrm{I}]\{\mathrm{w}_3\}_L &= \lambda([\mathrm{BB}]_{L\times 3N}[\mathrm{B}]^{-1}_{3N\times 3N}[\mathrm{K}]_{3N\times L} \\ &\quad +[\mathrm{KK}]_{L\times L})\{\mathrm{w}_3\}_L\end{aligned} \tag{4.41}$$

The equation (4.41) can be written as a standard eigenvalue problem equation as follows:

$$([\psi] - \frac{1}{\lambda}[\mathrm{I}])\{\mathrm{w}_3\}_L = 0 \tag{4.42}$$

where $[\psi] = [\mathbf{BB}]_{L\times 3N}\,[\mathbf{B}]^{-1}_{3N\times 3N}\,[\mathbf{K}]_{3N\times L} + [\mathbf{KK}]_{L\times L}$.

Buckling analysis of shear deformable plates has been presented as a standard eigenvalue problem. Buckling modes correspond to the problem can be obtained by solving equation (4.42).

4.6 Numerical Examples

Several numerical examples are presented to demonstrate the accuracy of the proposed method for analysis of plate buckling problems with different geometries, loadings and boundary conditions (see Figure 4-2). The BEM results are compared with analytical and finite element results. In the following examples, the buckling coefficient K is defined by

$$K = \frac{b^2}{\pi^2 D} T$$

where T is critical compression load σ_{cr} or critical shear load τ_{cr}, b is the width or diameter of plates and D is flexural rigidity of plate as described in Chapter 2.

4.6.1 Convergence study of simply supported square plate subjected to compression loads

In this example, a square plate as shown in Figure 4-3 is analysed. Six different BEM meshes of domain cells and domain points are used. A convergence study of the simply supported square plate is performed and the buckling coefficients K are compared with the analytical result [90].

The number of boundary elements and cell elements are shown in Table 4.1, and the number of domain points in Table 4.2. It can be seen, that convergence of the results is achieved with increasing number of cells and domain points. It can also be seen that the BEM results are in good agreement with analytical results.

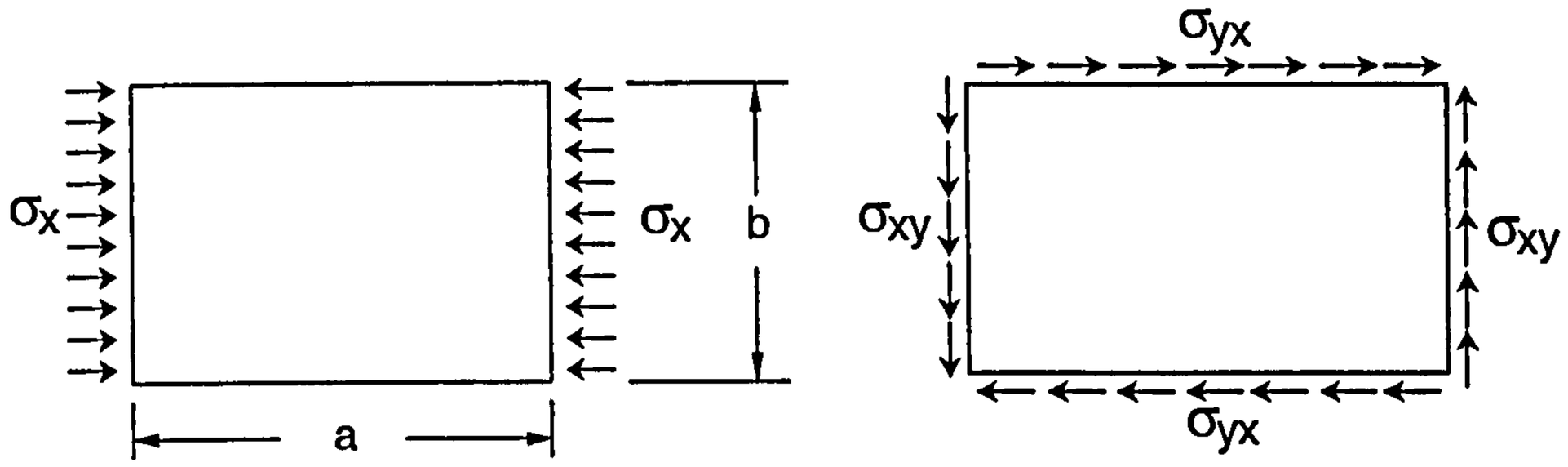

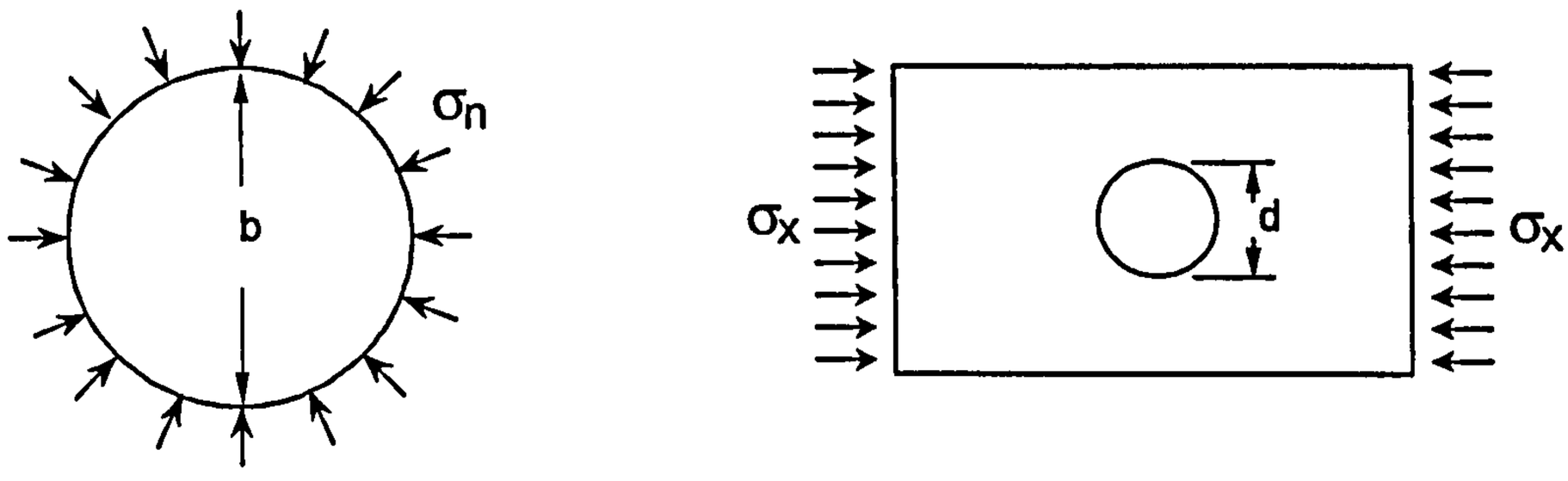

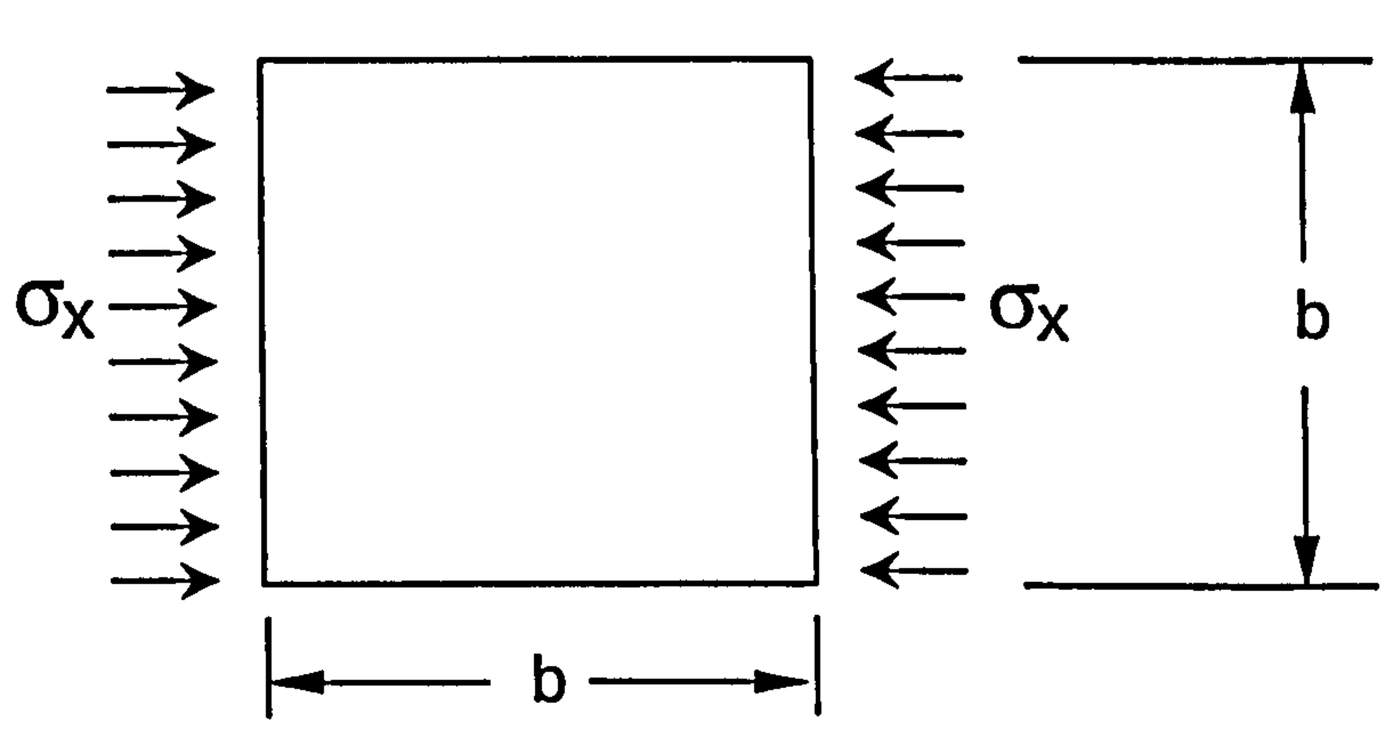

Figure 4-2: Plate buckling model with different geometries, loadings and boundary conditions.

Figure 4-3: Square plate subjected to compression loads.

Table 4.1: Buckling coefficients using domain cells.

No	Boundary	Domain	K BEM	K analytical	% error
1	20 elems	5 x 5 cells	4.241	4.000	6.030
2	24 elems	6 x 6 cells	4.173	4.000	4.325
3	28 elems	7 x 7 cells	4.143	4.000	3.575
4	32 elems	8 x 8 cells	4.079	4.000	1.975
5	36 elems	9 x 9 cells	4.068	4.000	1.700
6	40 elems	10 x 10 cells	4.041	4.000	1.025

Table 4.2: Buckling coefficients using the dual reciprocity technique.

No	Boundary	Domain	K BEM	K analytical	% error
1	32 elems	5 x 5 points	4.189	4.000	4.720
2	32 elems	6 x 6 points	4.141	4.000	3.515
3	32 elems	7 x 7 points	4.060	4.000	1.510
4	32 elems	8 x 8 points	4.032	4.000	0.808
5	32 elems	9 x 9 points	3.985	4.000	0.387
6	32 elems	10 x 10 points	3.999	4.000	0.025

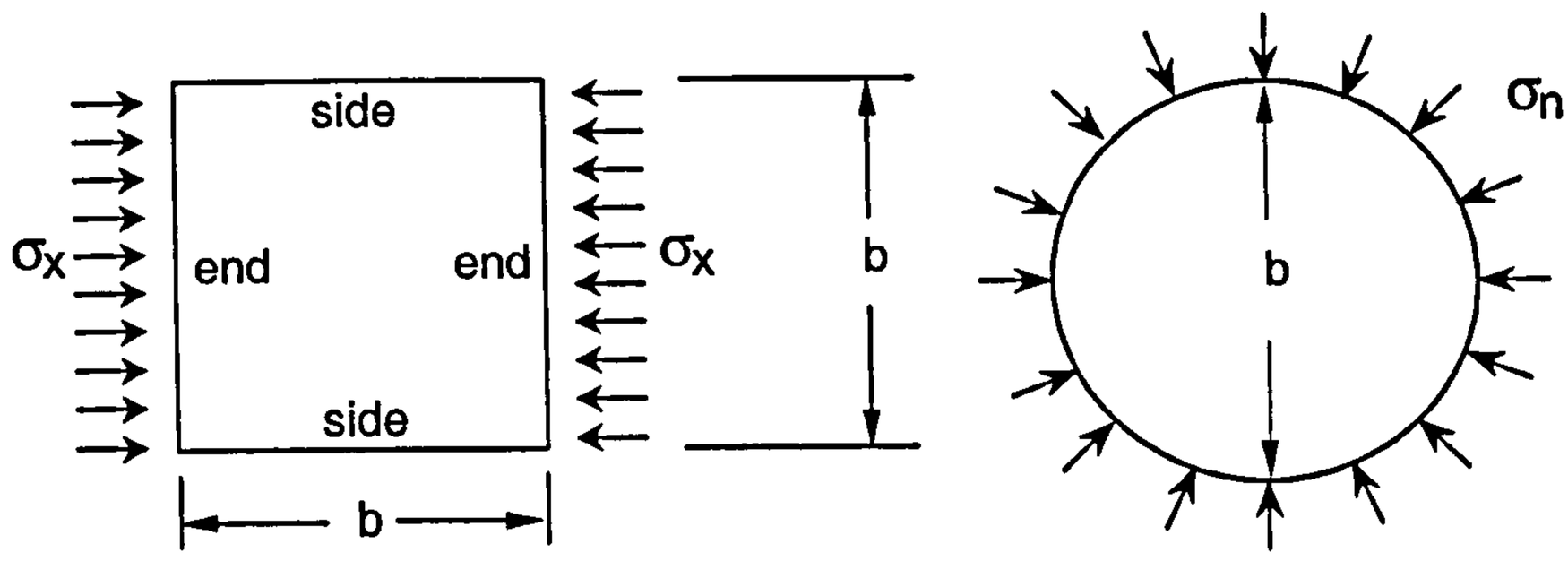

Figure 4-4: Square and circular buckling models.

4.6.2 Square and circular plates subjected to compression loads with different boundary conditions

Examples of buckling problems for square and circular plates subjected to compression loads with different boundary conditions are presented. The models are shown in Figure 4-4. Initially, the square plate is discretised into 40 boundary elements and 100 domain cells, and next analysed using the dual reciprocity technique with 32 boundary elements and 100 domain points. The circular plate is discretised using 16 boundary elements and 49 domain cells. It is also analysed using the dual reciprocity technique with 16 boundary elements and 32 domain points. Table 4.3 presents the BEM results of the examples as well as analytical and finite element results obtained using I-DEAS [48] with 400 quadratic elements for square plate and 240 quadratic elements for circular. As it can be seen from Table 4.3 that BEM results are in good agreement (the maximum error is less than 4%) with both analytical and finite element results.

Table 4.3: Buckling coefficients of square and circular plates.

Boundary Condition	Domain Cell	DRM	FEM	Analytical
I-A	10.387	10.142	10.392	10.070
I-B	4.041	3.999	4.011	4.000
I-C	7.757	7.683	7.796	7.690
I-D	6.972	6.781	6.882	6.740
I-E	1.724	1.712	1.718	1.700
I-F	1.417	1.428	1.422	1.440
II-A	5.779	5.889	5.921	5.910
II-B	1.661	1.689	1.714	1.702

I : square plate

II : circular plate

A : sides and ends clamped

B : sides and ends simply supported

C : sides clamped, ends simply supported

D : ends clamped, sides simply supported

E : one side free, one side clamped, end simply supported

F : one side free, the other side and ends simply supported

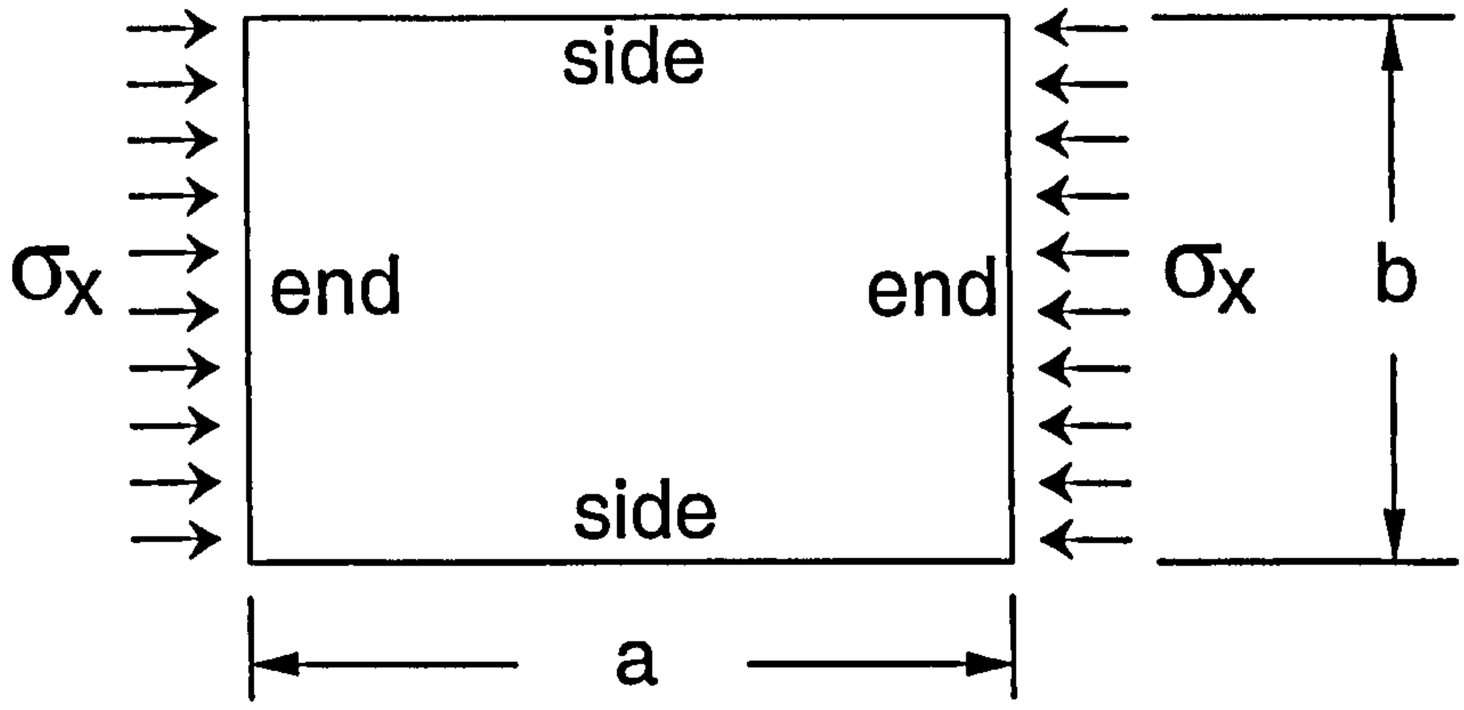

Figure 4-5: Rectangular plate subjected to compression loads.

4.6.3 Rectangular plate subjected to compression load with different boundary conditions

In this example, a rectangular plate (as in Figure 4-5) subjected to compression loads with different boundary conditions is presented. The buckling coefficients K for different aspect ratio a/b are presented in Figure 4-6 and the accuracy achieved by BEM can be considered satisfactory. The legends in the Figure 4-5 stand for boundary conditions as follows

cccc : sides and ends clamped

ssss : sides and ends simply supported

cscs : ends clamped, sides simply supported

sfsc : one side free, one side clamped, end simply supported

sssf : one side free, the other side and ends simply supported

The buckling contours and modes of simply supported rectangular plate are presented in Figures 4-7 and 4-8 respectively. From Figure 4-8, it can be seen that increasing the aspect ratio a/b will increase a number of half-waves. Contour plot presented in Figure 4-7 are related to the buckling modes.

4.6.4 Rectangular plate subjected to shear loads

In this example, shear buckling of rectangular plate with different aspect ratio a/b is presented. The buckling model is shown in Figure 4-9. Boundary conditions applied are simply supported and clamped. The results are plotted in Figure 4-10 and are

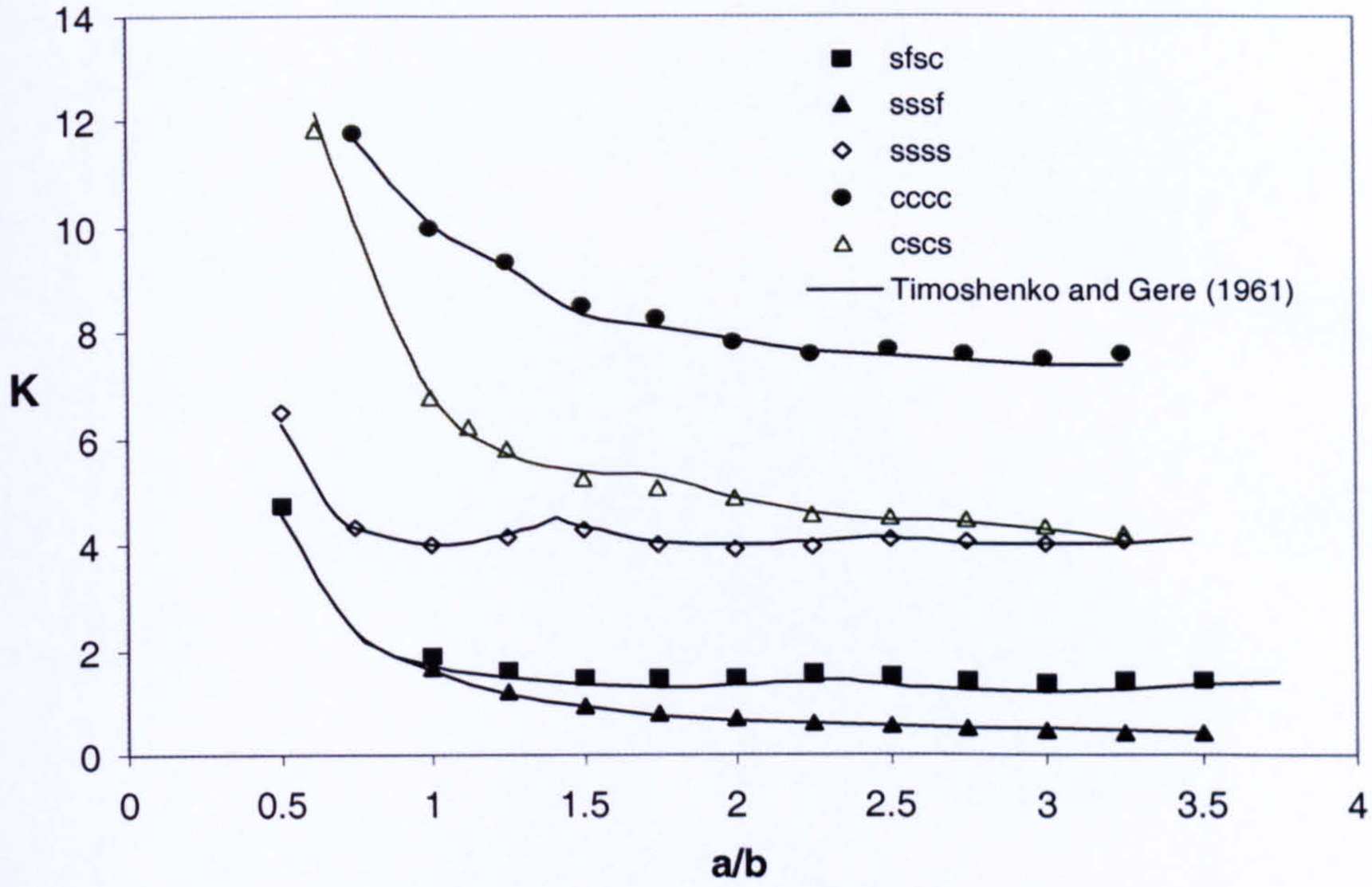

Figure 4-6: Buckling coefficients of rectangular plate with different boundary conditions.

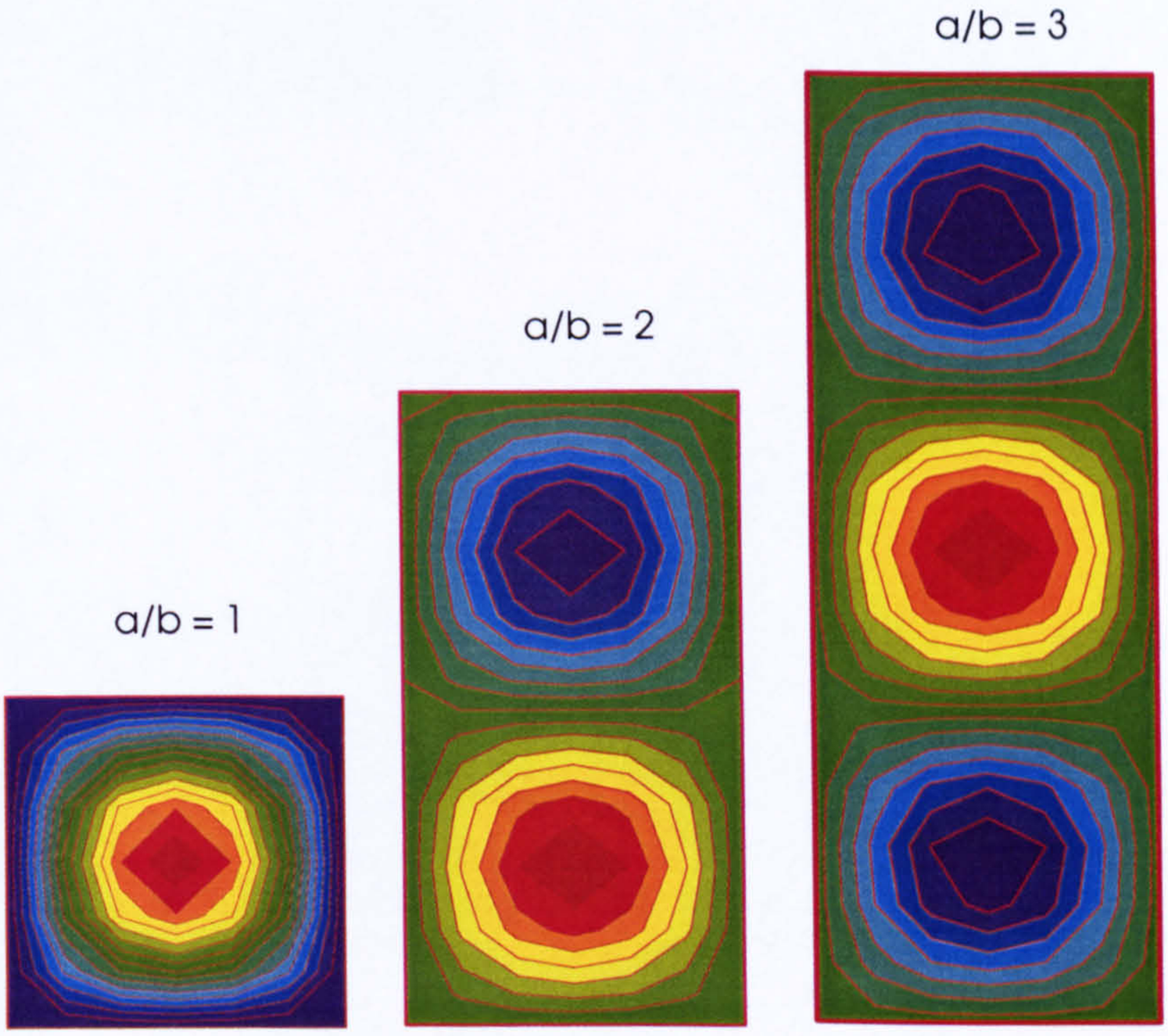

Figure 4-7: Contour plot of simply supported rectangular plate buckling.

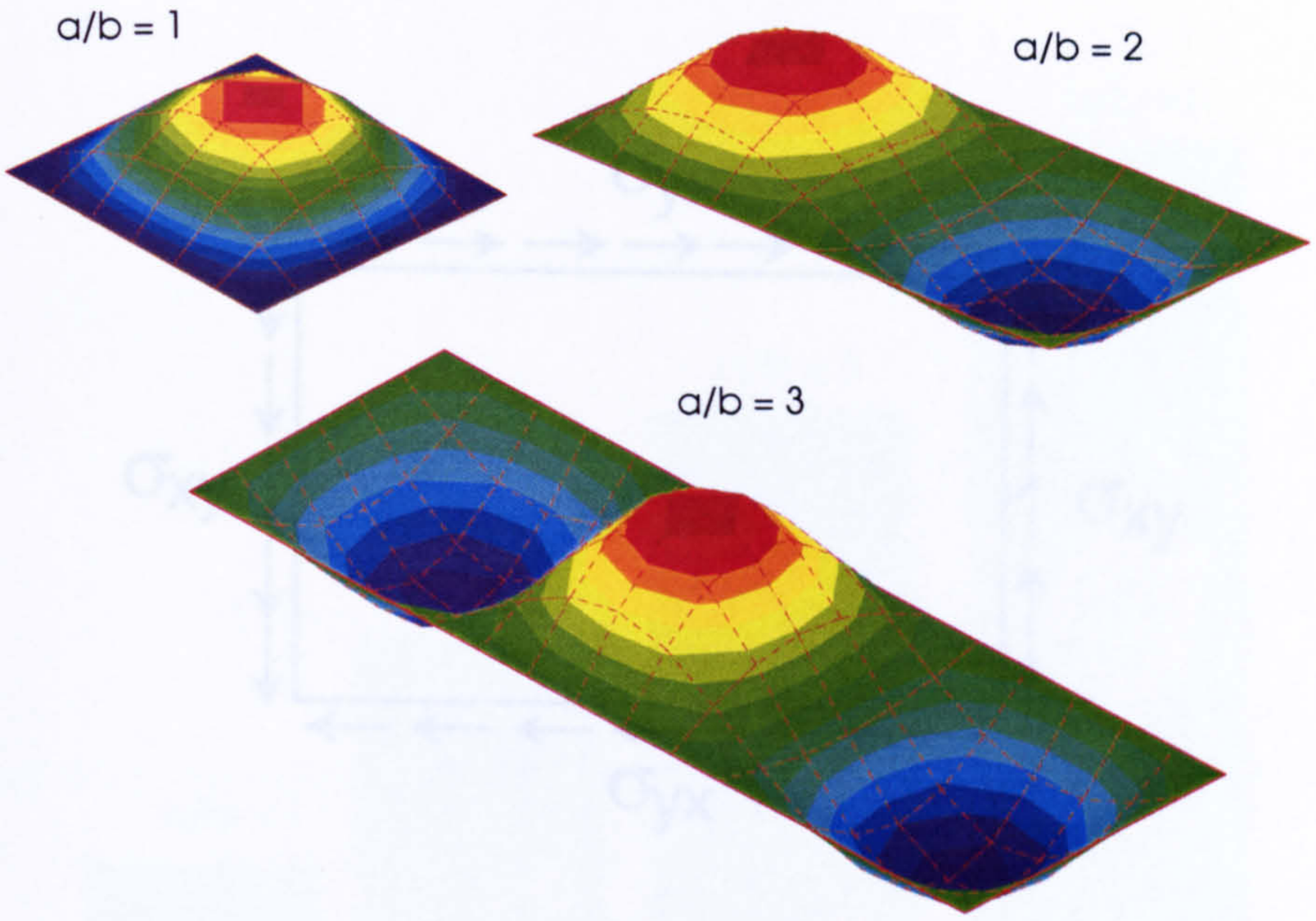

Figure 4-8: Buckling modes of simply supported rectangular plate.

compared with analytical and finite element results. Good agreements (< 1.5% error) is achieved in both cases. Buckling contours and modes of simply supported rectangular plate are also presented. The contour types of buckling is shown in Figure 4-11. The shear buckling modes of simply supported rectangular plate can be seen in Figure 4-12.

4.6.5 Rectangular plate with a hole subjected to compression loads

In this example, a rectangular plate with a hole (Figure 4-13) subjected to compression loads is presented. The aspect ratio of the plate is $a/b = 2$. The buckling coefficients with different aspect ratio d/b (diameter of hole to width of the plate) are plotted as shown in Figure 4-14. The results are compared and show good agreements (< 2.5% error) with finite element results.

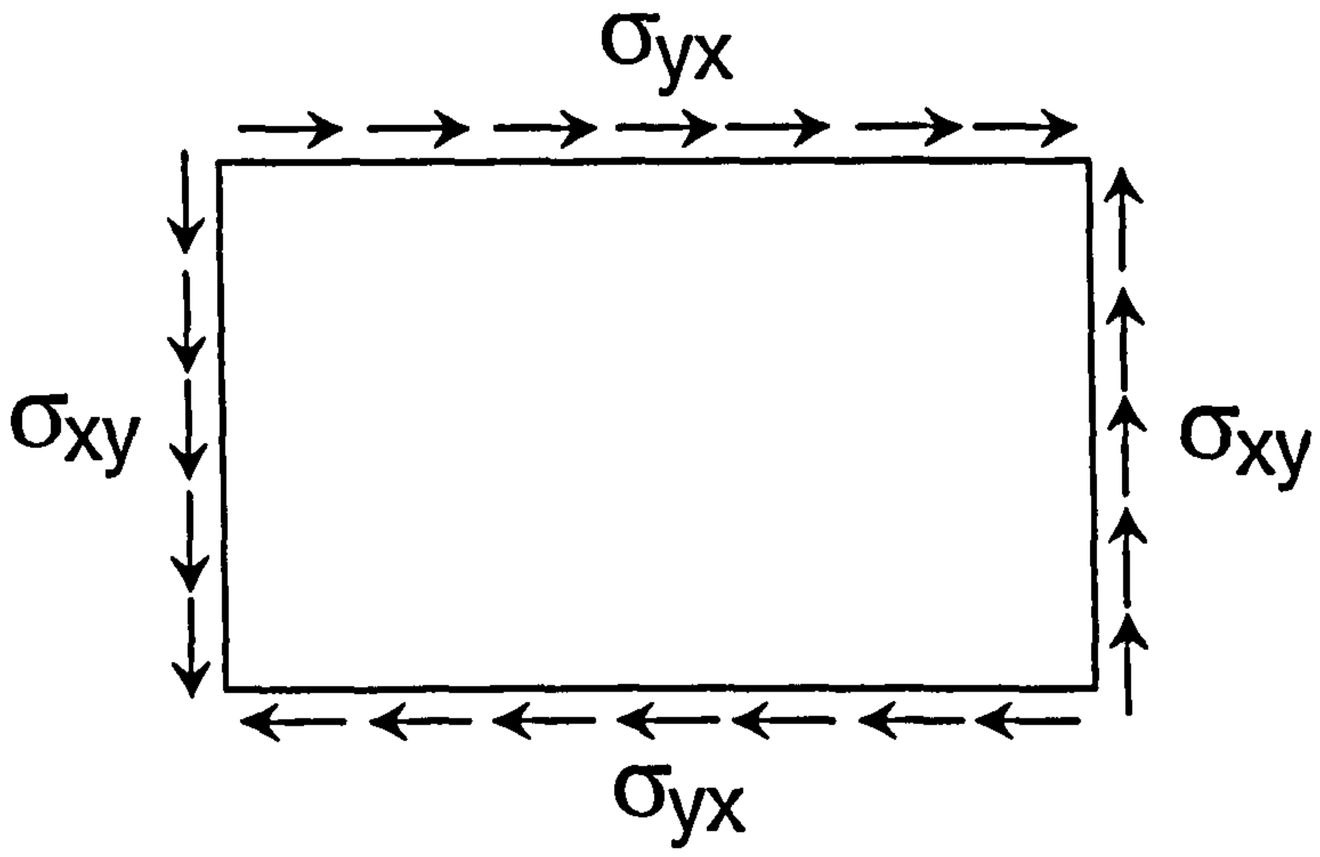

Figure 4-9: Rectangular plate subjected to shear loads.

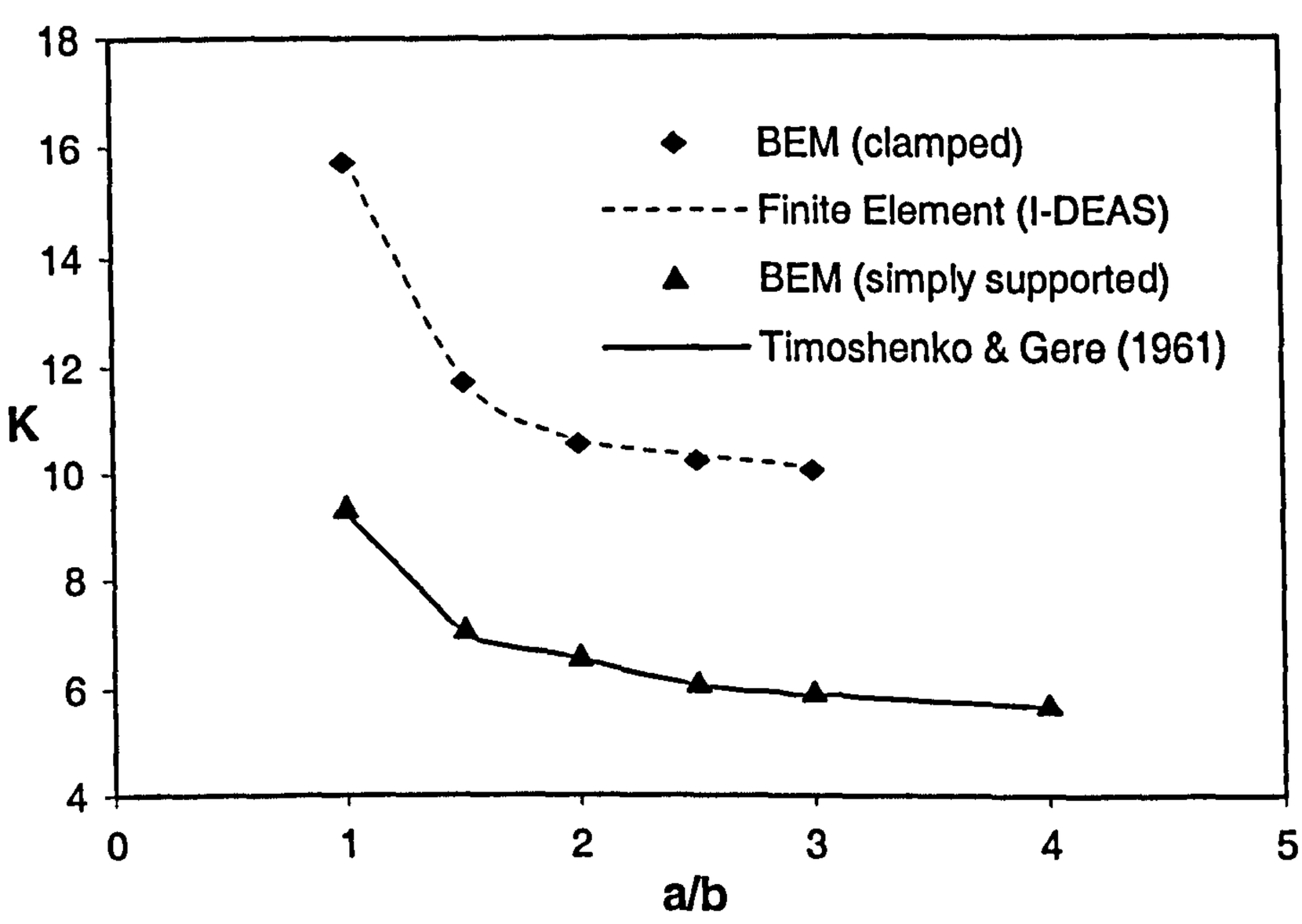

Figure 4-10: Shear buckling coefficient of rectangular plate.

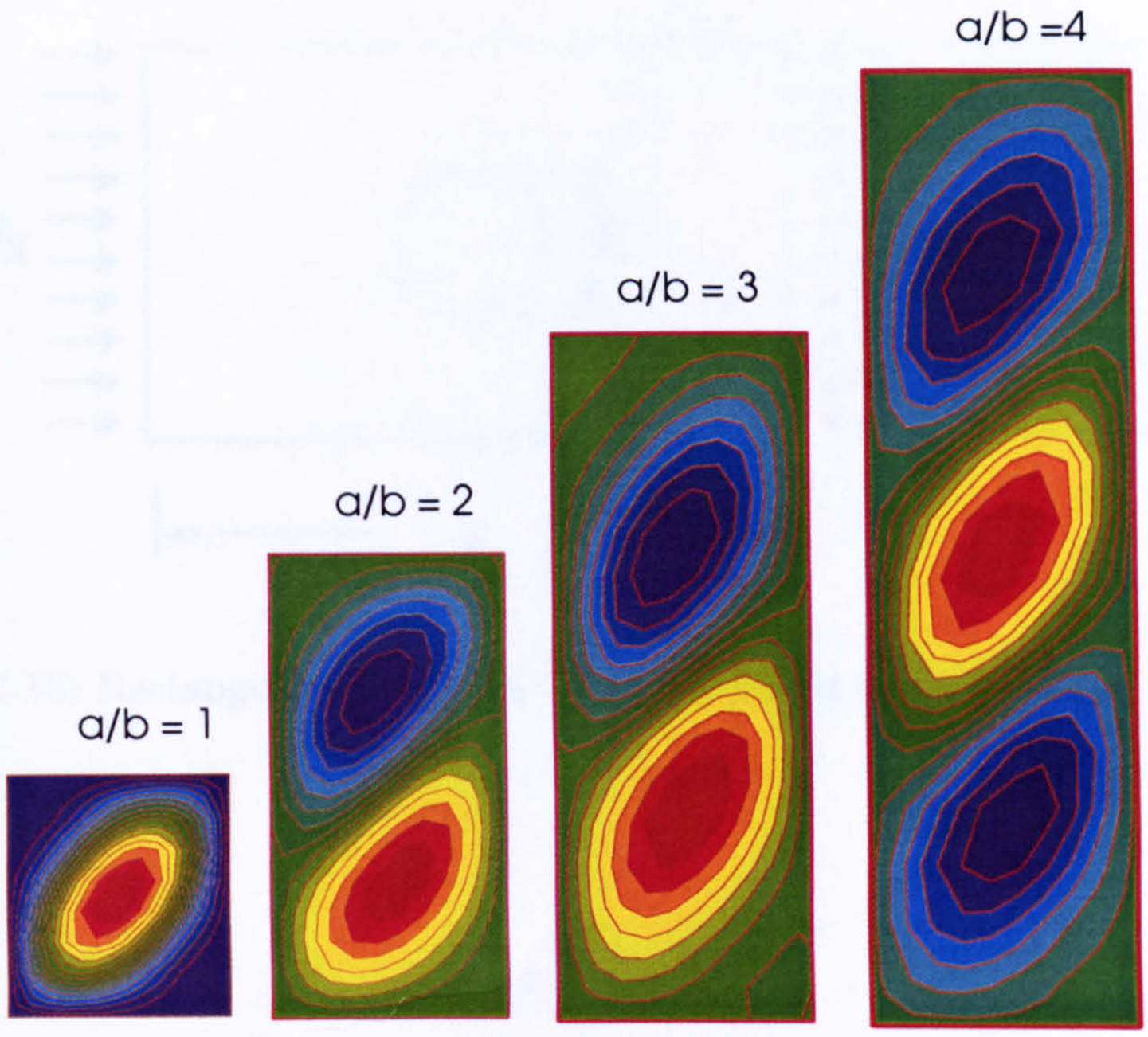

Figure 4-11: Contour plot of shear buckling of simply supported rectangular plate.

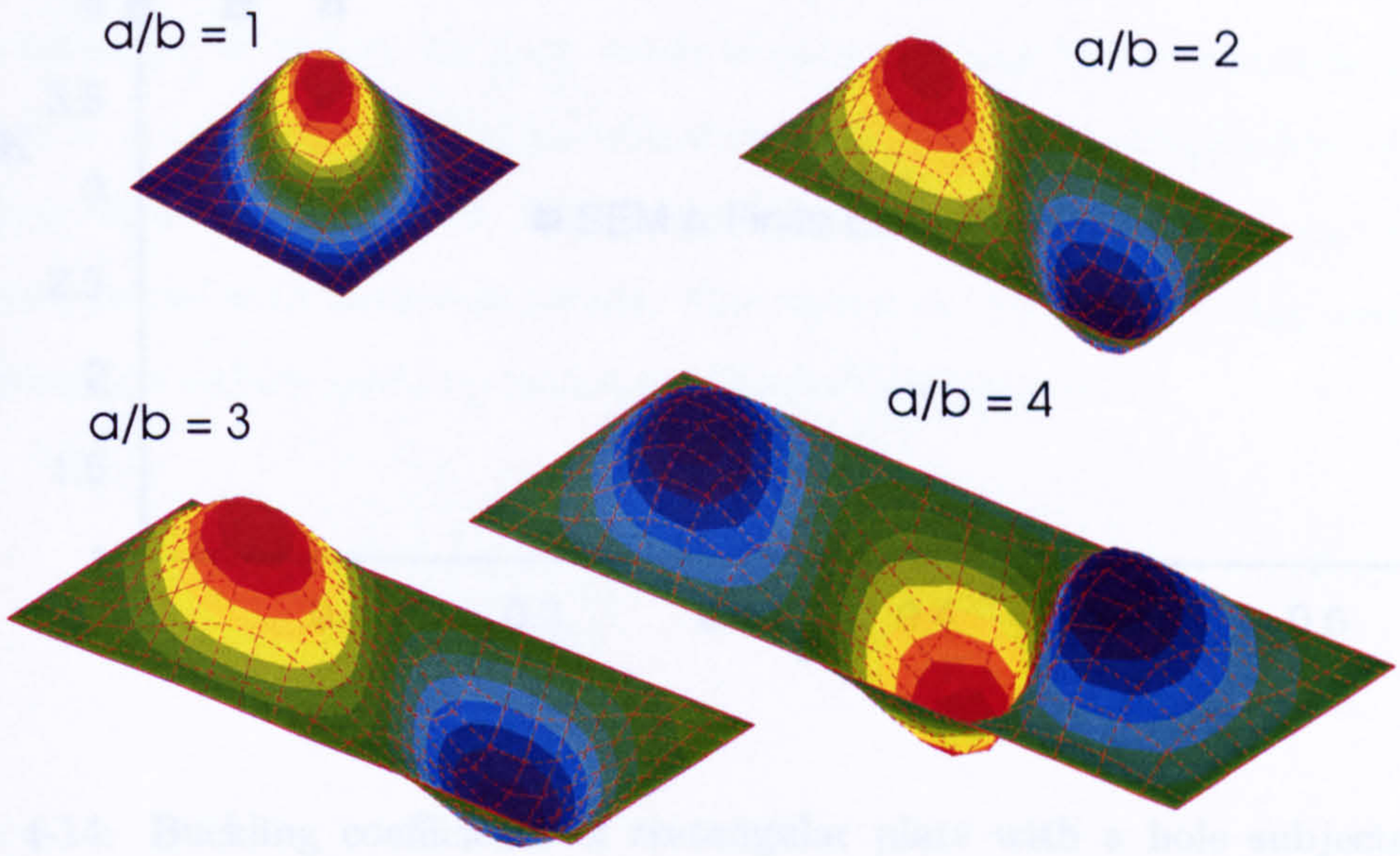

Figure 4-12: Shear buckling modes of simply supported rectangular plate.

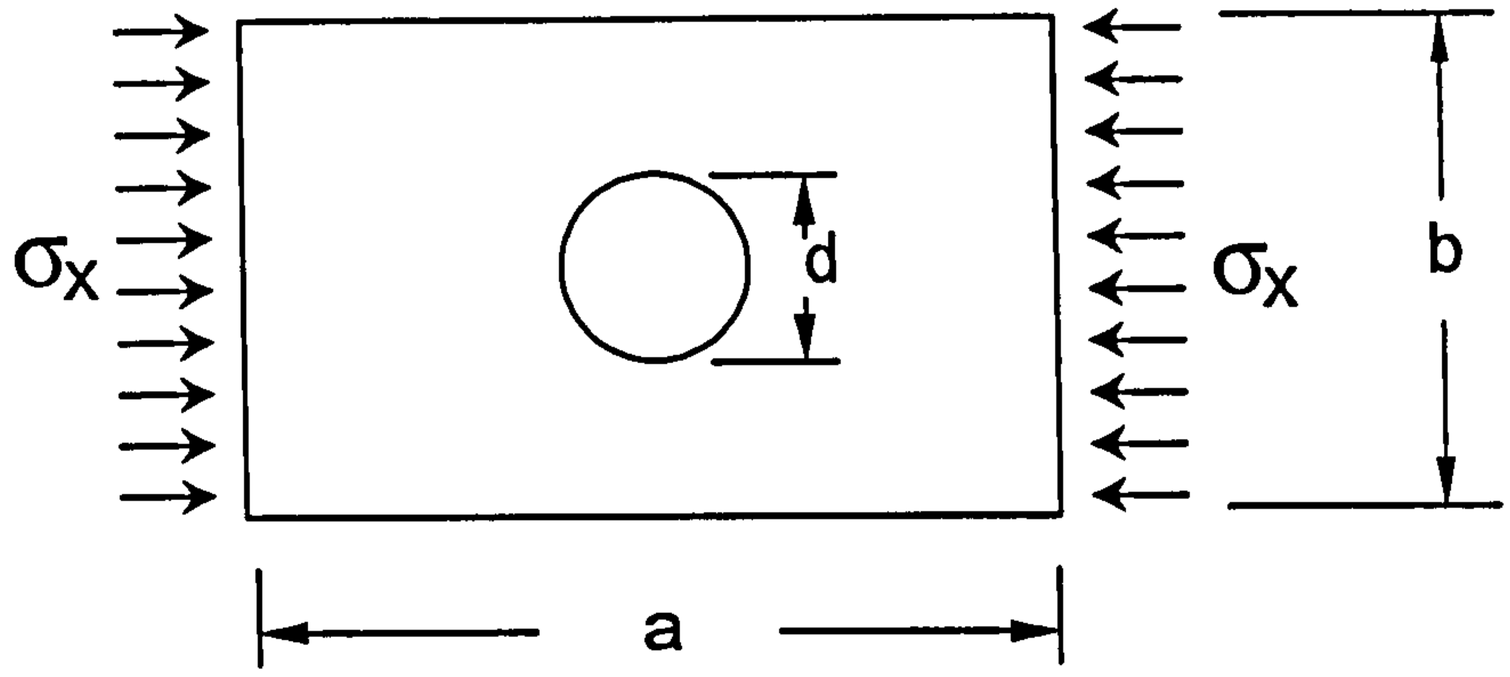

Figure 4-13: Rectangular plate with a hole subjected to compression loads.

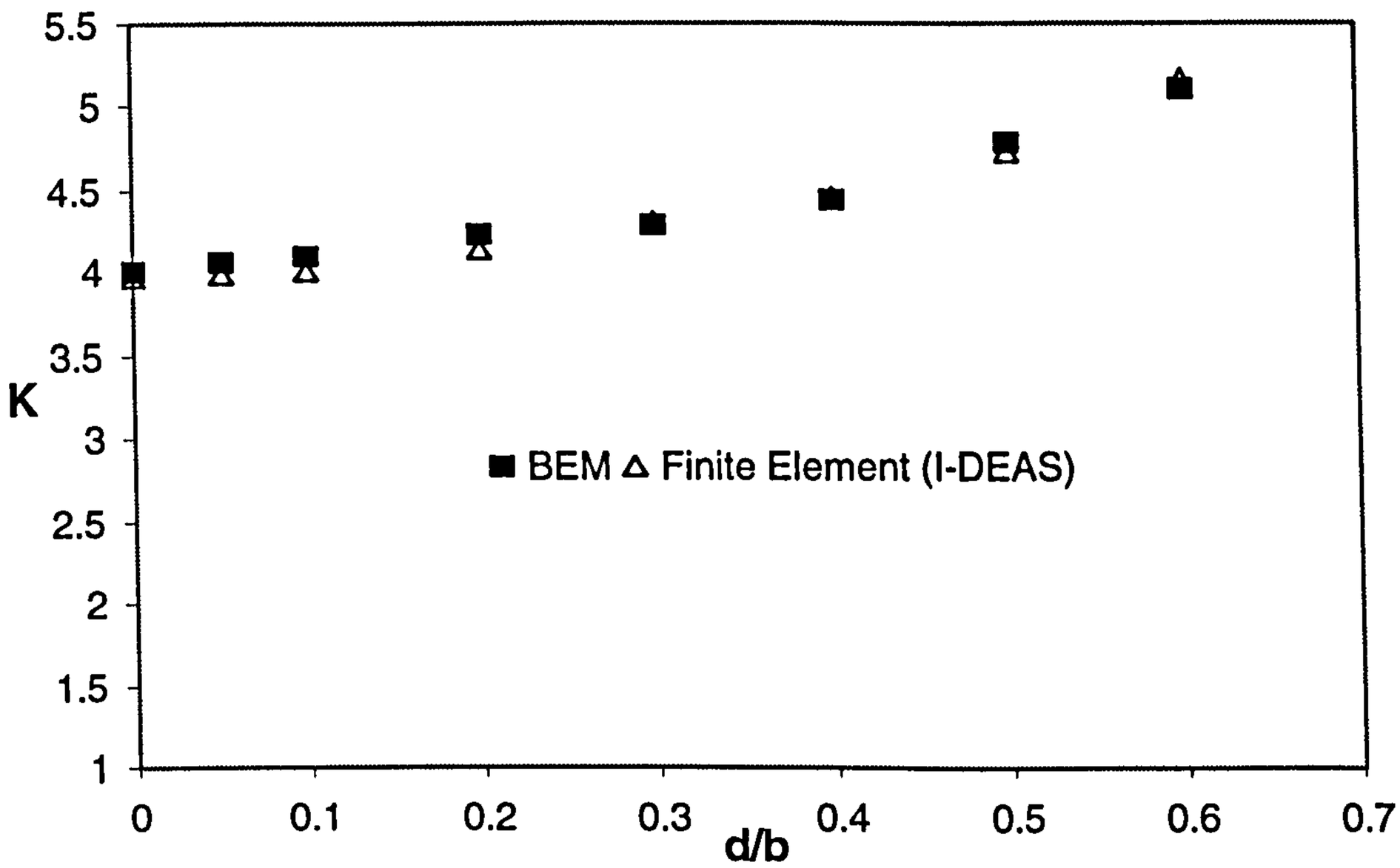

Figure 4-14: Buckling coefficients of rectangular plate with a hole subjected to compression loads.

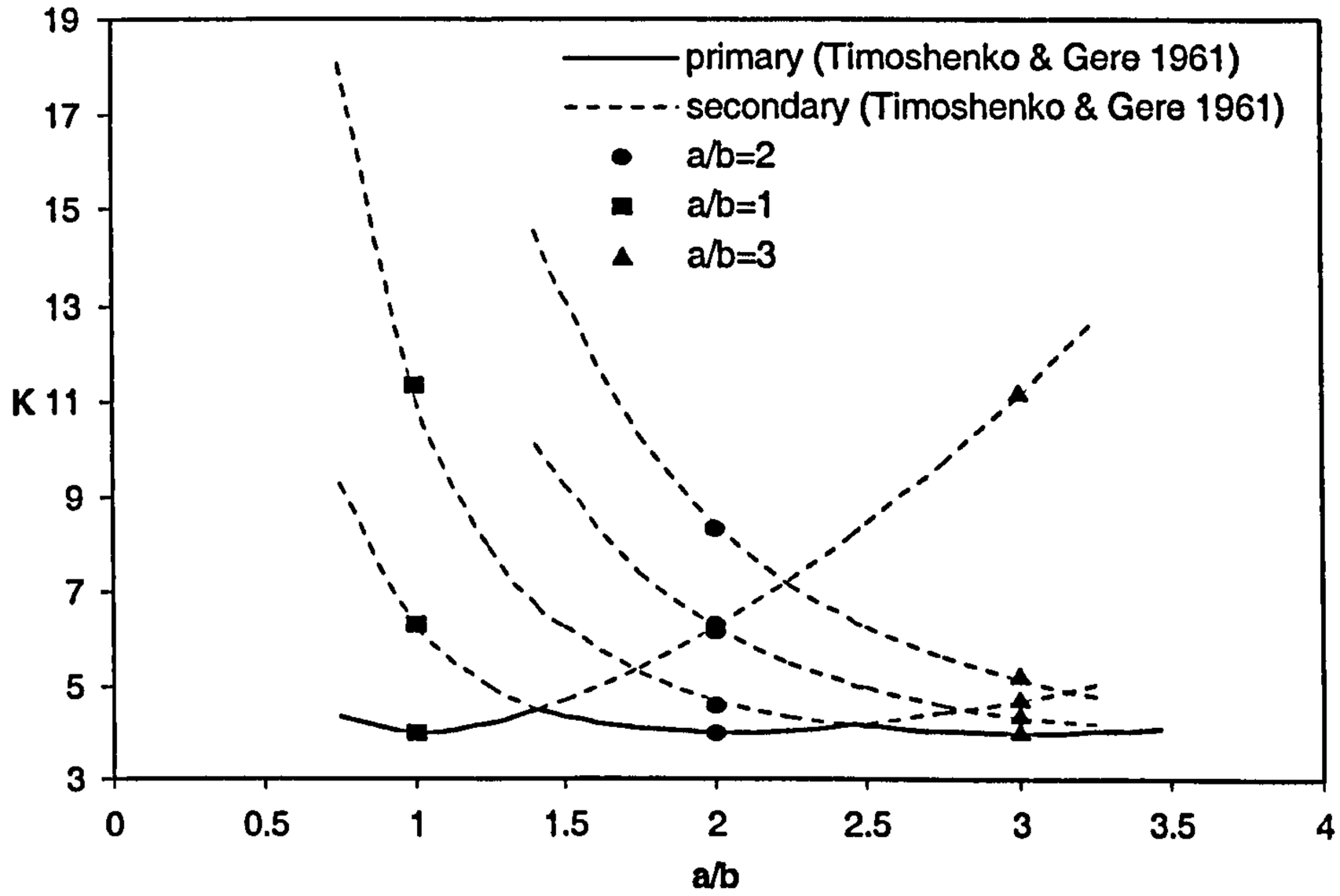

Figure 4-15: Secondary buckling coefficients of simply supported rectangular plate under compression loads

4.6.6 Secondary buckling of simply supported rectangular plate subjected to compression loads

In this example, secondary buckling mode of simply supported rectangular plate subjected to compression loads is investigated. The primary buckling mode of the example is shown in Figure 4-16. The results are plotted with different aspect ratio and are compared with analytical results. The results in Figure 4-15 are considered satisfactory. Secondary buckling modes are plotted in Figure 4-17 .

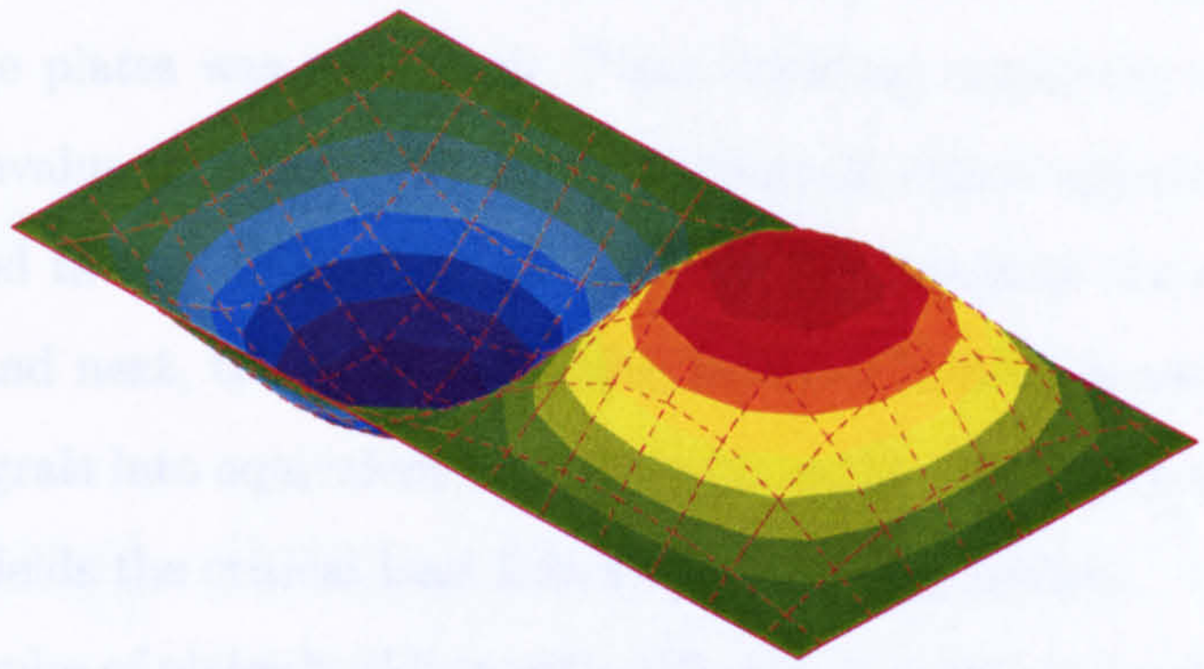

Figure 4-16: Primary buckling of simply supported rectangular plate under compression loads

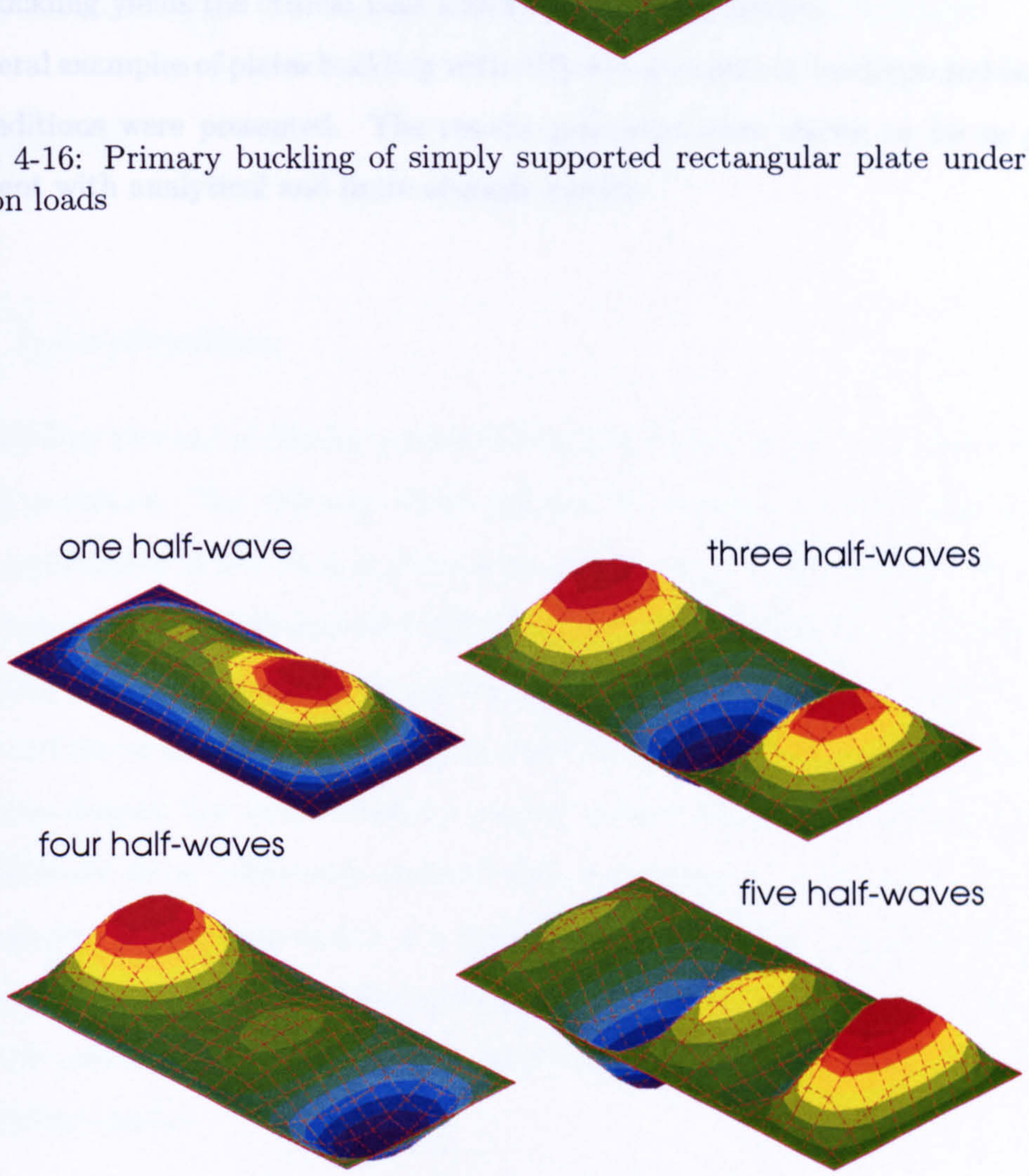

Figure 4-17: Secondary buckling mode of simply supported rectangular plate subjected to compression loads

4.7 Summary

In this chapter, the boundary element method formulation of buckling analysis of shear deformable plates was presented. Plate buckling equations were written as a standard eigenvalue problem. The domain integrals which appear in this formulation are treated in two different ways: initially the integrals are evaluated using constant cells, and next, the dual reciprocity method (DRM) is used to transform the domain integrals into equivalent boundary integrals. The eigenvalue problem of plate buckling yields the critical load factor and buckling modes.

Several examples of plates buckling with different geometries, loadings and boundary conditions were presented. The results presented were shown to be in good agreement with analytical and finite element results.

Chapter 5

Buckling Analysis of Cracked Plates

5.1 Introduction

The boundary element method is a powerful numerical tool for general stress analysis of crack problems. The difficulty which appears in modelling of crack problems is due to coincidence of the crack surfaces that makes point collocations on two crack surfaces generate identical equations [10]. To overcome this difficulty, several special techniques have been developed to model cracked structures. Among these the most general are the sub-region method [18] and the dual boundary element method [39].

In this chapter the dual boundary integral equations for the buckling analysis of the Reissner shear deformable cracked plate are presented. The domain integrals which appear in this formulation are transferred to boundary integrals using the dual reciprocity method. The plate buckling equations are presented as a standard eigenvalue problem, which would allow direct evaluation of the critical load factor and buckling modes.

5.2 The Dual Boundary Integral Equations

A cracked body shown in Figure 5-1 is considered with Γ^+ and Γ^- referring to the upper and lower crack surfaces respectively, and Γ_b denotes the rest of the boundary.

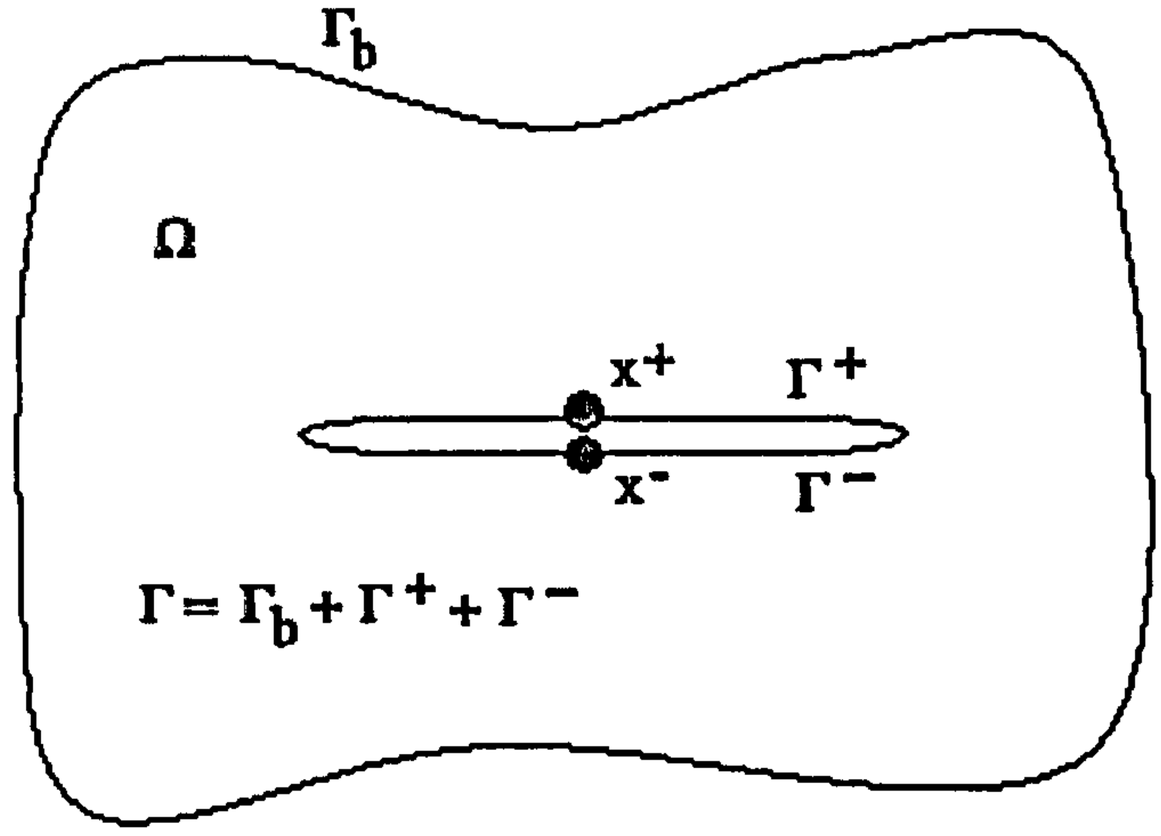

Figure 5-1: A cracked body.

The equations (4.1) and (4.4) can be recalled to represent the boundary integral of the displacement components u_α and w_i for collocation points on the upper crack surface, that is $\mathbf{x}^+ \in \Gamma^+$ [10],

$$\begin{aligned} & \frac{1}{2}u_\alpha(\mathbf{x}^+) + \frac{1}{2}u_\alpha(\mathbf{x}^-) + \int_\Gamma T^*_{\theta\alpha}(\mathbf{x}^+,\mathbf{x})u_\alpha(\mathbf{x})d\Gamma(\mathbf{x}) \\ = & \int_\Gamma U^*_{\theta\alpha}(\mathbf{x}^+,\mathbf{x})t^{linear}_\alpha(\mathbf{x})d\Gamma(\mathbf{x}) \end{aligned} \tag{5.1}$$

and

$$\begin{aligned} & \frac{1}{2}w_j(\mathbf{x}^+) + \frac{1}{2}w_j(\mathbf{x}^-) + \int_\Gamma P^*_{ij}(\mathbf{x}^+,\mathbf{x})w_j(\mathbf{x})\,d\Gamma(\mathbf{x}) \\ = & \int_\Gamma W^*_{ij}(\mathbf{x}^+,\mathbf{x})p_j(\mathbf{x})\,d\Gamma(\mathbf{x}) \\ & +\lambda\int_\Omega W^*_{i3}(\mathbf{x}^+,\mathbf{X})(N^{linear}_{\alpha\beta,\alpha}w_{3,\beta} + N^{linear}_{\alpha\beta}w_{3,\beta\alpha})(\mathbf{X})d\Omega(\mathbf{X}) \\ & +\lambda\int_\Omega W^*_{i3}(\mathbf{x}^+,\mathbf{X})q(\mathbf{X})d\Omega(\mathbf{X}) \end{aligned} \tag{5.2}$$

where $\mathbf{x}^+$ and $\mathbf{x}^-$ are referring to collocation points on the upper and lower crack surfaces respectively.

The deflection w_3 at the domain points $\mathbf{X}'$ is required as an additional equation to arrange an eigenvalue equation, by recalling equation (4.6) as follows:

$$\begin{aligned} w_3(\mathbf{X}') &= \int_\Gamma W^*_{3j}(\mathbf{X}',\mathbf{x}) p_j^{linear}(\mathbf{x}) d\Gamma - \int_\Gamma P^*_{3j}(\mathbf{X}',\mathbf{x}) w_j(\mathbf{x}) d\Gamma(\mathbf{x}) \\ &\quad + \lambda \int_\Omega W^*_{33}(\mathbf{X}',\mathbf{X}) q(\mathbf{X}) d\Omega(\mathbf{X}) \\ &\quad + \lambda \int_\Omega W^*_{33}(\mathbf{X}',\mathbf{X}) (N^{linear}_{\alpha\beta,\alpha} w_{3,\beta} + N^{linear}_{\alpha\beta} w_{3,\beta\alpha})(\mathbf{X}) d\Omega(\mathbf{X}) \end{aligned} \tag{5.3}$$

As the source point $\mathbf{x}^+$ is coincident with $\mathbf{x}^- \in \Gamma^-$, therefore the extra free terms $\frac{1}{2}u_\alpha(\mathbf{x}^-)$ and $\frac{1}{2}w_j(\mathbf{x}^-)$ will appear in equations (5.1) and (5.2). The collocation at $\mathbf{x}^-$ will also give the same integral equations as equations (5.1) and (5.2). This situation will provide an ill-conditioned system of algebraic equations.

In order to overcome the above difficulty, the traction integral equations are used for collocations at $\mathbf{x}^- \in \Gamma^-$. For collocations on $\mathbf{x}^- \in \Gamma^-$, the in-plane stress resultants boundary integral equation can be expressed as

$$\begin{aligned} &\frac{1}{2} N^{linear}_{\alpha\beta}(\mathbf{x}^-) + \frac{1}{2} N^{linear}_{\alpha\beta}(\mathbf{x}^+) + \int_\Gamma T^*_{\alpha\beta\gamma}(\mathbf{x}^-,\mathbf{x}) u_\gamma(\mathbf{x}) d\Gamma(\mathbf{x}) \\ &= \int_\Gamma U^*_{\alpha\beta\gamma}(\mathbf{x}^-,\mathbf{x}) t^{linear}_\gamma(\mathbf{x}) d\Gamma(\mathbf{x}) \end{aligned} \tag{5.4}$$

and the plate bending stress resultants boundary integral equation can be written as follows

$$\begin{aligned} &\frac{1}{2} M_{\alpha\beta}(\mathbf{x}^-) + \frac{1}{2} M_{\alpha\beta}(\mathbf{x}^+) + \int_\Gamma P^*_{\alpha\beta\gamma}(\mathbf{x}^-,\mathbf{x}) w_\gamma(\mathbf{x}) d\Gamma(\mathbf{x}) \\ &+ \int_\Gamma P^*_{\alpha\beta 3}(\mathbf{x}^-,\mathbf{x}) w_3(\mathbf{x}) d\Gamma(\mathbf{x}) \\ &= \int_\Gamma W^*_{\alpha\beta\gamma}(\mathbf{x}^-,\mathbf{x}) p_\gamma(\mathbf{x}) d\Gamma(\mathbf{x}) + \int_\Gamma W^*_{\alpha\beta 3}(\mathbf{x}^-,\mathbf{x}) p_3^{linear}(\mathbf{x}) d\Gamma(\mathbf{x}) \\ &\quad + \lambda \int_\Omega W^*_{\alpha\beta 3}(\mathbf{x}^-,\mathbf{X}) q d\Omega(\mathbf{X}) \\ &\quad + \lambda \int_\Omega W^*_{\alpha\beta 3}(\mathbf{x}^-,\mathbf{X}) (N^{linear}_{\theta\psi,\theta} w_{3,\varphi} + N^{linear}_{\theta\psi} w_{3,\varphi\theta})(\mathbf{X}) d\Omega(\mathbf{X}) \end{aligned} \tag{5.5}$$

and

$$\begin{aligned}
&\frac{1}{2}Q_\beta(\mathbf{x}^-)+\frac{1}{2}Q_\beta(\mathbf{x}^+)+\quad\int_\Gamma P^*_{3\beta\gamma}(\mathbf{x}^-,\mathbf{x})w_\gamma(\mathbf{x})d\Gamma(\mathbf{x})\\
&+\int_\Gamma P^*_{3\beta 3}(\mathbf{x}^-,\mathbf{x})w_3(\mathbf{x})d\Gamma(\mathbf{x})\\
=\quad&\int_\Gamma W^*_{3\beta\gamma}(\mathbf{x}^-,\mathbf{x})p_\gamma(\mathbf{x})d\Gamma(\mathbf{x})+\int_\Gamma W^*_{3\beta 3}(\mathbf{x}^-,\mathbf{x})p_3^{linear}(\mathbf{x})d\Gamma(\mathbf{x})\\
&+\lambda\int_\Omega W^*_{3\beta 3}(\mathbf{x}^-,\mathbf{X})qd\Omega(\mathbf{X})\\
&+\lambda\int_\Omega W^*_{3\beta 3}(\mathbf{x}^-,\mathbf{X})(N^{linear}_{\theta\psi,\theta}w_{3,\varphi}+N^{linear}_{\theta\psi}w_{3,\varphi\theta})(\mathbf{X})d\Omega(\mathbf{X})\qquad(5.6)
\end{aligned}$$

Multiplying equations (5.4 – 5.6) by the outward normal $n_\beta(\mathbf{x}^-)$ and denoting that $n_\beta(\mathbf{x}^+)=-n_\beta(\mathbf{x}^-)$, the traction integral equations for a boundary source point at lower crack surface $\mathbf{x}^-$ are as follows:

$$\begin{aligned}
&\frac{1}{2}t_\alpha^{linear}(\mathbf{x}^-)-\frac{1}{2}t_\alpha^{linear}(\mathbf{x}^+)+n_\beta(\mathbf{x}^-)\int_\Gamma T^*_{\alpha\beta\gamma}(\mathbf{x}^-,\mathbf{x})u_\gamma(\mathbf{x})d\Gamma(\mathbf{x})\\
=\quad&n_\beta(\mathbf{x}^-)\quad\int_\Gamma U^*_{\alpha\beta\gamma}(\mathbf{x}^-,\mathbf{x})t_\gamma^{linear}(\mathbf{x})d\Gamma(\mathbf{x})\qquad(5.7)
\end{aligned}$$

and

$$\begin{aligned}
&\frac{1}{2}p_\alpha(\mathbf{x}^-)-\frac{1}{2}p_\alpha(\mathbf{x}^+)+n_\beta(\mathbf{x}^-)\int_\Gamma P^*_{\alpha\beta\gamma}(\mathbf{x}^-,\mathbf{x})w_\gamma(\mathbf{x})d\Gamma(\mathbf{x})\\
&+n_\beta(\mathbf{x}^-)\int_\Gamma P^*_{\alpha\beta 3}(\mathbf{x}^-,\mathbf{x})w_3(\mathbf{x})d\Gamma(\mathbf{x})\\
=\quad&n_\beta(\mathbf{x}^-)\int_\Gamma W^*_{\alpha\beta\gamma}(\mathbf{x}^-,\mathbf{x})p_\gamma(\mathbf{x})d\Gamma(\mathbf{x})+n_\beta(\mathbf{x}')\int_\Gamma W^*_{\alpha\beta 3}(\mathbf{x}^-,\mathbf{x})p_3^{linear}(\mathbf{x})d\Gamma(\mathbf{x})\\
&+\lambda n_\beta(\mathbf{x}^-)\int_\Omega W^*_{\alpha\beta 3}(\mathbf{x}^-,\mathbf{X})qd\Omega(\mathbf{X})\\
&+\lambda n_\beta(\mathbf{x}^-)\int_\Omega W^*_{\alpha\beta 3}(\mathbf{x}^-,\mathbf{X})(N^{linear}_{\theta\psi,\theta}w_{3,\varphi}+N^{linear}_{\theta\psi}w_{3,\varphi\theta})(\mathbf{X})d\Omega(\mathbf{X})\qquad(5.8)
\end{aligned}$$

$$\frac{1}{2}p_3(\mathbf{x}^-)-\frac{1}{2}p_3(\mathbf{x}^+)+n_\beta(\mathbf{x}^-)\int_\Gamma P^*_{3\beta\gamma}(\mathbf{x}^-,\mathbf{x})w_\gamma(\mathbf{x})d\Gamma(\mathbf{x})$$

$$
\begin{aligned}
& +n_\beta(\mathbf{x}^-)\int_\Gamma P^*_{3\beta 3}(\mathbf{x}^-,\mathbf{x})w_3(\mathbf{x})d\Gamma(\mathbf{x}) \\
= \; & n_\beta(\mathbf{x}^-)\int_\Gamma W^*_{3\beta\gamma}(\mathbf{x}^-,\mathbf{x})p_\gamma(\mathbf{x})d\Gamma(\mathbf{x}) + n_\beta(\mathbf{x}^-)\int_\Gamma W^*_{3\beta 3}(\mathbf{x}^-,\mathbf{x})p_3^{linear}(\mathbf{x})d\Gamma(\mathbf{x}) \\
& +\lambda n_\beta(\mathbf{x}^-)\int_\Omega W^*_{3\beta 3}(\mathbf{x}^-,\mathbf{X})q d\Omega(\mathbf{X}) \\
& +\lambda n_\beta(\mathbf{x}^-)\int_\Omega W^*_{3\beta 3}(\mathbf{x}^-,\mathbf{X})(N^{linear}_{\theta\psi,\theta}w_{3,\varphi} + N^{linear}_{\theta\psi}w_{3,\varphi\theta})(\mathbf{X})d\Omega(\mathbf{X}) \qquad (5.9)
\end{aligned}
$$

To arrange an eigenvalue equation, the derivatives of w_3 have to be expressed in terms of $w_3(X)$, see section 4.2.3. Equation (5.2) can be written as

$$
\begin{aligned}
& \frac{1}{2}w_j(\mathbf{x}^+) + \frac{1}{2}w_j(\mathbf{x}^-) + \int_\Gamma P^*_{ij}(\mathbf{x}^+,\mathbf{x})w_j(\mathbf{x})\,d\Gamma(\mathbf{x}) \\
= \; & \int_\Gamma W^*_{ij}(\mathbf{x}^+,\mathbf{x})p_j^{linear}(\mathbf{x})\,d\Gamma(\mathbf{x}) \\
& +\lambda\int_\Omega W^*_{i3}(\mathbf{x}^+,\mathbf{X})(N^{linear}_{\alpha\beta,\alpha}\mathbf{f}(r)_{,\beta}\mathbf{F}^{-1}w_3)(\mathbf{X})d\Omega(\mathbf{X}) \\
& +\lambda\int_\Omega W^*_{i3}(\mathbf{x}^+,\mathbf{X})(N^{linear}_{\alpha\beta}\mathbf{f}(r)_{,\alpha}\mathbf{F}^{-1}\mathbf{f}(r)_{,\beta}\mathbf{F}^{-1}w_3)(\mathbf{X})d\Omega(\mathbf{X}) \\
& +\lambda\int_\Omega W^*_{i3}(\mathbf{x}^+,\mathbf{X})q(\mathbf{X})d\Omega(\mathbf{X}) \qquad (5.10)
\end{aligned}
$$

The plate bending stress resultants equations (5.5) and (5.6) are written as

$$
\begin{aligned}
& \frac{1}{2}M_{\alpha\beta}(\mathbf{x}^-) + \frac{1}{2}M_{\alpha\beta}(\mathbf{x}^+) + \int_\Gamma P^*_{\alpha\beta\gamma}(\mathbf{x}^-,\mathbf{x})w_\gamma(\mathbf{x})d\Gamma(\mathbf{x}) \\
& + \int_\Gamma P^*_{\alpha\beta 3}(\mathbf{x}^-,\mathbf{x})w_3(\mathbf{x})d\Gamma(\mathbf{x}) \\
= \; & \int_\Gamma W^*_{\alpha\beta\gamma}(\mathbf{x}^-,\mathbf{x})p_\gamma(\mathbf{x})d\Gamma(\mathbf{x}) + \int_\Gamma W^*_{\alpha\beta 3}(\mathbf{x}^-,\mathbf{x})p_3^{linear}(\mathbf{x})d\Gamma(\mathbf{x}) \\
& +\lambda\int_\Omega W^*_{\alpha\beta 3}(\mathbf{x}^-,\mathbf{X})q d\Omega(\mathbf{X}) \\
& +\lambda\int_\Omega W^*_{\alpha\beta 3}(\mathbf{x}^-,\mathbf{X})(N^{linear}_{\theta\psi,\theta}\mathbf{f}(r)_{,\psi}\mathbf{F}^{-1}w_3)(\mathbf{X})d\Omega(\mathbf{X}) \\
& +\lambda\int_\Omega W^*_{\alpha\beta 3}(\mathbf{x}^-,\mathbf{X})(N^{linear}_{\theta\psi}\mathbf{f}(r)_{,\theta}\mathbf{F}^{-1}\mathbf{f}(r)_{,\psi}\mathbf{F}^{-1}w_3)(\mathbf{X})d\Omega(\mathbf{X}) \qquad (5.11)
\end{aligned}
$$

and

$$
\begin{aligned}
&\frac{1}{2}Q_\beta(\mathbf{x}^-)+\frac{1}{2}Q_\beta(\mathbf{x}^+)+\int_\Gamma P^*_{3\beta\gamma}(\mathbf{x}^-,\mathbf{x})w_\gamma(\mathbf{x})d\Gamma(\mathbf{x})\\
&+\int_\Gamma P^*_{3\beta 3}(\mathbf{x}^-,\mathbf{x})w_3(\mathbf{x})d\Gamma(\mathbf{x})\\
=\;&\int_\Gamma W^*_{3\beta\gamma}(\mathbf{x}^-,\mathbf{x})p_\gamma(\mathbf{x})d\Gamma(\mathbf{x})+\int_\Gamma W^*_{3\beta 3}(\mathbf{x}^-,\mathbf{x})p_3^{linear}(\mathbf{x})d\Gamma(\mathbf{x})\\
&+\lambda\int_\Omega W^*_{3\beta 3}(\mathbf{x}^-,\mathbf{X})qd\Omega(\mathbf{X})\\
&+\lambda\int_\Omega W^*_{3\beta 3}(\mathbf{x}^-,\mathbf{X})(N^{linear}_{\theta\psi,\theta}\mathbf{f}(r)_{,\psi}\mathbf{F}^{-1}w_3)(\mathbf{X})d\Omega(\mathbf{X})\\
&+\lambda\int_\Omega W^*_{3\beta 3}(\mathbf{x}^-,\mathbf{X})(N^{linear}_{\theta\psi}\mathbf{f}(r)_{,\theta}\mathbf{F}^{-1}\mathbf{f}(r)_{,\psi}\mathbf{F}^{-1}w_3)(\mathbf{X})d\Omega(\mathbf{X})
\end{aligned}
\tag{5.12}
$$

Traction boundary integral equations for plate bending can be expressed as

$$
\begin{aligned}
&\frac{1}{2}p_\alpha(\mathbf{x}^-)-\frac{1}{2}p_\alpha(\mathbf{x}^+)+n_\beta(\mathbf{x}^-)\int_\Gamma P^*_{\alpha\beta\gamma}(\mathbf{x}^-,\mathbf{x})w_\gamma(\mathbf{x})d\Gamma(\mathbf{x})\\
&+n_\beta(\mathbf{x}^-)\int_\Gamma P^*_{\alpha\beta 3}(\mathbf{x}^-,\mathbf{x})w_3(\mathbf{x})d\Gamma(\mathbf{x})\\
=\;&n_\beta(\mathbf{x}^-)\int_\Gamma W^*_{\alpha\beta\gamma}(\mathbf{x}^-,\mathbf{x})p_\gamma(\mathbf{x})d\Gamma(\mathbf{x})+n_\beta(\mathbf{x}')\int_\Gamma W^*_{\alpha\beta 3}(\mathbf{x}^-,\mathbf{x})p_3(\mathbf{x})d\Gamma(\mathbf{x})\\
&+\lambda n_\beta(\mathbf{x}^-)\int_\Omega W^*_{\alpha\beta 3}(\mathbf{x}^-,\mathbf{X})qd\Omega(\mathbf{X})\\
&+\lambda n_\beta(\mathbf{x}^-)\int_\Omega W^*_{\alpha\beta 3}(\mathbf{x}^-,\mathbf{X})(N^{linear}_{\theta\psi,\theta}\mathbf{f}(r)_{,\psi}\mathbf{F}^{-1}w_3)(\mathbf{X})d\Omega(\mathbf{X})\\
&+\lambda n_\beta(\mathbf{x}^-)\int_\Omega W^*_{\alpha\beta 3}(\mathbf{x}^-,\mathbf{X})(N^{linear}_{\theta\psi}\mathbf{f}(r)_{,\theta}\mathbf{F}^{-1}\mathbf{f}(r)_{,\psi}\mathbf{F}^{-1}w_3)(\mathbf{X})d\Omega(\mathbf{X})
\end{aligned}
\tag{5.13}
$$

and

$$
\begin{aligned}
&\frac{1}{2}p_3(\mathbf{x}^-)-\frac{1}{2}p_3(\mathbf{x}^+)+n_\beta(\mathbf{x}^-)\int_\Gamma P^*_{3\beta\gamma}(\mathbf{x}^-,\mathbf{x})w_\gamma(\mathbf{x})d\Gamma(\mathbf{x})\\
&+n_\beta(\mathbf{x}^-)\int_\Gamma P^*_{3\beta 3}(\mathbf{x}^-,\mathbf{x})w_3(\mathbf{x})d\Gamma(\mathbf{x})\\
=\;&n_\beta(\mathbf{x}^-)\int_\Gamma W^*_{3\beta\gamma}(\mathbf{x}^-,\mathbf{x})p_\gamma(\mathbf{x})d\Gamma(\mathbf{x})+n_\beta(\mathbf{x}^-)\int_\Gamma W^*_{3\beta 3}(\mathbf{x}^-,\mathbf{x})p_3(\mathbf{x})d\Gamma(\mathbf{x})\\
&+\lambda n_\beta(\mathbf{x}^-)\int_\Omega W^*_{3\beta 3}(\mathbf{x}^-,\mathbf{X})qd\Omega(\mathbf{X})\\
&+\lambda n_\beta(\mathbf{x}^-)\int_\Omega W^*_{3\beta 3}(\mathbf{x}^-,\mathbf{X})(N^{linear}_{\theta\psi,\theta}\mathbf{f}(r)_{,\psi}\mathbf{F}^{-1}w_3)(\mathbf{X})d\Omega(\mathbf{X})
\end{aligned}
$$

$$+\lambda n_\beta(\mathbf{x}^-)\int_\Omega W^*_{3\beta 3}(\mathbf{x}^-,\mathbf{X})(N^{linear}_{\theta\psi}\mathbf{f}(r)_{,\theta}\mathbf{F}^{-1}\mathbf{f}(r)_{,\psi}\mathbf{F}^{-1}w_3)(\mathbf{X})d\Omega(\mathbf{X}) \quad (5.14)$$

By recalling equation (4.8), the deflection equation w_3 at the domain points $\mathbf{X}'$ as

$$\begin{aligned} w_3(\mathbf{X}') &= \int_\Gamma W^*_{3j}(\mathbf{X}',\mathbf{x})p_j^{linear}(\mathbf{x})d\Gamma(\mathbf{x}) \\ &\quad -\int_\Gamma P^*_{3j}(\mathbf{X}',\mathbf{x})w_j(\mathbf{x})d\Gamma(\mathbf{x}) \\ &\quad +\lambda\int_\Omega W^*_{33}(\mathbf{X}',\mathbf{X})q(\mathbf{X})d\Omega(\mathbf{X}) \\ &\quad +\lambda\int_\Omega W^*_{33}(\mathbf{X}',\mathbf{X})(N^{linear}_{\alpha\beta,\alpha}\mathbf{f}(r)_{,\beta}\mathbf{F}^{-1}w_3)(\mathbf{X})d\Omega(\mathbf{X}) \\ &\quad +\lambda\int_\Omega W^*_{33}(\mathbf{X}',\mathbf{X})(N^{linear}_{\alpha\beta}\mathbf{f}(r)_{,\alpha}\mathbf{F}^{-1}\mathbf{f}(r)_{,\beta}\mathbf{F}^{-1}w_3)\,(\mathbf{X})\,d\Omega(\mathbf{X}) \end{aligned} \quad (5.15)$$

By recalling equation (4.10) as

$$f_b = q + N^{linear}_{\alpha\beta,\alpha}\mathbf{f}(r)_{,\beta}\mathbf{F}^{-1}\mathbf{w}_3 + N^{linear}_{\alpha\beta}\mathbf{f}(r)_{,\alpha}\mathbf{F}^{-1}\mathbf{f}(r)_{,\beta}\mathbf{F}^{-1}\mathbf{w}_3 \quad (5.16)$$

Therefore equation (5.10) can be expressed as

$$\begin{aligned} &\frac{1}{2}w_j(\mathbf{x}^+)+\frac{1}{2}w_j(\mathbf{x}^-)+\int_\Gamma P^*_{ij}(\mathbf{x}^+,\mathbf{x})w_j\,(\mathbf{x})\,d\Gamma\,(\mathbf{x}) \\ =\ &\int_\Gamma W^*_{ij}(\mathbf{x}^+,\mathbf{x})p_j^{linear}\,(\mathbf{x})\,d\Gamma\,(\mathbf{x}) \\ &+\lambda\int_\Omega W^*_{i3}(\mathbf{x}^+,\mathbf{X})f_b(\mathbf{X})d\Omega(\mathbf{X}) \end{aligned} \quad (5.17)$$

The equations (5.11) and (5.12) are written as

$$\begin{aligned} &\frac{1}{2}M_{\alpha\beta}(\mathbf{x}^-)+\frac{1}{2}M_{\alpha\beta}(\mathbf{x}^+)+\int_\Gamma P^*_{\alpha\beta\gamma}(\mathbf{x}^-,\mathbf{x})w_\gamma(\mathbf{x})d\Gamma(\mathbf{x}) \\ &+\int_\Gamma P^*_{\alpha\beta 3}(\mathbf{x}^-,\mathbf{x})w_3(\mathbf{x})d\Gamma(\mathbf{x}) \\ =\ &\int_\Gamma W^*_{\alpha\beta\gamma}(\mathbf{x}^-,\mathbf{x})p_\gamma(\mathbf{x})d\Gamma(\mathbf{x})+\int_\Gamma W^*_{\alpha\beta 3}(\mathbf{x}^-,\mathbf{x})p_3^{linear}(\mathbf{x})d\Gamma(\mathbf{x}) \\ &+\lambda\int_\Omega W^*_{\alpha\beta 3}(\mathbf{x}^-,\mathbf{X})f_b d\Omega(\mathbf{X}) \end{aligned} \quad (5.18)$$

and

$$\begin{aligned}
&\frac{1}{2}Q_\beta(\mathbf{x}^-)+\frac{1}{2}Q_\beta(\mathbf{x}^+)+\int_\Gamma P^*_{3\beta\gamma}(\mathbf{x}^-,\mathbf{x})w_\gamma(\mathbf{x})d\Gamma(\mathbf{x})\\
&+\int_\Gamma P^*_{3\beta 3}(\mathbf{x}^-,\mathbf{x})w_3(\mathbf{x})d\Gamma(\mathbf{x})\\
=\;&\int_\Gamma W^*_{3\beta\gamma}(\mathbf{x}^-,\mathbf{x})p_\gamma(\mathbf{x})d\Gamma(\mathbf{x})+\int_\Gamma W^*_{3\beta 3}(\mathbf{x}^-,\mathbf{x})p_3(\mathbf{x})d\Gamma(\mathbf{x})\\
&+\lambda\int_\Omega W^*_{3\beta 3}(\mathbf{x}^-,\mathbf{X})f_b d\Omega(\mathbf{X})
\end{aligned}\tag{5.19}$$

The traction boundary integral equations (5.13) and (5.14)

$$\begin{aligned}
&\frac{1}{2}p_\alpha(\mathbf{x}^-)-\frac{1}{2}p_\alpha(\mathbf{x}^+)+n_\beta(\mathbf{x}^-)\int_\Gamma P^*_{\alpha\beta\gamma}(\mathbf{x}^-,\mathbf{x})w_\gamma(\mathbf{x})d\Gamma(\mathbf{x})\\
&+n_\beta(\mathbf{x}^-)\int_\Gamma P^*_{\alpha\beta 3}(\mathbf{x}^-,\mathbf{x})w_3(\mathbf{x})d\Gamma(\mathbf{x})\\
=\;&n_\beta(\mathbf{x}^-)\int_\Gamma W^*_{\alpha\beta\gamma}(\mathbf{x}^-,\mathbf{x})p_\gamma(\mathbf{x})d\Gamma(\mathbf{x})+n_\beta(\mathbf{x}')\int_\Gamma W^*_{\alpha\beta 3}(\mathbf{x}^-,\mathbf{x})p_3^{linear}(\mathbf{x})d\Gamma(\mathbf{x})\\
&+\lambda n_\beta(\mathbf{x}^-)\int_\Omega W^*_{\alpha\beta 3}(\mathbf{x}^-,\mathbf{X})f_b d\Omega(\mathbf{X})
\end{aligned}\tag{5.20}$$

$$\begin{aligned}
&\frac{1}{2}p_3(\mathbf{x}^-)-\frac{1}{2}p_3(\mathbf{x}^+)+n_\beta(\mathbf{x}^-)\int_\Gamma P^*_{3\beta\gamma}(\mathbf{x}^-,\mathbf{x})w_\gamma(\mathbf{x})d\Gamma(\mathbf{x})\\
&+n_\beta(\mathbf{x}^-)\int_\Gamma P^*_{3\beta 3}(\mathbf{x}^-,\mathbf{x})w_3(\mathbf{x})d\Gamma(\mathbf{x})\\
=\;&n_\beta(\mathbf{x}^-)\int_\Gamma W^*_{3\beta\gamma}(\mathbf{x}^-,\mathbf{x})p_\gamma(\mathbf{x})d\Gamma(\mathbf{x})+n_\beta(\mathbf{x}^-)\int_\Gamma W^*_{3\beta 3}(\mathbf{x}^-,\mathbf{x})p_3^{linear}(\mathbf{x})d\Gamma(\mathbf{x})\\
&+\lambda n_\beta(\mathbf{x}^-)\int_\Omega W^*_{3\beta 3}(\mathbf{x}^-,\mathbf{X})f_b d\Omega(\mathbf{X})
\end{aligned}\tag{5.21}$$

The deflection equation w_3 at the domain points $\mathbf{X}'$ can be written as follows

$$\begin{aligned}
w_3(\mathbf{X}') \;=\;&\int_\Gamma W^*_{3j}(\mathbf{X}',\mathbf{x})p_j^{linear}(\mathbf{x})d\Gamma(\mathbf{x})\\
&-\int_\Gamma P^*_{3j}(\mathbf{X}',\mathbf{x})w_j(\mathbf{x})d\Gamma(\mathbf{x})\\
&+\lambda\int_\Omega W^*_{33}(\mathbf{X}',\mathbf{X})f_b\;d\Omega(\mathbf{X})
\end{aligned}\tag{5.22}$$

Equations (5.1) and (5.2) and (5.7, 5.20, 5.21) represent displacement and traction integral equations respectively on the crack surfaces, and together with the use of the displacement integral equations in equation (4.1) and (4.9), that is

$$c_{\theta\alpha}\left(\mathbf{x}'\right)u_\alpha(\mathbf{x}') + \int_\Gamma T^*_{\theta\alpha}(\mathbf{x}',\mathbf{x})u_\alpha(\mathbf{x})d\Gamma(\mathbf{x})$$

$$= \int_\Gamma U^*_{\theta\alpha}(\mathbf{x}',\mathbf{x})t^{linear}_\alpha(\mathbf{x})d\Gamma(\mathbf{x}) \tag{5.23}$$

and

$$c_{ij}(\mathbf{x}')w_j(\mathbf{x}') + \int_\Gamma P^*_{ij}(\mathbf{x}',\mathbf{x})w_j\left(\mathbf{x}\right)d\Gamma\left(\mathbf{x}\right) = \int_\Gamma W^*_{ij}(\mathbf{x}',\mathbf{x})p^{linear}_j\left(\mathbf{x}\right)d\Gamma\left(\mathbf{x}\right)$$

$$+\lambda\int_\Omega W^*_{i3}(\mathbf{x}',\mathbf{X})f_b(\mathbf{X})d\Omega(\mathbf{X}) \tag{5.24}$$

for collocation points on the rest of the boundary Γ_b, form the dual boundary integral formulation.

Domain integrals which appear in the formulation are transferred to the boundary by employing the dual reciprocity technique as described in sections 3.5 and 4.4. As the source point $\mathbf{x}^+ \in \Gamma^+$ is coincident with $\mathbf{x}^- \in \Gamma^-$, it is important to note when the dual reciprocity technique is applied to a structure containing cracks, domain integrals will contain extra free terms as in equations (5.17 – 5.19).
The domain integral in equation (5.17) is rewritten as:

$$\begin{aligned}
&\int_\Omega W^*_{i3}(\mathbf{x}',\mathbf{X})f_b(X)d\Omega(X) \\
&= \sum_{m=1}^{M}[\frac{1}{2}\hat{w}_{mj}(\mathbf{x}^+) + \frac{1}{2}\hat{w}_{mj}(\mathbf{x}^-) + \int_\Gamma P^*_{ij}(\mathbf{x}',\mathbf{x})\hat{w}_{mj}(\mathbf{x})d\Gamma(\mathbf{x}) \\
&\quad - \int_\Gamma W^*_{ij}(\mathbf{x}',\mathbf{x})\hat{p}_{mj}(\mathbf{x})d\Gamma(\mathbf{x})]\mathbf{F}^{-1}f_b
\end{aligned} \tag{5.25}$$

The domain integral in equation (5.18) is rewritten as:

$$\int_\Omega W^*_{\alpha\beta 3}(\mathbf{x}^-,\mathbf{X})f_{b2}(\mathbf{X})d\Omega(\mathbf{X}) \;=\; \{\sum_{m=1}^{M}[\,\frac{1}{2}\hat{M}_{m\alpha\beta}(\mathbf{x}^-) + \frac{1}{2}\hat{M}_{m\alpha\beta}(\mathbf{x}^+)$$

$$
\begin{aligned}
&+\int_{\Gamma} P^*_{\alpha\beta\gamma}(\mathbf{x}^-,\mathbf{x})\hat{w}_{m\gamma}(\mathbf{x})d\Gamma(\mathbf{x}) \\
&+\int_{\Gamma} P^*_{\alpha\beta 3}(\mathbf{x}^-,\mathbf{x})\hat{w}_{m3}(\mathbf{x})d\Gamma(\mathbf{x}) \\
&-\int_{\Gamma} W^*_{\alpha\beta\gamma}(\mathbf{x}^-,\mathbf{x})\hat{p}_{m\gamma}(\mathbf{x})d\Gamma(\mathbf{x}) \qquad (5.26) \\
&-\int_{\Gamma} W^*_{\alpha\beta 3}(\mathbf{x}^-,\mathbf{x})\hat{p}_{m3}(\mathbf{x})d\Gamma(\mathbf{x})]\mathbf{F}^{-1}f_b\}
\end{aligned}
$$

The domain integral in equation (5.19) is rewritten as:

$$
\begin{aligned}
\int_{\Omega} W^*_{3\beta 3}(\mathbf{x}^-,\mathbf{X})f_{b2}(\mathbf{X})d\Omega(\mathbf{X}) \;=\; &\{\sum_{m=1}^{M}[\frac{1}{2}\hat{Q}_{m\beta}(\mathbf{x}^-)+\frac{1}{2}\hat{Q}_{m\beta}(\mathbf{x}^+) \\
&+\int_{\Gamma} P^*_{3\beta\gamma}(\mathbf{x}^-,\mathbf{x})\hat{w}_{m\gamma}(\mathbf{x})d\Gamma(\mathbf{x}) \\
&+\int_{\Gamma} P^*_{3\beta 3}(\mathbf{x}^-,\mathbf{x})\hat{w}_{m3}(\mathbf{x})d\Gamma(\mathbf{x}) \\
&-\int_{\Gamma} W^*_{3\beta\gamma}(\mathbf{x}^-,\mathbf{x})\hat{p}_{m\gamma}(\mathbf{x})d\Gamma(\mathbf{x}) \qquad (5.27) \\
&-\int_{\Gamma} W^*_{3\beta 3}(\mathbf{x}^-,\mathbf{x})\hat{p}_{m3}(\mathbf{x})d\Gamma(\mathbf{x})]\mathbf{F}^{-1}f_b\}
\end{aligned}
$$

5.3 Numerical Implementation

5.3.1 Crack modelling strategy

As described in Chapters 3 and 4, to discretise the boundary including crack surfaces into elements, isoparametric quadratic elements are used. Discontinuous elements as shown in Figure 5-2 are used for modelling the crack surfaces to satisfy the continuity requirements of displacements and tractions at collocation points for displacement and traction integral equations.

The general modelling strategies used in this work are similar to those used in [63] and can be summarized as follows:

- crack boundaries are modelled with discontinuous quadratic elements, as shown in Figure 5-3, in such a way that each node of one of the crack surfaces is coincident with the node on the opposite surfaces;

- the traction equations (5.7), (5.20) and (5.21) are applied for collocation on one of the crack surfaces;

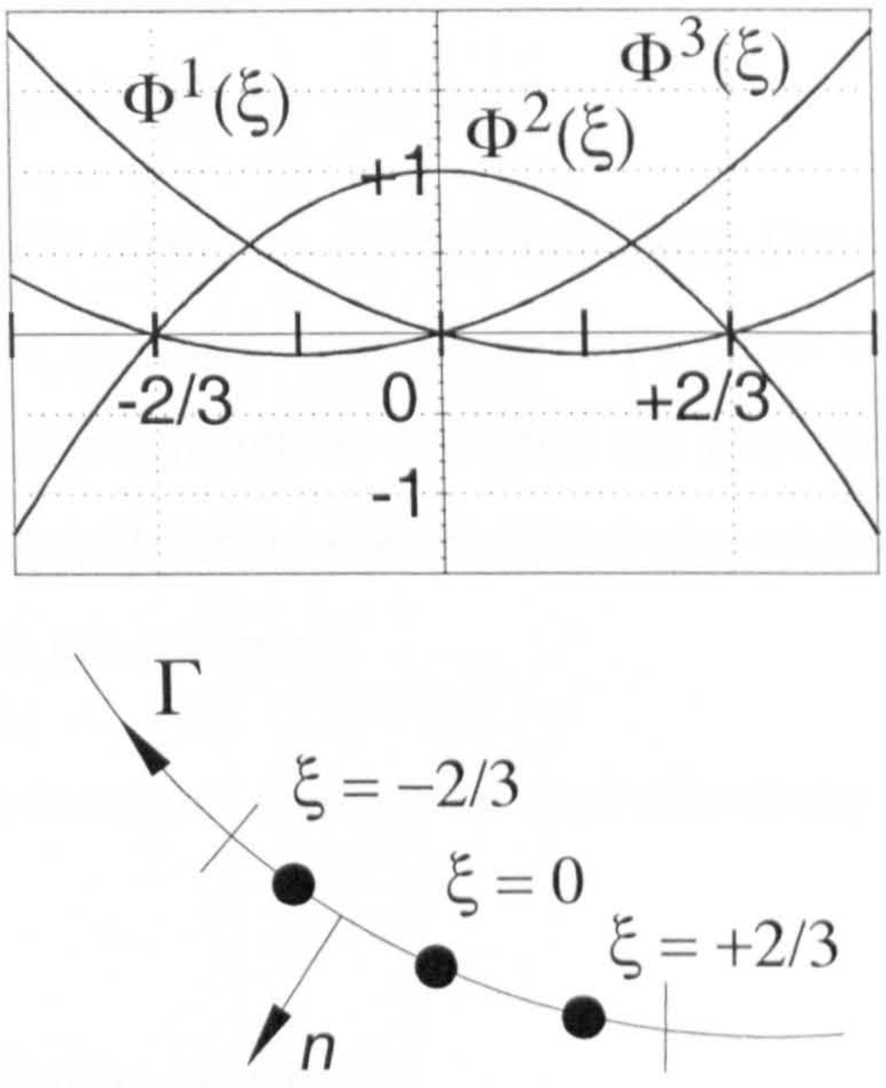

Figure 5-2: Shape functions for discontinous elements.

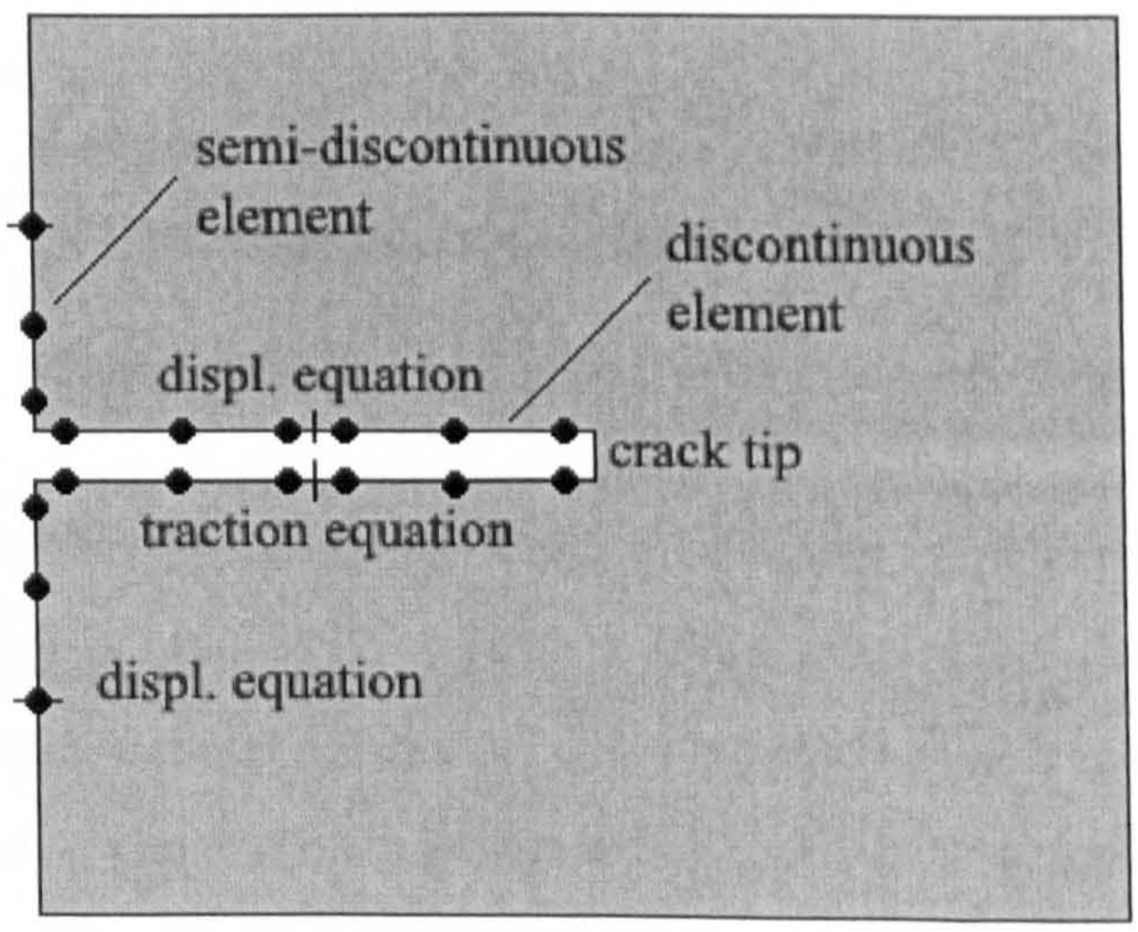

Figure 5-3: A cracked plate.

- the displacement equations (5.1) and (5.17) are applied for collocation on the opposite crack surface and for the other non-crack boundaries the displacement equations (5.23) and (5.24) are employed;

- continuous quadratic elements are applied along the remaining boundary of the body, except at the intersection between a crack and an edge, where discontinuous or semi-discontinuous elements are required on the edge in order to avoid a common node at intersection, and also at boundary corners, where semi-discontinuous are preferred.

This simple strategy is robust and can be used effectively to model general crack problems by DBEM.

5.3.2 Special crack-tip elements

To deal with the $\sqrt{r}$ behaviour of displacement fields near the crack tip, a set of special shape function has been used for crack tip elements similar to those reported by Mi and Aliabadi [57] for three dimensional elasticity problems. In this work, a discontinuous quadratic element with $\xi = -\frac{2}{3}, 0, +\frac{2}{3}$ is used. The quadratic shape function Φ_D^m for a discontinuous quadratic element are given as:

$$\begin{aligned} \Phi_D^1(\xi) &= \frac{3}{4}\xi(\frac{3}{2}\xi - 1) \\ \Phi_D^2(\xi) &= (1 - \frac{3}{2}\xi)(1 + \frac{3}{2}\xi) \\ \Phi_D^3(\xi) &= \frac{3}{4}\xi(\frac{3}{2}\xi + 1) \end{aligned} \tag{5.28}$$

The variation of the displacements along the element is required to have the form of $u(\xi) = u^\alpha N^\alpha(\xi) = a_1^\alpha + a_2^\alpha\sqrt{r} + a_3^\alpha(r)$. If the crack tip is located at $\xi = -1$, then the shape function in the form $N^\alpha(\xi) = a_1^\alpha + a_2^\alpha\sqrt{1+\xi} + a_3^\alpha(1+\xi)$ is used. On the other hand, if the crack tip is located at $\xi = +1$, then the shape function in the form $N^\alpha(\xi) = b_1^\alpha + b_2^\alpha\sqrt{1-\xi} + b_3^\alpha(1-\xi)$ is used. If $N^\alpha(\xi)$ is set to equal 1 at the collocation node α, and 0 at the other nodes, a set of linear system of equations are established and the unknown constants can be obtained.

Therefore, the shape functions for crack tip elements with the crack tip located

at $\xi = -1$ are

$$N_1^{(-1)}(\xi) = \frac{3}{2}\frac{\left(3-\sqrt{15}\right)\xi + 2\sqrt{1+\xi} - 2}{\sqrt{15}+\sqrt{3}-6} \tag{5.29}$$

$$N_2^{(-1)}(\xi) = \frac{3\left(\sqrt{15}-\sqrt{3}\right)\xi - 12\sqrt{1+\xi} + 2\left(\sqrt{15}+\sqrt{3}\right)}{2\left(\sqrt{15}+\sqrt{3}-6\right)} \tag{5.30}$$

$$N_3^{(-1)}(\xi) = \frac{3}{2}\frac{\left(\sqrt{3}-3\right)\xi + 2\sqrt{1+\xi} - 2}{\sqrt{15}+\sqrt{3}-6} \tag{5.31}$$

and for crack tip element with the crack tip located at $\xi = +1$ are

$$N_1^{(+1)}(\xi) = \frac{3}{2}\frac{\left(3-\sqrt{3}\right)\xi + 2\sqrt{1-\xi} - 2}{\sqrt{15}+\sqrt{3}-6} \tag{5.32}$$

$$N_2^{(+1)}(\xi) = \frac{3\left(\sqrt{3}-\sqrt{15}\right)\xi - 12\sqrt{1-\xi} + 2\left(\sqrt{15}+\sqrt{3}\right)}{2\left(\sqrt{15}+\sqrt{3}-6\right)} \tag{5.33}$$

$$N_3^{(+1)}(\xi) = \frac{3}{2}\frac{\left(\sqrt{15}-3\right)\xi + 2\sqrt{1-\xi} - 2}{\sqrt{15}+\sqrt{3}-6} \tag{5.34}$$

5.3.3 Crack modelling consideration of the dual reciprocity technique

In the implementation of the dual reciprocity technique for the dual boundary element analysis, difficulties will appear due to the coincidence nodes along crack surfaces. The existence of two coincident collocation points would make the coefficient matrix **F** singular and requires a special treatment. However, as will be shown next, this difficulty is overcome due to the cancelling of the integrals over the two crack surfaces.

Similar to the discussion reported in Salgado and Aliabadi [73], the contribution of the integration over crack boundaries can be calculated by considering a collocation point $\mathbf{x}'$ and two coincidence nodes $\mathbf{x}^-$ and $\mathbf{x}^+$ on opposite crack surfaces. The integrals can be written in matrix form as

$$\Psi \;=\; \left[\; \mathbf{H}(\mathbf{x}',\mathbf{x}^+) \quad \mathbf{H}(\mathbf{x}',\mathbf{x}^-) \;\right] \left\{ \begin{array}{c} \hat{\mathbf{w}}_k(\mathbf{x}',\mathbf{x}^+) \\ \hat{\mathbf{w}}_k(\mathbf{x}',\mathbf{x}^-) \end{array} \right\} \tag{5.35}$$

$$-\left[\begin{array}{cc} \mathbf{G}(\mathbf{x}',\mathbf{x}^+) & \mathbf{G}(\mathbf{x}',\mathbf{x}^-) \end{array}\right]\left\{\begin{array}{c} \hat{\mathbf{p}}_k(\mathbf{x}',\mathbf{x}^+) \\ \hat{\mathbf{p}}_k(\mathbf{x}',\mathbf{x}^-) \end{array}\right\}$$

It can be observed that particular solutions and fundamental solutions have properties as follows:

$$\begin{array}{lll}
\hat{p}_k(\mathbf{x}',\mathbf{x}^+) = -\hat{p}_k(\mathbf{x}',\mathbf{x}^-); & \text{and} & \hat{t}_\beta(\mathbf{x}',\mathbf{x}^+) = -\hat{t}_\beta(\mathbf{x}',\mathbf{x}^-) \\
\hat{w}_k(\mathbf{x}',\mathbf{x}^+) = \hat{w}_k(\mathbf{x}',\mathbf{x}^-); & \text{and} & \hat{u}_\beta(\mathbf{x}',\mathbf{x}^+) = \hat{u}_\beta(\mathbf{x}',\mathbf{x}^-) \\
P^*_{ik}(\mathbf{x}',\mathbf{x}^+) = -P^*_{ik}(\mathbf{x}',\mathbf{x}^-); & \text{and} & T^*_{\alpha\beta}(\mathbf{x}',\mathbf{x}^+) = -T^*_{\alpha\beta}(\mathbf{x}',\mathbf{x}^-) \\
P^*_{i\beta k}(\mathbf{x}',\mathbf{x}^+) = -P^*_{i\beta k}(\mathbf{x}',\mathbf{x}^-); & \text{and} & T^*_{\alpha\beta\gamma}(\mathbf{x}',\mathbf{x}^+) = -T^*_{\alpha\beta\gamma}(\mathbf{x}',\mathbf{x}^-) \\
W^*_{ik}(\mathbf{x}',\mathbf{x}^+) = W^*_{ik}(\mathbf{x}',\mathbf{x}^-); & \text{and} & U^*_{\alpha\beta}(\mathbf{x}',\mathbf{x}^+) = U^*_{\alpha\beta}(\mathbf{x}',\mathbf{x}^-) \\
W^*_{i\beta k}(\mathbf{x}',\mathbf{x}^+) = W^*_{i\beta k}(\mathbf{x}',\mathbf{x}^-); & \text{and} & U^*_{\alpha\beta\gamma}(\mathbf{x}',\mathbf{x}^+) = U^*_{\alpha\beta\gamma}(\mathbf{x}',\mathbf{x}^-)
\end{array} \tag{5.36}$$

Substituting properties in equation (5.36) into the matrix in equation (5.35), it can be seen that the contribution of the integration over crack boundaries to the coefficient matrix is equal to zero. Therefore, it is not necessary to include the crack boundaries in the integration process of domain integrals. In that case, the difficulties mentioned above are eliminated since the exclusion of crack boundary also means that there will be no dual reciprocity collocation points along the crack boundaries.

5.3.4 Treatment of the singularities

There are three different orders of singularities occurring in the dual boundary integral equations, i.e. weakly singular, strongly singular and hypersingular integrals. The weakly singular integrals are cancelled using a bi-cubic nonlinear coordinate transformation as described in Appendix C. Strongly singular integrals along the non-crack boundaries are evaluated indirectly using the consideration of generalised rigid body movements as described in Chapter 3.

On the crack boundaries, the strongly singular and the hypersingular integrals are evaluated using a singularity subtraction method based on the Taylor series expansion around the singular point for bending and shear integrals, and subsequently, the singular terms are integrated analytically [5]. For straight elements along the

crack, the evaluation of the strongly singular and the hypersingular integrals in membrane integral equations are most effectively carried out using direct analytic integrations. Details of the singularity subtraction method and direct analytic integrations are described in Appendix C.

5.4 Numerical Procedure

Similar to the procedures described in Chapter 4, a numerical procedure of cracked plate buckling analysis by the dual boundary element method is presented. The first step is to solve the dual boundary integrals of in-plane problem and then calculate the stress resultants at the domain points. The second step is to solve the dual boundary integral formulation for buckling problems.

5.4.1 Determination of the in-plane stresses

After discretising and introducing boundary conditions into equations (4.1), (5.1) and (5.7), the system of algebraic equation can be arranged in terms of the known and unknown quantities as follows:

$$[\mathbf{A}]\{\mathbf{X}\} = \{\mathbf{F}\} \tag{5.37}$$

where matrix $\mathbf{X}$ contains the unknown vectors of displacements $\mathbf{u}$ and tractions $\mathbf{t}$. The vector $\mathbf{F}$ is obtained by multiplying the related coefficient matrices by the known vectors of displacements $\mathbf{u}$ or tractions $\mathbf{t}$.

Once equation (5.37) has been solved, in-plane stresses N_{11}, N_{12}, and N_{22} in the domain (equation (4.3)) can be calculated. The stresses are required to solve the cracked plate buckling problem.

5.4.2 Solving the plate buckling problem

After applying the boundary conditions to equations (5.24), (5.17), (5.20) and (5.21), they can be written in a matrix form as:

$$[\mathrm{C}]\{\mathrm{w}\} + [\mathrm{H}^p]\{\mathrm{w}\} = [\mathrm{G}^p]\{\mathrm{p}\} + \lambda[\mathrm{G}^p_{eq}]\{\mathrm{f}_b\} \tag{5.38}$$

in which $\mathbf{H}^p$and $\mathbf{G}^p$ are boundary element influence matrices for plate bending, $\hat{\mathrm{w}}$ and $\hat{\mathrm{p}}$ are matrices of node values of particular solution on the boundary and $\mathbf{G}^p_{eq} = (\mathbf{H}^p\hat{\mathbf{w}} - \mathbf{G}^p\hat{\mathbf{p}})\mathbf{F}^{-1}$. The $q(\mathrm{X})$ quantities in the equations (??) and (??) are set to zero. Then, the term $f_b(\mathrm{X})$ in equation (5.16) can be expressed in term of $w_3(\mathrm{X})$, as follows

$$f_b(\mathrm{X}) = \mathrm{f}_{bw}(\mathrm{X})w_3(\mathrm{X}) \tag{5.39}$$

where $\mathrm{f}_{bw} = N^{linear}_{\alpha\beta,\alpha}\mathrm{f}(r)_{,\beta}\mathbf{F}^{-1} + N^{linear}_{\alpha\beta}\mathrm{f}(r)_{,\alpha}\mathrm{f}(r)_{,\beta}\mathbf{F}^{-1}$

Equation (5.38) can be arranged in a similar manner as equation (5.37), and give

$$[\mathrm{B}]_{3N\times 3N}\{\mathrm{Y}\}_{3N} = \lambda[\mathrm{K}]_{3N\times L}\{\mathrm{w}_3\}_L \tag{5.40}$$

$$\mathbf{K} = \mathbf{G}^p_{eq}\mathrm{f}_{bw} \tag{5.41}$$

where the matrix B contains the coefficient matrices $\mathbf{H}^p$ and $\mathbf{G}^p$. N and L are the number of boundary elements and domain points, respectively.

The equation (5.22) can be also written in matrix form as follows:

$$[\mathrm{I}]\{\mathrm{w}_3\}_L = [\mathrm{BB}]_{L\times 3N}\{\mathrm{Y}\}_{3N} + \lambda[\mathrm{KK}]_{L\times L}\{\mathrm{w}_3\}_L \tag{5.42}$$

where matrix [I] is an identity matrix. The matrix [BB] contains coefficient matrices related to fundamental solutions. The matrix [KK] are obtained by multiplication of coefficient matrices related to the fundamental solutions with matrix f_{bw}.

The equation (5.40) can be rearranged in term of unknown vector $\{\mathrm{Y}\}_{3N}$,

$$\{\mathrm{Y}\}_{3N} = \lambda[\mathrm{B}]^{-1}_{3N\times 3N}[\mathrm{K}]_{3N\times L}\{\mathrm{w}_3\}_L \tag{5.43}$$

where matrix $\mathbf{B}^{-1}$ is the inverse matrix of $\mathbf{B}$.

The substitution of the equation (5.43) into the equation (5.42) yields:

$$\begin{aligned}[\mathbf{I}]\{\mathbf{w_3}\}_L &= \lambda[\mathbf{BB}]_{L\times 3N}[\mathbf{B}]^{-1}_{3N\times 3N}[\mathbf{K}]_{3N\times L}\{\mathbf{w_3}\}_L \\ &\quad +\lambda[\mathbf{KK}]_{L\times L}\{\mathbf{w_3}\}_L \end{aligned} \tag{5.44}$$

Then,

$$\begin{aligned}[\mathbf{I}]\{\mathbf{w_3}\}_L &= \lambda([\mathbf{BB}]_{L\times 3N}[\mathbf{B}]^{-1}_{3N\times 3N}[\mathbf{K}]_{3N\times L} \\ &\quad +[\mathbf{KK}]_{L\times L})\{\mathbf{w_3}\}_L \end{aligned} \tag{5.45}$$

The equation (5.45) can be written as a standard eigenvalue problem equation as follows:

$$([\psi]-\frac{1}{\lambda}[\mathbf{I}])\{\mathbf{w_3}\}_L = 0 \tag{5.46}$$

where $[\psi] = [\mathbf{BB}]_{L\times 3N}[\mathbf{B}]^{-1}_{3N\times 3N}[\mathbf{K}]_{3N\times L} + [\mathbf{KK}]_{L\times L}$.

Analysis of shear deformable cracked plate buckling problems has been presented as a standard eigenvalue problem. Buckling coefficients correspond to the problem can be obtained by the solution of equation (5.46).

5.5 Numerical Examples

Several numerical examples are presented to demonstrate the ability of the proposed method to solve cracked plate buckling problems with different geometries, loadings and boundary conditions. The buckling coefficients K are defined as described in section 4.6. The calculated values of K are compared with analytical [78] and differential quadrature element method [54] results.

5.5.1 Convergence study of simply supported rectangular cracked plates subjected to compression loads

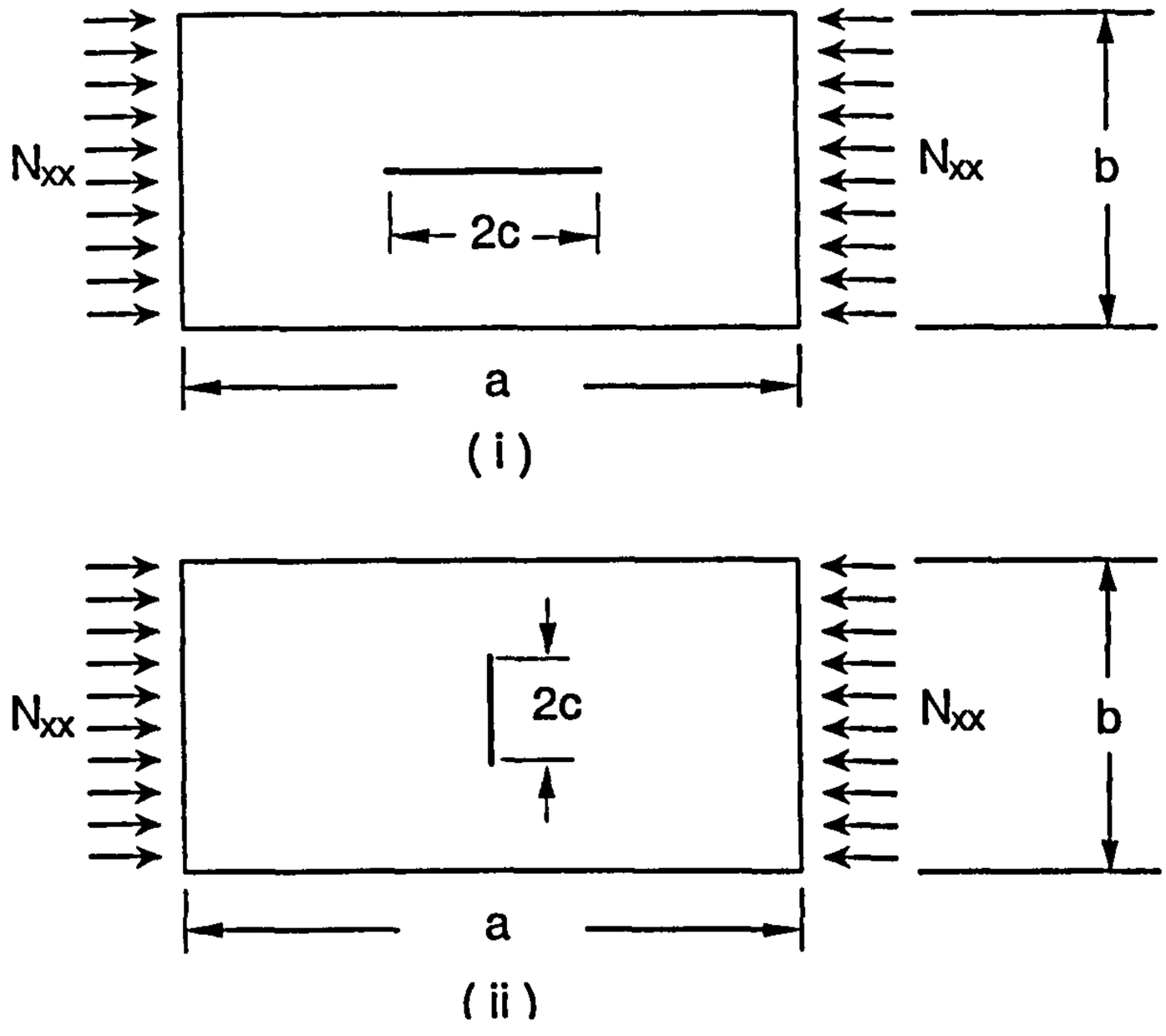

Figure 5-4: Rectangular plates with a central crack subjected to compression loads.

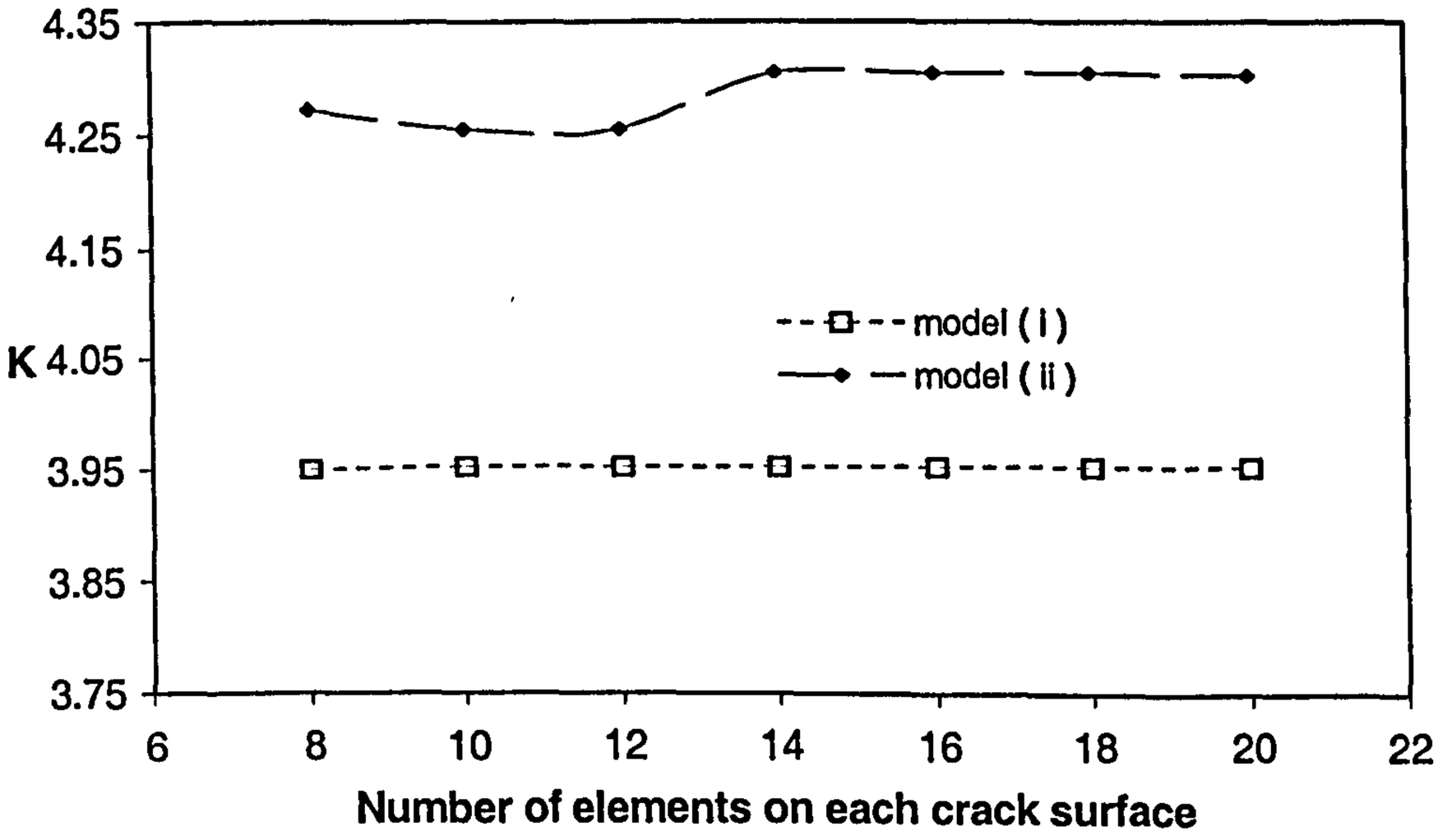

Figure 5-5: Convergence study for the problem of cracked plates buckling.

In this example, convergence of the presented formulation is assessed by solving a simply supported cracked plate as shown in Figure 5-4. Two configurations of rectangular plate with aspect ratio $a/b = 2$ are considered here: (i) a longitudinal central crack with $2c/a = 0.25$ and (ii) a transverse central crack with $2c/b = 0.25$. Both models are discretised into 8 elements on the long sides and 4 elements on the short sides. Each model has different meshes on the crack surfaces. The BEM results are shown in Figure 5-5. As it can be seen, the buckling coefficient for model (i) in Figure 5-4 is not sensitive to the number of elements on the crack surfaces and convergence is achieved with only 8 elements on the crack surfaces. The convergence for model (ii) can be achieved after the crack surfaces are modelled using 14 elements.

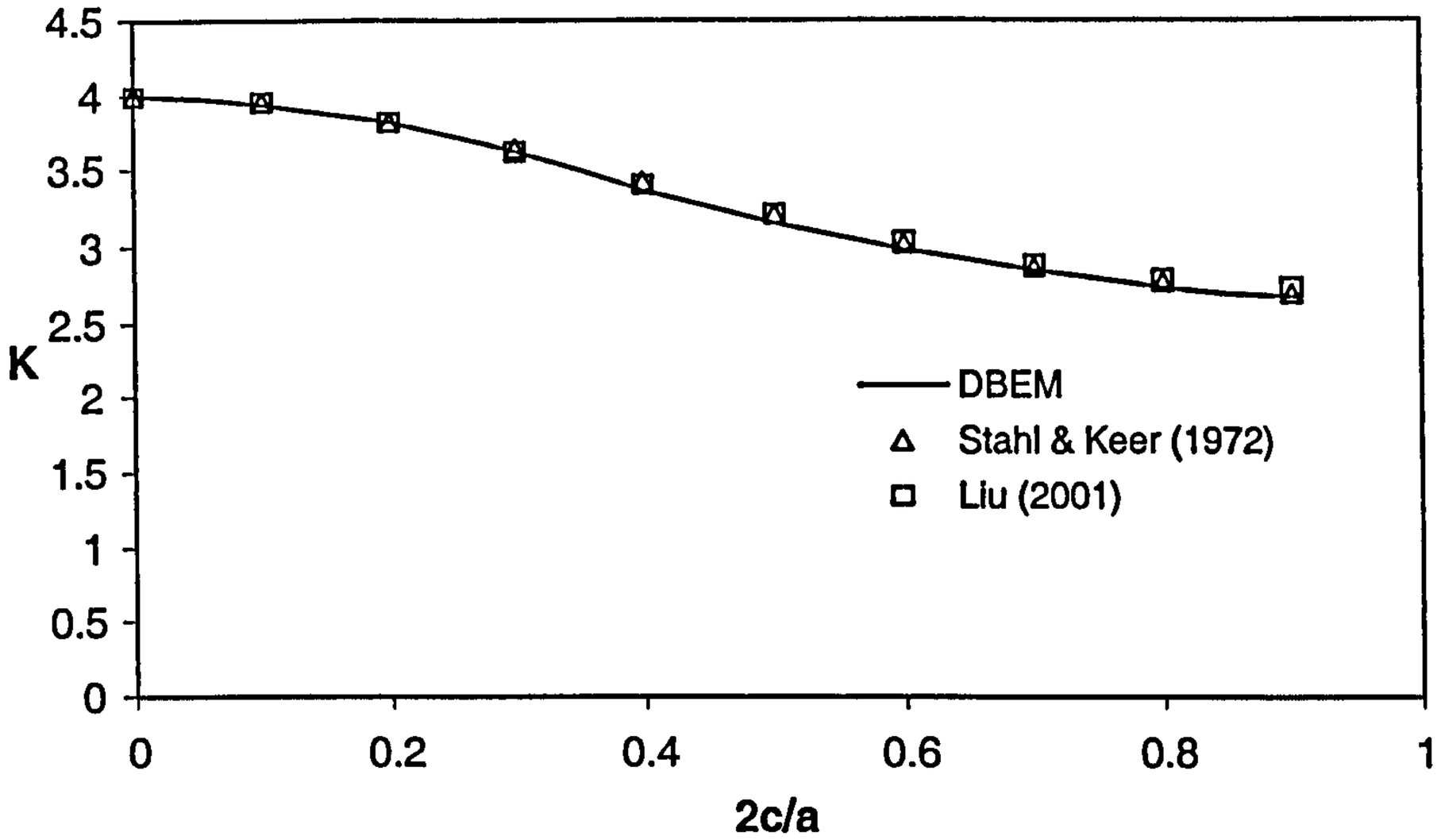

Figure 5-6: Variation of buckling coefficients for the plate (aspect ratio $a/b = 1$) with a longitudinal central crack.

5.5.2 Simply supported rectangular plates with a longitudinal central crack

Here, the problem of the rectangular plate with a longitudinal central crack subjected to compression loads is studied again. The model is similar to that shown in Figure 5-4 (i) but the aspect ratio of the plate is varied. Two configurations are considered: (a) the plate with aspect ratio $a/b = 1$ and (b) the plate with aspect ratio $a/b = 2$. Stahl and Keer [78] have analysed the first case. Both cases were analysed by Liu [54]. Buckling coefficients for different aspect ratios of crack length to the length of plate $2c/a$ are presented in Figures 5-6 and 5-7. Figures 5-8 and 5-9 present the change in the buckling modes of rectangular plate with aspect ratio $a/b = 2$. For the case of short cracks (aspect ratio $2c/a$ up to 0.25), the buckling modes are illustrated in Figure 5-8. When the aspect ratio $2c/a$ is greater than 0.25, the buckling modes change as shown in Figure 5-9. It can be seen from the Figures that the present results are in very good agreements (less than 1% difference) with those presented in Stahl and Keer [78] and Liu [54].

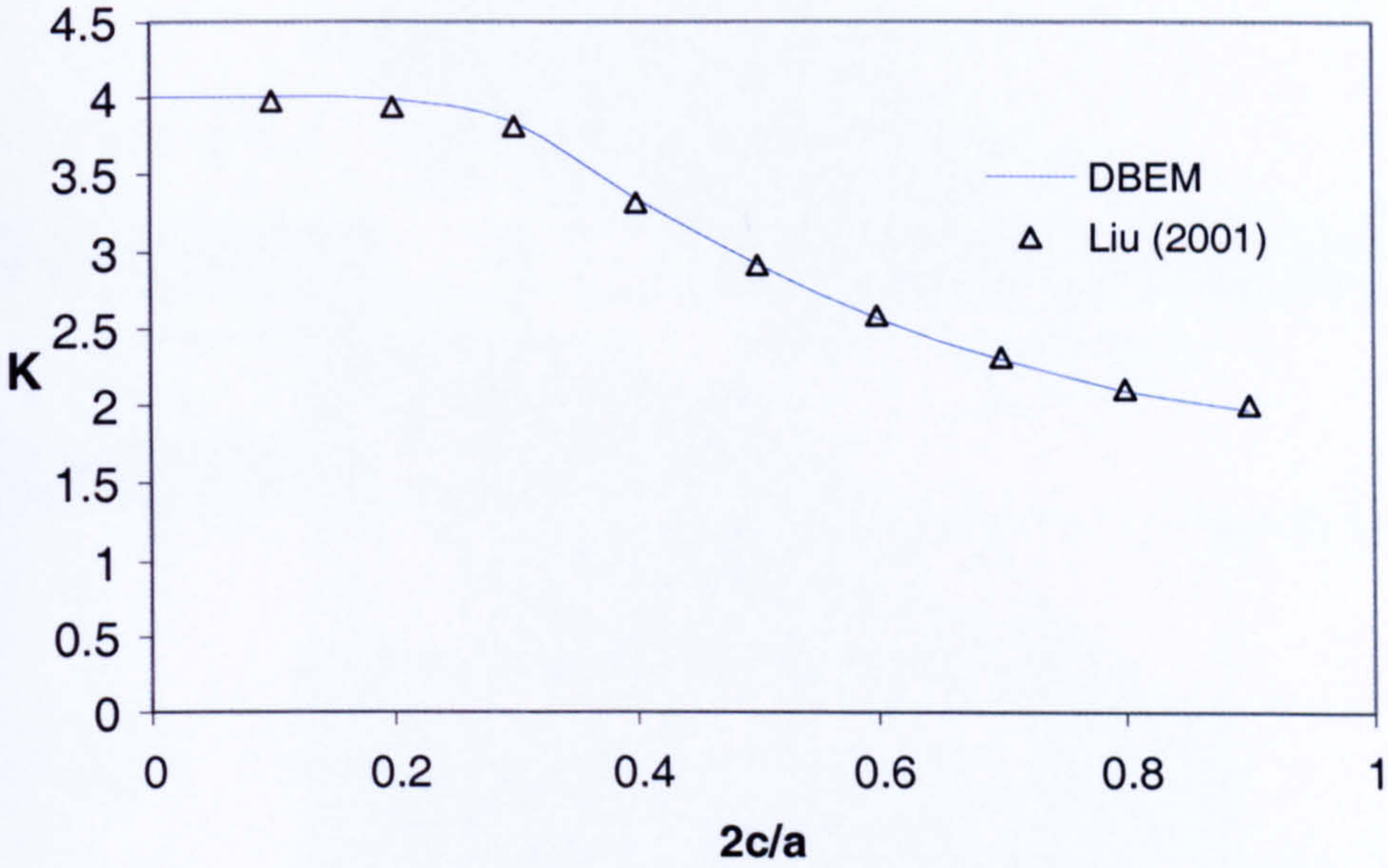

Figure 5-7: Variation of buckling coefficients for the plate (aspect ratio $a/b = 2$) with a longitudinal central crack.

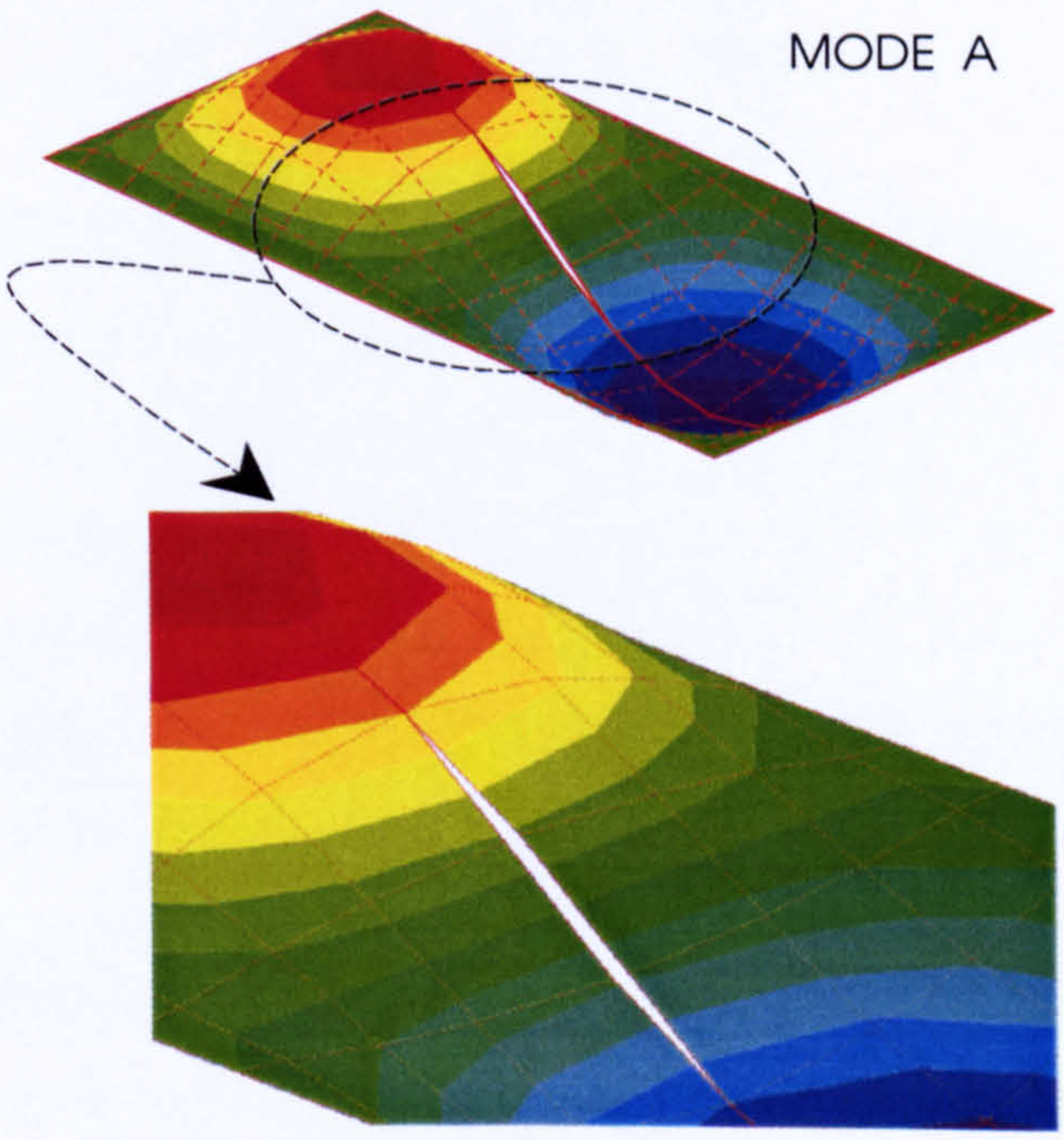

Figure 5-8: Mode A: initial mode of simply supported rectangular plate with a longitudinal central crack.

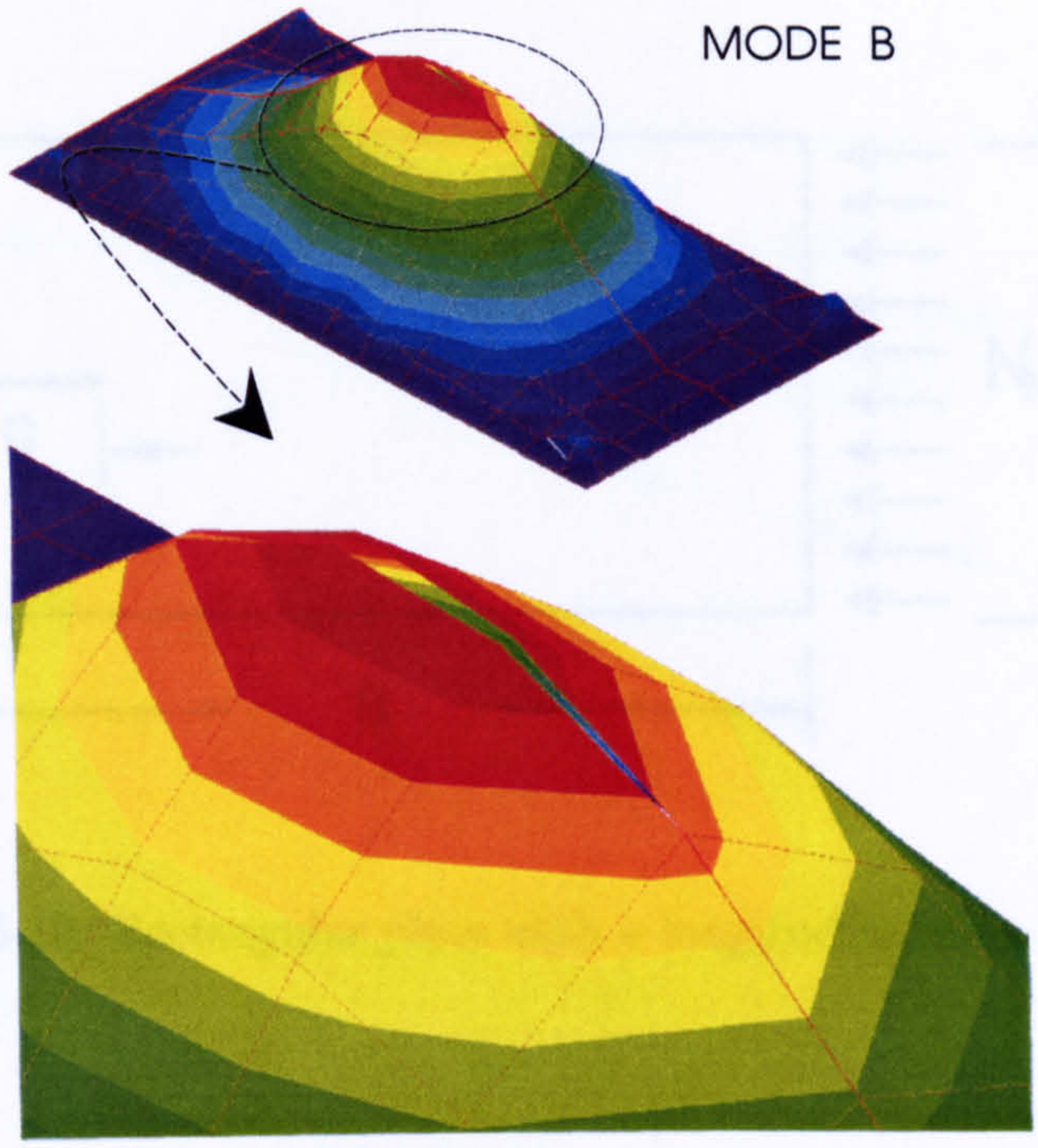

Figure 5-9: Mode B: second mode of simply supported rectangular plate with a longitudinal central crack.

5.5.3 Simply supported rectangular plates with a longitudinal edge crack

In this example, a rectangular plate with a longitudinal edge crack subjected to compression loads is presented. The model is shown in Figure 5-10. Two configurations of edge crack plate are considered: (a) aspect ratio $a/b = 1$ and (b) aspect ratio $a/b = 2$. The second case has been analysed by Stahl and Keer [78], and Liu [54] has investigated both cases. Buckling coefficients for different aspect ratios of crack length to the length of plate c/a are presented in Figures 5-11 and 5-12. It can be seen from the Figures that good agreements (less 1.5% difference) are achieved with those presented in Stahl and Keer [78] and Liu [54].

5.5.4 Rectangular plates with a longitudinal central crack and different boundary conditions

A rectangular plate with a longitudinal central crack subjected to compression

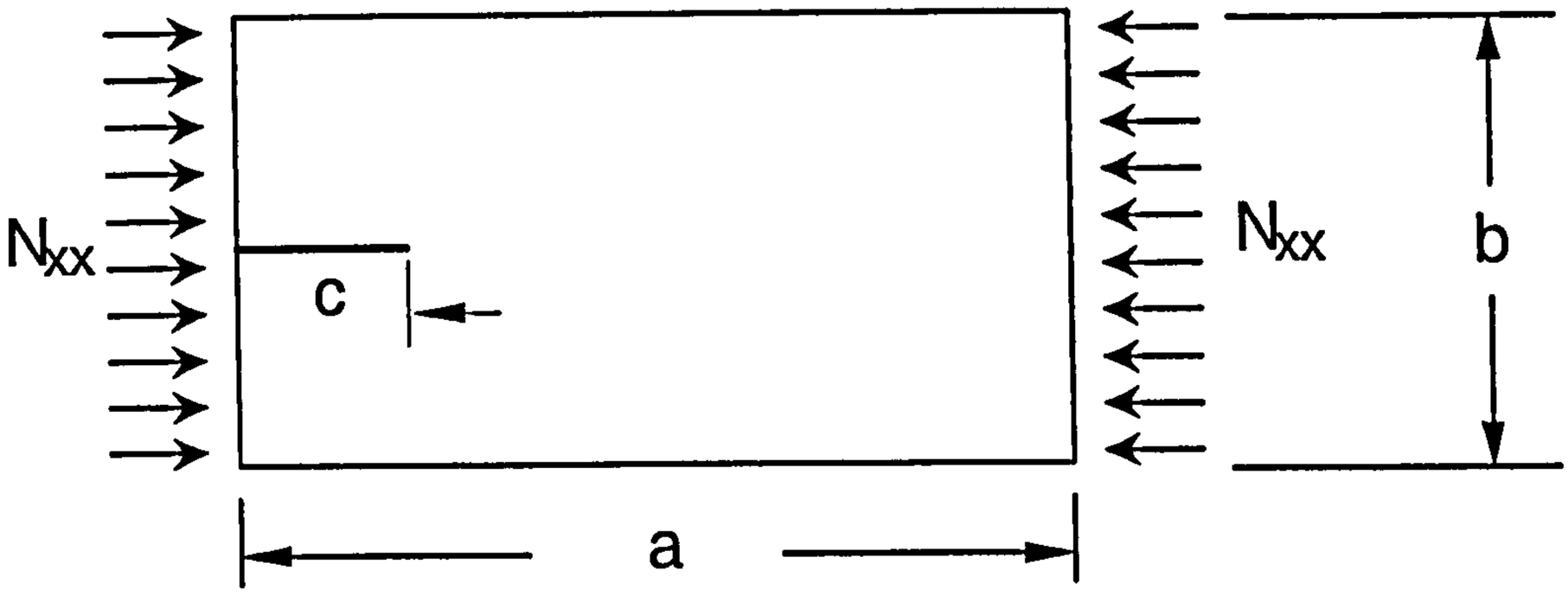

Figure 5-10: Rectangular plate with a longitudinal edge crack.

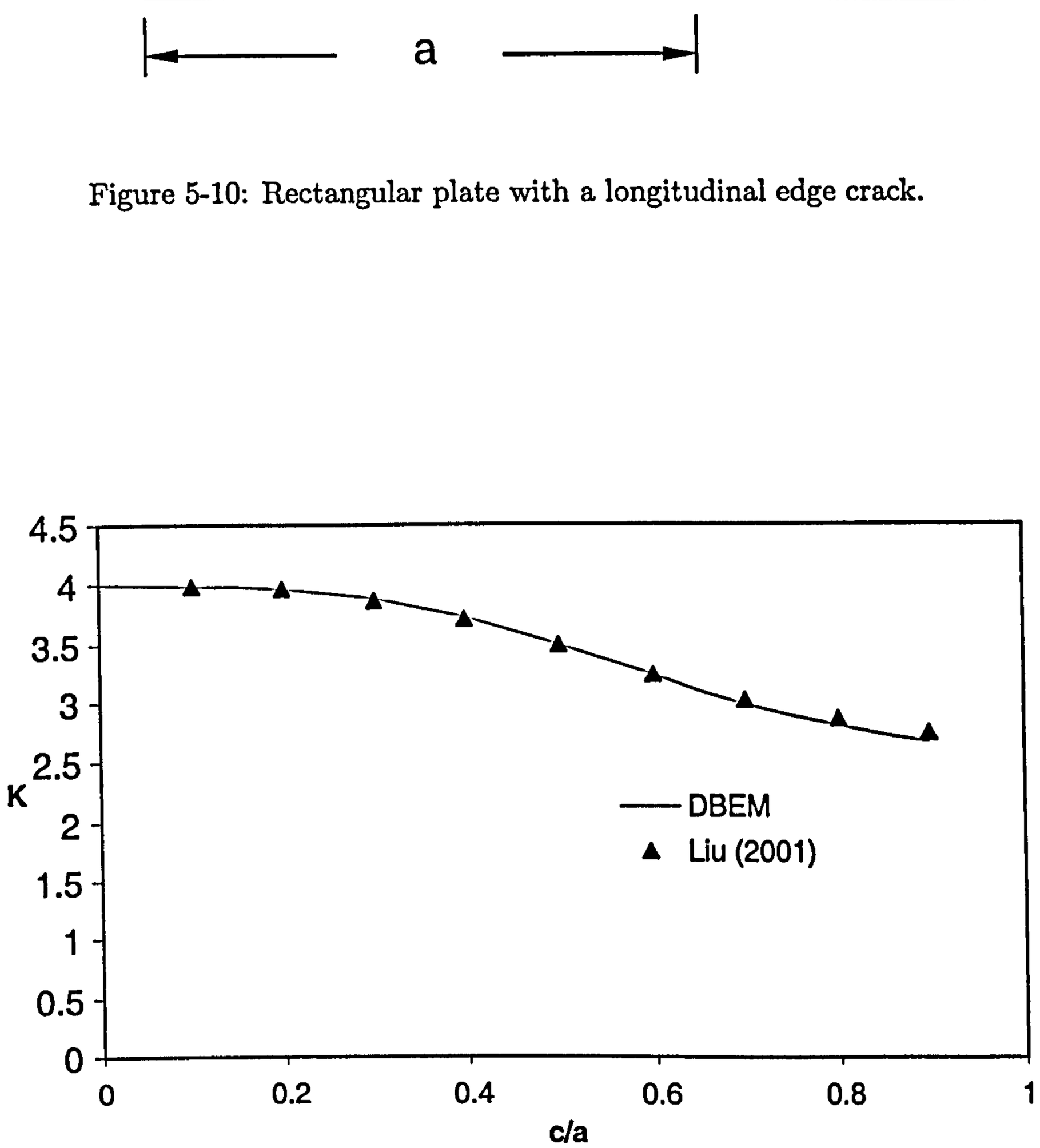

Figure 5-11: Variation of buckling coefficients for the plate (aspect ratio $a/b = 1$) with edge crack.

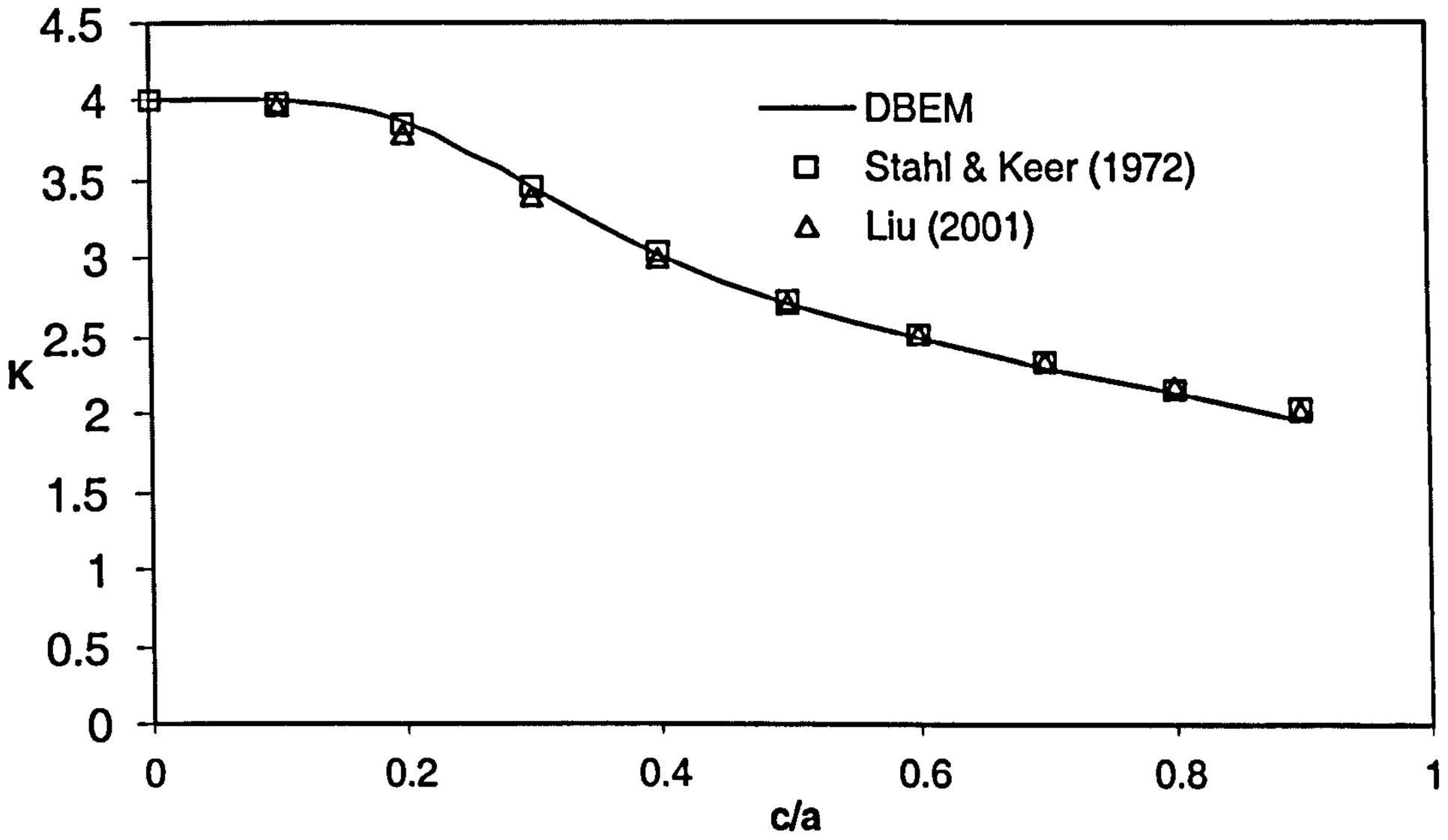

Figure 5-12: Variation of buckling coefficients for the plate (aspect ratio $a/b = 2$) with edge crack.

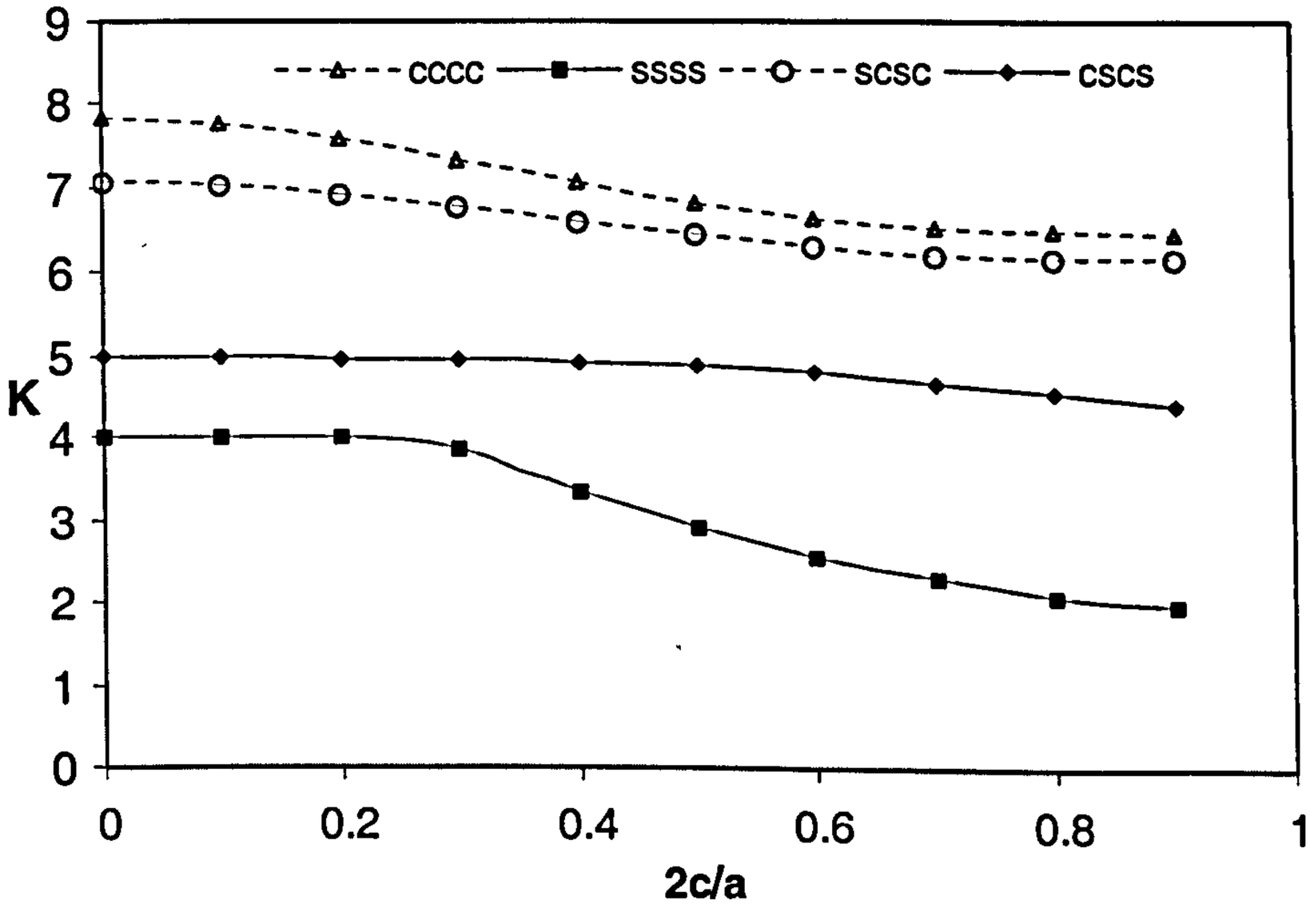

Figure 5-13: Variation of buckling coefficients for the plate (aspect ratio $a/b = 2$) with a longitudinal central crack and different boundary conditions.

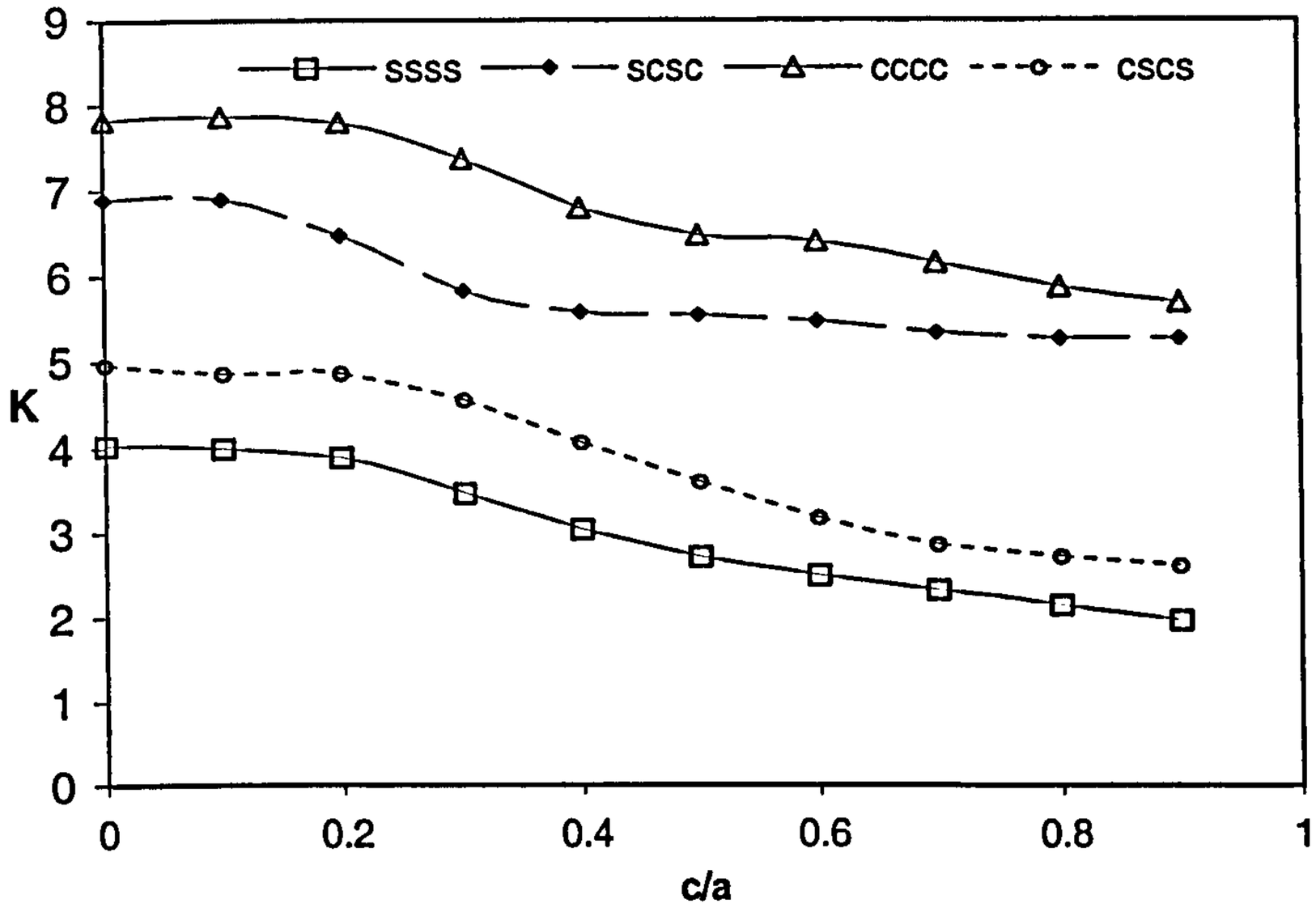

Figure 5-14: Rectangular plates $a/b = 2$ with a longitudinal edge crack and different boundary conditions.

loads with different boundary conditions is presented. The model is similar as shown in Figure 5-4 (i) with aspect ratio of the plate $a/b = 2$. Buckling coefficients for different aspect ratios of crack length to the length of plate $2c/a$ are presented in Figure 5-13. The legends in the Figure 5-13 are similar to those defined in section 4.6.3, i.e.

cccc : sides and ends clamped

ssss : sides and ends simply supported

cscs : ends clamped, sides simply supported

scsc : sides clamped, ends simply supported

As it can be seen, the buckling coefficients decrease with increasing $2c/a$ for all four different boundary conditions. The buckling coefficient is the highest for cccc and the lowest for ssss.

5.5.5 Rectangular plates with a longitudinal edge crack and different boundary conditions

Here, a rectangular plate with a longitudinal edge crack subjected to compression

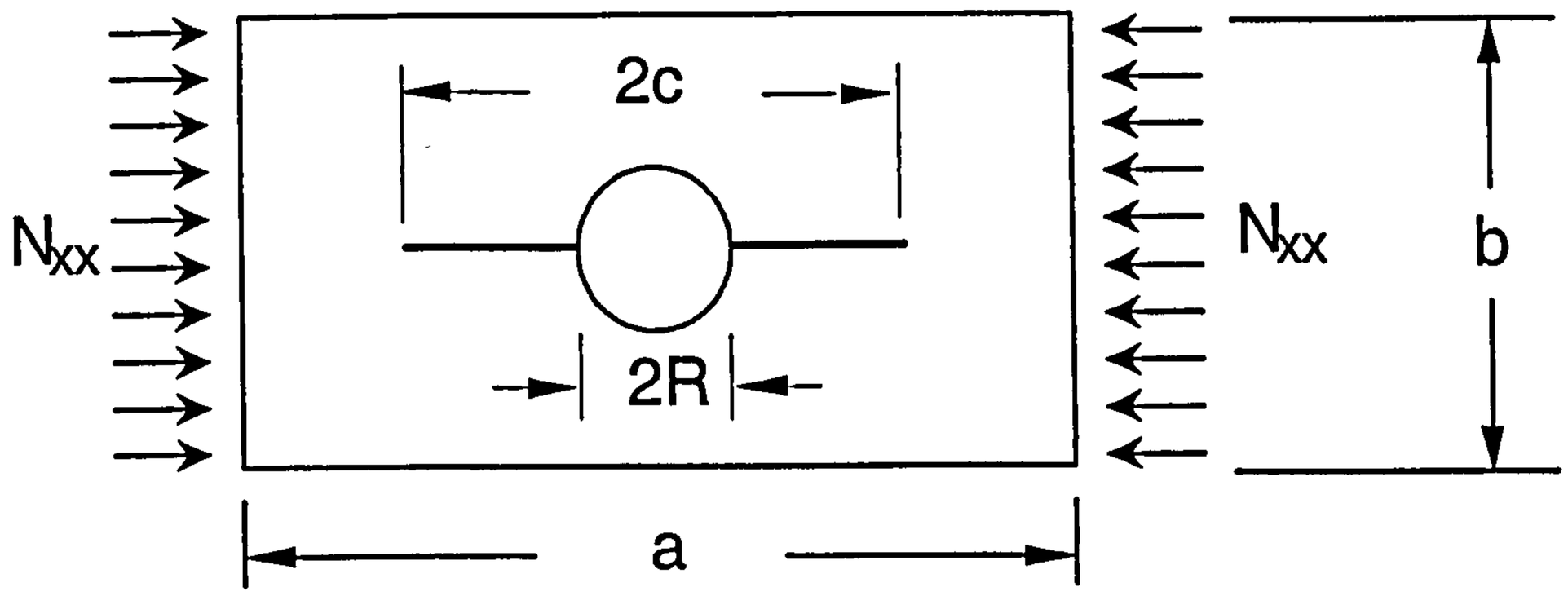

Figure 5-15: Rectangular plate with two symmetric cracks emanating from a hole.

loads with different boundary conditions is analysed. The model is similar to that shown in Figure 5-10 with aspect ratio of the plate $a/b = 2$. Buckling coefficients for different aspect ratios of crack length to the length of plate c/a are presented. The results of this example are shown in Figure 5-14. The legends in the Figure 5-14 are similar with those described in section 5.5.4. The buckling coefficients are shown to decrease with increasing crack length to width ratio.

5.5.6 Rectangular plate with two symmetric cracks emanating from a hole

This example involved a simply supported rectangular plate with two symmetric cracks emanating from a hole subjected to compression loads with different boundary conditions. The model is shown in Figure 5-15 . The aspect ratio of length to width of the plate $a/b = 2$. Buckling coefficients for different aspect ratios of crack length to the length of plate $2c/a$, and two different hole sizes $R/b = 0.1$ and $R/b = 0.25$ are presented in Figure 5-16.

The K value for $R/b = 0.1$ and 0.25 are higher than $R/b = 0$. In all cases, the buckling coefficients decrease with increasing ratio of $2c/a$.

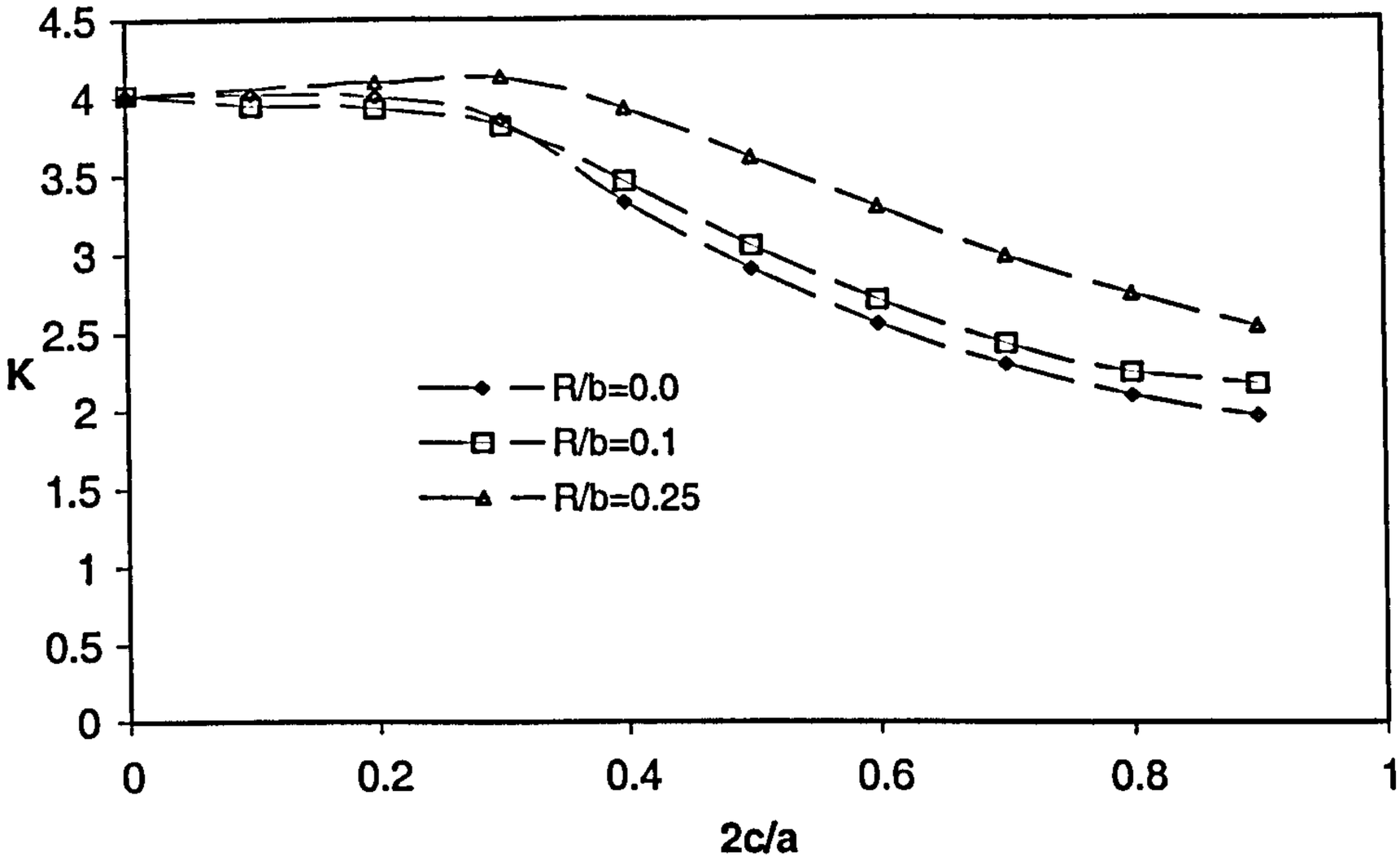

Figure 5-16: Variation of buckling coefficients for simply supported plate (aspect ratio $a/b = 2$) with two symmetric cracks emanating from a hole.

5.5.7 Rectangular plate with two collinear cracks

In this example, a rectangular plate with two collinear cracks subjected to compression loads with different boundary conditions is analysed. The model is shown in Figure 5-17 with aspect ratio of the plate $a/b = 2$. Buckling coefficients for different aspect ratios of crack length to the length of plate $2c/a$ and $2e = 0.5a$ are presented in Figures 5-18. The buckling coefficients for ssss are almost half of those obtained for cccc.

5.5.8 Rectangular plates with a transverse edge crack

In this example, a rectangular plate with a transverse edge crack as shown in Figure 5-19 subjected to compression loads is analysed. Aspect ratio of the plate $a/b = 2$. Two boundary conditions are applied: (a) all sides simply supported (ssss) and (b) One long side clamped and the others simply supported (sssc). Buckling coefficients in different aspect ratios of crack length to the length of plate c/b are presented in Figure 5-20. As expected the values of K for ssss are lower than sssc.

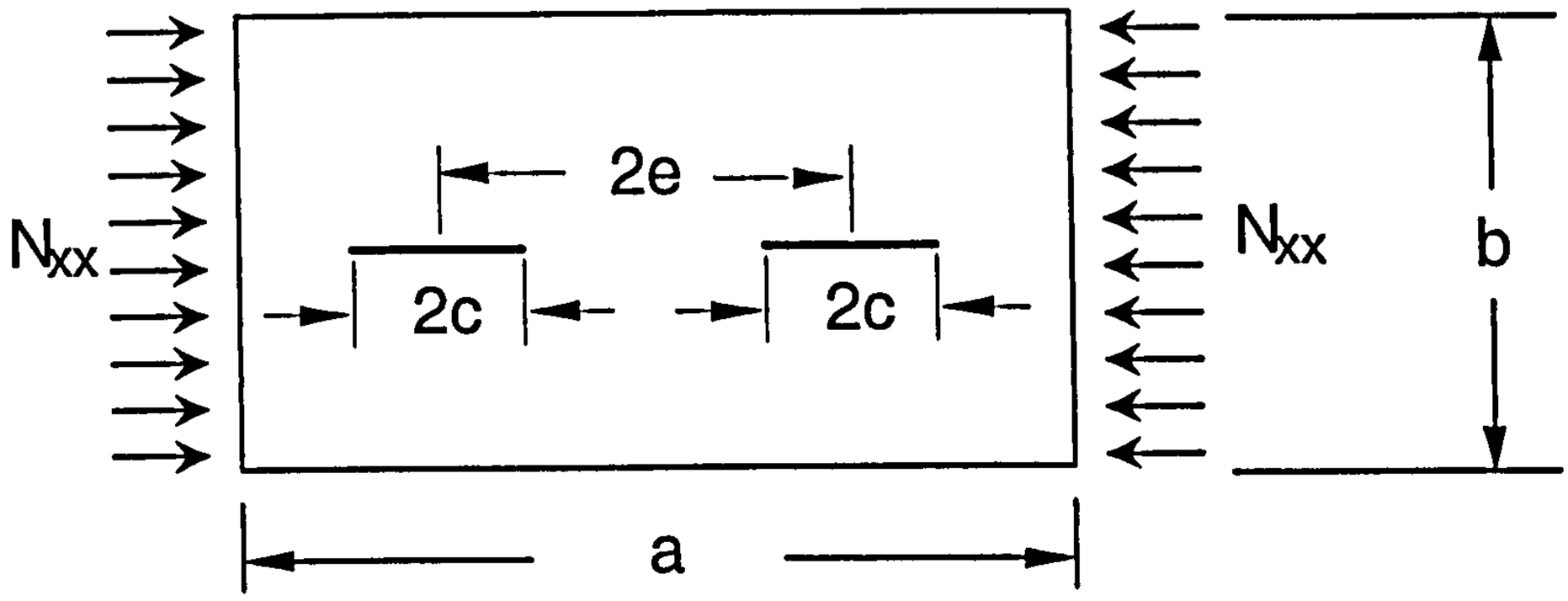

Figure 5-17: Rectangular plate with two collinear cracks.

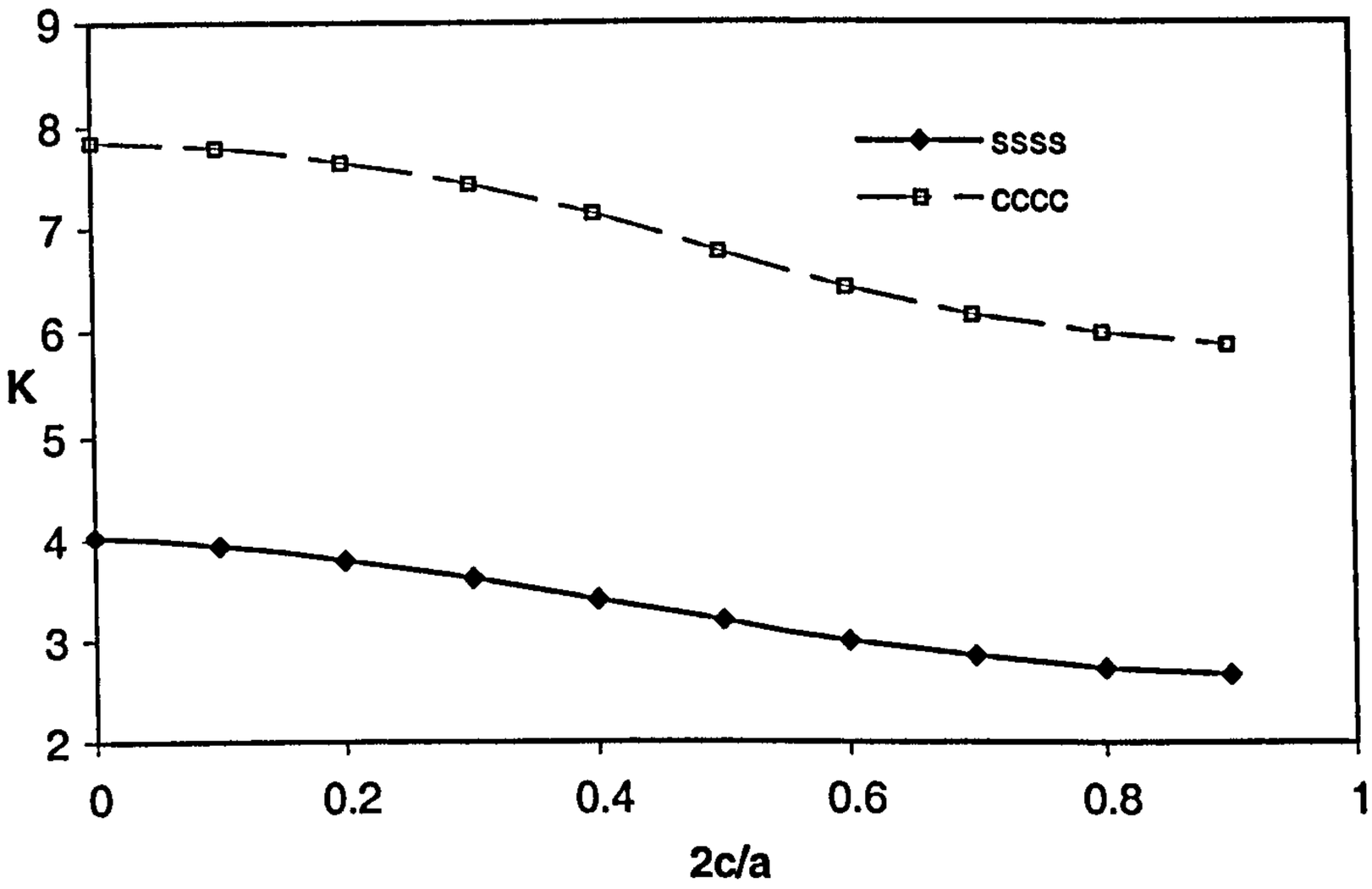

Figure 5-18: Variation of buckling coefficients for simply supported plate (aspect ratio $a/b = 2$) with two collinear cracks.

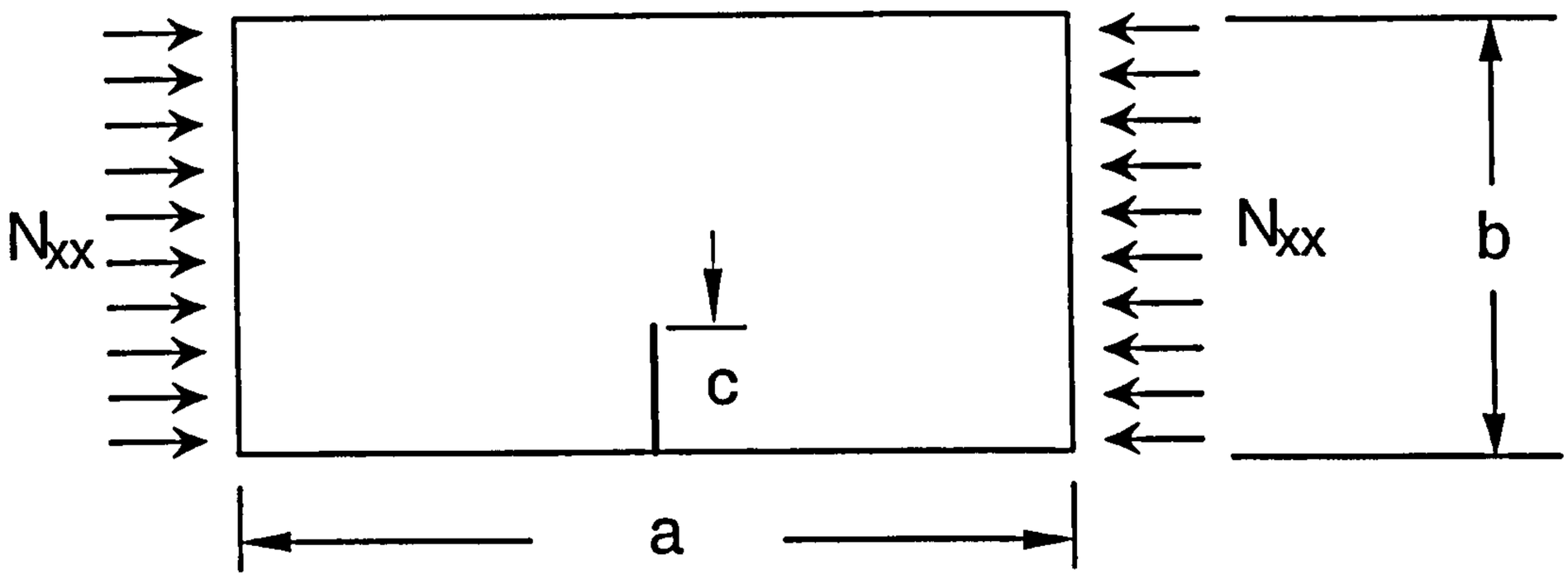

Figure 5-19: Rectangular plate with a transverse edge crack.

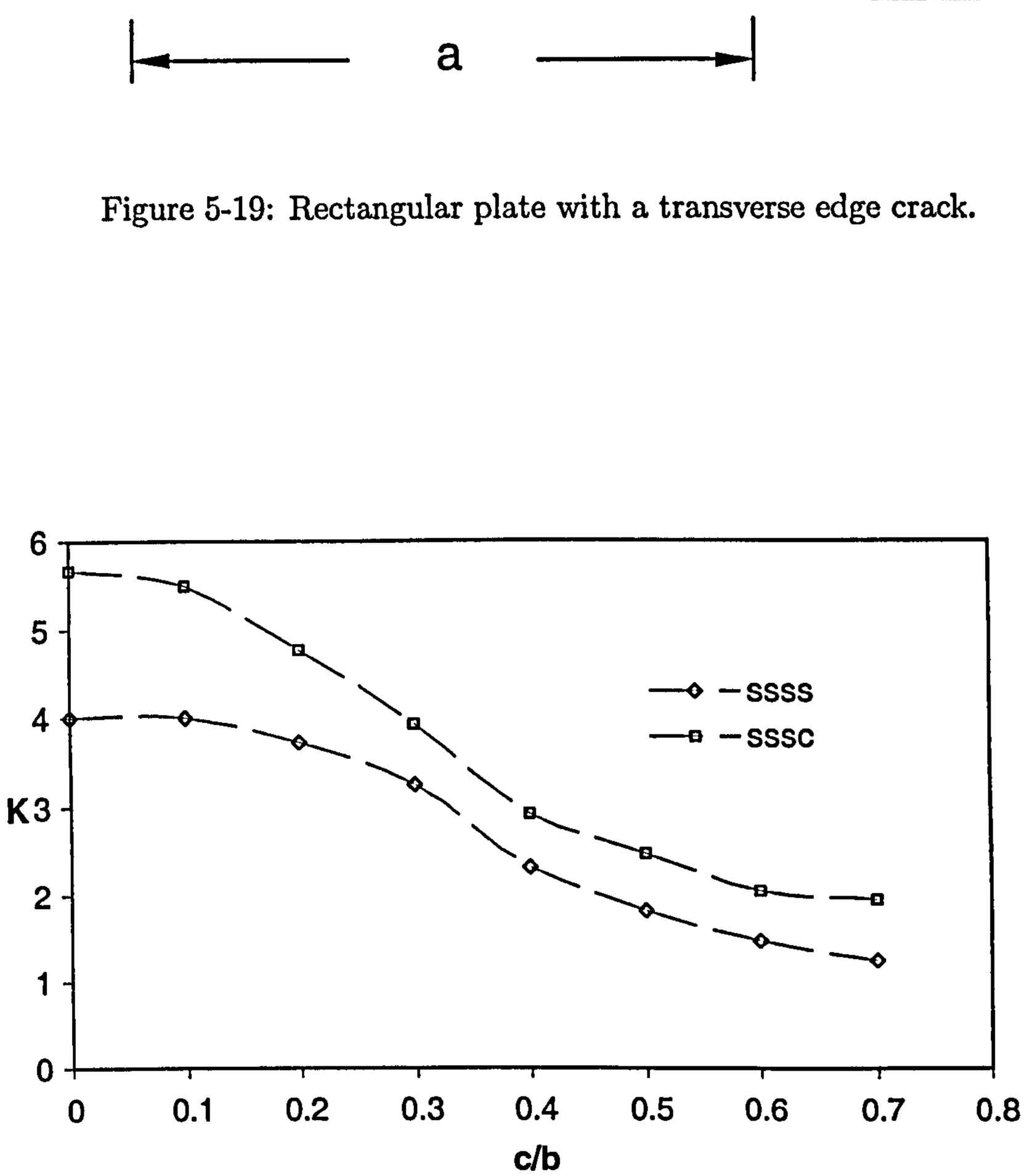

Figure 5-20: Variation of buckling coefficients for rectangular plate (aspect ratio $a/b = 2$) with a transverse edge crack.

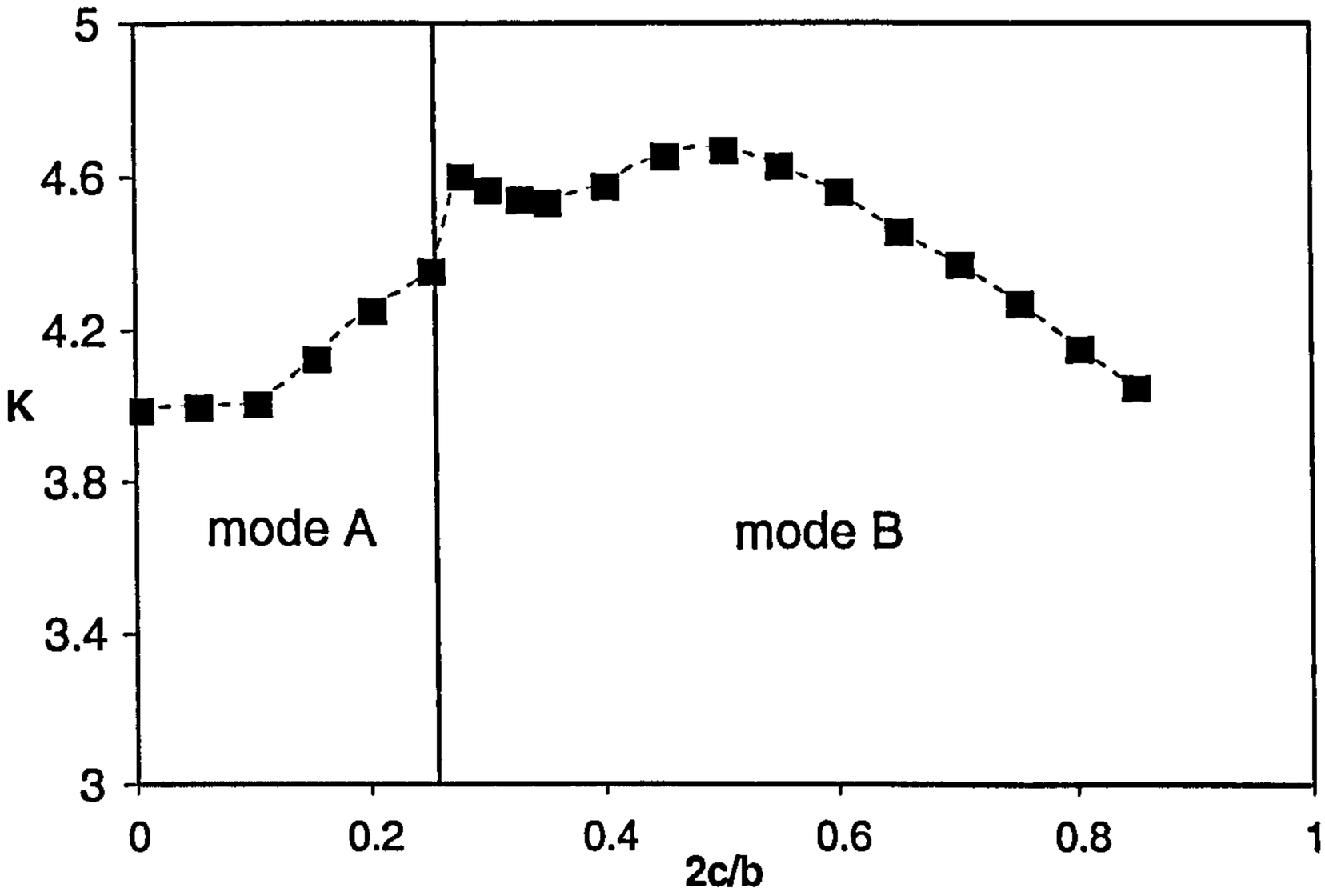

Figure 5-21: Rectangular plates with a transverse central crack subjected to compression loads.

5.5.9 Simply supported rectangular plates with a transverse central crack

In this example, a simply supported rectangular plate with a transverse central crack subjected to compression loads is analysed. The model is similar to that shown in Figure 5-4 (ii) with aspect ratio of the plate $a/b = 2$. Buckling coefficients for different aspect ratios of crack length to the length of plate c/b are presented in Figures 5-21. Mode A in Figure 5-21 denotes initial modes for the case of a short crack ($c/b = 0.0$ to $c/b = 0.25$) as shown in Figure 5-22. It can be seen from Figure 5-21, as the crack length reaches ratio c/b between $0.25 - 0.275$, the buckling coefficient has a big jump. After the crack length reaches ratio $c/b = 0.275$, the buckling modes change as shown in Figure 5-23. This phenomena occurs due to the change of buckling mode.

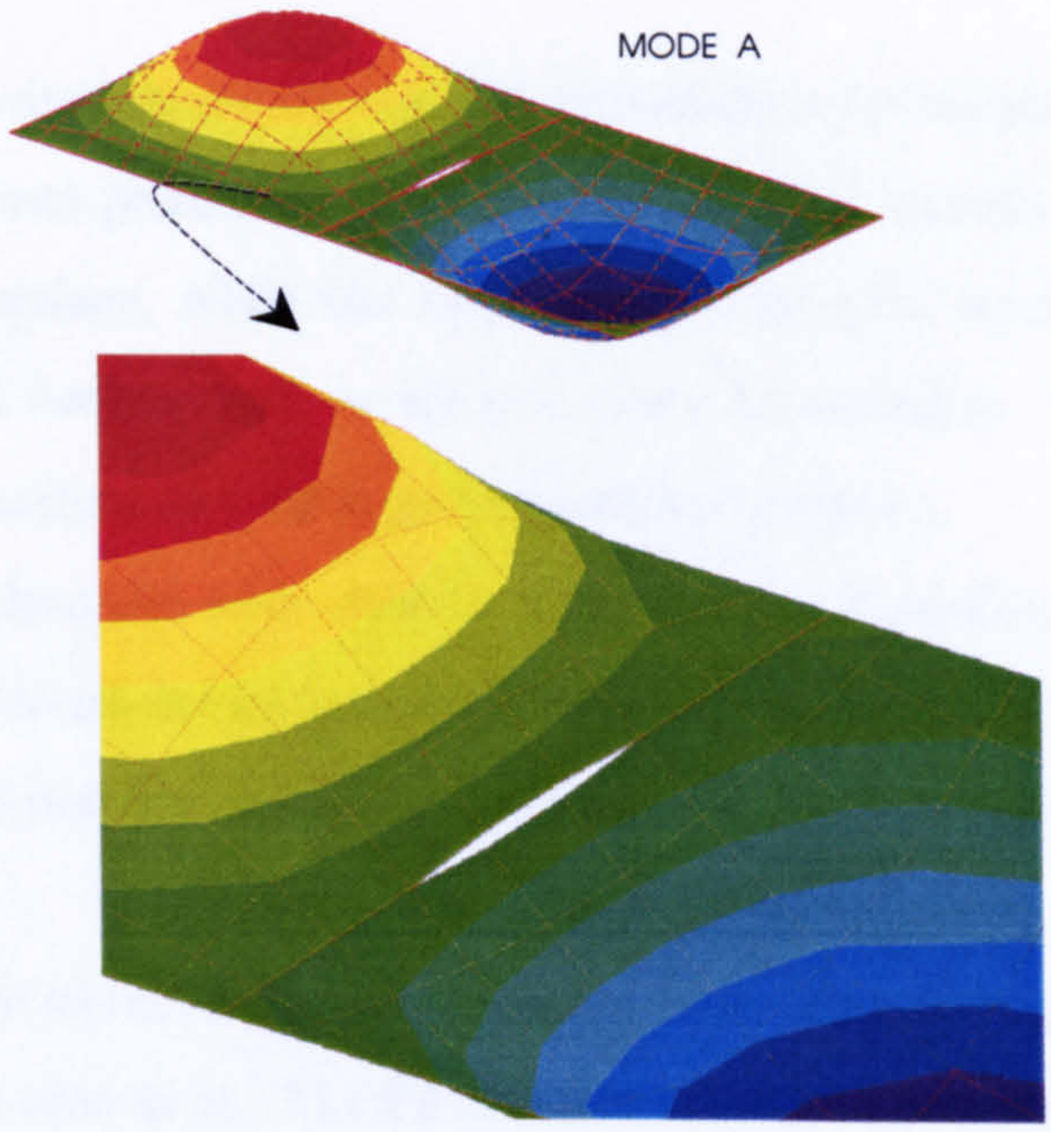

Figure 5-22: Mode A: an initial mode of simply supported rectangular plate with a transverse central crack.

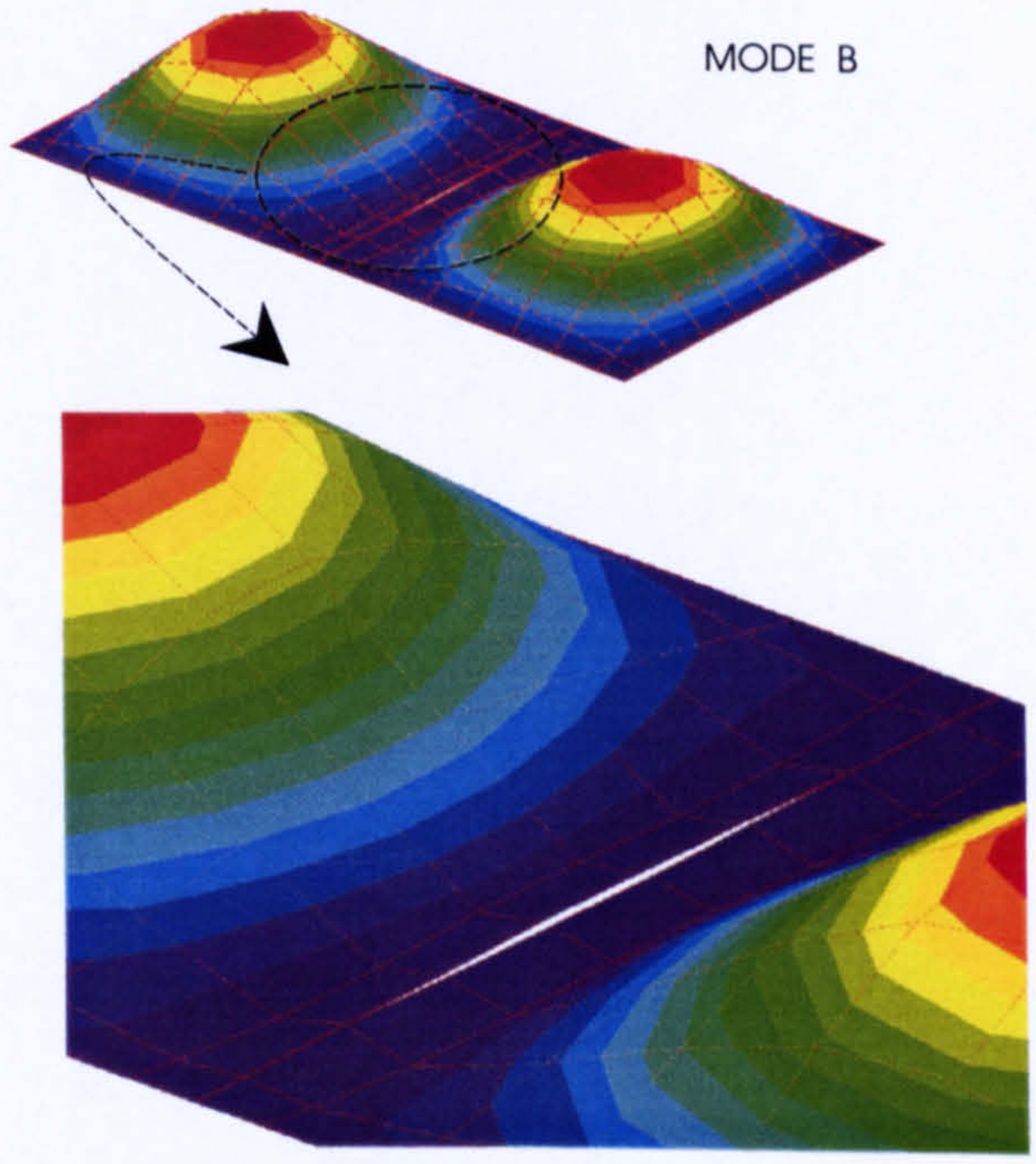

Figure 5-23: Mode B: second mode of simply supported rectangular plate with a transverse central crack.

5.6 Summary

In this chapter, the dual boundary element formulation for buckling analysis of shear deformable plates was presented. The traction integral equations were applied on one of the crack surface, while the displacement integral equations were applied on the other crack surface and on all non-crack boundaries. The plate buckling equations were presented as a standard eigenvalue problem.

Discontinuous elements were used to discretise crack surfaces, while continuous elements were used to model all non-crack boundaries, except for corners boundaries and the intersection between a crack and an edge, where semi-discontinuous elements were used.

Several examples of cracked plates buckling with different geometries and boundary conditions were presented. The BEM results presented were shown to be in good agreements with analytical and other numerical results.

Chapter 6

Geometrically Nonlinear Analysis of Plates

6.1 Introduction

Geometrically nonlinear behaviour in solid mechanics is one of the important problems in engineering practice. Bending of rectangular plates with large deflection was presented by Levy [50][51] using a solution of von Karman's equation in term of trigonometric series. An approximate analysis of large deflections for plates was introduced by Berger [17] which has become known as the Berger equation. The application of BEM to geometrically nonlinear problems is relatively new. Tanaka [84] presented a coupled boundary and inner domain integral equations in terms of stress and displacement functions based on the von Karman's equation. Kamiya and Sawaki [43] investigated the large deflection of elastic plates based on the Berger equation. Ye and Lin [102] analysed the finite deflection of thin plate by boundary element method. Based on the general nonlinear differential equations of finite deflection of the plate, an integral equation formulation for the geometrically nonlinear analysis of the shear deformable type plate has been proposed by Lei, Huang and Wang [49]. Sun, He and Qin [66] derived an exact boundary equation for the analysis of the nonlinear Reissner plate based on a variational principle.

The boundary element method has also been applied to analyse nonlinear problems in the plate stability. Contribution to BEM analysis of nonlinear buckling of

thin plates have been made Manolis and Beskos [55], Kamiya, Sawaki and Nakamura [42], Costa and Brebbia [24], Kawabe [46], Qin and Huang [67], and Tanaka, Matsumoto and Zheng [86]. The review of the application of BEM to the stability analysis of thin plate can be found in Liu [53] and Syngellakis [83].

In the analysis of the geometrically nonlinear plate bending problems, one of the difficulties is to evaluate domain integrals in the boundary integral equations. The domain integrals consist of coupling of the plate bending and membrane terms.

Here, for large deformation analysis, initially the domain is discretised using constant cells. Then meshless domain using the dual reciprocity technique is presented. An approximation function is used to calculate the derivatives of the nonlinear terms in the domain integral.

The nonlinear buckling of thin plate is also presented in this chapter. Two models of imperfections are introduced in the formulation, i.e. a small uniform transverse load and distributed transverse load based on eigenvectors. A load incremental numerical algorithm is presented to analyse the nonlinear problems.

Next, large deformation analysis of cracked plates is presented. The analysis is performed using the dual boundary element method. Five stress intensity factors are obtained, i.e. three SIFs from plate bending problem and two SIFs from membrane problem.

Finally, the nonlinear buckling of cracked plates is presented. The problem is analysed using the formulations for nonlinear buckling of thin plates and large deformation for cracked plates.

Several examples are presented and comparisons are made to demonstrate the accuracy of the proposed method with analytical results and other numerical results results.

6.2 Boundary Integral Equations

The integral equations for the geometrically nonlinear shear deformable plate bending problems can be derived by considering the integral representations of governing equations (2.37 - 2.39). The integral representation related to the governing equations for bending and transverse stress resultants as:

$$\int_{\Omega}[(M_{\alpha\beta,\beta}-Q_{\alpha})W_{\alpha}^{*}+(Q_{\alpha,\alpha}+(N_{\alpha\beta}w_{3,\beta})_{,\alpha}+q)W_{3}^{*}]d\Omega=0 \tag{6.1}$$

while the integral representation related to the governing equations for membrane stress resultants can written as

$$\int_{\Omega}N_{\alpha\beta,\beta}U_{\alpha}^{*}d\Omega=0 \tag{6.2}$$

Derivation of boundary integral equations for the geometrically nonlinear plate bending problems is similar to the linear analysis as described in Chapter 3. Applying the Betti's reciprocal theorem to the governing equations for bending and transverse stress resultants at arbitrary domain point $\mathbf{X}'$, gives:

$$\begin{aligned} & w_i(\mathbf{X}')+\int_{\Gamma}P_{ij}^{*}(\mathbf{X}',\mathbf{x})w_j(\mathbf{x})d\Gamma(\mathbf{x}) \\ = & \int_{\Gamma}W_{ij}^{*}(\mathbf{X}',\mathbf{x})p_j^{linear}(\mathbf{x})d\Gamma(\mathbf{x})+\int_{\Omega}W_{i3}^{*}(\mathbf{X}',\mathbf{X})q(\mathbf{X})d\Omega(\mathbf{X}) \\ & +\int_{\Omega}W_{i3}^{*}(\mathbf{X}',\mathbf{X})(N_{\alpha\beta}w_{3,\beta})_{,\alpha}(\mathbf{X})d\Omega(\mathbf{X}) \end{aligned} \tag{6.3}$$

In the same way, boundary integral equation for the displacements of two dimensional elasticity at domain point $\mathbf{X}'$ can be presented as

$$\begin{aligned} & u_{\alpha}(\mathbf{X}')+\int_{\Gamma}T_{\theta\alpha}^{*}(\mathbf{X}',\mathbf{x})u_{\alpha}(\mathbf{x})d\Gamma(\mathbf{x}) \\ = & \int_{\Gamma}U_{\theta\alpha}^{*}(\mathbf{X}',\mathbf{x})t_{\alpha}^{linear}(\mathbf{x})d\Gamma(\mathbf{x})+\int_{\Omega}U_{\theta\alpha}^{*}(\mathbf{X}',\mathbf{X})N_{\alpha\gamma,\gamma}^{nonlinear}(\mathbf{X})d\Omega(\mathbf{X}) \end{aligned} \tag{6.4}$$

Then after taking the point $\mathbf{X}'$ to the boundary, that is $\mathbf{X}'\rightarrow\mathbf{x}'$ at Γ, boundary integral equations are obtained as follows:

$$\begin{aligned} & C_{ij}w_i(\mathbf{x}')+\int_{\Gamma}P_{ij}^{*}(\mathbf{x}',\mathbf{x})w_j(\mathbf{x})d\Gamma(\mathbf{x}) \\ = & \int_{\Gamma}W_{ij}^{*}(\mathbf{x}',\mathbf{x})p_j^{linear}(\mathbf{x})d\Gamma(\mathbf{x})+\int_{\Omega}W_{i3}^{*}(\mathbf{x}',\mathbf{X})q(\mathbf{X})d\Omega(\mathbf{X}) \end{aligned}$$

$$+\int_{\Omega} W^*_{i3}(\mathbf{x}',\mathbf{X})(N_{\alpha\beta}w_{3,\beta})_{,\alpha}(\mathbf{X})d\Omega(\mathbf{X}) \tag{6.5}$$

for plate bending problems and $C_{ij} = \delta_{ij}/2$.

$$\begin{aligned} & C_{\theta\alpha}u_\alpha(\mathbf{x}') + \int_{\Gamma} T^*_{\theta\alpha}(\mathbf{x}',\mathbf{x})u_\alpha(\mathbf{x})d\Gamma(\mathbf{x}) \\ = & \int_{\Gamma} U^*_{\theta\alpha}(\mathbf{x}',\mathbf{x})t^{linear}_\alpha(\mathbf{x})d\Gamma(\mathbf{x}) + \int_{\Omega} U^*_{\theta\alpha}(\mathbf{x}',\mathbf{X})N^{nonlinear}_{\alpha\gamma,\gamma}(\mathbf{X})d\Omega(\mathbf{X}) \end{aligned} \tag{6.6}$$

for in-plane problems and $C_{\theta\alpha} = \delta_{\theta\alpha}/2$.

6.3 Large Deformation Analysis

In this section, two methods related to the evaluation of domain integrals which appear in the formulation, i.e. domain integral method and approximation function method are presented.

6.3.1 Domain Integral Method

The nonlinear terms which appear in the domain integrals are calculated directly using a domain integration procedure. Integrating by parts the last terms of the equations (6.5) and (6.6), gives:

$$\begin{aligned} & C_{ij}w_i(\mathbf{x}') + \int_{\Gamma} P^*_{ij}(\mathbf{x}',\mathbf{x})w_j(\mathbf{x})d\Gamma(\mathbf{x}) \\ = & \int_{\Gamma} W^*_{ij}(\mathbf{x}',\mathbf{x})p^{linear}_j(\mathbf{x})d\Gamma(\mathbf{x}) + \int_{\Omega} W^*_{i3}(\mathbf{x}',\mathbf{X})q(\mathbf{X})d\Omega(\mathbf{X}) \\ & + \int_{\Gamma} W^*_{i3}(\mathbf{x}',\mathbf{x})(N_{\alpha\beta}w_{3,\beta})\, n_\alpha(\mathbf{x})d\Gamma(\mathbf{x}) \\ & - \int_{\Omega} W^*_{i3}(\mathbf{x}',\mathbf{X})(N_{\alpha\beta}w_{3,\beta})(\mathbf{X})d\Omega(\mathbf{X}) \end{aligned} \tag{6.7}$$

and

$$\begin{aligned} & C_{\theta\alpha}u_\alpha(\mathbf{x}') + \int_{\Gamma} T^*_{\theta\alpha}(\mathbf{x}',\mathbf{x})u_\alpha(\mathbf{x})d\Gamma(\mathbf{x}) \\ = & \int_{\Gamma} U^*_{\theta\alpha}(\mathbf{x}',\mathbf{x})t^{linear}_\alpha(\mathbf{x})d\Gamma(\mathbf{x}) + \int_{\Gamma} U^*_{\theta\alpha}(\mathbf{x}',\mathbf{x})N^{nonlinear}_{\alpha\gamma}n_\gamma(\mathbf{x})d\Gamma(\mathbf{x}) \end{aligned}$$

$$- \int_{\Omega} U^*_{\theta\alpha,\gamma}(\mathbf{x}', \mathbf{X}) N^{nonlinear}_{\alpha\gamma}(\mathbf{X}) d\Omega(\mathbf{X}) \tag{6.8}$$

Equations (6.7) and (6.8) can be simplified as follows:

$$\begin{aligned} C_{ij} w_i(\mathbf{x}') + \int_{\Gamma} P^*_{ij}(\mathbf{x}', \mathbf{x}) w_j(\mathbf{x}) d\Gamma(\mathbf{x}) \\ = \int_{\Gamma} W^*_{ij}(\mathbf{x}', \mathbf{x}) p_j(\mathbf{x}) d\Gamma(\mathbf{x}) + \int_{\Omega} W^*_{i3}(\mathbf{x}', \mathbf{X}) q(\mathbf{X}) d\Omega(\mathbf{X}) \\ - \int_{\Omega} W^*_{i3}(\mathbf{x}', \mathbf{X}) (N_{\alpha\beta} w_{3,\beta})(\mathbf{X}) d\Omega(\mathbf{X}) \end{aligned} \tag{6.9}$$

and

$$\begin{aligned} C_{\theta\alpha} u_{\alpha}(\mathbf{x}') + \int_{\Gamma} T^*_{\theta\alpha}(\mathbf{x}', \mathbf{x}) u_{\alpha}(\mathbf{x}) d\Gamma(\mathbf{x}) \\ = \int_{\Gamma} U^*_{\theta\alpha}(\mathbf{x}', \mathbf{x}) t_{\alpha}(\mathbf{x}) d\Gamma(\mathbf{x}) - \int_{\Omega} U^*_{\theta\alpha,\gamma}(\mathbf{x}', \mathbf{X}) N^{nonlinear}_{\alpha\gamma}(\mathbf{X}) d\Omega(\mathbf{X}) \end{aligned} \tag{6.10}$$

in which,

$$\{p\} = [M_{\alpha\beta} n_{\beta}, Q_{\alpha} n_{\alpha}] \text{ and } \{t\} = [N_{\alpha\beta} n_{\beta}]$$

To calculate the nonlinear terms for this approach, two additional integral equations are required: the derivative of deflection $w_{3,\gamma}$ equation,

$$\begin{aligned} w_{3,\gamma}(\mathbf{X}') = \int_{\Gamma} W^*_{3j,\gamma}(\mathbf{X}', \mathbf{x}) p_j(\mathbf{x}) d\Gamma(\mathbf{x}) - \int_{\Gamma} P^*_{3j,\gamma}(\mathbf{X}', \mathbf{x}) w_j(\mathbf{x}) d\Gamma(\mathbf{x}) + \\ \int_{\Omega} W^*_{33,\gamma}(\mathbf{X}', \mathbf{X}) q(\mathbf{X}) d\Omega(\mathbf{X}) \\ - \int_{\Omega} W^*_{33,\gamma\alpha}(\mathbf{X}', \mathbf{X}) (N_{\alpha\beta} w_{3,\beta})\ (\mathbf{X})\ d\Omega(\mathbf{X}) \end{aligned} \tag{6.11}$$

and membrane stress resultant $N^{linear}_{\alpha\beta}$ equation as:

$$\begin{aligned} N^{linear}_{\alpha\beta}(\mathbf{X}') = \int_{\Gamma} U^*_{\Delta\alpha\beta}(\mathbf{X}', \mathbf{x}) t_{\Delta}(\mathbf{x}) d\Gamma(\mathbf{x}) - \int_{\Gamma} T^*_{\Delta\alpha\beta}(\mathbf{X}', \mathbf{x}) u_{\Delta}(\mathbf{x}) d\Gamma(\mathbf{x}) \\ - \int_{\Omega} U^*_{\Delta\alpha\beta,\gamma}(\mathbf{X}', \mathbf{X}) N^{nonlinear}_{\Delta\gamma,\gamma}(\mathbf{X}) d\Omega(\mathbf{X}) \end{aligned} \tag{6.12}$$

6.3.2 Approximation Function Method

An alternative formulation is presented here for dealing with the domain integrals due to the nonlinear terms. The main reason for proposing this new formulation is to avoid direct calculation of the hypersingular integral which arises in equation (6.11). Although, the evaluation of these integrals is not too demanding with constant cells, higher order cells will pose some difficulties. The approximate function method proposed here would avoid the difficulties for higher order cells. The boundary integral equations can be expressed by recalling equations (6.5) and (6.6) as:

$$\begin{aligned} & C_{ij}w_i(\mathbf{x}') + \int_\Gamma P^*_{ij}(\mathbf{x}',\mathbf{x})w_j(\mathbf{x})d\Gamma(x) \\ = & \int_\Gamma W^*_{ij}(\mathbf{x}',\mathbf{x})p_j^{linear}(\mathbf{x})d\Gamma(\mathbf{x}) + \int_\Omega W^*_{i3}(\mathbf{x}',\mathbf{X})q(\mathbf{X})d\Omega(\mathbf{X}) \\ & + \int_\Omega W^*_{i3}(\mathbf{x}',\mathbf{X})(N_{\alpha\beta}w_{3,\beta})_{,\alpha}(\mathbf{X})d\Omega(\mathbf{X}) \end{aligned} \tag{6.13}$$

and

$$\begin{aligned} & C_{\theta\alpha}u_\alpha(\mathbf{x}') + \int_\Gamma T^*_{\theta\alpha}(\mathbf{x}',\mathbf{x})u_\alpha(\mathbf{x})d\Gamma(\mathbf{x}) \\ = & \int_\Gamma U^*_{\theta\alpha}(\mathbf{x}',\mathbf{x})t_\alpha^{linear}(\mathbf{x})d\Gamma(\mathbf{x}) + \int_\Omega U^*_{\theta\alpha}(\mathbf{x}',\mathbf{X})N^{nonlinear}_{\alpha\gamma,\gamma}(\mathbf{X})d\Omega(\mathbf{X}) \end{aligned} \tag{6.14}$$

in which,

$$\{p^{linear}\} = [M_{\alpha\beta}n_\beta, Q_\alpha^{linear}n_\alpha];\ \{t^{linear}\} = [N_{\alpha\beta}^{linear}n_\beta]$$

To calculate the nonlinear terms, three additional integral equations are needed. The first equation is obtained by recalling equation (6.3), that is

$$\begin{aligned} & w_i(\mathbf{X}') + \int_\Gamma P^*_{ij}(\mathbf{X}',\mathbf{x})w_j(\mathbf{x})d\Gamma(\mathbf{x}) \\ = & \int_\Gamma W^*_{ij}(\mathbf{X}',\mathbf{x})p_j^{linear}(\mathbf{x})d\Gamma(\mathbf{x}) + \int_\Omega W^*_{i3}(\mathbf{X}',\mathbf{X})q(\mathbf{X})d\Omega(\mathbf{X}) \\ & + \int_\Omega W^*_{i3}(\mathbf{X}',\mathbf{X})(N_{\alpha\beta}w_{3,\beta})_{,\alpha}(\mathbf{X})d\Omega(\mathbf{X}) \end{aligned} \tag{6.15}$$

The second equation is the derivative of deflection $w_{3,\gamma}$ given as

$$\begin{aligned} w_{3,\gamma}(\mathbf{X}') &= \int_\Gamma W^*_{3j,\gamma}(\mathbf{X}',\mathbf{x}) p_j^{linear}(\mathbf{x}) d\Gamma(\mathbf{x}) - \int_\Gamma P^*_{3j,\gamma}(\mathbf{X}',\mathbf{x}) w_j(\mathbf{x}) d\Gamma(\mathbf{x}) + \\ &\int_\Omega W^*_{33,\gamma}(\mathbf{X}',\mathbf{X}) q(\mathbf{X}) d\Omega(\mathbf{X}) \\ &+ \int_\Omega W^*_{33,\gamma}(\mathbf{X}',\mathbf{X}) (N_{\alpha\beta} w_{3,\beta})_{,\alpha}\ (\mathbf{X})\ d\Omega(\mathbf{X}) \end{aligned} \tag{6.16}$$

The third equation is the membrane stress resultant $N^{linear}_{\alpha\beta}$ equation as

$$\begin{aligned} N^{linear}_{\alpha\beta}(\mathbf{X}') &= \int_\Gamma U^*_{\Delta\alpha\beta}(\mathbf{X}',\mathbf{x}) t^{linear}_\Delta(\mathbf{x}) d\Gamma(\mathbf{x}) - \int_\Gamma T^*_{\Delta\alpha\beta}(\mathbf{X}',\mathbf{x}) u_\Delta(\mathbf{x}) d\Gamma(\mathbf{x}) \\ &+ \int_\Omega U^*_{\Delta\alpha\beta}(\mathbf{X}',\mathbf{X}) N^{nonlinear}_{\Delta\gamma,\gamma}(\mathbf{X}) d\Omega(\mathbf{X}) \end{aligned} \tag{6.17}$$

As it can be seen, the nonlinear domain terms are now represented on $(N_{\alpha\beta} w_{3,\beta})_{,\alpha}$. The fundamental solution $W^*_{33,\gamma}$ in equation (6.16) has a lower order of singularity than $W^*_{33,\gamma\alpha}$ appearing in equation (6.11).

Equations (6.3), (6.5) and (6.16) can be rewritten in the other forms as follows:

$$\begin{aligned} & w_i(\mathbf{X}') + \int_\Gamma P^*_{ij}(\mathbf{X}',\mathbf{x}) w_j(\mathbf{x}) d\Gamma(\mathbf{x}) \\ = & \int_\Gamma W^*_{ij}(\mathbf{X}',\mathbf{x}) p_j^{linear}(\mathbf{x}) d\Gamma(\mathbf{x}) + \int_\Omega W^*_{i3}(\mathbf{X}',\mathbf{X}) q(\mathbf{X}) d\Omega(\mathbf{X}) \\ & + \int_\Omega W^*_{i3}(\mathbf{X}',\mathbf{X}) (N_{\alpha\beta} w_{3,\beta})_{,\alpha}(\mathbf{X}) d\Omega(\mathbf{X}) \end{aligned} \tag{6.18}$$

$$\begin{aligned} & C_{ij} w_i(\mathbf{x}') + \int_\Gamma P^*_{ij}(\mathbf{x}',\mathbf{x}) w_j(\mathbf{x}) d\Gamma(\mathbf{x}) \\ = & \int_\Gamma W^*_{ij}(\mathbf{x}',\mathbf{x}) p_j^{linear}(\mathbf{x}) d\Gamma(\mathbf{x}) + \int_\Omega W^*_{i3}(\mathbf{x}',\mathbf{X}) q(\mathbf{X}) d\Omega(\mathbf{X}) \\ & + \int_\Omega W^*_{i3}(\mathbf{x}',\mathbf{X}) (N_{\alpha\beta,\alpha} w_{3,\beta} + N_{\alpha\beta} w_{3,\alpha\beta})(\mathbf{X}) d\Omega(\mathbf{X}) \end{aligned} \tag{6.19}$$

$$
\begin{aligned}
w_{3,\gamma}(\mathbf{X}') &= \int_\Gamma W^*_{3j,\gamma}(\mathbf{X}',\mathbf{x}) p_j^{linear}(\mathbf{x}) d\Gamma(\mathbf{x}) \\
&\quad - \int_\Gamma P^*_{3j,\gamma}(\mathbf{X}',\mathbf{x}) w_j(\mathbf{x}) d\Gamma(\mathbf{x}) \\
&\quad + \int_\Omega W^*_{33,\gamma}(\mathbf{X}',\mathbf{X}) q(\mathbf{X}) d\Omega(\mathbf{X}) \\
&\quad + \int_\Omega W^*_{33,\gamma}(\mathbf{X}',\mathbf{X}) (N_{\alpha\beta,\alpha} w_{3,\beta} + N_{\alpha\beta} w_{3,\alpha\beta})\ (\mathbf{X})\ d\Omega(\mathbf{X}) \quad (6.20)
\end{aligned}
$$

The domain integrals which appear in equations (6.17 - 6.20) are also evaluated using the dual reciprocity technique as described in sections 3.5 and 4.4.

To calculate the derivatives of the nonlinear terms, the nonlinear terms are approximated by the approximation function $f(r)$ as described in section 4.2.3. The nonlinear terms $N^{nonlinear}_{\Delta\gamma,\gamma}$ which appear in the in-plane equations (6.6) and (6.17) are evaluated as:

$$
N^{nonlinear}_{\Delta\gamma}(x_1,x_2) = \sum_{m=1}^{M} f(r)^m \Psi^m \quad (6.21)
$$

where M is a number of selected points.

$$
\Psi = \mathbf{F}^{-1}\{N^{nonlinear}_{\Delta\gamma}\} \quad (6.22)
$$

$$
N^{nonlinear}_{\Delta\gamma,\gamma}(x_1,x_2) = \mathrm{f}(r)_{,\gamma}\mathbf{F}^{-1}\{N^{nonlinear}_{\Delta\gamma}\} \quad (6.23)
$$

There are four approximations to calculate the nonlinear terms which appear in the plate bending equation as follows:

Approximation Function Method I

The nonlinear terms $(N_{\alpha\beta}w_{3,\beta})_{,\alpha}$ in the equations (6.3), (6.5) and (6.16) are calculated as:

$$
(N_{\alpha\beta}w_{3,\beta})(x_1,x_2) = \sum_{m=1}^{M} f(r)^m \Psi^m \quad (6.24)
$$

$$\Psi = \mathbf{F}^{-1}\{N_{\alpha\beta} w_{3,\beta}\} \tag{6.25}$$

$$(N_{\alpha\beta} w_{3,\beta})_{,\alpha}(x_1, x_2) = \mathrm{f}(r)_{,\alpha} \mathbf{F}^{-1}\{N_{\alpha\beta} w_{3,\beta}\} \tag{6.26}$$

Approximation Function Method II

The nonlinear terms $(N_{\alpha\beta,\alpha} w_{3,\beta} + N_{\alpha\beta} w_{3,\alpha\beta})$ in the equations (6.18), (6.13) and (6.20) are calculated as:

For $N_{\alpha\beta,\alpha}$:

$$N_{\alpha\beta}(x_1, x_2) = \sum_{m=1}^{M} f(r)^m \Psi^m \tag{6.27}$$

$$\Psi = \mathbf{F}^{-1}\{N_{\alpha\beta}\} \tag{6.28}$$

$$N_{\alpha\beta,\alpha}(x_1, x_2) = \mathrm{f}(r)_{,\alpha} \mathbf{F}^{-1}\{N_{\alpha\beta}\} \tag{6.29}$$

For $w_{3,\alpha\beta}$:

$$w_{3,\beta}(x_1, x_2) = \sum_{m=1}^{M} f(r)^m \Psi^m \tag{6.30}$$

$$\Psi = \mathbf{F}^{-1}\{w_{3,\beta}\} \tag{6.31}$$

$$w_{3,\alpha\beta}(x_1, x_2) = \mathrm{f}(r)_{,\alpha} \mathbf{F}^{-1}\{w_{3,\beta}\} \tag{6.32}$$

Approximation Function Method III

The term $N_{\alpha\beta,\alpha}$ is calculated in the same way as the equations (6.27), (6.28) and (6.29). But the terms $w_{3,\beta}$ and $w_{3,\alpha\beta}$ in the equations (6.18), (6.13) and (6.20) are calculated as follows:

$$w_3(x_1,x_2) = \sum_{m=1}^{M} f(r)^m \Psi^m \tag{6.33}$$

$$\Psi = \mathbf{F}^{-1}\{w_3\} \tag{6.34}$$

$$w_{3,\beta}(x_1,x_2) = \mathbf{f}(r)_{,\beta}\mathbf{F}^{-1}\{w_3\} \tag{6.35}$$

$$w_{3,\alpha\beta}(x_1,x_2) = \mathbf{f}(r)_{,\alpha}\mathbf{F}^{-1}\mathbf{f}(r)_{,\beta}\mathbf{F}^{-1}\{w_3\} \tag{6.36}$$

Approximation Function Method IV

This approximation is the same as approximation III, but comprises of selected points on the boundary and in the domain. That is

$$w_3(x_1,x_2) = \sum_{m=1}^{N+M} f(r)^m \Psi^m \tag{6.37}$$

where N is a number of boundary nodes.

6.4 Incremental Approach and Solution Procedures

In this section four methods are presented for dealing with the nonlinear problem.

6.4.1 Total incremental method

In this method, the load is divided in the small load steps, and the equations are represented as a system of algebraic equations as follows:

$$[H^p]\{w^{k+1}\} + [G^p]\{p^{k+1}\} = [B^p]\{(N_{\alpha\beta}w_{3,\beta})^k_{,\alpha} + (k+1)\ \overset{\circ}{q}\} \tag{6.38}$$

$$[H^m]\{u^{k+1}\} + [G^m]\{t^{k+1}\} = [B^m]\{N^{nonlinear\ (k)}_{\alpha\beta,\beta}\} \tag{6.39}$$

where k denotes incremental step-th; superscript $\overset{\circ}{(.)}$ is incremental of term.

Once the matrices $[H^p]$, $[G^p]$, $[B^p]$, $[H^m]$, $[G^m]$ and $[B^m]$ have been formed, they can be stored and used in each increment without any further change. Moreover, the re-solution of the system of equations can be carried out fast if the LU-decomposition method is adopted. The LU-decomposition is slightly modified to store the matrix coefficients in the core, which are reused in each increment.

In the process of loading step, the approximation $(k+1)^{th}$ is estimated using the approximation k^{th} for the terms on the right hand side. Suppose that $\overset{\circ}{N}_{\alpha\beta}{}^{(k)}$ and $\overset{\circ}{w}_{3,\beta}{}^{(k)}$ express the approximations k^{th}. The initial values of the first loading step $(k=1)$ can be set for example $\overset{\circ}{N}_{\alpha\beta}{}^{linear\,(k)} = 0$ and $\overset{\circ}{w}_{3,\beta}{}^{(k)} = 0$. The loading step in each increment, $q = (k+1)\,\overset{\circ}{q}$.

Relaxation procedures are adopted to improve the numerical results. When the nonlinear terms are calculated in each step of increment , the deflection w_3 and its derivative $w_{3,\beta}$ can be modified as follows:

$$w_3^{k+1} = \varepsilon\, w_3^{k+1} + (1-\varepsilon)\, w_3^k \tag{6.40}$$

$$w_{3,\beta}^{k+1} = \varepsilon\, w_{3,\beta}^{k+1} + (1-\varepsilon)\, w_{3,\beta}^k \tag{6.41}$$

where ε is chosen as 0.5 and $k \geq 2$. Flow chart of the total increment method is shown in Figure 6-1.

6.4.2 Accumulative load incremental method

Alternatively the total load could be presented as an accumulative load incremental method. The $\overset{\circ}{N}_{\alpha\beta}{}^{nonlinear}$ are written as

$$\begin{aligned}\overset{\circ}{N}_{11}{}^{nonlinear\,(k)} &= \frac{B}{2}[2w_{3,1}^{k-1}\,\overset{\circ}{w}{}^{k}_{3,1} + \overset{\circ}{w}{}^{k}_{3,1}\overset{\circ}{w}{}^{k}_{3,1} + \\ &\quad 2\nu(w_{3,2}^{k-1}\,\overset{\circ}{w}{}^{k}_{3,2} + \overset{\circ}{w}{}^{k}_{3,2}\overset{\circ}{w}{}^{k}_{3,2})]\end{aligned} \tag{6.42}$$

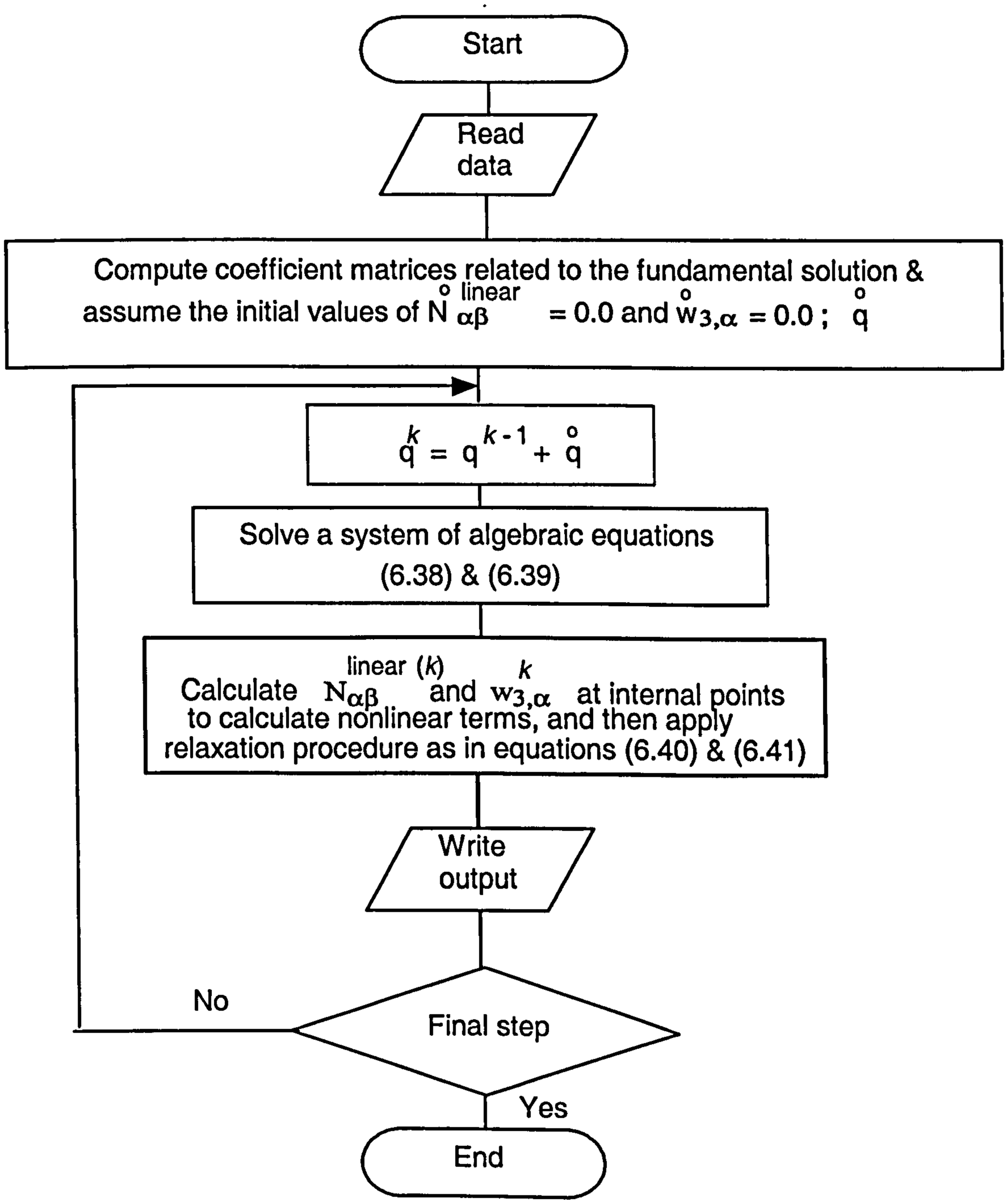

Figure 6-1: Flow chart of the total increment method.

$$\overset{\circ}{N}_{22}{}^{nonlinear\ (k)} = \frac{B}{2}[2w_{3,2}^{k-1}\ \overset{\circ}{w}{}_{3,2}^{k} + \overset{\circ}{w}{}_{3,2}^{k}\overset{\circ}{w}{}_{3,2}^{k} + 2\nu(w_{3,1}^{k-1}\ \overset{\circ}{w}{}_{3,1}^{k} + \overset{\circ}{w}{}_{3,1}^{k}\overset{\circ}{w}{}_{3,1}^{k})] \tag{6.43}$$

$$\overset{\circ}{N}_{12}{}^{nonlinear\ (k)} = \frac{1-\nu}{2}B[w_{3,1}^{k-1}\ \overset{\circ}{w}{}_{3,2}^{k} + \overset{\circ}{w}{}_{3,1}^{k}\overset{\circ}{w}{}_{3,2}^{k} + w_{3,2}^{k-1}\ \overset{\circ}{w}{}_{3,1}^{k}] \tag{6.44}$$

The equations can be written in terms of the incremental values. The loads is divided in small load steps, and the equations are represented as an incremental system of algebraic equations:

$$[H^p]\{\overset{\circ}{w}{}^{k+1}\} + [G^p]\{\overset{\circ}{p}{}^{k+1}\} = [B^p]\{(\overset{\circ}{N}_{\alpha\beta}\overset{\circ}{w}_{3,\beta})_{,\alpha}^{k} + \overset{\circ}{q}\} \tag{6.45}$$

$$[H^m]\{\overset{\circ}{u}{}^{k+1}\} + [G^m]\{\overset{\circ}{t}{}^{k+1}\} = [B^m]\{\overset{\circ}{N}_{\alpha\beta,\beta}{}^{nonlinear\ (k)}\} \tag{6.46}$$

where k denotes incremental step-th; superscript $\overset{\circ}{(.)}$ is incremental of term.

Similar to the total incremental method, once the matrices $[H^p]$, $[G^p]$, $[B^p]$, $[H^m]$, $[G^m]$ and $[B^m]$ have been calculated, they can be used in each step of increment. The loading is provided in small constant loading step $\overset{\circ}{q}$. Then the incremental quantities obtained at each loading step are simply summed up. The modified LU-decomposition is adopted to solve the system of equations. The relaxation procedures as described in equations (6.40) and (6.41) are applied. Flow chart of sub-incremental accumulative method is shown in Figure 6-2.

6.4.3 Euler method

The Euler method is similar to the accumulative load incremental method, but the $\overset{\circ}{N}_{\alpha\beta}{}^{nonlinear}$ are now expressed as first derivative of $N_{\alpha\beta}$ as follows;

$$\overset{\circ}{N}_{11}{}^{nonlinear\ (k)} = B(w_{3,1}^{k}\ \overset{\circ}{w}{}_{3,1}^{k} + \nu w_{3,2}^{k}\ \overset{\circ}{w}{}_{3,2}^{k}) \tag{6.47}$$

$$\overset{\circ}{N}_{22}{}^{nonlinear\ (k)} = B(w_{3,2}^{k}\ \overset{\circ}{w}{}_{3,2}^{k} + \nu w_{3,1}^{k}\ \overset{\circ}{w}{}_{3,1}^{k}) \tag{6.48}$$

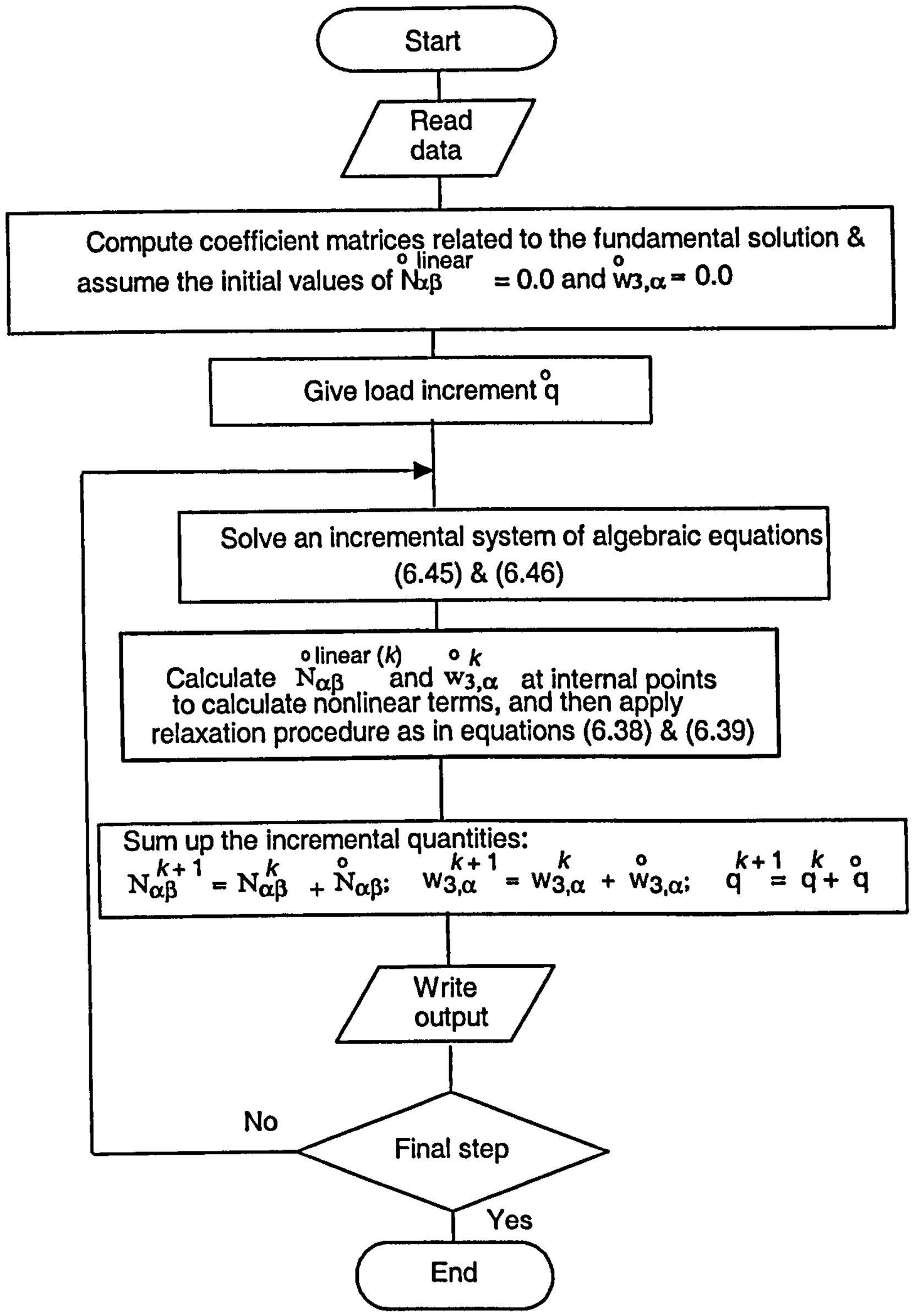

Figure 6-2: Flow chart of accumulative load incremental method.

$$\overset{\circ}{N}_{12}{}^{nonlinear\ (k)} = \frac{1-\nu}{2} B(w_{3,1}^k \overset{\circ}{w}{}_{3,2}^k + w_{3,2}^k \overset{\circ}{w}{}_{3,1}^k) \tag{6.49}$$

where $w_{3,\alpha}^{k+1} = w_{3,\alpha}^k + \overset{\circ}{w}{}_{3,\alpha}^k$

Therefore the system algebraic equations can be written as follows:

$$[B]\{\overset{\circ}{w}{}^{k+1}\} + [C]\{\overset{\circ}{p}{}^{k+1}\} = [D]\{(N_{\alpha\beta}^k \overset{\circ}{w}{}_{3,\alpha}^k + \overset{\circ}{N}{}_{\alpha\beta}^k w_{3,\beta}^k)_{,\alpha} + \overset{\circ}{q}\} \tag{6.50}$$

$$[E]\{\overset{\circ}{u}{}^{k+1}\} + [F]\{\overset{\circ}{t}{}^{k+1}\} = [G]\{\overset{\circ}{N}_{\alpha\beta,\beta}{}^{nonlinear\ (k)}\} \tag{6.51}$$

where $N_{\alpha\beta}^{k+1} = N_{\alpha\beta}^k + \overset{\circ}{N}{}_{\alpha\beta}^k$

The loading is also provided in small loading step $\overset{\circ}{q}$. The previous incremental quantities obtained are simply summed up in each loading step. The modified LU-decomposition is also adopted to solve the system of equations. The relaxation procedures as described in equations (6.40) and (6.41) are applied. Flow chart of Euler method is similar to the flow chart for sub-incremental accumulative method.

6.4.4 Nonlinear System of Equation Method

This method can only be applied to the domain integral method. By introducing the increment terms into the equations (6.9), (6.10), (6.11) and (6.12) , such as

$w_i^{k+1} = w_i^k + \overset{\circ}{w}_i; \qquad u_\alpha^{k+1} = u_\alpha^k + \overset{\circ}{u}_\alpha; \qquad etc.$

The boundary integral equations for plate bending can be rewritten as

$$\begin{aligned} C_{ij}(w_i^k(\mathbf{x}') + \overset{\circ}{w}_i(\mathbf{x}')) + \int_\Gamma P_{ij}^*(\mathbf{x}', \mathbf{x})(w_j^k(\mathbf{x}) + \overset{\circ}{w}_j(\mathbf{x}))d\Gamma(\mathbf{x}) \\ = \int_\Gamma W_{ij}^*(\mathbf{x}', \mathbf{x})(p_j^k(\mathbf{x}) + \overset{\circ}{p}_j(\mathbf{x}))d\Gamma(\mathbf{x}) + \\ \int_\Omega W_{i3}^*(\mathbf{x}', \mathbf{X})(q^k(\mathbf{X}) + \overset{\circ}{q}(\mathbf{X}))d\Omega(\mathbf{X}) \\ - \int_\Omega W_{i3}^*(\mathbf{x}', \mathbf{X})((N_{\alpha\beta}^k + \overset{\circ}{N}_{\alpha\beta})(w_{3,\beta}^k + \overset{\circ}{w}_{3,\beta}))(\mathbf{X})d\Omega(\mathbf{X}) \end{aligned} \tag{6.52}$$

Ignore the higher order incremental terms, gives

$$
\begin{aligned}
& C_{ij}(w_i^k(\mathbf{x}')+ w_i(\overset{\circ}{\mathbf{x}}')) + \int_\Gamma P_{ij}^*(\mathbf{x}',\mathbf{x})(w_j^k(\mathbf{x})+ \overset{\circ}{w}_j\ (\mathbf{x}))d\Gamma(\mathbf{x}) \\
= & \int_\Gamma W_{ij}^*(\mathbf{x}',\mathbf{x})(p_j^k(\mathbf{x})+ p_j(\overset{\circ}{\mathbf{x}}))\ d\Gamma(\mathbf{x}) \\
& + \int_\Omega W_{i3}^*(\mathbf{x}',\mathbf{X})(q^k(\mathbf{X})+ q(\overset{\circ}{\mathbf{X}}))\ d\Omega(\mathbf{X}) \\
& - \int_\Omega W_{i3}^*(\mathbf{x}',\mathbf{X})(N_{\alpha\beta}^k w_{3,\beta}^k + N_{\alpha\beta}^k\ w_{3,\beta}^\circ)(\mathbf{X})d\Omega(\mathbf{X}) \\
& - \int_\Omega W_{i3}^*(\mathbf{x}',\mathbf{X})((\frac{1-\nu}{2}B(w_{3,\beta}^k\ w_{3,\alpha}^\circ + \\
& w_{3,\beta}^\circ\ w_{3,\alpha}^k + 2\frac{\nu}{1-\nu}w_{3,\gamma}^k\ w_{3,\gamma}^\circ\ \delta_{\alpha\beta}))w_{3,\beta}^k)(\mathbf{X})d\Omega(\mathbf{X}) \\
& - \int_\Omega W_{i3}^*(\mathbf{x}',\mathbf{X})(\overset{\circ}{N}_{\alpha\beta}^{\ \ linear}\ w_{3,\beta}^k)(\mathbf{X})d\Omega(\mathbf{X})
\end{aligned}
\tag{6.53}
$$

The boundary integral equations for membrane:

$$
\begin{aligned}
& C_{\theta\alpha}(u_\alpha^k(\mathbf{x}')+ \overset{\circ}{u}_\alpha\ (\mathbf{x}')) + \int_\Gamma T_{\theta\alpha}^*(\mathbf{x}',\mathbf{x})(u_\alpha^k(\mathbf{x})+ \overset{\circ}{u}_\alpha\ (\mathbf{x}))d\Gamma(\mathbf{x}) \\
= & \int_\Gamma U_{\theta\alpha}^*(\mathbf{x}',\mathbf{x})(t_\alpha^k(\mathbf{x})+ \overset{\circ}{t}_\alpha\ (\mathbf{x}))d\Gamma(\mathbf{x}) \\
& - \int_\Omega U_{\theta\alpha,\gamma}^*(\mathbf{x}',\mathbf{X})N_{\alpha\gamma}^{nonlinear\ k}(\mathbf{X})d\Omega(\mathbf{X}) \\
& - \int_\Omega U_{\theta\alpha,\gamma}^*(\mathbf{x}',\mathbf{X})(\frac{1-\nu}{2}B(w_{3,\alpha}^k\ w_{3,\gamma}^\circ \\
& + w_{3,\alpha}^\circ\ w_{3,\gamma}^k + 2\frac{\nu}{1-\nu}w_{3,\eta}^k\ w_{3,\eta}^\circ\ \delta_{\alpha\beta}))(\mathbf{X})d\Omega(\mathbf{X})
\end{aligned}
\tag{6.54}
$$

Derivative of the out of plane displacement:

$$
\begin{aligned}
w_{3,\gamma}^k(\mathbf{X}')+ w_{3,\gamma}^\circ\ (\mathbf{X}') \ = \ & \int_\Gamma W_{3j,\gamma}^*(\mathbf{X}',\mathbf{x})(p_j^k(\mathbf{x})+ p_j(\overset{\circ}{\mathbf{x}}))\ d\Gamma(\mathbf{x}) - \\
& \int_\Gamma P_{3j,\gamma}^*(\mathbf{X}',\mathbf{x})(w_j^k(\mathbf{x}) + w_j^\circ(\mathbf{x}))\ d\Gamma(\mathbf{x}) + \\
& \int_\Omega W_{33,\gamma}^*(\mathbf{X}',\mathbf{X})(q^k(\mathbf{X})+ q(\overset{\circ}{\mathbf{X}}))\ d\Omega(\mathbf{X}) - \\
& \int_\Omega W_{33,\gamma\alpha}^*(\mathbf{X}',\mathbf{X})(N_{\alpha\beta}^k w_{3,\beta}^k + N_{\alpha\beta}^k\ w_{3,\beta}^\circ)(\mathbf{X})\ d\Omega(\mathbf{X})
\end{aligned}
$$

$$\int_\Omega W^*_{33,\gamma\alpha}(\mathbf{X}',\mathbf{X})(\frac{1-\nu}{2}B(w^k_{3,\beta}\,\overset{\circ}{w}_{3,\alpha}+\overset{\circ}{w}_{3,\beta}\,w^k_{3,\alpha}$$
$$+2\frac{\nu}{1-\nu}w^k_{3,\gamma}\,\overset{\circ}{w}_{3,\gamma}\,\delta_{\alpha\beta})w^k_{3,\beta})(\mathbf{X})d\Omega(\mathbf{X})$$
$$\int_\Omega W^*_{33,\gamma\alpha}(\mathbf{X}',\mathbf{X})(\overset{\circ}{N}{}^{linear}_{\alpha\beta}\;w^k_{3,\beta})(\mathbf{X})d\Omega(\mathbf{X}) \qquad (6.55)$$

Membrane stress resultants can be written as:

$$N^{linear\ k}_{\alpha\beta}(\mathbf{X}')+\overset{\circ}{N}{}^{linear}_{\alpha\beta}(\mathbf{X}') = \int_\Gamma U^*_{\Delta\alpha\beta}(\mathbf{X}',\mathbf{x})(t^k_\Delta(\mathbf{x})+\overset{\circ}{t}_\Delta(\mathbf{x}))d\Gamma(\mathbf{x}) -$$
$$\int_\Gamma T^*_{\Delta\alpha\beta}(\mathbf{X}',\mathbf{x})(u^k_\Delta(\mathbf{x})+\overset{\circ}{u}_\Delta(\mathbf{x}))d\Gamma(\mathbf{x})$$
$$-\int_\Omega U^*_{\Delta\alpha\beta,\gamma}(\mathbf{X}',\mathbf{X})N^{nonlinear\ k}_{\Delta\gamma}(\mathbf{X})d\Omega(\mathbf{X})$$
$$-\int_\Omega U^*_{\Delta\alpha\beta,\gamma}(\mathbf{X}',\mathbf{X})(\frac{1-\nu}{2}B(w^k_{3,\Delta}\,\overset{\circ}{w}_{3,\gamma} \qquad (6.56)$$
$$+\overset{\circ}{w}_{3,\Delta}\,w^k_{3,\gamma}+2\frac{\nu}{1-\upsilon}w^k_{3,\eta}\,\overset{\circ}{w}_{3,\eta}\,\delta_{\alpha\beta}))(\mathbf{X})d\Omega(\mathbf{X})$$

Rearranging the equations (6.53), (6.54), (6.55) and (6.56), so all the unknown incremental terms are on the left hand side as given:

$$C_{ij}\,\overset{\circ}{w}_i(\mathbf{x}')) + \int_\Gamma P^*_{ij}(\mathbf{x}',\mathbf{x})\,\overset{\circ}{w}_j(\mathbf{x})\,d\Gamma(\mathbf{x}) - \int_\Gamma W^*_{ij}(\mathbf{x}',\mathbf{x})\,\overset{\circ}{p}_j(\mathbf{x})\,d\Gamma(\mathbf{x}) +$$
$$\int_\Omega W^*_{i3}(\mathbf{x}',\mathbf{X})(N^k_{\alpha\beta}\,\overset{\circ}{w}_{3,\beta})(\mathbf{X})d\Omega(\mathbf{X}) + \int_\Omega W^*_{i3}(\mathbf{x}',\mathbf{X})(w^k_{3,\beta}$$
$$(\frac{1-\nu}{2}B(w^k_{3,\beta}\,\overset{\circ}{w}_{3,\alpha}+\overset{\circ}{w}_{3,\beta}\,w^k_{3,\alpha}+2\frac{\nu}{1-\nu}w_{3,\gamma}\,\overset{\circ}{w}_{3,\gamma}\,\delta_{\alpha\beta})))(\mathbf{X})d\Omega(\mathbf{X}) +$$
$$\int_\Omega W^*_{i3}(\mathbf{x}',\mathbf{X})(w^k_{3,\beta}\,\overset{\circ}{N}{}^{linear}_{\alpha\beta})(\mathbf{X})d\Omega(\mathbf{X})$$
$$= \int_\Omega W^*_{i3}(\mathbf{x}',\mathbf{X})(q^k(\mathbf{X})+\overset{\circ}{q}(\mathbf{X}))\,d\Omega(\mathbf{X}) - C_{ij}w^k_i(\mathbf{x}') + \int_\Gamma W^*_{ij}(\mathbf{x}',\mathbf{x})p^k_j(\mathbf{x})d\Gamma(\mathbf{x}) +$$
$$-\int_\Omega W^*_{i3}(\mathbf{x}',\mathbf{X})(N^k_{\alpha\beta}w^k_{3,\beta})(\mathbf{X})d\Omega(\mathbf{X}) - \int_\Gamma P^*_{ij}(\mathbf{x}',\mathbf{x})w^k_j(\mathbf{x})d\Gamma(\mathbf{x}) \qquad (6.57)$$

for plate bending problems.

$$
\begin{aligned}
& C_{\theta\alpha}\,\overset{\circ}{u}_{\alpha}\,(\mathbf{x}') + \int_{\Gamma} T^{*}_{\theta\alpha}(\mathbf{x}',\mathbf{x})\,\overset{\circ}{u}_{\alpha}\,(\mathbf{x})d\Gamma(\mathbf{x}) - \int_{\Gamma} U^{*}_{\theta\alpha}(\mathbf{x}',\mathbf{x})\,\overset{\circ}{t}_{\alpha}\,(\mathbf{x})d\Gamma(\mathbf{x}) + \\
& \int_{\Omega} U^{*}_{\theta\alpha,\gamma}(\mathbf{x}',\mathbf{X})(\frac{1-\nu}{2}B(w^{k}_{3,\alpha}\,\overset{\circ}{w}_{3,\gamma} + \overset{\circ}{w}_{3,\alpha}\,w^{k}_{3,\gamma} + 2\frac{\nu}{1-\nu}w^{k}_{3,\eta}\,\overset{\circ}{w}_{3,\eta}\,\delta_{\alpha\beta}))(\mathbf{X})d\Omega(\mathbf{X}) \\
= & \int_{\Gamma} U^{*}_{\theta\alpha}(\mathbf{x}',\mathbf{x})t^{k}_{\alpha}(\mathbf{x})d\Gamma(\mathbf{x}) - C_{\theta\alpha}u^{k}_{\alpha}(\mathbf{x}') - \int_{\Omega} U^{*}_{\theta\alpha,\gamma}(\mathbf{x}',\mathbf{X})N^{nonlinear\ k}_{\alpha\gamma}(\mathbf{X})d\Omega(\mathbf{X}) - \\
& \int_{\Gamma} T^{*}_{\theta\alpha}(\mathbf{x}',\mathbf{x})u^{k}_{\alpha}(\mathbf{x})d\Gamma(\mathbf{x})
\end{aligned}
\tag{6.58}
$$

for membrane problems.

$$
\begin{aligned}
& \overset{\circ}{w}_{3,\gamma}\,(\mathbf{X}') - \int_{\Gamma} W^{*}_{3j,\gamma}(\mathbf{X}',\mathbf{x})\,\overset{\circ}{p_j}(\mathbf{x})\,d\Gamma(\mathbf{x}) + \int_{\Gamma} P^{*}_{3j,\gamma}(\mathbf{X}',\mathbf{x})\,\overset{\circ}{w_j}(\mathbf{x})\,d\Gamma(\mathbf{x}) - \\
& \int_{\Omega} W^{*}_{33,\gamma\alpha}(\mathbf{X}',\mathbf{X})(w^{k}_{3,\beta}(\frac{1-\nu}{2}B(w^{k}_{3,\beta}\,\overset{\circ}{w}_{3,\alpha} + \overset{\circ}{w}_{3,\beta}\,w^{k}_{3,\alpha} + \\
& 2\frac{\nu}{1-\nu}w^{k}_{3,\gamma}\,\overset{\circ}{w}_{3,\gamma}\,\delta_{\alpha\beta})))(\mathbf{X})d\Omega(\mathbf{X}) - \int_{\Omega} W^{*}_{33,\gamma\alpha}(\mathbf{X}',\mathbf{X})(N^{k}_{\alpha\beta}\,\overset{\circ}{w}_{3,\beta})(\mathbf{X})\,d\Omega(\mathbf{X}) \\
& - \int_{\Omega} W^{*}_{33,\gamma\alpha}(\mathbf{X}',\mathbf{X})(\overset{\circ}{N}{}^{linear}_{\alpha\beta}\,w^{k}_{3,\beta})(\mathbf{X})d\Omega(\mathbf{X}) \\
= & \int_{\Gamma} W^{*}_{3j,\gamma}(\mathbf{X}',\mathbf{x})p^{k}_{j}(\mathbf{x})d\Gamma(\mathbf{x}) - w^{k}_{3,\gamma}(\mathbf{X}') - \int_{\Omega} W^{*}_{33,\gamma\alpha}(\mathbf{X}',\mathbf{X})(N^{k}_{\alpha\beta}w^{k}_{3,\beta})(\mathbf{X})\,d\Omega(\mathbf{X}) + \\
& \int_{\Omega} W^{*}_{33,\gamma}(\mathbf{X}',\mathbf{X})(q^{k}(\mathbf{X}) + q(\overset{\circ}{\mathbf{X}}))\,d\Omega(X) - \int_{\Gamma} P^{*}_{3j,\gamma}(\mathbf{X}',\mathbf{x})w^{k}_{j}(\mathbf{x})d\Gamma(\mathbf{x})
\end{aligned}
\tag{6.59}
$$

for the derivative of deflection.

$$
\begin{aligned}
& \overset{\circ}{N}{}^{linear}_{\alpha\beta}\,(\mathbf{X}') - \int_{\Gamma} U^{*}_{\Delta\alpha\beta}(\mathbf{X}',\mathbf{x})\,\overset{\circ}{t}_{\Delta}\,(\mathbf{x})d\Gamma(\mathbf{x}) + \int_{\Gamma} T^{*}_{\Delta\alpha\beta}(\mathbf{X}',\mathbf{x})\,\overset{\circ}{u}_{\Delta}\,(\mathbf{x})d\Gamma(\mathbf{x}) + \\
& \int_{\Omega} U^{*}_{\Delta\alpha\beta,\gamma}(\mathbf{X}',\mathbf{X})(\frac{1-\nu}{2}B(w_{3,\Delta}\,\overset{\circ}{w}_{3,\gamma} + \overset{\circ}{w}_{3,\Delta}\,w_{3,\gamma} + \\
& 2\frac{\nu}{1-\nu}w_{3,\eta}\,\overset{\circ}{w}_{3,\eta}\,\delta_{\alpha\beta}))(\mathbf{X})d\Omega(\mathbf{X}) \\
= & \int_{\Gamma} U^{*}_{\Delta\alpha\beta}(\mathbf{X}',\mathbf{x})t_{\Delta}(\mathbf{x})d\Gamma(\mathbf{x}) - N^{linear}_{\alpha\beta}(\mathbf{X}') - \int_{\Gamma} T^{*}_{\Delta\alpha\beta}(\mathbf{X}',\mathbf{x})u_{\Delta}(\mathbf{x})d\Gamma(\mathbf{x}) \\
& - \int_{\Omega} U^{*}_{\Delta\alpha\beta,\gamma}(\mathbf{X}',\mathbf{X})N^{nonlinear}_{\Delta\gamma}(\mathbf{X})d\Omega(\mathbf{X})
\end{aligned}
\tag{6.60}
$$

for linear membrane stress resultants.

It can be seen that there are ten unknown incremental variables $\overset{\circ}{p}\,(x), \overset{\circ}{w}\,(x)$,

$\overset{\circ}{t}(x)$ and $\overset{\circ}{u}(x)$ on the boundary, and five variables $\overset{\circ}{N}_{\alpha\beta}^{linear}$, $\overset{\circ}{w}_{3,\Delta}$ in the domain. The equations (6.57), (6.58), (6.59) and (6.60) can be solved simultaneously and gives the final system of equations:

$$A\,\Delta \mathbf{X} \;=\; \Delta F \tag{6.61}$$

In this case, matrix A is updated in each load increment.

For an iteration process, Newton-Raphson procedure is adopted together with the equations (6.57), (6.58), (6.59) and (6.60). The matrix A is updated in each iteration. The iteration calculation is repeated until satisfying the following convergence condition for k^{th} iteration and $(k+1)^{th}$ iteration:

$$\left| \frac{w_{\max}^{k+1} - w_{\max}^{k}}{w_{\max}^{k}} \right| \;\leq\; \epsilon \tag{6.62}$$

where is ϵ is a small convergence parameter. Flow chart of simultaneous integral method is shown in Figure 6-3.

6.5 Numerical Examples

To assess the accuracy of the proposed methods for analysis of the large deformation problems, several examples with two restraint models as shown in Figure 6-5 and combination of them are presented. BEM models for domain cell integration and the dual reciprocity methods are shown in Figure 6-4. Comparison are made with other numerical methods and analytical results. In the following examples, the non-dimensionalised parameters are expressed as follows:

$$Q = \frac{q\,a^4}{E\,h^4} \tag{6.63}$$

$$Z = \frac{w_3^{\max}}{h} \tag{6.64}$$

where a denotes the radius of circular plate or width of square plate, h is the plate

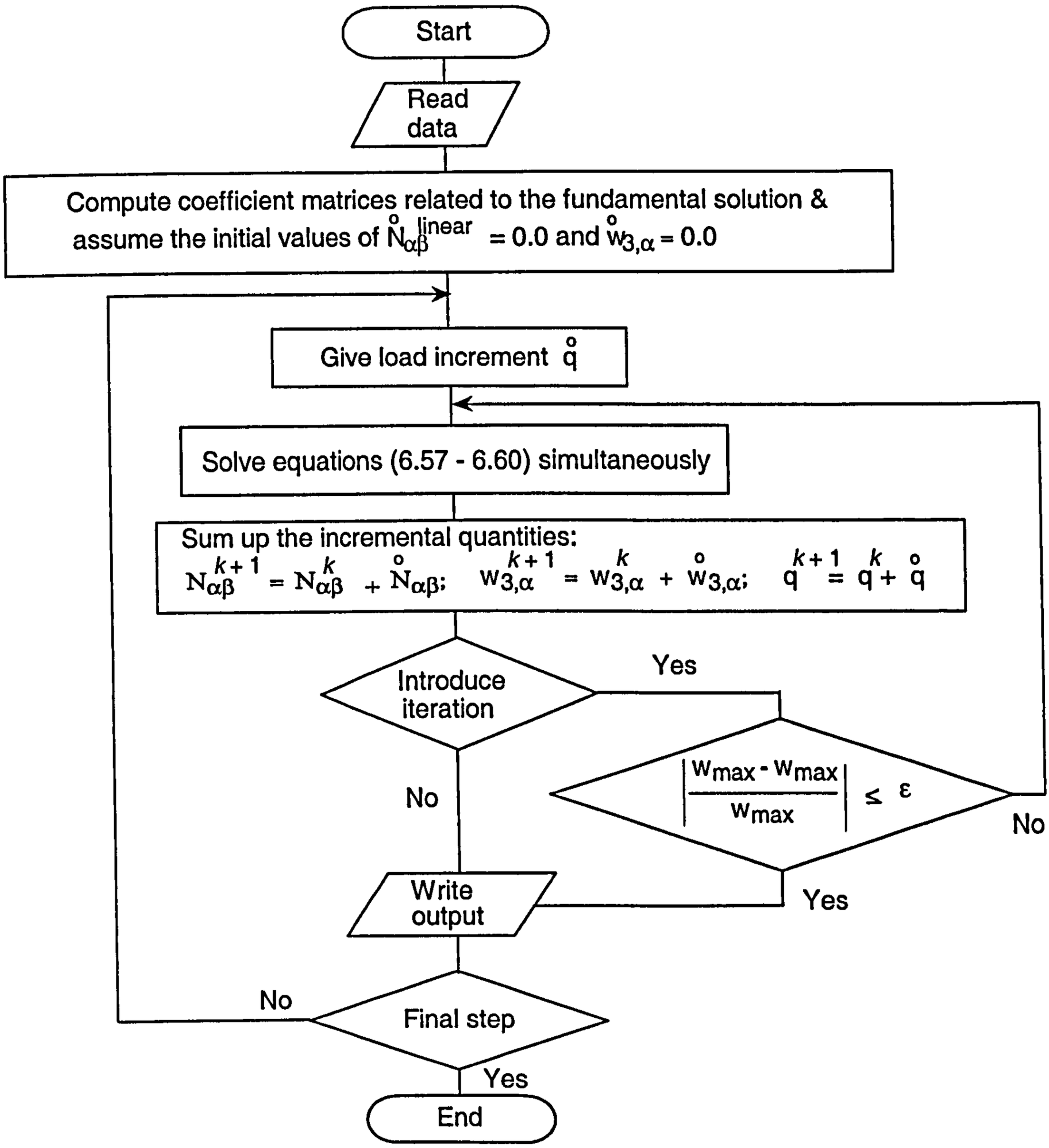

Figure 6-3: Flow chart of nonlinear system of equation method.

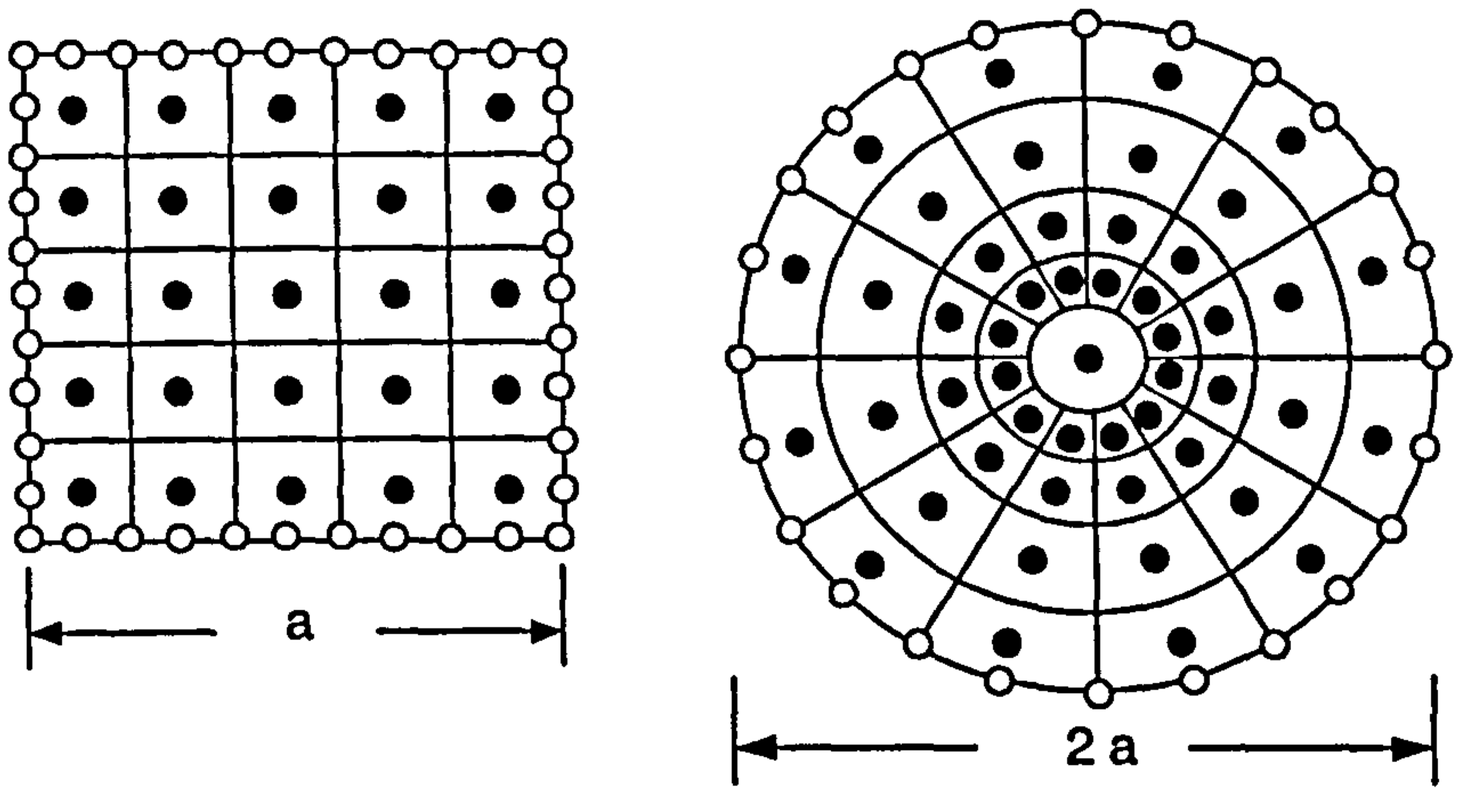

a. Domain cell model

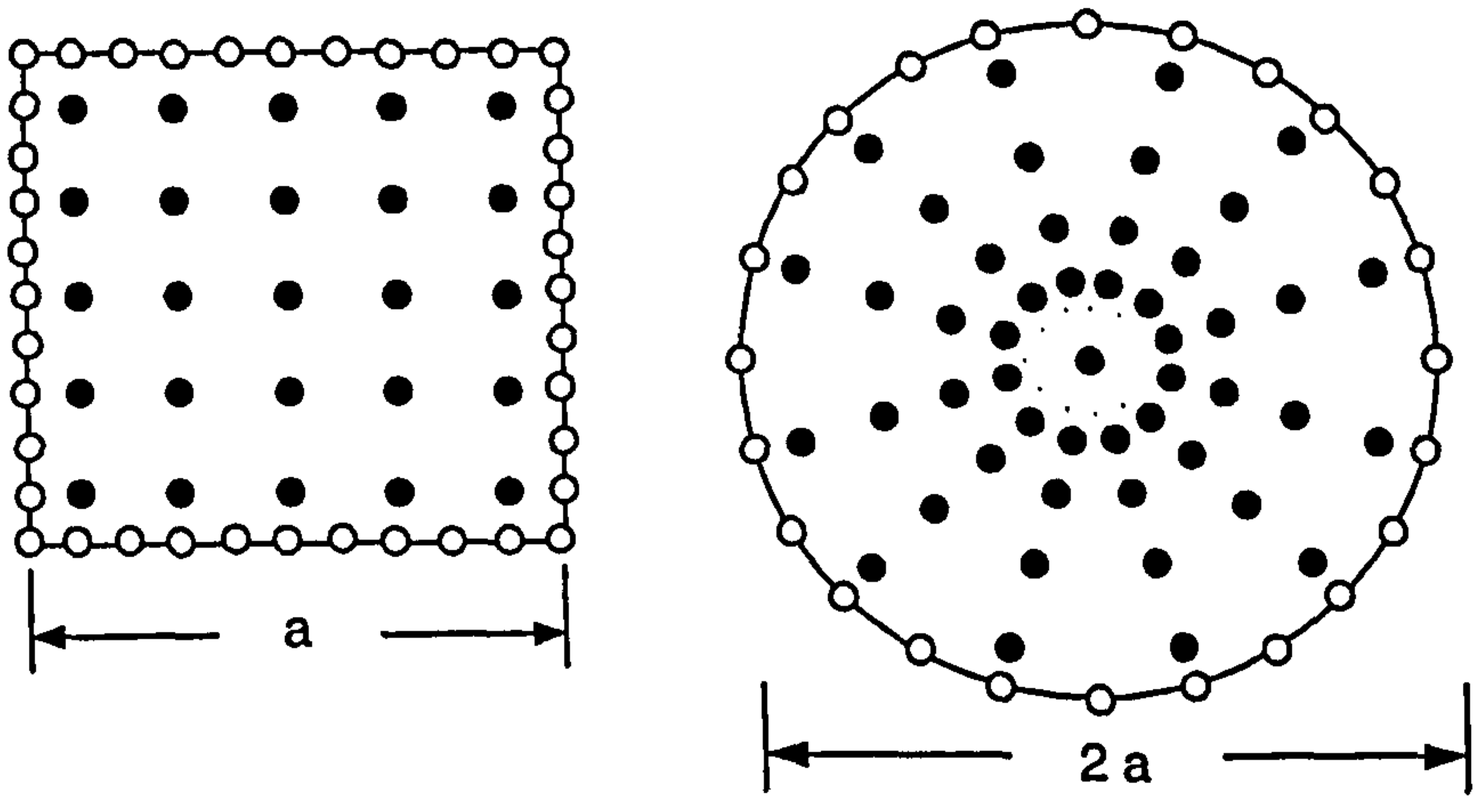

b. DRM model

Figure 6-4: BEM models.

Figure 6-5: Restraint models.

thickness, q is the uniformly lateral distributed load, E is modulus of elasticity and w_3 is lateral deflection. The abbreviations used are:

AFM : approximation function method (domain cells)

DIM : domain integral method (domain cells)

DRM : dual reciprocity method

for domain integral evaluations.

TIM : total increment method

Euler : Euler method

NSEM : nonlinear system of equation method

for solution procedures.

6.5.1 Study of different approximation functions

This example is used to study the accuracy of the different approximation function methods proposed for large deformation analysis. Four different approximations as described in section 6.3.2 are used to evaluate the nonlinear terms which appear in plate bending equation. A simply supported square plate subjected to uniform transverse loads is solved. Assuming the center of plate is at the origin of coordinate system (0.0,0.0), then the boundary condition for this case as follows:

Along $x = \pm\, a/2$: $\quad u_1 = u_2 = w_3 = 0$

Along $y = \pm\, a/2$: $\quad u_1 = u_2 = w_3 = 0$

BEM meshes with 20 quadratic boundary elements, 25 domain cells (for domain integration) and 25 domain points (for DRM) are used (as shown in Figure 6-4). The normalised maximum deflection values Z are plotted in Figure 6-6 and 6-7 and compared with finite element results [60]. It can be seen from the Figures 6-6 and 6-7 that the results of all approximations are in good agreements (less than 1.5% difference) with finite element results.

6.5.2 Total incremental method vs. accumulative load incremental method

In this example, the accuracy and efficiency of the total increment method and the sub increment method are compared. A comparison is also made of both methods in case of the implementation of the relaxation procedure described in section 6.6.1.

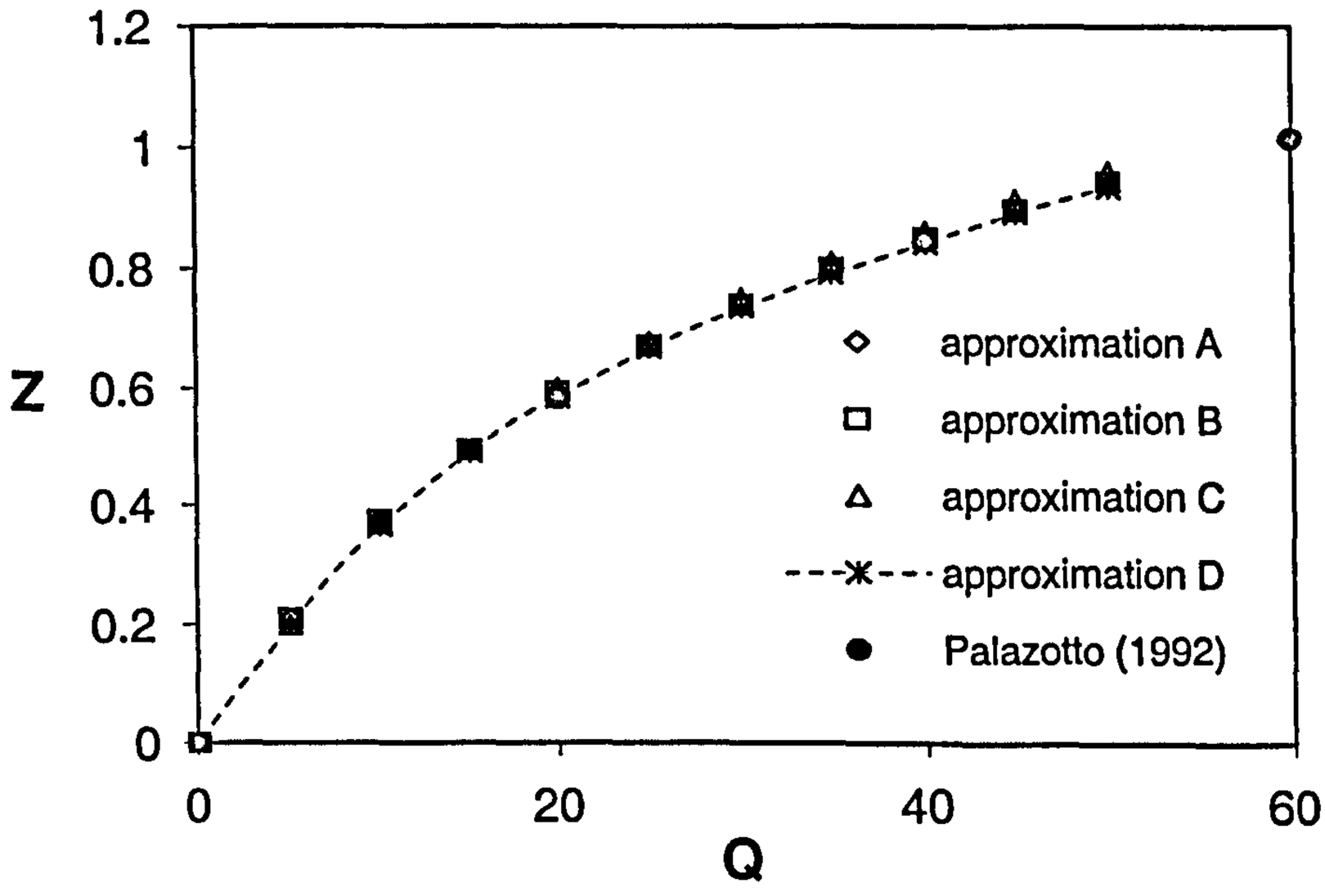

Figure 6-6: Simply supported square plate subjected to uniform transverse loads q with the domain integrals treated using the domain cell technique.

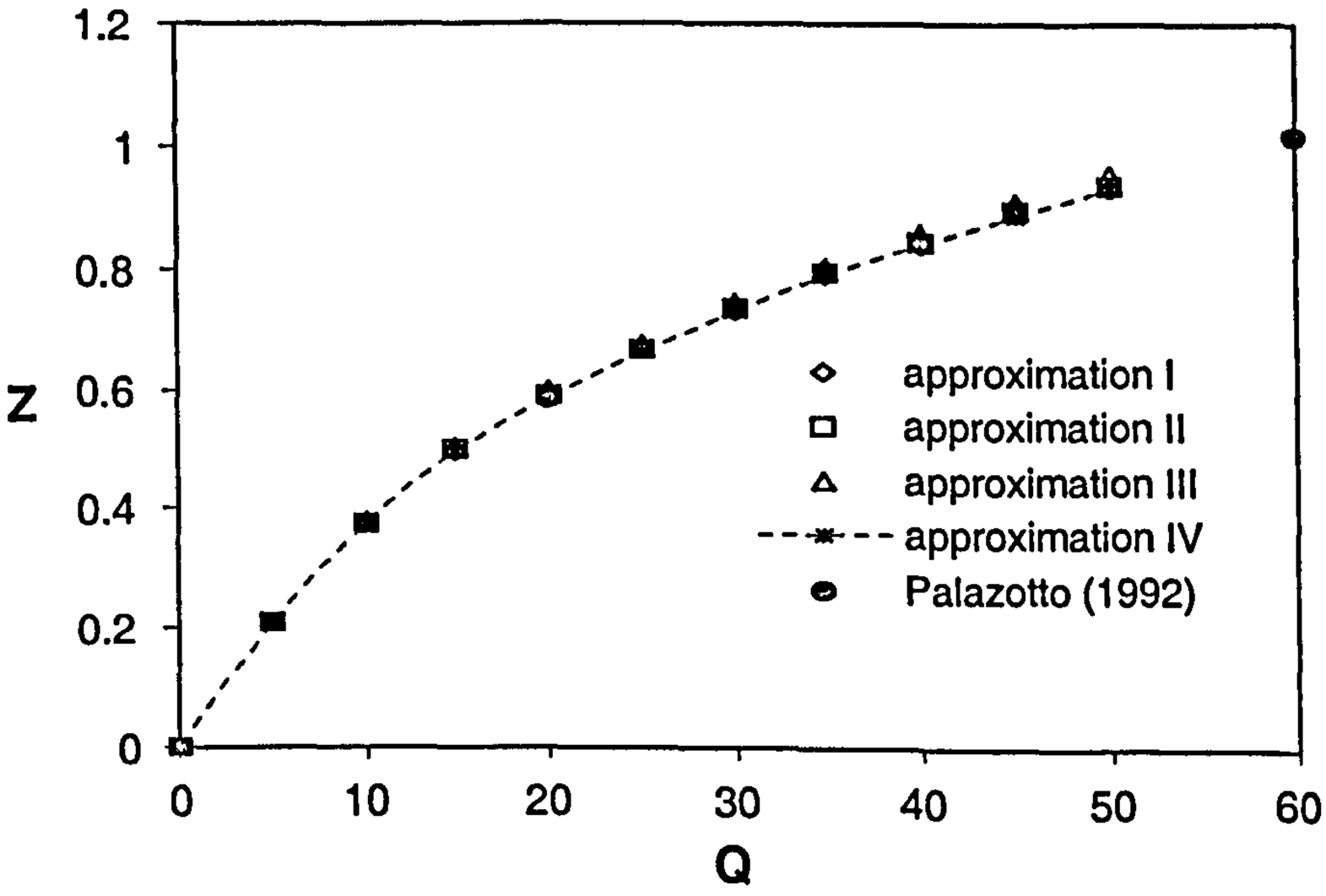

Figure 6-7: Simply supported square plate subjected to uniform transverse loads q with the domain integrals treated using the dual reciprocity technique.

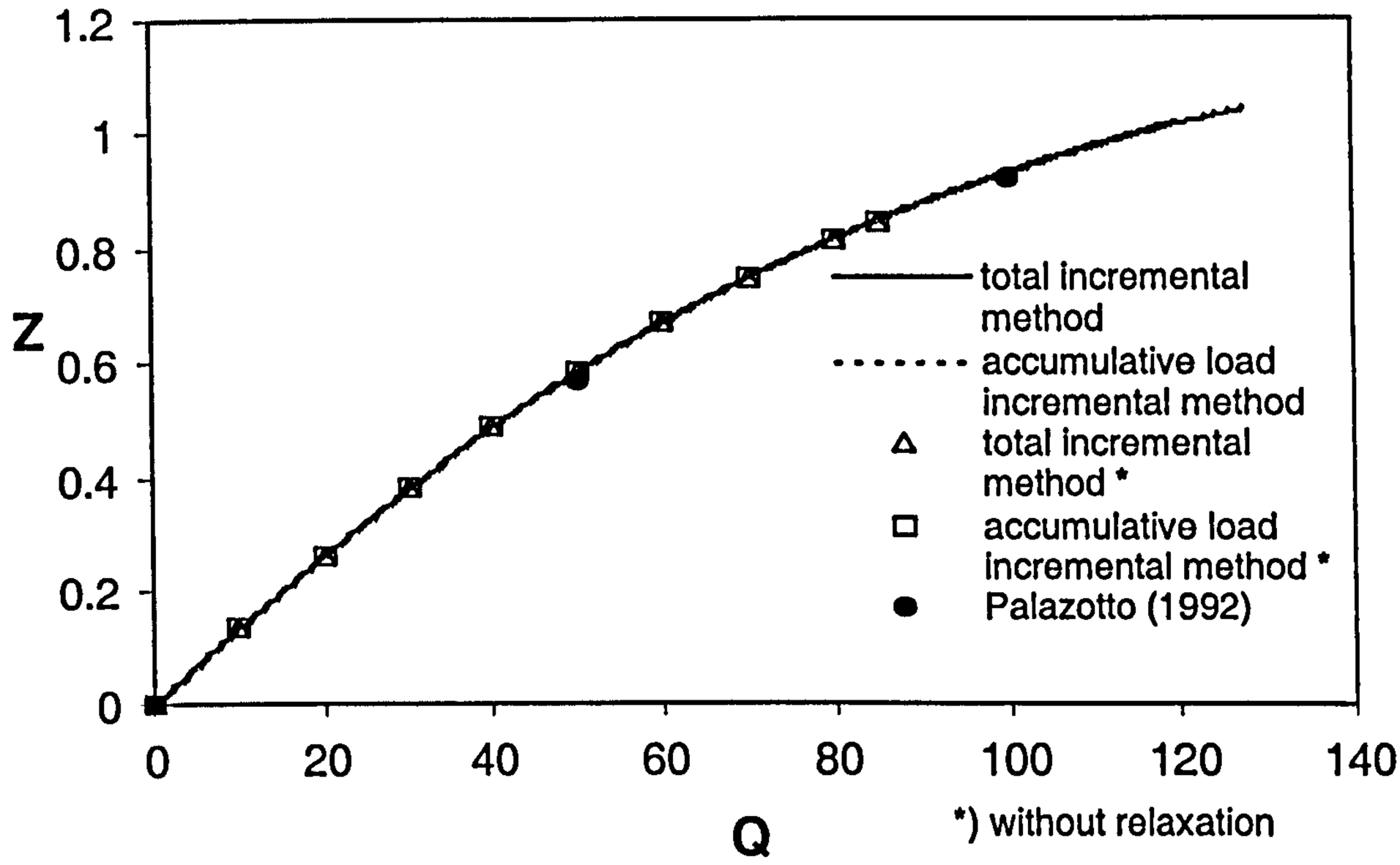

Figure 6-8: Comparison of total increment method and sub increment method.

In this case study, a clamped square plate subjected to a uniform transverse loads q is analysed. If the origin point (0.0,0.0) is located at the center of plate, then the boundary condition for this case as follows:

Along $x = \pm\, a/2$: $\quad u_1 = u_2 = w_1 = w_2 = w_3 = 0$

Along $y = \pm\, a/2$: $\quad u_1 = u_2 = w_1 = w_2 = w_3 = 0$

BEM meshes with 20 quadratic boundary elements and 25 domain points are used in this analysis. The normalised maximum deflection values $\underline{w}$ are plotted as shown in Figure 6-8 and compared with finite element results [60]. It can be seen from the Figure 6-8, that the accumulative load incremental method is identical with the total incremental method. The results of both methods are in good agreements with the reference results. By introducing the relaxation procedure, the numerical results can be improved. Without relaxation procedure, the increment process may have less step of increments.

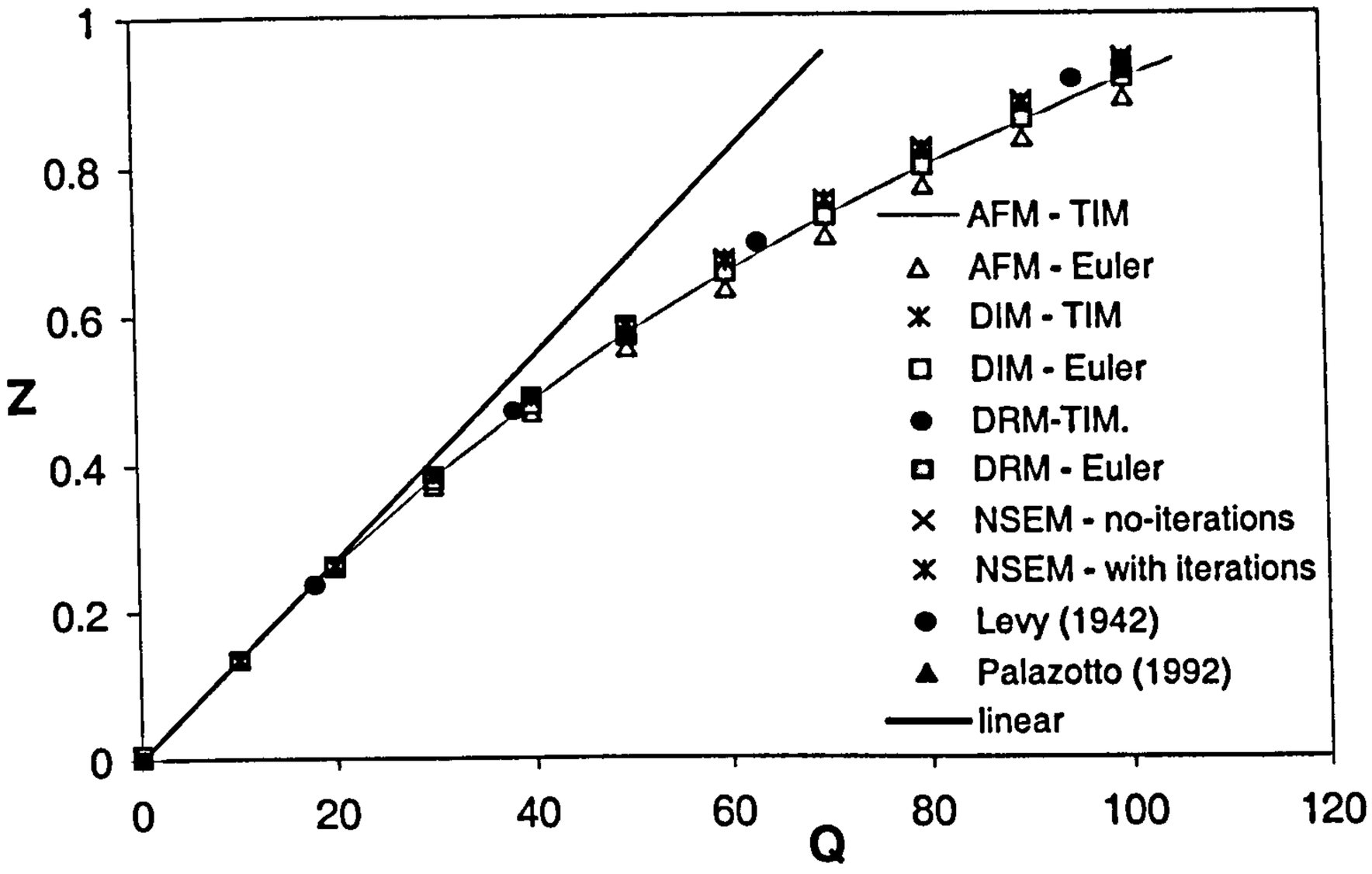

Figure 6-9: Clamped square plate subjected to a uniform load q.

6.5.3 Clamped square plate

In this example, a plate subjected to a uniform distribution load q (see Figure 6-4 and Figure 6-5) is presented. Considering the origin point (0.0,0.0) as a center of the plate, then the boundary condition for this case as follows:

Along $x = \pm\, a/2$: $\quad u_1 = u_2 = w_1 = w_2 = w_3 = 0$

Along $y = \pm\, a/2$: $\quad u_1 = u_2 = w_1 = w_2 = w_3 = 0$

BEM meshes with 20 quadratic boundary elements, 25 domain cells (for domain integration) and 25 domain points (for DRM) are used (as shown in Figure 6-4). The problem is analysed with different solution procedures, i.e. total increment method, Euler method and nonlinear system of equation method with iterations and no iterations. The normalised maximum deflection values Z are plotted in Figure 6-9.

The results are compared with the finite element result [60] and analytical result [51]. Most BEM results are less than 3% differences with the references but the results obtained using approximation function method with solution procedure of

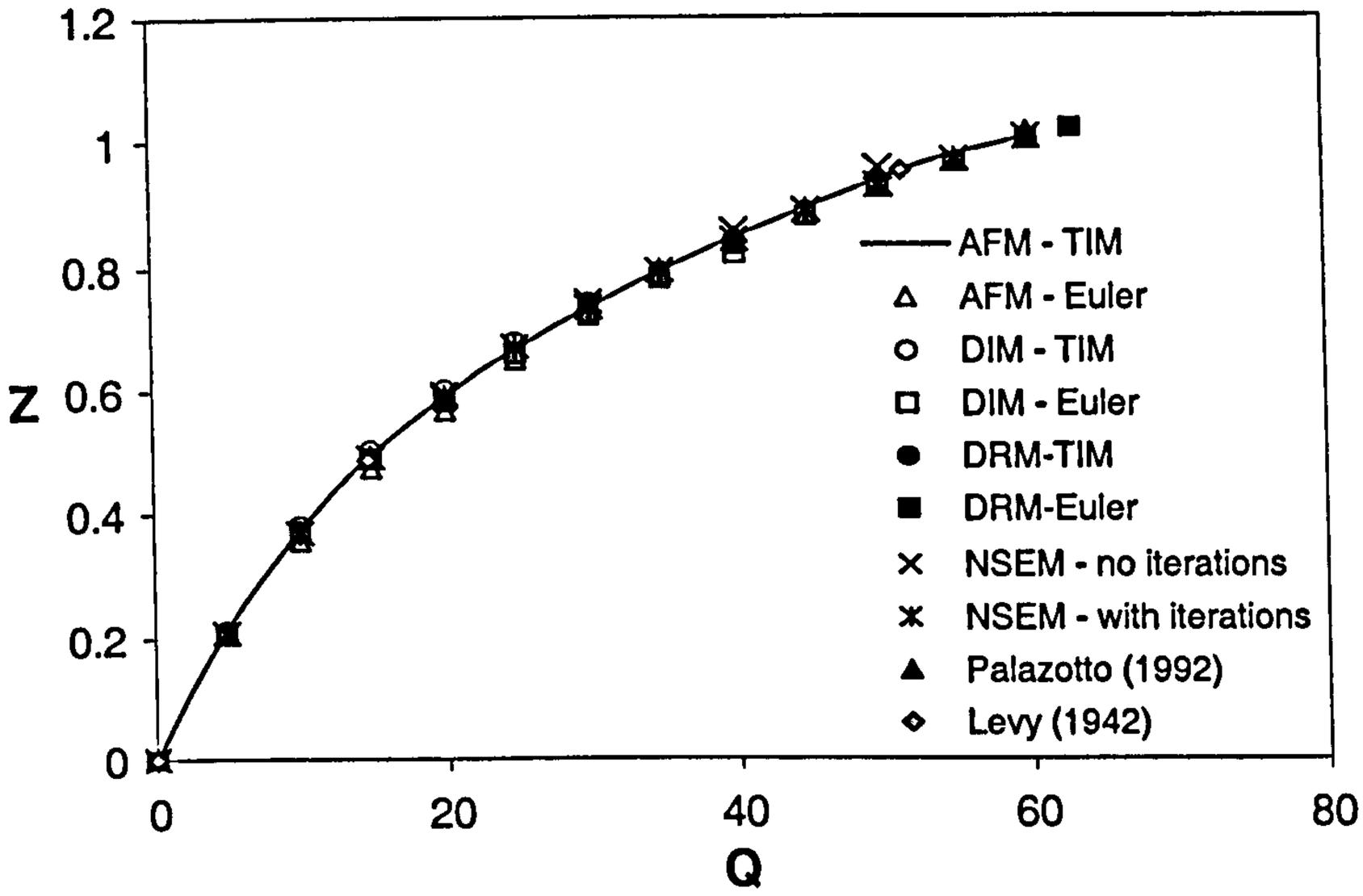

Figure 6-10: Simply supported square plate subjected to a uniform load q.

Euler method provide higher errors with increasing values of Q.

6.5.4 Simply supported square plate

Here a simply supported plate subjected to a uniform distribution load q (see Figure 6-4 and Figure 6-5) is analysed. The other boundary conditions are: $u_1 = u_2 = w_3 = 0$ along all sides.

BEM meshes with 20 quadratic boundary elements, 25 domain cells (for domain integration) and 25 domain points (for DRM) are used (as shown in Figure 6-4). The problem is analysed with different solution procedures, i.e. total increment method, Euler method and nonlinear system of equation method with iterations and no iterations. The normalised maximum deflection values Z are plotted in Figure 6-10. The normalised BEM values of maximum deflection of the plate, finite element result [60] and the analytical result [51] are plotted in Figure 6-10. Good agreement ($< 2\%$ difference) is achieved with the references.

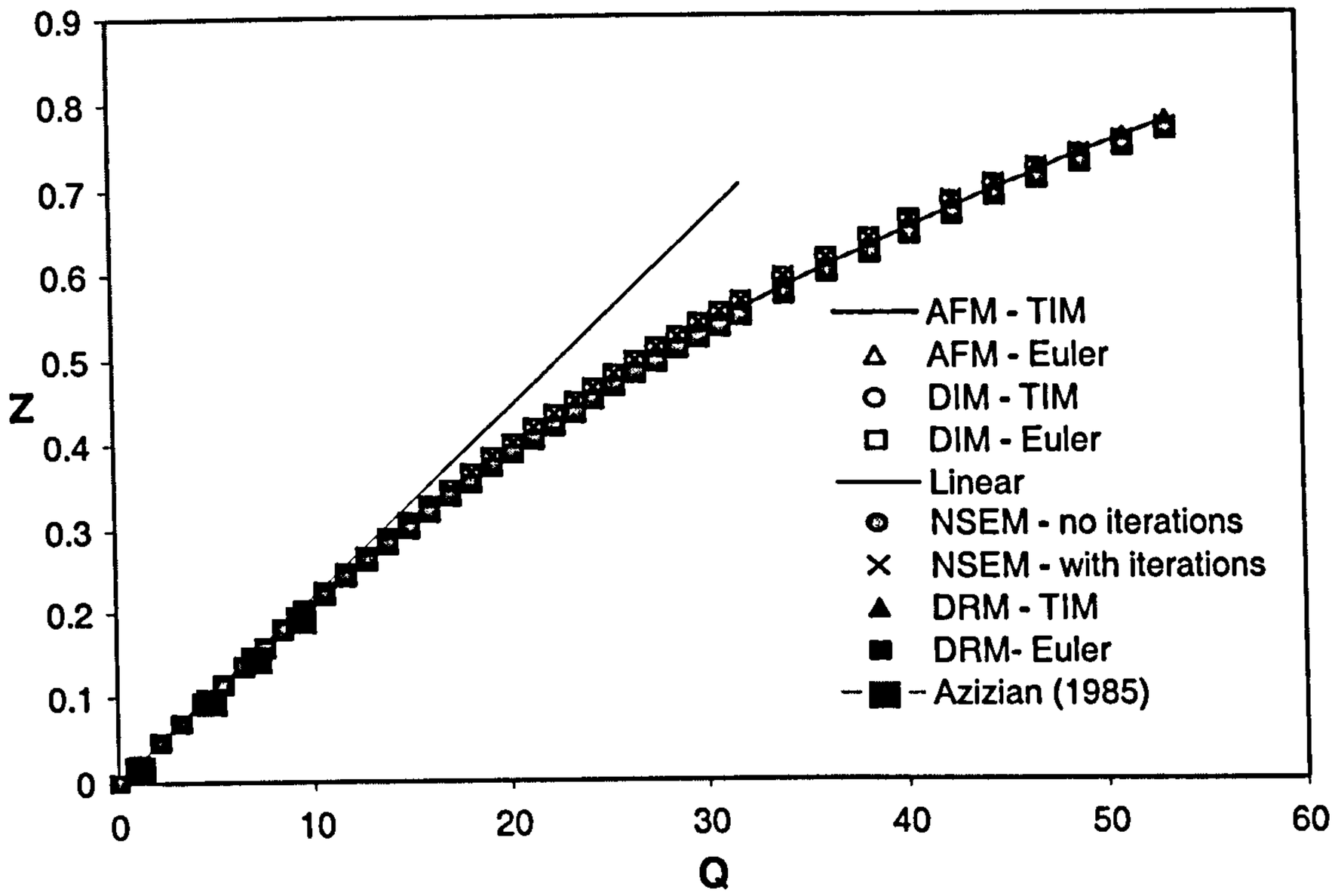

Figure 6-11: A square plate subjected to a uniform load q with two opposite edges clamped and the others simply supported.

6.5.5 A square plate with two opposite edges clamped and the others simply supported

A plate subjected to a uniform transverse load q (see Figure 6-4 and Figure 6-5) is analysed. The boundary conditions for this case are as follows (the origin point (0.0,0.0) as the center of the plate):

Along $x = \pm\, a/2$: $\quad u_1 = u_2 = w_1 = w_2 = w_3 = 0$

Along $y = \pm\, a/2$: $\quad u_1 = u_2 = w_3 = 0$

BEM meshes with 20 quadratic boundary elements, 25 domain cells (for domain integration) and 25 domain points (for DRM) are used. The problem is analysed with different solution procedures, i.e. total increment method, Euler method and nonlinear system of equation method with iterations and no iterations. The normalised maximum deflection values Z of the present method are plotted in Figure 6-11 and compared with the finite strip results [13]. The present results are in good agreement with the reference.

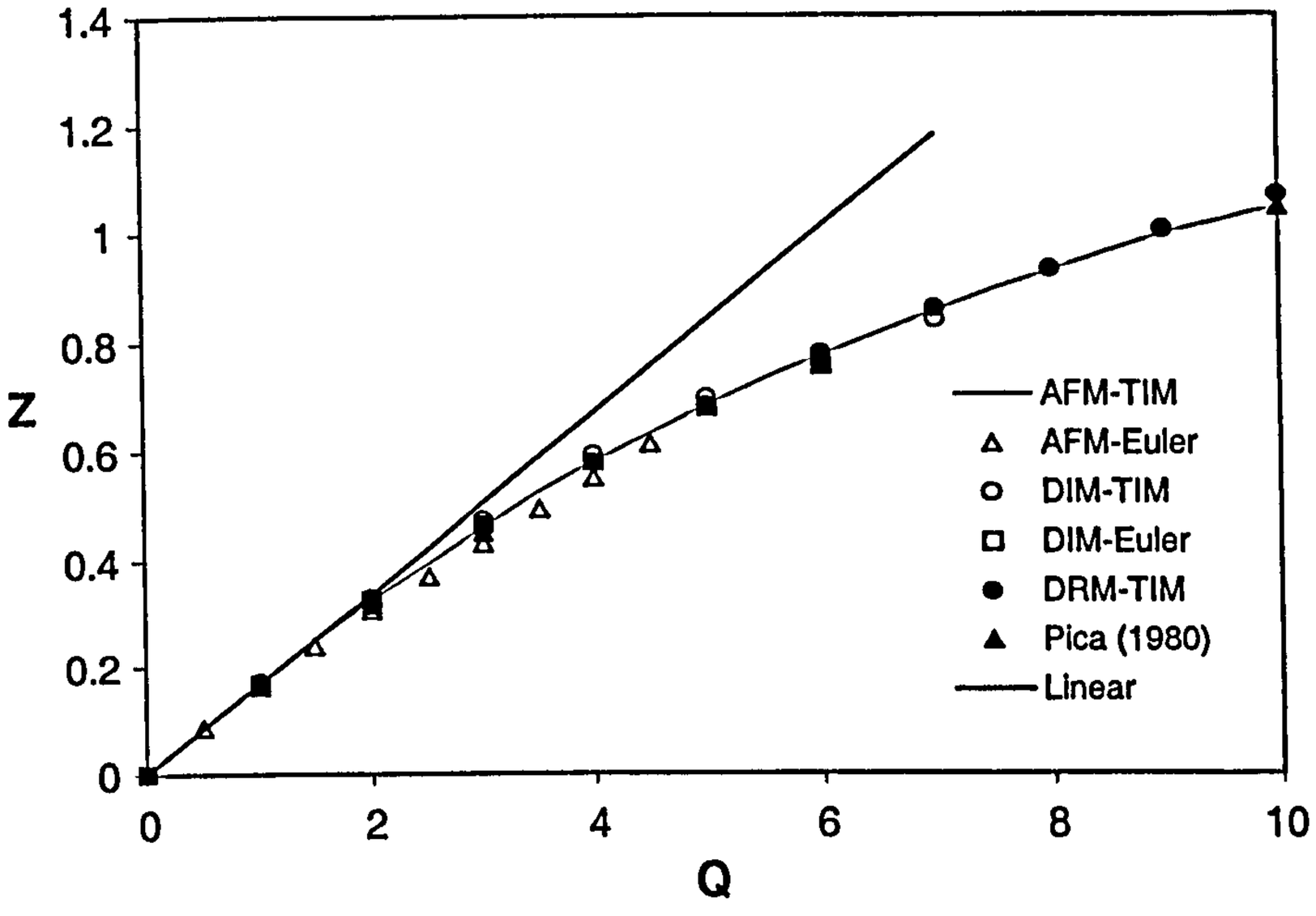

Figure 6-12: Clamped circular plate subjected to a uniform load q.

6.5.6 Clamped circular plate

A circular plate subjected to a uniform distribution load q (see Figure 6-4 and Figure 6-5) is analysed. The perimeter of the plate is restrained from rotations and translations; $u_1 = u_2 = w_1 = w_2 = w_3 = 0$. BEM meshes with 16 quadratic boundary elements, 49 domain cells (for domain integration) and 25 domain points (for DRM) are used (as shown in Figure 6-4). The normalised maximum deflection values Z of the present method are plotted in Figure 6-12 and compared with the finite element results [62]. BEM results are largely in good agreement with the reference (less than 1% difference). But the results obtained using approximation function method with solution procedure of Euler method provide the highest errors.

6.6 Nonlinear Buckling Analysis

The nonlinear buckling analysis can be analysed by making use of equations for large deformation analysis, which the nonlinear terms are approximated by the approximation function. Equation (6.6) can be rewritten as

$$\begin{aligned} & C_{\theta\alpha}u_\alpha(\mathbf{x}') + \int_\Gamma T^*_{\theta\alpha}(\mathbf{x}',\mathbf{x})u_\alpha(\mathbf{x})d\Gamma(\mathbf{x}) \\ = & \int_\Gamma U^*_{\theta\alpha}(\mathbf{x}',\mathbf{x})t_\alpha(\mathbf{x})d\Gamma(\mathbf{x}) - n_\gamma(\mathbf{x})\int_\Gamma U^*_{\theta\alpha}(\mathbf{x}',\mathbf{x})N^{nonlinear}_{\alpha\gamma}(\mathbf{x})d\Gamma(\mathbf{x}) \\ & + \int_\Omega U^*_{\theta\alpha}(\mathbf{x}',\mathbf{X})N^{nonlinear}_{\alpha\gamma,\gamma}(\mathbf{X})d\Omega(\mathbf{X}) \end{aligned} \tag{6.65}$$

The internal in-plane stress resultants can be expressed as

$$\begin{aligned} N^{linear}_{\alpha\beta}(\mathbf{X}') = & \int_\Gamma U^*_{\Delta\alpha\beta}(\mathbf{X}',\mathbf{x})t_\Delta(\mathbf{x})d\Gamma(\mathbf{x}) - \int_\Gamma T^*_{\Delta\alpha\beta}(\mathbf{X}',\mathbf{x})u_\Delta(\mathbf{x})d\Gamma(\mathbf{x}) \\ & -n_\gamma(\mathbf{x})\int_\Gamma U^*_{\Delta\alpha\beta}(\mathbf{X}',\mathbf{x})N^{nonlinear}_{\Delta\gamma}(\mathbf{x})d\Gamma(\mathbf{x}) \\ & + \int_\Omega U^*_{\Delta\alpha\beta}(\mathbf{X}',\mathbf{X})N^{nonlinear}_{\Delta\gamma,\gamma}(\mathbf{X})d\Omega(\mathbf{X}) \end{aligned} \tag{6.66}$$

where traction boundary condition is expressed as

$$\begin{aligned} t^{linear}_\alpha &= t_\alpha - t^{nonlinear}_\alpha \\ t^{nonlinear}_\alpha &= N^{nonlinear}_{\alpha\gamma} n_\gamma \end{aligned} \tag{6.67}$$

Recalling equation (2.44) as

$$N^{nonlinear}_{\alpha\gamma} = \frac{1-\upsilon}{2}B(w_{3,\gamma}w_{3,\alpha} + \frac{\nu}{1-\nu}w_{3,\beta}w_{3,\beta}\delta_{\alpha\gamma}) \tag{6.68}$$

Derivatives of deflection $w_{3,\gamma}$ on the boundary can be approximated by considering a radial basis function $f(r)$ as described in section 4.2.3. The deflection can be approximated as follows

$$w_3(x_1, x_2) = \sum_{m=1}^{N+M} f(r)^m \Psi^m \tag{6.69}$$

where N and M are selected points on the boundary and in the domain respectively

$$\Psi = \mathbf{F}^{-1}\{w_3\} \tag{6.70}$$

We can now define the derivatives as

$$w_{3,\gamma}(x_1, x_2) = \mathrm{f}(r)_{,\gamma}\mathbf{F}^{-1}\{w_3\} \tag{6.71}$$

Therefore the nonlinear membrane traction $t_\alpha^{nonlinear}$ can be calculated by making use of equations (6.68) and (2.31). Equations (6.16) and (6.17) are used to calculate nonlinear terms at internal points.

6.6.1 Initial Imperfections

In this chapter, initial imperfections are introduced to analyse nonlinear buckling problems. Two initial imperfection models as shown in Figure 6-13 are presented for this analysis:

i. Uniform distribution of the transverse loads q_0 in the domain Ω

ii. Distributed transverse loads $q_0(x, y)$ in the domain Ω related to the eigenvectors of the eigenvalue problem.

The first model is shown in Figure 6-13 a. This model allow for only few nonlinear buckling problems to be analysed accurately, especially for geometries of square and circular models. The second model shown in Figure 6-13 b is generally recommended, as imperfections can be modelled based on the eigenvectors. The eigenvectors are related to the buckling modes, so the second model can represent the initial imperfections that should be distributed in the domain.

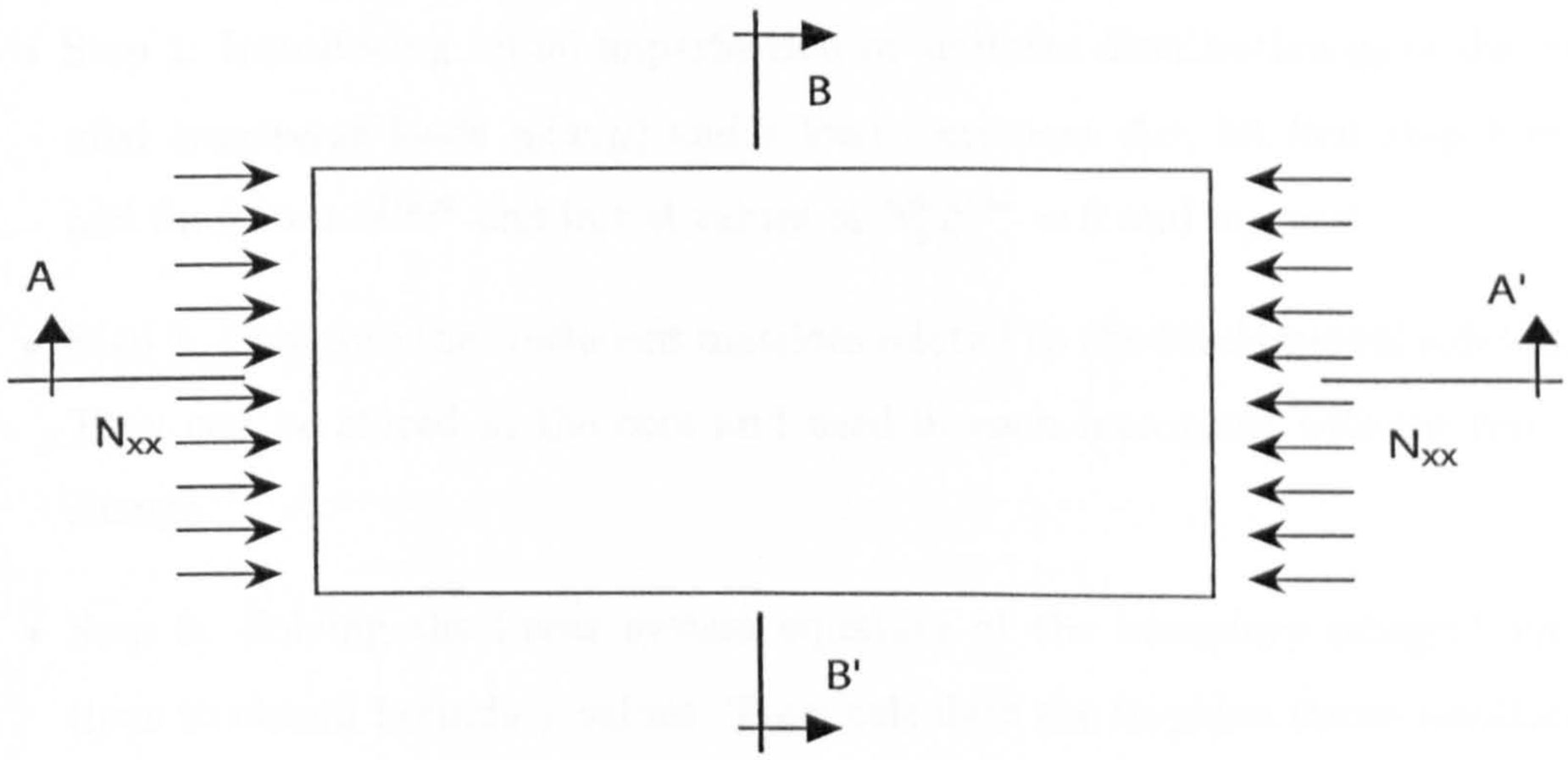

VIEW A-A'

VIEW B-B'

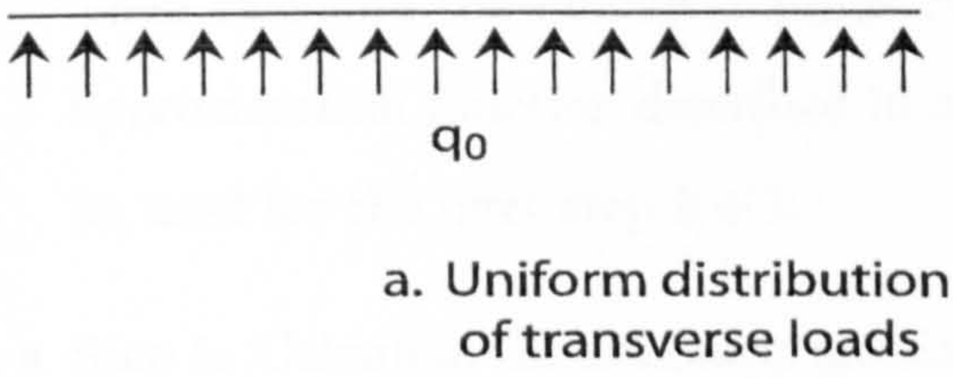

a. Uniform distribution of transverse loads

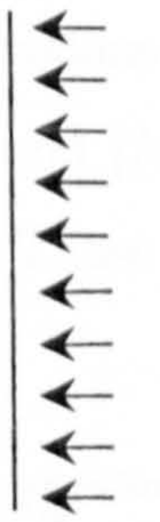

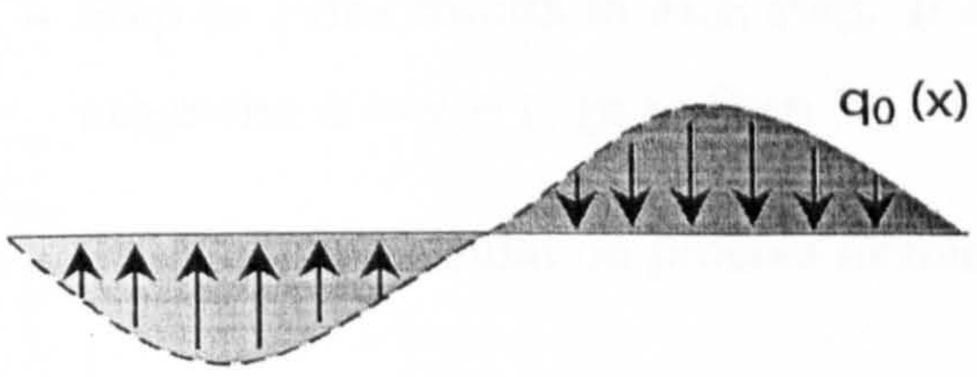

b. Distributed transverse loads

Figure 6-13: Initial imperfection models.

6.6.2 Numerical Algorithms

A simple numerical algorithm can be performed to analyse nonlinear buckling, in which no iterations are required. The algorithm can be summarized as follows:

- Step 1: Introducing initial imperfection by uniform distribution q_0 or distributed transverse loads $q_0(x, y)$ and a load increment $\Delta\sigma$, let first step $k = 1$ and final step k^{final} and initial values of $N_{\alpha\beta}^{linear} = 0$ and $w_{,\alpha} = 0$.

- Step 2: Compute the coefficient matrices related to the fundamental solutions. They can be stored in the core and used in each increment without further change.

- Step 3: Solving the linear system equation of the boundary integral equations to obtain boundary values. Then calculate the in-plane stress resultants $N_{\alpha\beta}^{linear}$ and derivative of deflection $w_{,\alpha}$ in the domain.

- Step 4: Apply the relaxation procedure (see equations (6.40) and (6.41)). Then calculate the nonlinear terms $N_{\alpha\gamma,\gamma}^{nonlinear\ (k)}$ and $[N_{\alpha\beta}w_{3,\beta}]_{,\alpha}^{(k)}$ using the approximation function described in section 6.3.2. These nonlinear terms will be used for the next step $k + 1$.

- Step 5: Calculate the nonlinear membrane traction $t_{\alpha}^{nonlinear}$ on the boundary.

- Step 6: Print results in each step. If step k is final step k^{final}, go to Step 7, otherwise $k = k + 1$, go to Step 3.

- Step 7: The calculation process terminates.

The flow chart that represents the detail of procedures described above is presented in Figure 6-14.

6.7 Numerical Examples

Several numerical examples are presented to demonstrate the ability of the proposed method to analyse nonlinear buckling problems with different geometries, loadings

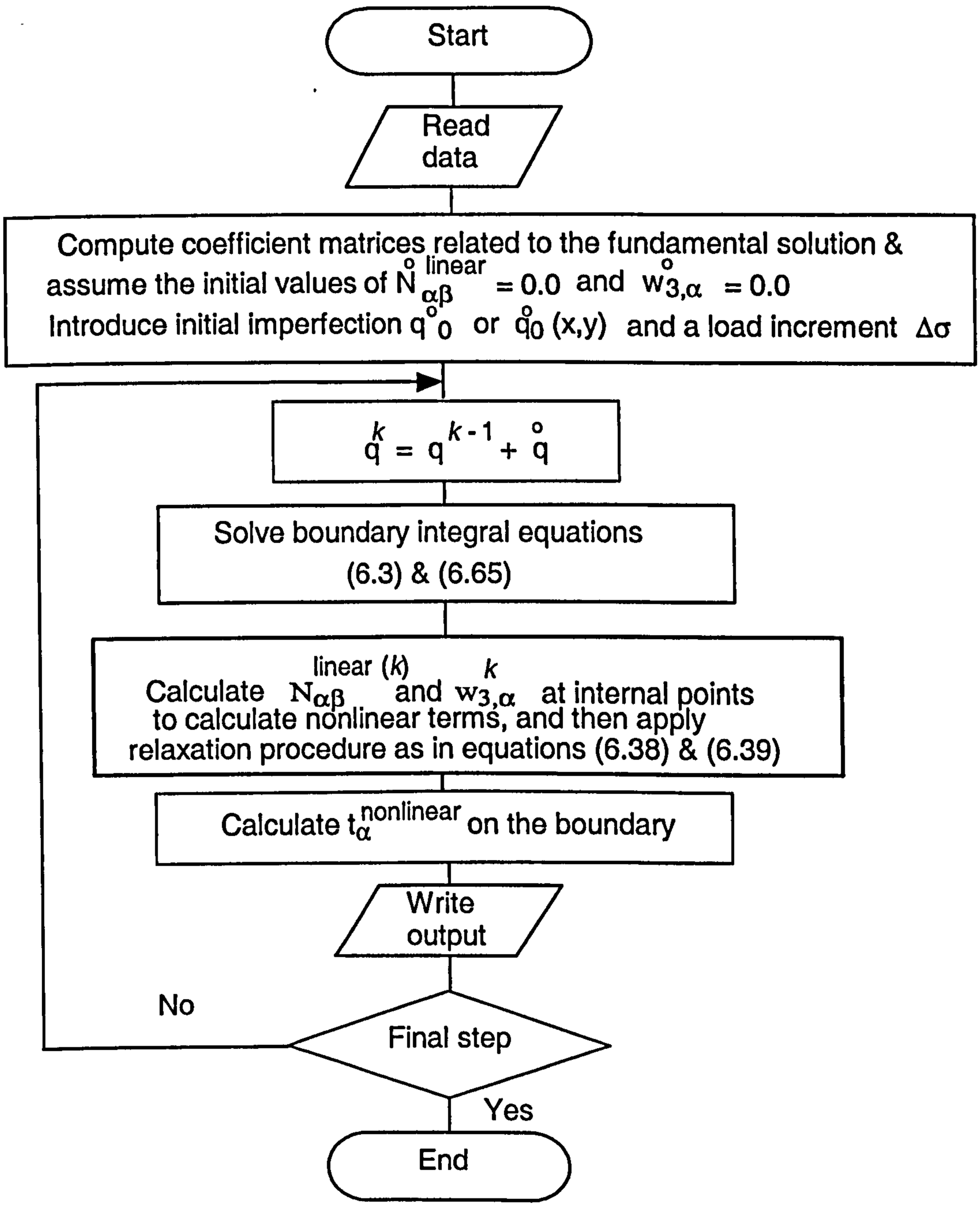

Figure 6-14: Flow chart of the nonlinear buckling analysis.

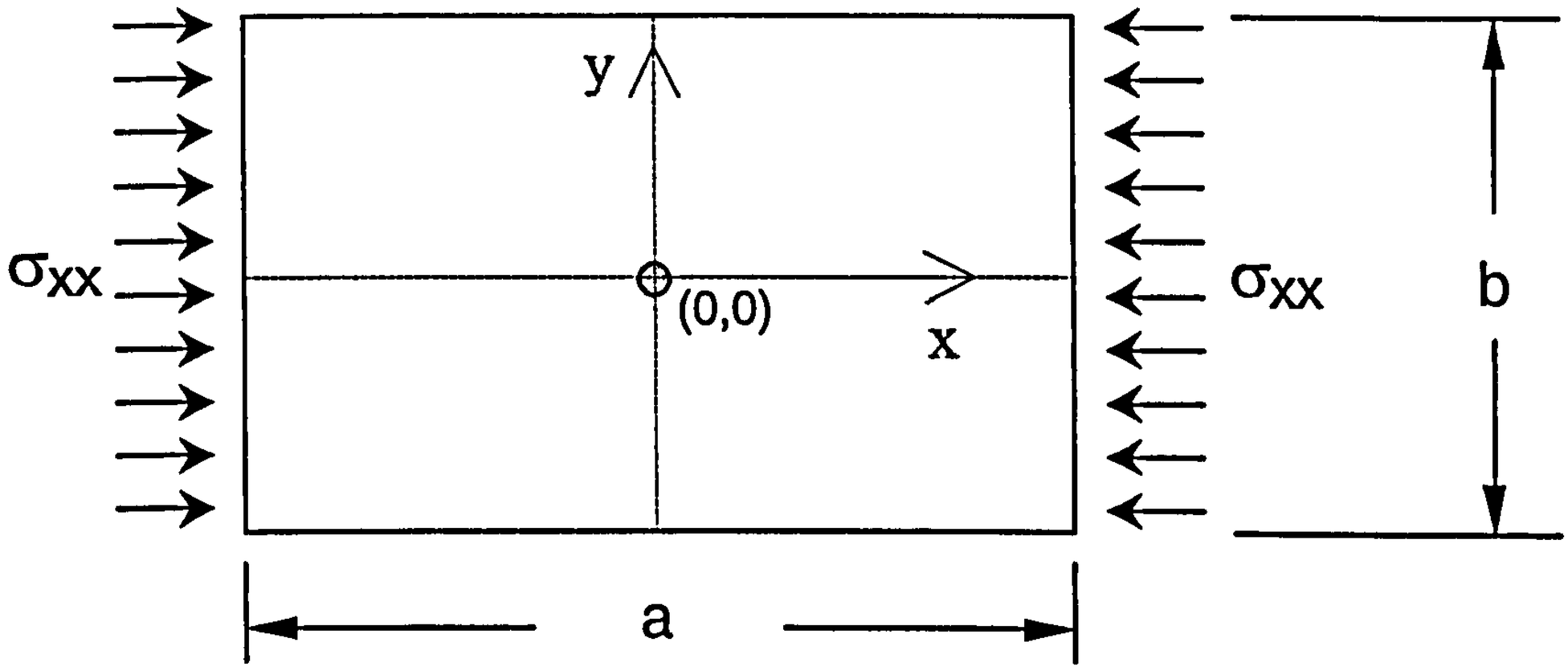

Figure 6-15: Nonlinear buckling model.

and boundary conditions. The nonlinear buckling model is shown in Figure 6-15. In the following examples, the normalized compression stresses K_{nl} are defined by

$$K_{nl} = \frac{b^2}{\pi^2 D}\sigma \tag{6.72}$$

where σ is compression stress, b is the width or diameter of plates and D is flexural rigidity of plate as described in chapter 3. The normalised deflection Z is given by equation (6.64).

6.7.1 Convergence study of a simply supported square plate subjected to uni-axial compression loads

In this example, a square plate modelled using 20 quadratic boundary elements subjected to compression loads at its ends as shown in Figure 6-15 is analysed. Five different distributions of domain points are used for the dual reciprocity calculations. The initial imperfection is introduced by a uniform transverse load $q_0 = 0.005$ units and in the case of $\Delta\sigma = 4$ units. Convergence study of the simply supported square plate is performed and the relationship between the normalized compression stresses K_{nl} and the normalized deflection Z are plotted in Figure 6-16. The results given by Levy [50] are also plotted in Figure 6-16. Following conclusions can be summarized from the Figure 6-16:

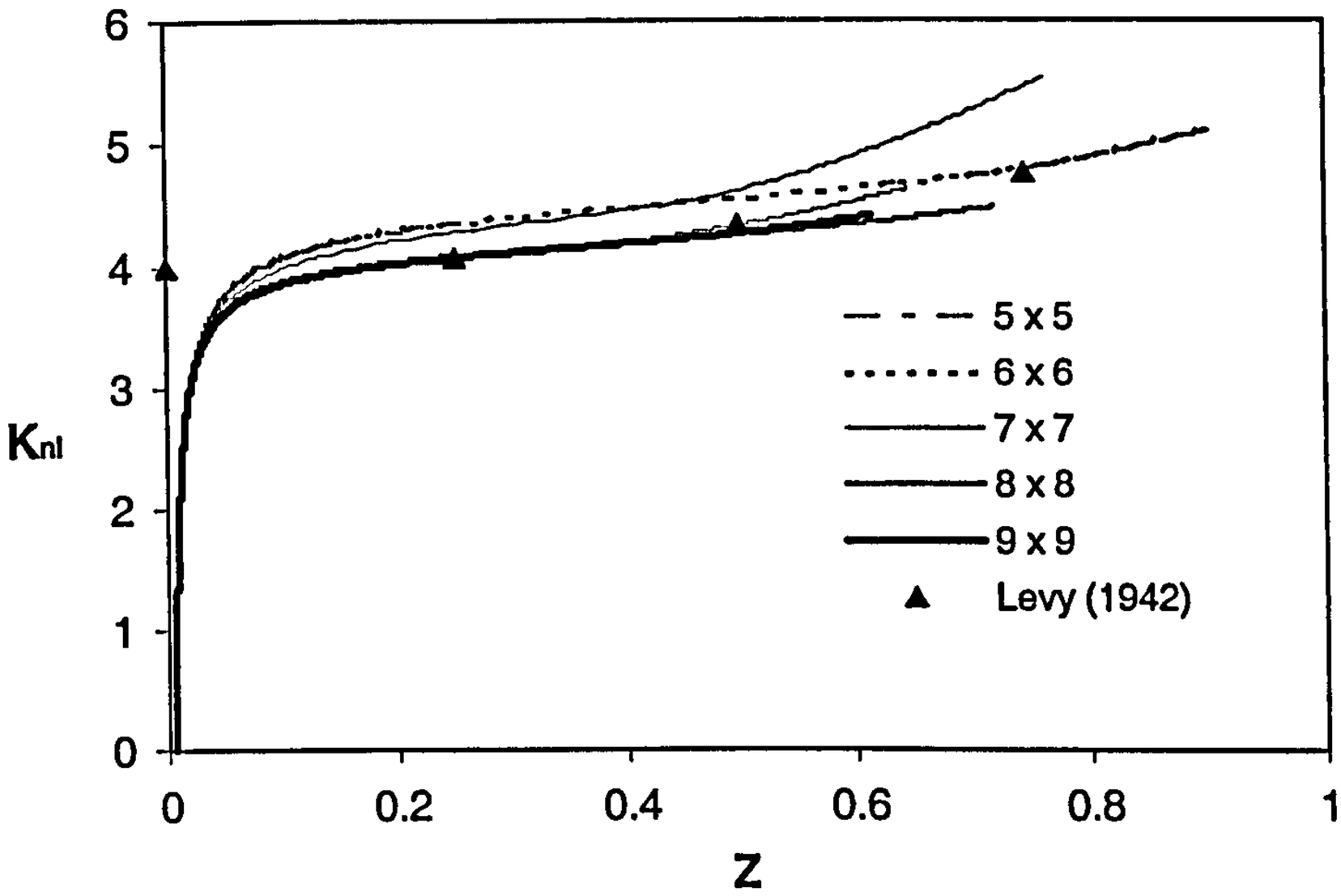

Figure 6-16: Convergence of the normalized compression stresses K_{nl} and deflection Z for different number of domain points.

- The convergence of the results can be achieved with 49 domain points.
- The critical value of the normalized compression stress is in good agreement with the analytical result, that is $K_{nl} \approx 4$.
- The BEM results are in good agreement with Levy's exact solutions [50].

6.7.2 Simply supported square plate subjected to uni-axial compression loads with different initial imperfections and increments of load

In this example, a simply supported square plate subjected to uni-axial compression load is analysed with different imperfections and increments of the load. A BEM mesh with 20 quadratic boundary elements and 49 domain points are used. The relationship between the normalized compression stresses K_{nl} and deflection Z for different initial imperfections and in the case of $\Delta\sigma = 4$ units of compression loads are plotted in Figure 6-17.

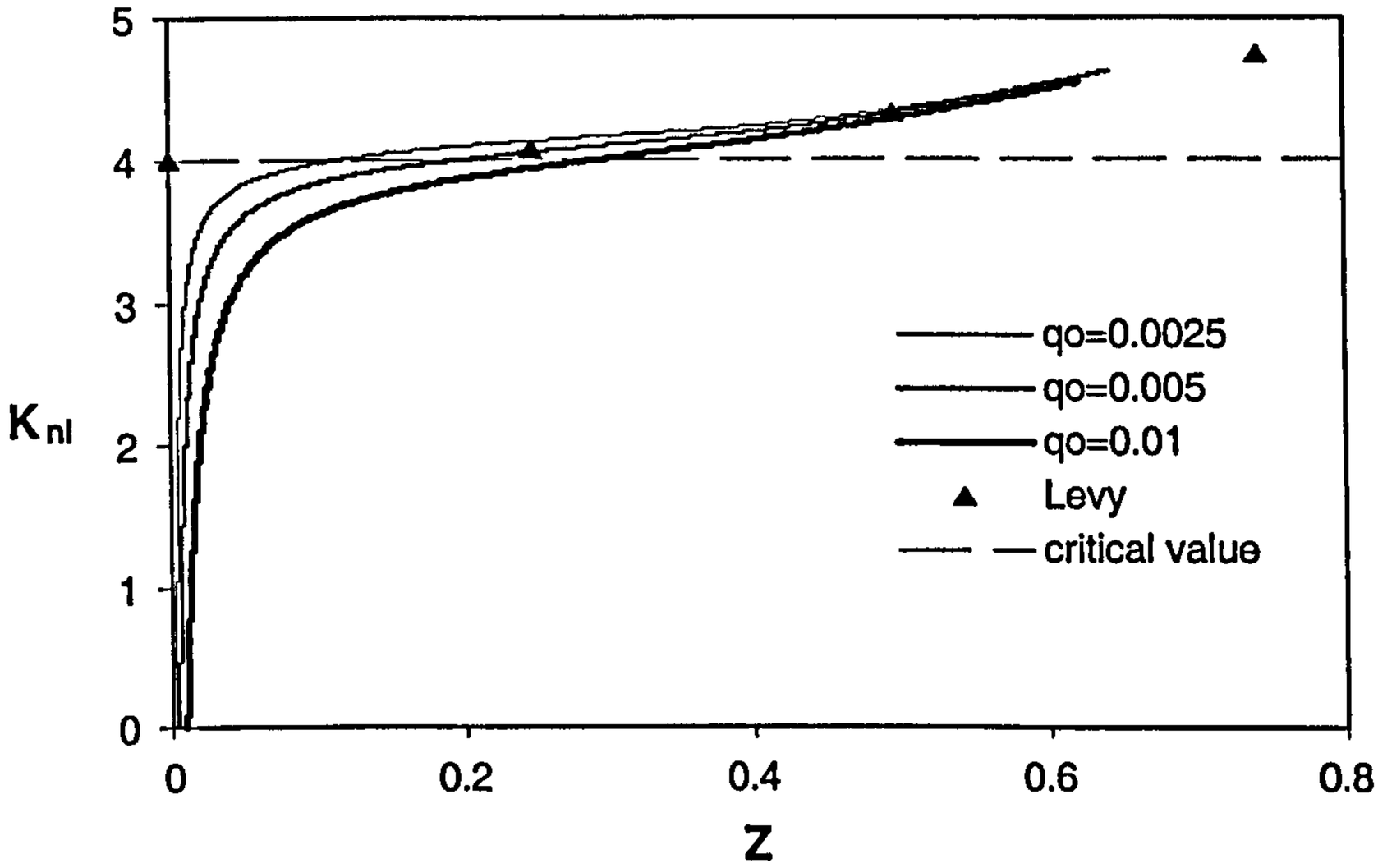

Figure 6-17: Nonlinear buckling of the simply supported square plate for different imperfections.

The relationship between the normalized compression stresses K_{nl} and deflection Z for different increment of compression loads and in the case of $q_0 = 0.005$ units of uniform transverse load are plotted in Figure 6-18. It can be seen from Figure 6-17 that the bigger value of initial imperfection provides a lower critical buckling load. While Figure 6-18 shows that the bigger value of compression load increment provides a bigger critical buckling load. Good agreements are achieved when the increments of compression loads are applied as $\Delta\sigma = 4$ units.

6.7.3 Circular and square plates subjected to a uniform normal compression loads

Here nonlinear buckling analysis of circular and square plates as shown in Figure 6-19 subjected to uniform normal compression loads are presented. Two boundary conditions, i.e. simply supported and clamped are applied. BEM meshes with 16 quadratic boundary elements and 33 domain points for circular plate, and 20 quadratic boundary elements and 25 domain points for square plate are used. In this

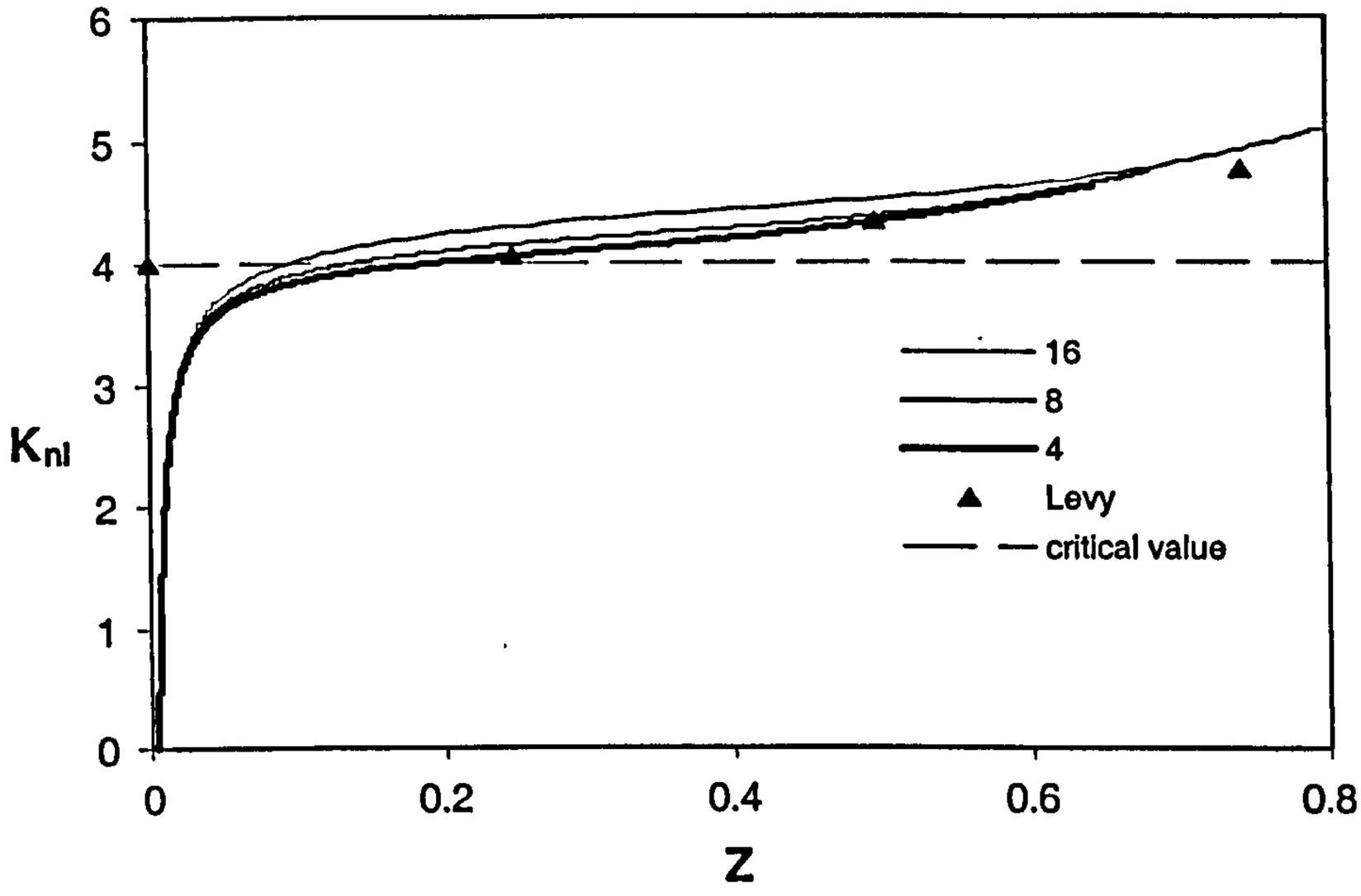

Figure 6-18: Nonlinear buckling of the simply supported square plate for different increments of compression loads.

case, the increments of compression loads as $\Delta\sigma = 4$ units and initial imperfection as $q_0 = 0.005$ units are applied. The normalized compression stresses K_{nl} and the normalized deflection Z together with critical value of each model are plotted in Figure 6-20. It can be seen from Figure 6-20 that the results are in agreement with the analytical critical values.

The legends in Figure 6-20 are denoted as follows:

c-ssss	:	simply supported circular plate
s-ssss	:	simply supported square plate
c-cccc	:	clamped circular plate
s-cccc	:	clamped square plate
cv-c-ssss	:	critical value of simply supported circular plate
cv-s-ssss	:	critical value of simply supported square plate
cv-c-cccc	:	critical value of clamped circular plate
cv-s-cccc	:	critical value of clamped square plate

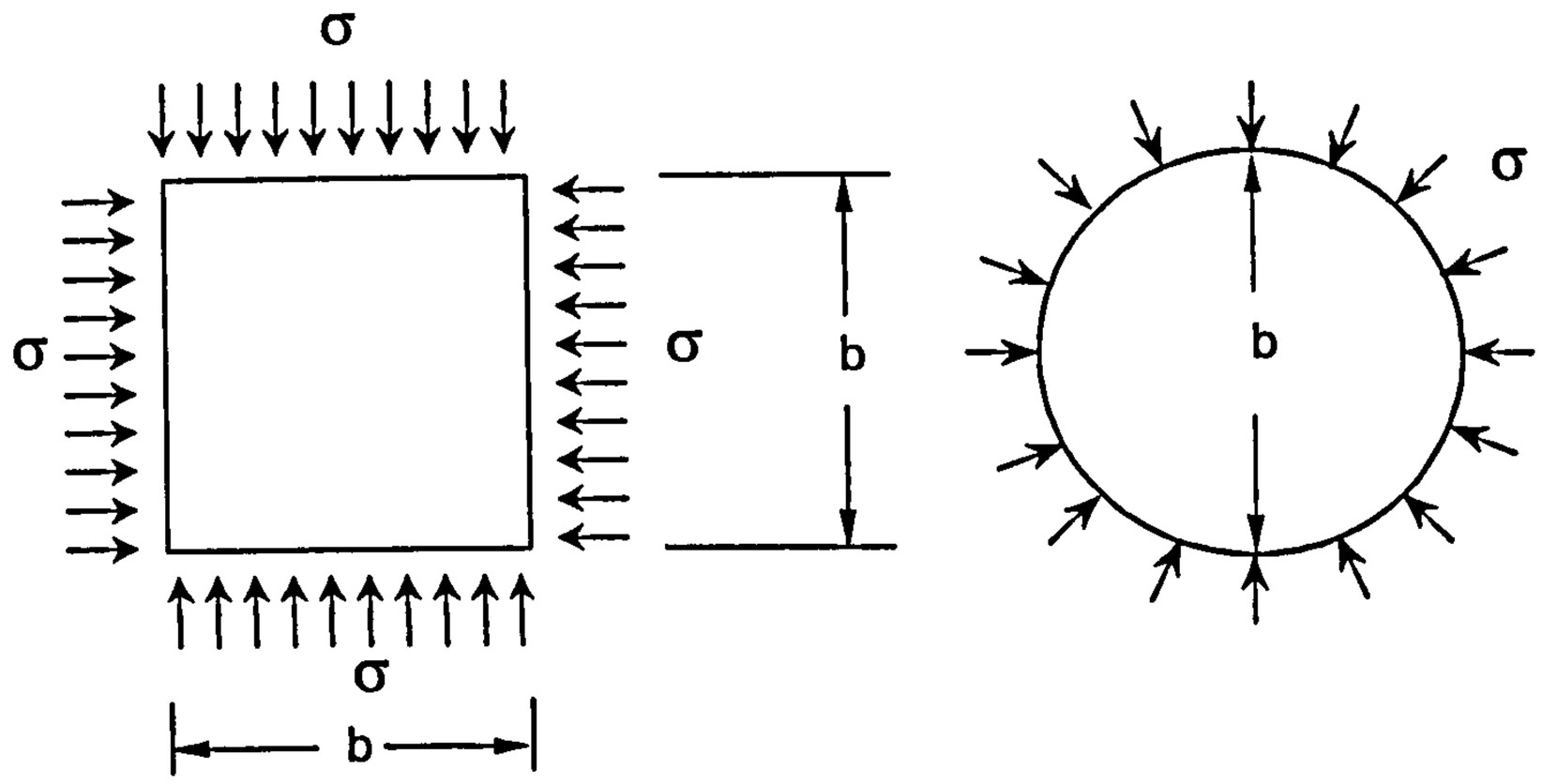

Figure 6-19: Circular and square plates subjected to uniform normal compression loads.

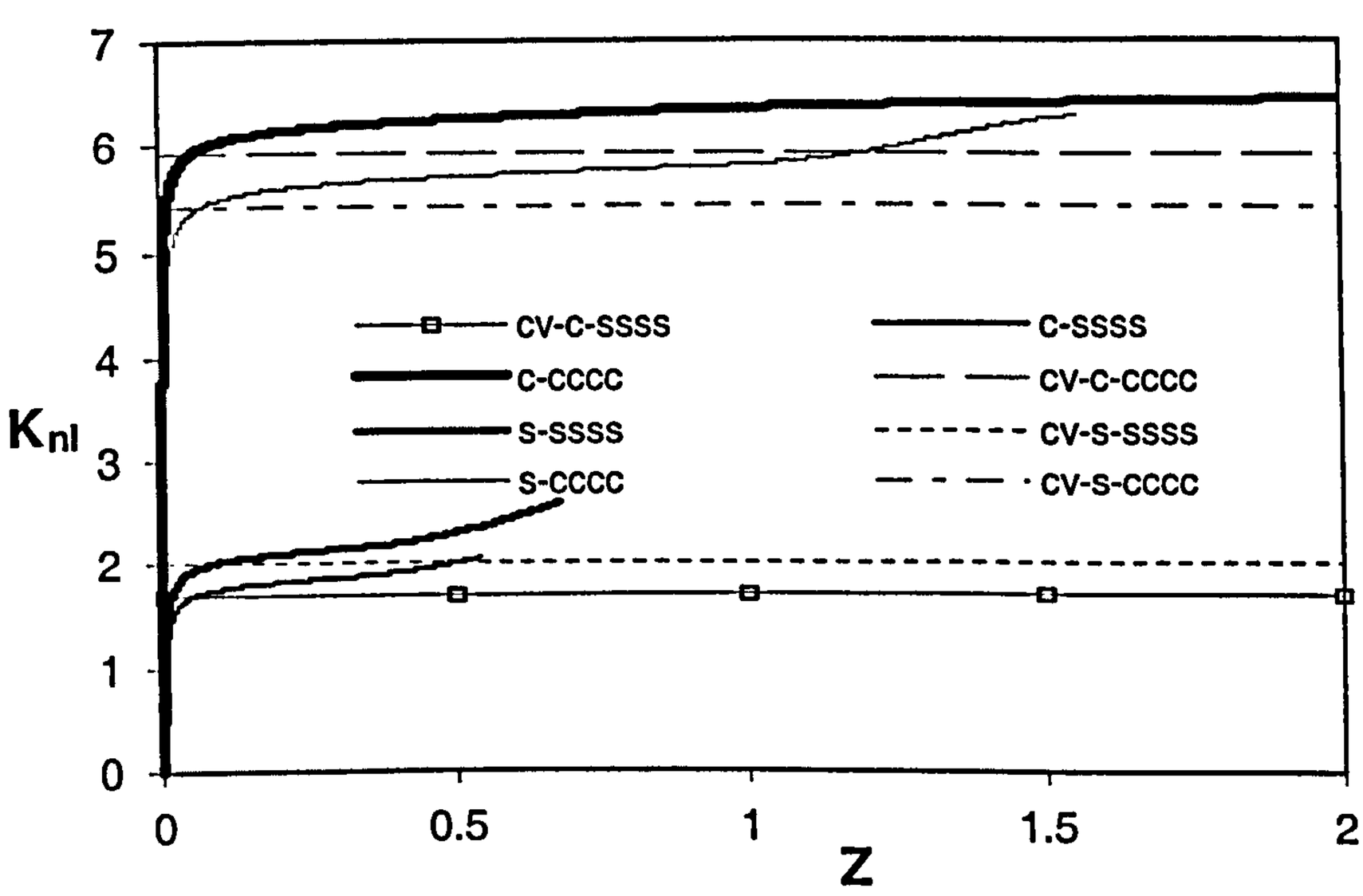

Figure 6-20: Nonlinear buckling of the circular and square plates subjected to uniform normal compression loads.

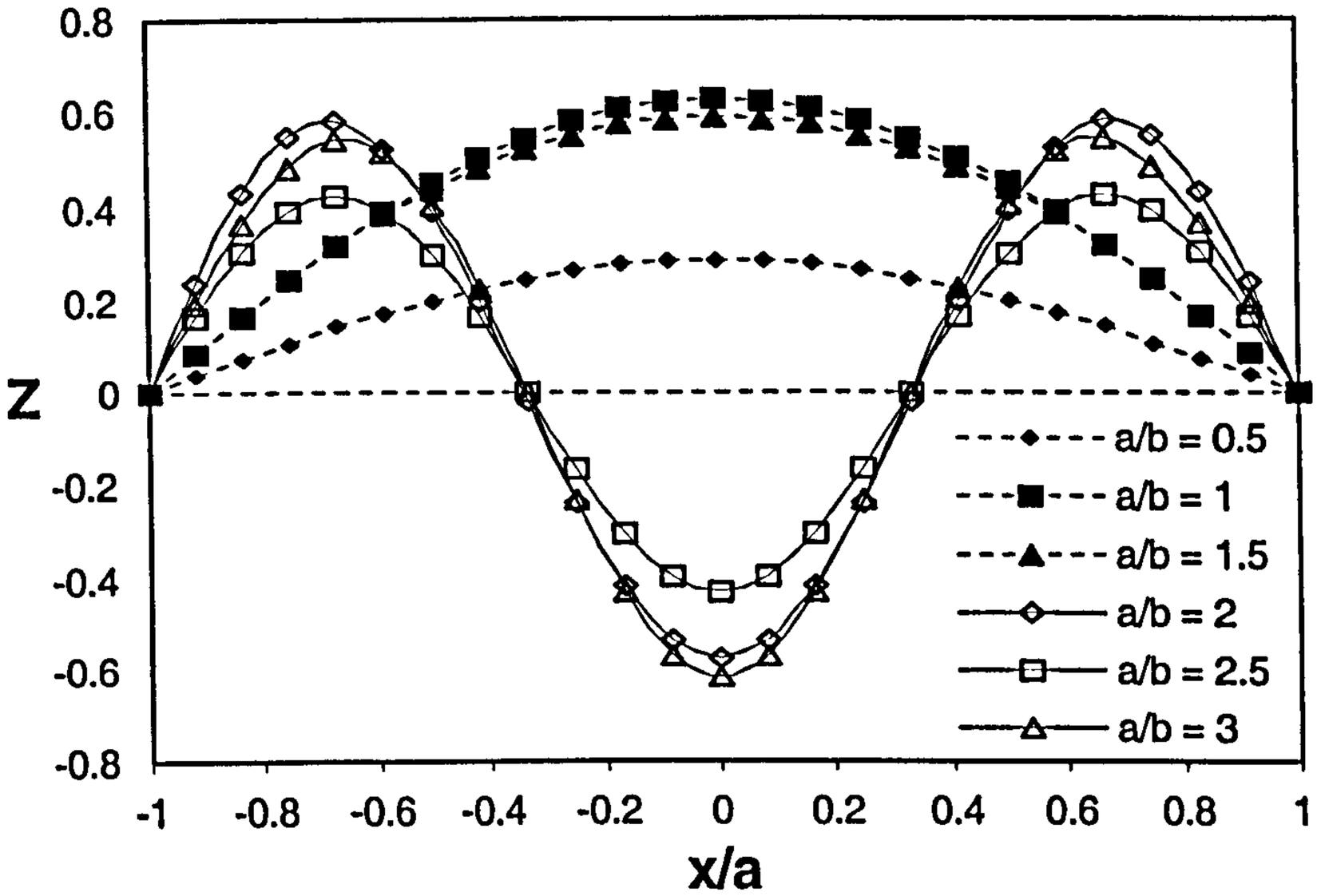

Figure 6-21: Half-wave modes for rectangular plates with different aspect ratio a/b due to uniform imperfections.

6.7.4 Analysis of the uniform distribution and distributed imperfections

In this example, two imperfection models, i.e. uniform distribution and distributed transverse loads (as described in section 6.4.1) are assessed. A simply supported rectangular plate as shown in Figure 6-15 is used to investigate the proposed imperfection models. Considering the origin point (0.0,0.0) as a center of the plate. In the case of uniform distribution, the increments of compression loads as $\Delta\sigma = 4$ units and initial imperfection as $q_0 = 0.005$ units are applied.

Normalized deflections Z $(= \frac{w_3}{h})$ for the points along x-axis are plotted in Figure 6-21. It can be seen from the Figure that due to uniform imperfections, the plate will buckle in odd number of half-waves for different aspect ratio a/b.

In the case of distributed model, imperfections are introduced based on the buckling modes of eigenvalue results for the same geometry. For the rectangular plate, distribution of imperfections can be introduced and modelled as shown in Figure 6-22.

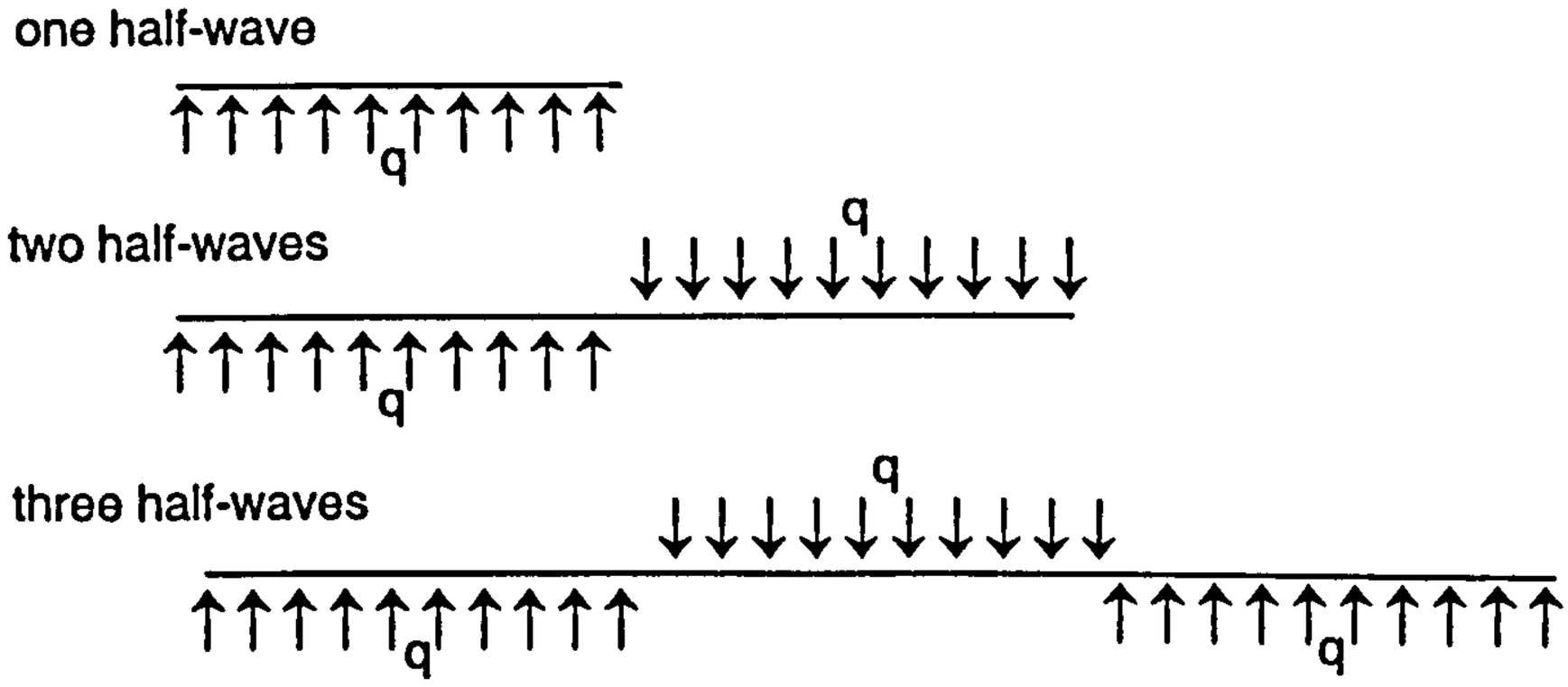

Figure 6-22: Simplified imperfections for rectangular plates.

The normalized compression stresses K_{nl} for different aspect ratio of the plates are plotted in Figure 6-23. It can be seen from Figure 6-23 that the uniform imperfection of transverse loads provides inaccurate results with the increasing of aspect ratios, while the results of the distributed one is in good agreements with analytical results.

6.7.5 Nonlinear buckling analysis of a rectangular plate with different boundary conditions

Here nonlinear buckling analysis of a rectangular plate as shown in Figure 6-15 subjected to a uniform normal compression loads is presented. Three boundary conditions are applied, i.e.

- model 1: all sides clamped (cccc)
- model 2: two opposite loaded side clamped and two others simply supported (cscs)
- model 3: three sides simply supported and one unloaded side free (sssf)

The normalized compression stresses K_{nl} and the normalized deflection Z together with critical value of each model are plotted in Figure 6-24 for model 1, Figure 6-25 for model 2 and Figure 6-26 for model 3. Deformations for rectangular plates with the above boundary conditions are shown in Figure 6-27.

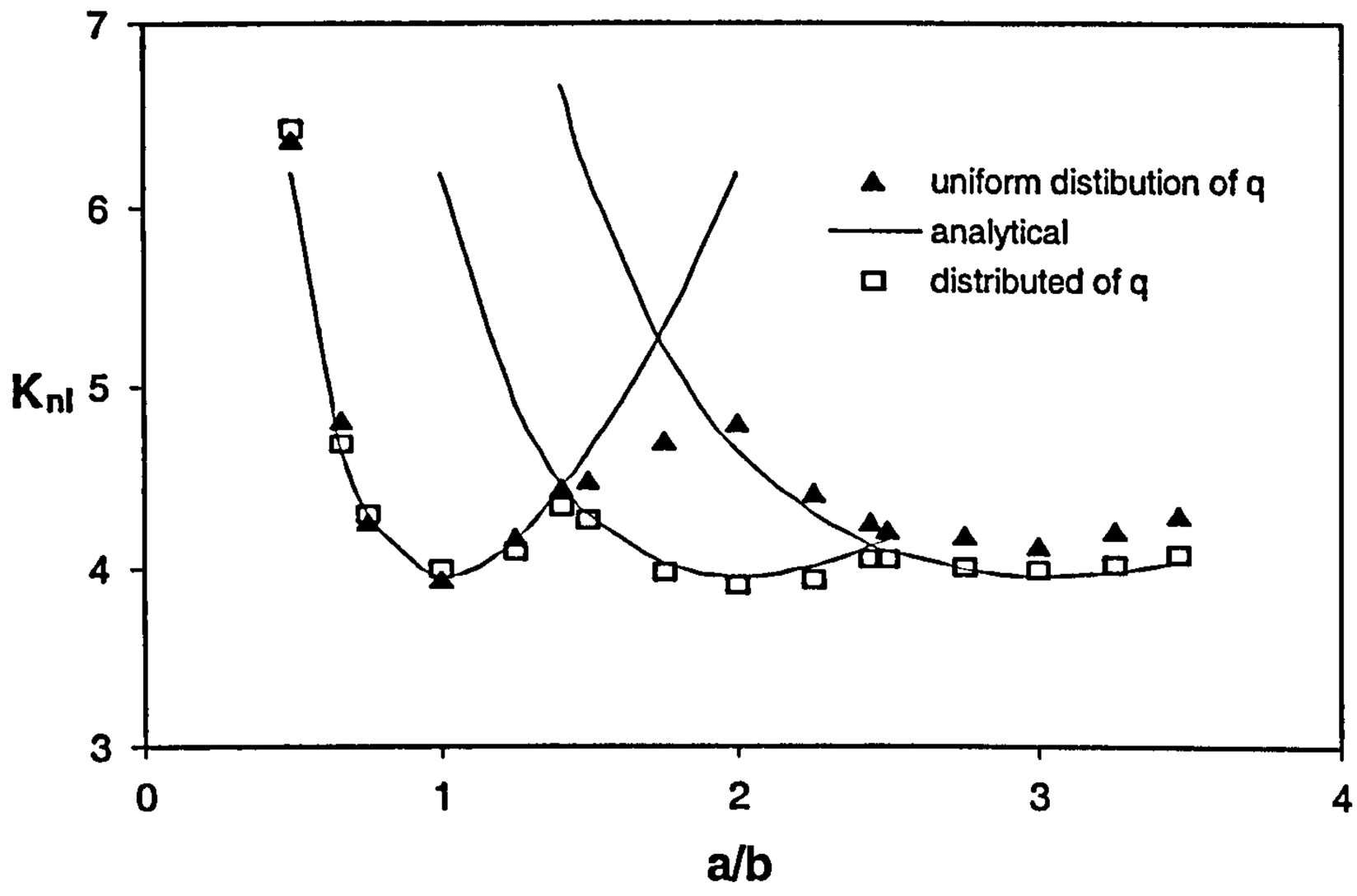

Figure 6-23: The normalized compression stresses K_{nl} for different aspect ratio of the simply supported rectangular plates

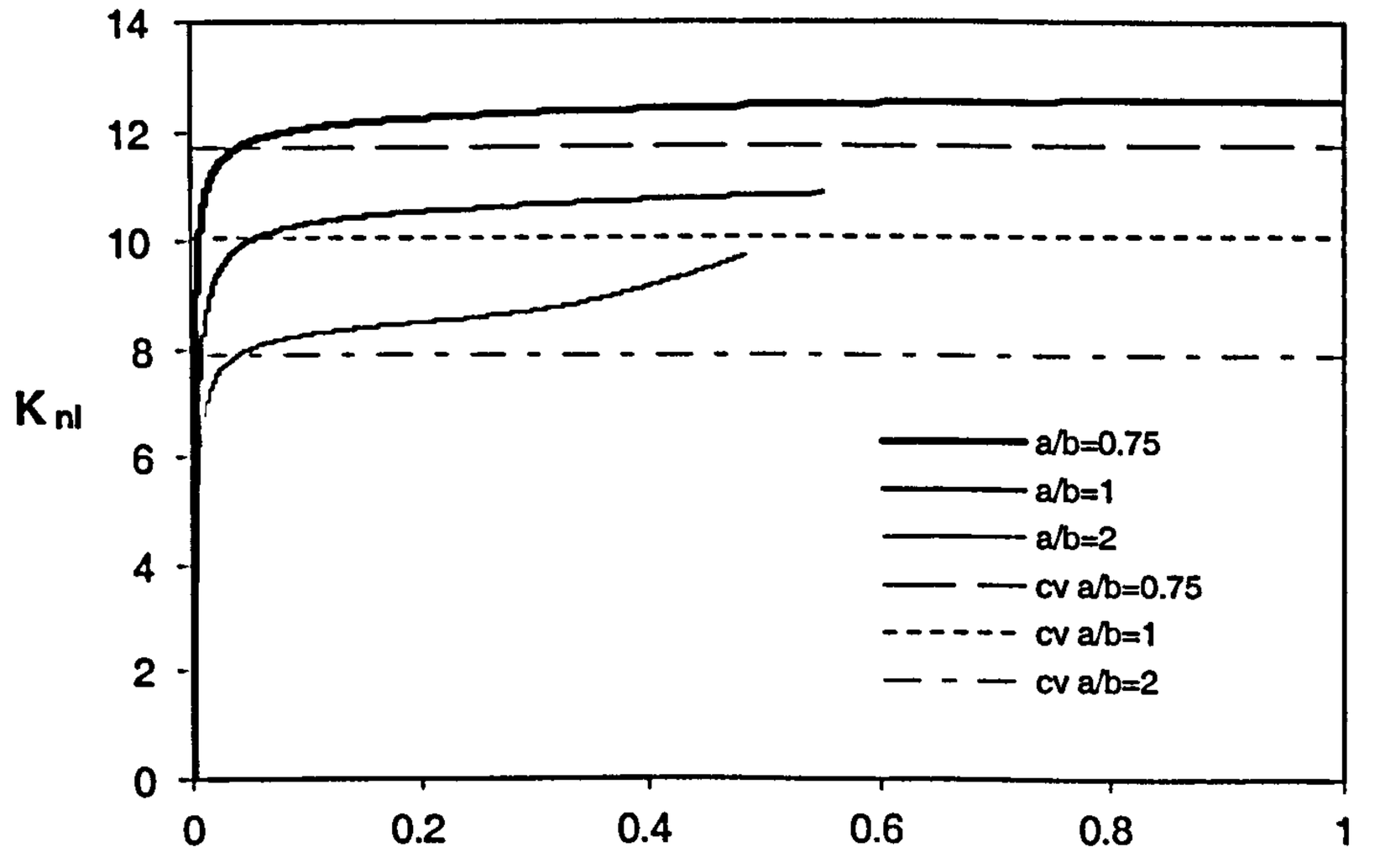

Figure 6-24: Nonlinear buckling analysis of rectangular plates with all sides clamped.

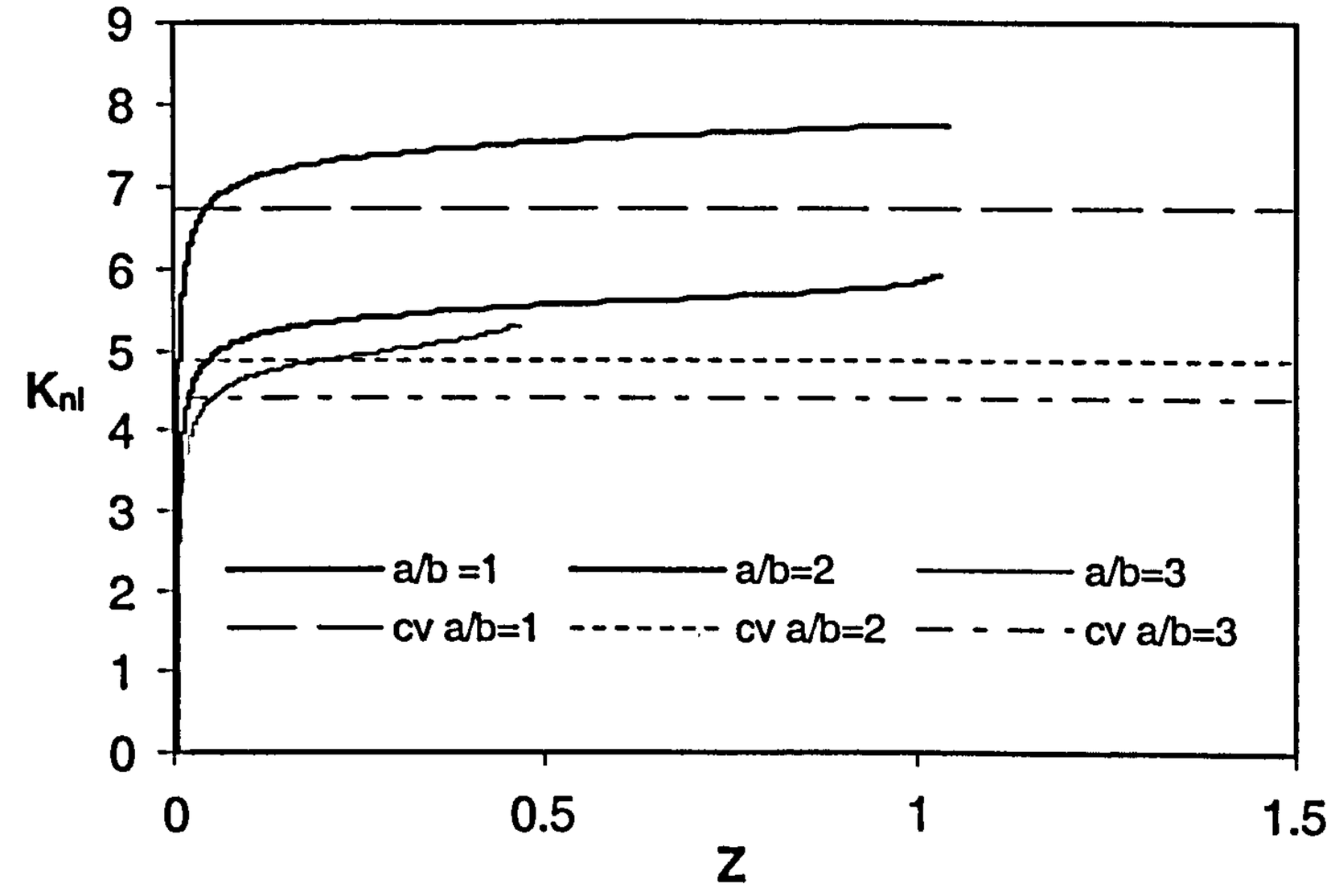

Figure 6-25: Nonlinear buckling analysis of rectangular plates with two opposite loaded side clamped and two others simply supported.

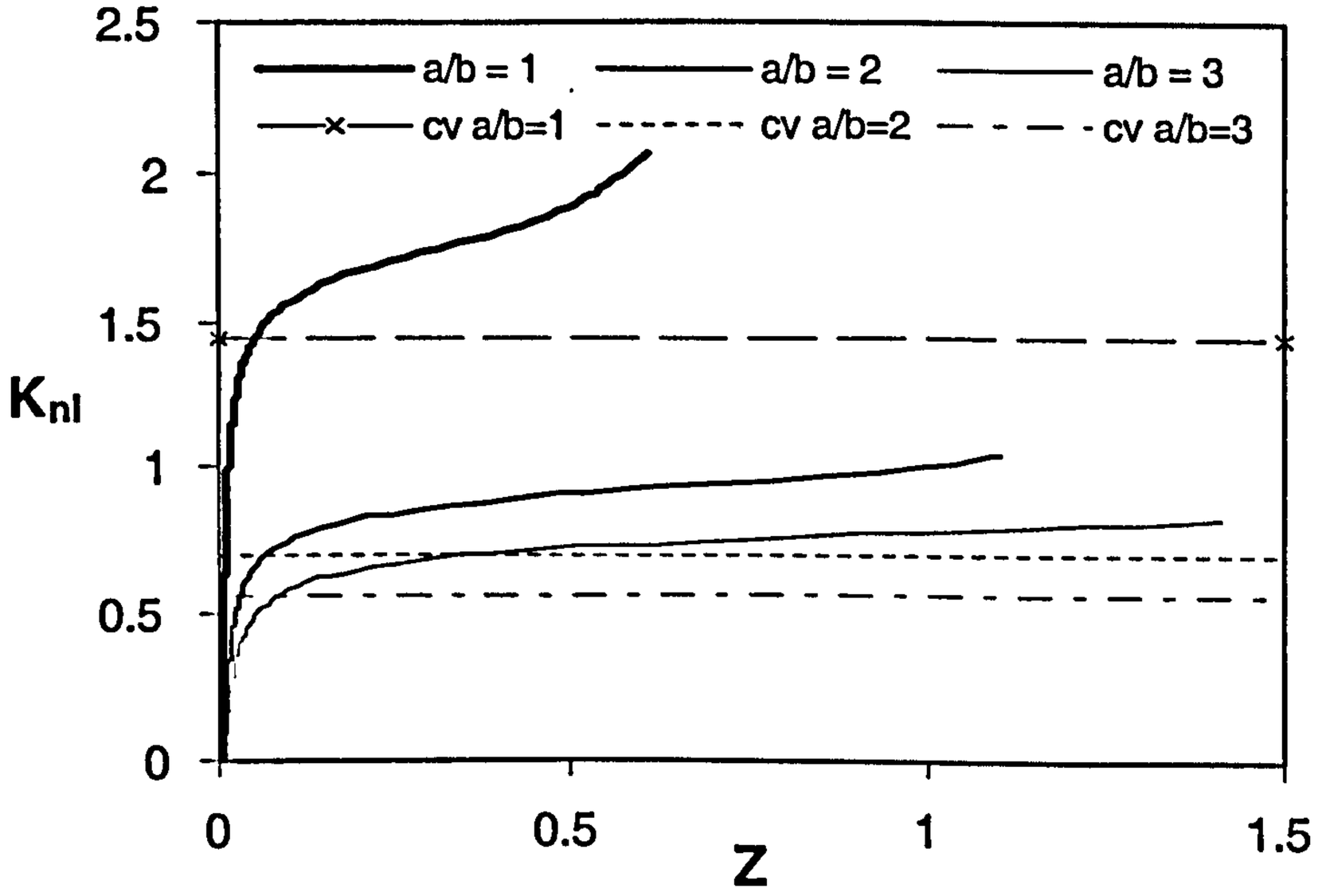

Figure 6-26: Nonlinear buckling analysis of rectangular plates with three sides simply supported and one unloaded side free.

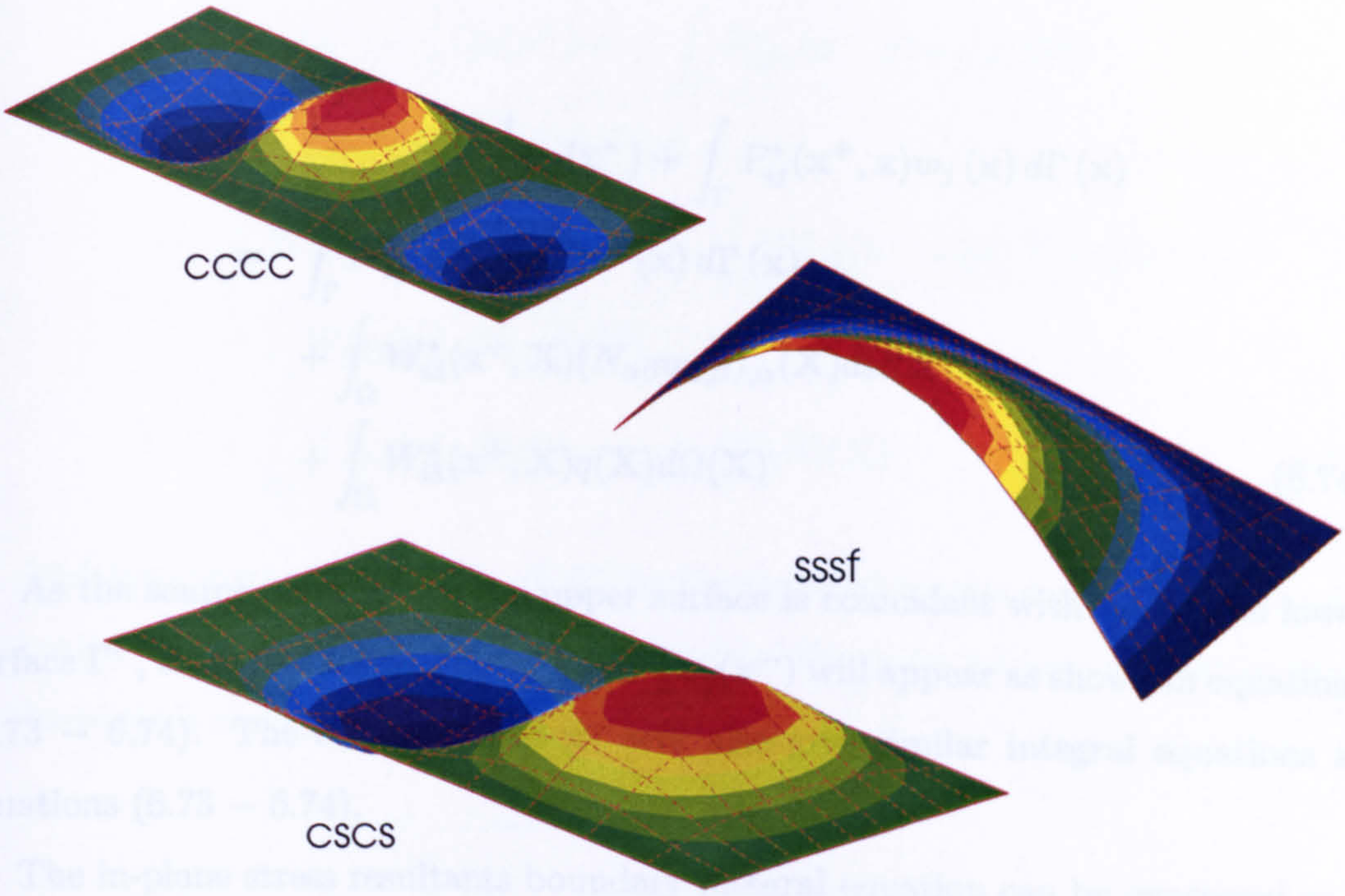

Figure 6-27: Nonlinear buckling deformations for rectangular plates with different boundary conditions.

It can be seen from Figure 6-24, that the results are in agreements with the analytical critical values.

6.8 Fracture Mechanics Analysis

The procedures described in Chapter 5 will be used to analyse the large deformation of cracked plates. The boundary integrals on the upper crack surface Γ^+ are expressed as follows:

$$\begin{aligned} & \frac{1}{2}u_\alpha(\mathbf{x}^+) + \frac{1}{2}u_\alpha(\mathbf{x}^-) + \int_\Gamma T^*_{\theta\alpha}(\mathbf{x}^+, \mathbf{x}) u_\alpha(\mathbf{x}) d\Gamma(\mathbf{x}) \\ = & \int_\Gamma U^*_{\theta\alpha}(\mathbf{x}^+, \mathbf{x}) t^{linear}_\alpha(\mathbf{x}) d\Gamma(\mathbf{x}) + \int_\Omega U^*_{\theta\alpha}(\mathbf{x}^+, \mathbf{X}) N^{nonlinear}_{\alpha\gamma,\gamma}(\mathbf{X}) d\Omega(\mathbf{X}) \quad (6.73) \end{aligned}$$

and

$$
\begin{aligned}
&\frac{1}{2}w_j(\mathbf{x}^+) + \frac{1}{2}w_j(\mathbf{x}^-) + \int_\Gamma P^*_{ij}(\mathbf{x}^+,\mathbf{x})w_j(\mathbf{x})\,d\Gamma(\mathbf{x}) \\
= &\int_\Gamma W^*_{ij}(\mathbf{x}^+,\mathbf{x})p_j^{linear}(\mathbf{x})\,d\Gamma(\mathbf{x}) \\
&+ \int_\Omega W^*_{i3}(\mathbf{x}^+,\mathbf{X})(N_{\alpha\beta}w_{3,\beta})_{,\alpha}(\mathbf{X})d\Omega(\mathbf{X}) \\
&+ \int_\Omega W^*_{i3}(\mathbf{x}^+,\mathbf{X})q(\mathbf{X})d\Omega(\mathbf{X})
\end{aligned} \tag{6.74}
$$

As the source point $\mathbf{x}^+$ on the upper surface is coincident with $\mathbf{x}^-$ on the lower surface Γ^-, extra free terms $\frac{1}{2}u_\alpha(\mathbf{x}^-)$ and $\frac{1}{2}w_j(\mathbf{x}^-)$ will appear as shown in equations (6.73 – 6.74). The collocation at $\mathbf{x}^-$ will also give similar integral equations as equations (6.73 – 6.74).

The in-plane stress resultants boundary integral equation can be expressed as

$$
\begin{aligned}
&\frac{1}{2}N_{\alpha\beta}^{linear}(\mathbf{x}^-) + \frac{1}{2}N_{\alpha\beta}^{linear}(\mathbf{x}^+) + \int_\Gamma T^*_{\Delta\alpha\beta}(\mathbf{x}^+,\mathbf{x})u_\Delta(\mathbf{x})d\Gamma(\mathbf{x}) \\
= &\int_\Gamma U^*_{\Delta\alpha\beta}(\mathbf{x}^+,\mathbf{x})t_\Delta^{linear}(\mathbf{x})d\Gamma(\mathbf{x}) \\
&+ \int_\Omega U^*_{\Delta\alpha\beta}(\mathbf{x}^+,\mathbf{X})N^{nonlinear}_{\Delta\gamma,\gamma}(\mathbf{X})d\Omega(\mathbf{X})
\end{aligned} \tag{6.75}
$$

and the plate bending stress resultants boundary integral equation can be written as follows

$$
\begin{aligned}
&\frac{1}{2}M_{\alpha\beta}(\mathbf{x}^-) + \frac{1}{2}M_{\alpha\beta}(\mathbf{x}^+) + \int_\Gamma P^*_{\alpha\beta\gamma}(\mathbf{x}^-,\mathbf{x})w_\gamma(\mathbf{x})d\Gamma(\mathbf{x}) \\
&+ \int_\Gamma P^*_{\alpha\beta3}(\mathbf{x}^-,\mathbf{x})w_3(\mathbf{x})d\Gamma(\mathbf{x}) \\
= &\int_\Gamma W^*_{\alpha\beta\gamma}(\mathbf{x}^-,\mathbf{x})p_\gamma(\mathbf{x})d\Gamma(\mathbf{x}) + \int_\Gamma W^*_{\alpha\beta3}(\mathbf{x}^-,\mathbf{x})p_3^{linear}(\mathbf{x})d\Gamma(\mathbf{x}) \\
&+ \int_\Omega W^*_{\alpha\beta3}(\mathbf{x}^-,\mathbf{X})qd\Omega(\mathbf{X}) \\
&+ \int_\Omega W^*_{\alpha\beta3}(\mathbf{x}^-,\mathbf{X})(N_{\theta\psi}w_{3,\varphi})_{,\theta}(\mathbf{X})d\Omega(\mathbf{X})
\end{aligned} \tag{6.76}
$$

$$
\begin{aligned}
&\frac{1}{2}Q_\beta(\mathrm{x}^-)+\frac{1}{2}Q_\beta(\mathrm{x}^+)+\quad\int_\Gamma P^*_{3\beta\gamma}(\mathrm{x}^-,\mathrm{x})w_\gamma(\mathrm{x})d\Gamma(\mathrm{x})\\
&+\int_\Gamma P^*_{3\beta 3}(\mathrm{x}^-,\mathrm{x})w_3(\mathrm{x})d\Gamma(\mathrm{x})\\
=\quad&\int_\Gamma W^*_{3\beta\gamma}(\mathrm{x}^-,\mathrm{x})p_\gamma(\mathrm{x})d\Gamma(\mathrm{x})+\int_\Gamma W^*_{3\beta 3}(\mathrm{x}^-,\mathrm{x})p_3^{linear}(\mathrm{x})d\Gamma(\mathrm{x})\\
&+\int_\Omega W^*_{3\beta 3}(\mathrm{x}^-,\mathrm{X})q d\Omega(\mathrm{X})\\
&+\int_\Omega W^*_{3\beta 3}(\mathrm{x}^-,\mathrm{X})(N_{\theta\psi}w_{3,\varphi})_{,\theta}(\mathrm{X})d\Omega(\mathrm{X})
\end{aligned}
\tag{6.77}
$$

Multiplying equations (6.76 – 6.77) by the outward normal $n_\beta(\mathrm{x}^-)$ and denoting that $n_\beta(\mathrm{x}^+)=-n_\beta(\mathrm{x}^-)$, the traction integral equations for a boundary source point at lower crack surface x^- are as follows:

$$
\begin{aligned}
&\frac{1}{2}t_\alpha^{linear}(\mathrm{x}^-)-\frac{1}{2}t_\alpha^{linear}(\mathrm{x}^+)+n_\beta(\mathrm{x}^-)\int_\Gamma T^*_{\Delta\alpha\beta}(\mathrm{x}^-,\mathrm{x})u_\Delta(\mathrm{x})d\Gamma(\mathrm{x})\\
=\quad&n_\beta(\mathrm{x}^-)\int_\Gamma U^*_{\Delta\alpha\beta}(\mathrm{x}^-,\mathrm{x})t_\Delta^{linear}(\mathrm{x})d\Gamma(\mathrm{x})\\
&+n_\beta(\mathrm{x}^-)\int_\Omega U^*_{\Delta\alpha\beta}(\mathrm{x}^-,\mathrm{X})N_{\Delta\gamma,\gamma}^{nonlinear}(\mathrm{X})d\Omega(\mathrm{X})
\end{aligned}
\tag{6.78}
$$

and

$$
\begin{aligned}
&\frac{1}{2}p_\alpha(\mathrm{x}^-)-\frac{1}{2}p_\alpha(\mathrm{x}^+)+n_\beta(\mathrm{x}^-)\int_\Gamma P^*_{\alpha\beta\gamma}(\mathrm{x}^-,\mathrm{x})w_\gamma(\mathrm{x})d\Gamma(\mathrm{x})\\
&+n_\beta(\mathrm{x}^-)\int_\Gamma P^*_{\alpha\beta 3}(\mathrm{x}^-,\mathrm{x})w_3(\mathrm{x})d\Gamma(\mathrm{x})\\
=\quad&n_\beta(\mathrm{x}^-)\int_\Gamma W^*_{\alpha\beta\gamma}(\mathrm{x}^-,\mathrm{x})p_\gamma(\mathrm{x})d\Gamma(\mathrm{x})+n_\beta(\mathrm{x}')\int_\Gamma W^*_{\alpha\beta 3}(\mathrm{x}^-,\mathrm{x})p_3^{linear}(\mathrm{x})d\Gamma(\mathrm{x})\\
&+n_\beta(\mathrm{x}^-)\int_\Omega W^*_{\alpha\beta 3}(\mathrm{x}^-,\mathrm{X})q d\Omega(\mathrm{X})\\
&+n_\beta(\mathrm{x}^-)\int_\Omega W^*_{\alpha\beta 3}(\mathrm{x}^-,\mathrm{X})(N_{\theta\psi}w_{3,\varphi})_{,\theta}(\mathrm{X})d\Omega(\mathrm{X})
\end{aligned}
\tag{6.79}
$$

$$
\begin{aligned}
&\frac{1}{2}p_3(\mathrm{x}^-)-\frac{1}{2}p_3(\mathrm{x}^+)+n_\beta(\mathrm{x}^-)\int_\Gamma P^*_{3\beta\gamma}(\mathrm{x}^-,\mathrm{x})w_\gamma(\mathrm{x})d\Gamma(\mathrm{x})\\
&+n_\beta(\mathrm{x}^-)\int_\Gamma P^*_{3\beta 3}(\mathrm{x}^-,\mathrm{x})w_3(\mathrm{x})d\Gamma(\mathrm{x})
\end{aligned}
$$

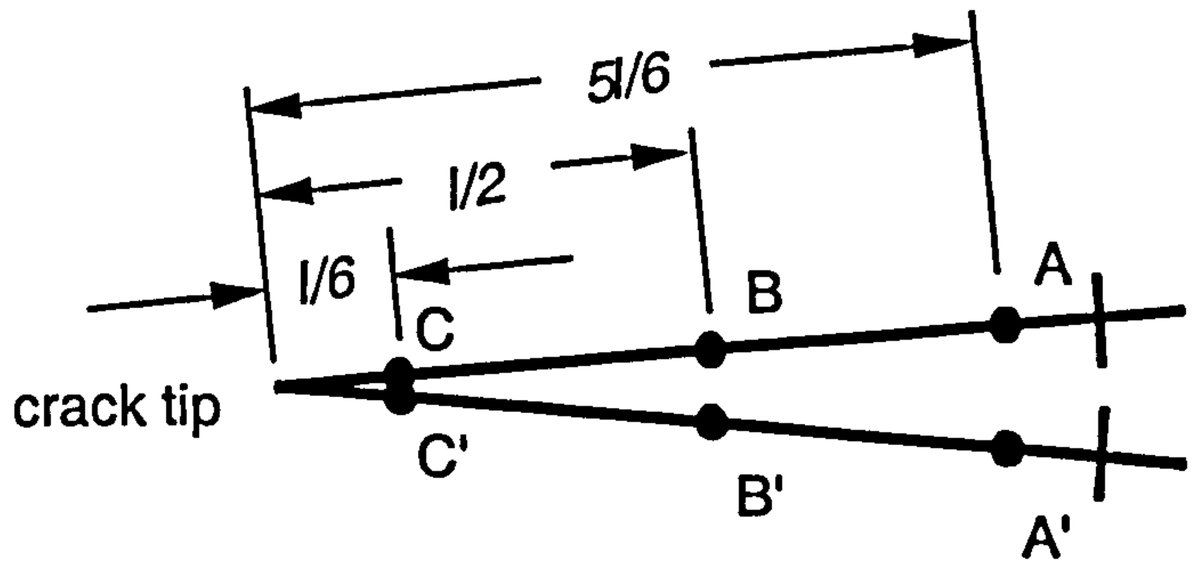

Figure 6-28: Crack tip element.

$$
\begin{aligned}
= \; & n_\beta(\mathbf{x}^-)\int_\Gamma W^*_{3\beta\gamma}(\mathbf{x}^-,\mathbf{x})p_\gamma(\mathbf{x})d\Gamma(\mathbf{x}) + n_\beta(\mathbf{x}^-)\int_\Gamma W^*_{3\beta 3}(\mathbf{x}^-,\mathbf{x})p_3^{linear}(\mathbf{x})d\Gamma(\mathbf{x}) \\
& + n_\beta(\mathbf{x}^-)\int_\Omega W^*_{3\beta 3}(\mathbf{x}^-,\mathbf{X})q d\Omega(\mathbf{X}) \\
& + n_\beta(\mathbf{x}^-)\int_\Omega W^*_{3\beta 3}(\mathbf{x}^-,\mathbf{X})(N_{\theta\psi}w_{3,\varphi})_{,\theta}(\mathbf{X})d\Omega(\mathbf{X}) \qquad (6.80)
\end{aligned}
$$

To calculate the nonlinear terms, additional integral equations are required, i.e. equations (6.15), (6.16) and (6.17).

6.9 Stress Intensity Factors Evaluation

The displacements on the crack surfaces near the crack tip can be obtained as discussed in Chapter 2. Five stress intensity factors (SIFs), three SIFs for plate bending problem and two due to membrane loads have to be computed. The stress intensity factors are carried out using the Crack Opening Displacement (COD).

Crack surfaces are discretised using discontinuous elements with nodes located at $\xi = -\frac{2}{3}, 0, +\frac{2}{3}$, then the distance of every node at crack tip elements is given in Figure 6-28. The value of SIFs can be obtained at any point in crack tip elements as follows:

$$\{K\}^{AA'} = \sqrt{\frac{6}{5l}}\,[\mathbf{Fc}]\left(\{w\}^A - \{w\}^{A'}\right) \qquad (6.81)$$

and

$$\{K\}^{BB'} = \sqrt{\frac{2}{l}}\,[\mathbf{Fc}]\left(\{w\}^B - \{w\}^{B'}\right) \qquad (6.82)$$

where **Fc** is defined in equation (2.74).

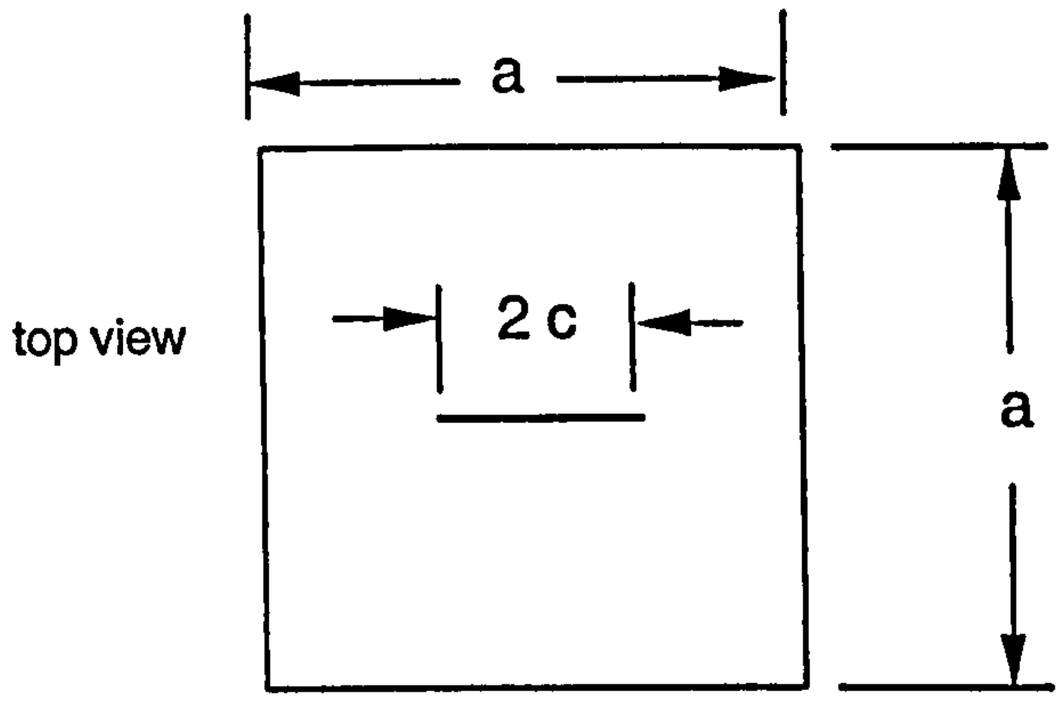

Figure 6-29: A cracked square plate.

Using extrapolation technique to the crack tip elements, SIFs can be obtained as follows

$$\{K\}^{tip} = \frac{r_{AA'}}{r_{AA'} - r_{BB'}} \left(\{K\}^{BB'} - \frac{r_{BB'}}{r_{AA'}} \{K\}^{AA'} \right) \tag{6.83}$$

where $r_{AA'} = \frac{5}{6}l$ and $r_{BB'} = \frac{1}{2}l$.

6.10 Numerical Examples

Numerical examples are presented to assess the ability of the proposed method to analyse large deformation of cracked plates. The cracked plate model is shown in Figure 6-29. In the following examples, the normalized stress intensity factors for plate bending are defined by

$$K_{1bn} = \frac{K_{1b}}{(Eh^4\sqrt{\pi c}/a^2)} \tag{6.84}$$

While the normalized stress intensity factors for membrane are defined by

$$K_{1mn} = \frac{K_{1m}}{(Eh^2\sqrt{\pi c}/a)} \tag{6.85}$$

where K_{1b} and K_{1m} are defined in equation (2.73).

In this example, large deformation analysis of the cracked square plate as shown in Figure 6-29 subjected to a uniform transverse loads q is presented. Two different boundary conditions are applied , i.e. fully clamped and simply supported. For full clamped condition is given as follows :

$$\text{Along } x = \pm\, a/2: \qquad u_1 = u_2 = w_1 = w_2 = w_3 = 0$$

$$\text{Along } y = \pm\, a/2: \qquad u_1 = u_2 = w_1 = w_2 = w_3 = 0$$

and simply supported as

$$\text{Along } x = \pm\, a/2: \qquad u_1 = u_2 = w_3 = 0$$

$$\text{Along } y = \pm\, a/2: \qquad u_1 = u_2 = w_3 = 0$$

where the origin point (0.0,0.0) as a center of the plate

The analysed model is summarized as follows:

- Modulus elasticity $E = 30000000$ units
- Thickness $h = 0.01$ units
- Poisson ratio $\upsilon = 0.316$
- Plate dimension = 2 by 2 unit square.
- Crack length, $2c = 0.4$ units
- Increment load $\overset{\circ}{q} = 0.01$ units

The normalized stress intensity factors for the clamped boundary condition are shown in Figures 6-30 and 6-31. While the normalized stress intensity factors for the simply supported boundary condition are shown in Figures 6-32 and 6-33. The non-dimensionalised parameter Q is defined in equation (6.63).

It can be seen from the Figures 6-31 and 6-33, that the normalized stress intensity factors in membrane increase significantly after few increment of loads. While the normalized stress intensity factors in bending as shown in Figures 6-30 and 6-32 decrease if compared with the linear results.

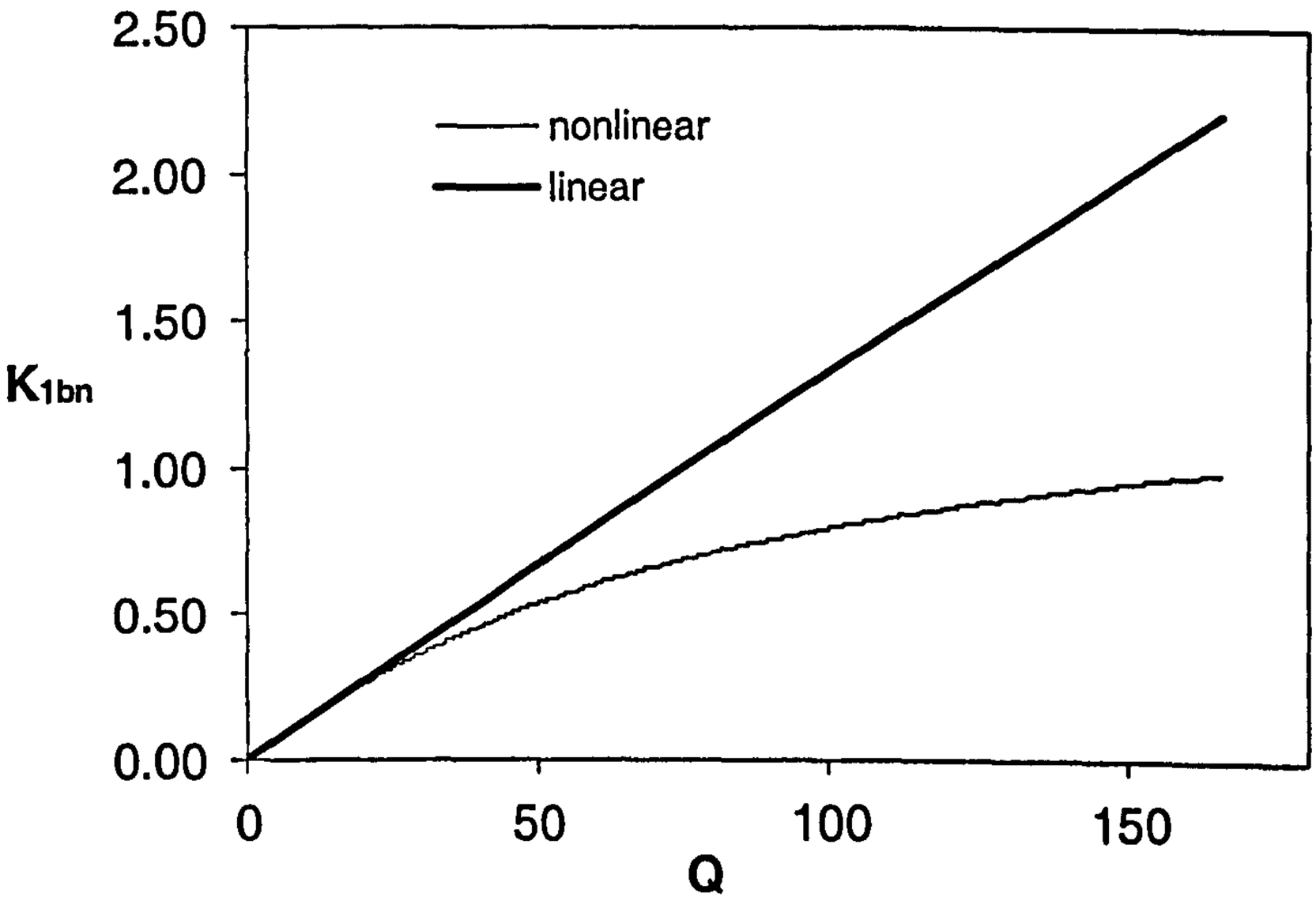

Figure 6-30: The normalized stress intensity factors in bending of the clamped cracked square plate ($2a = 0.4$).

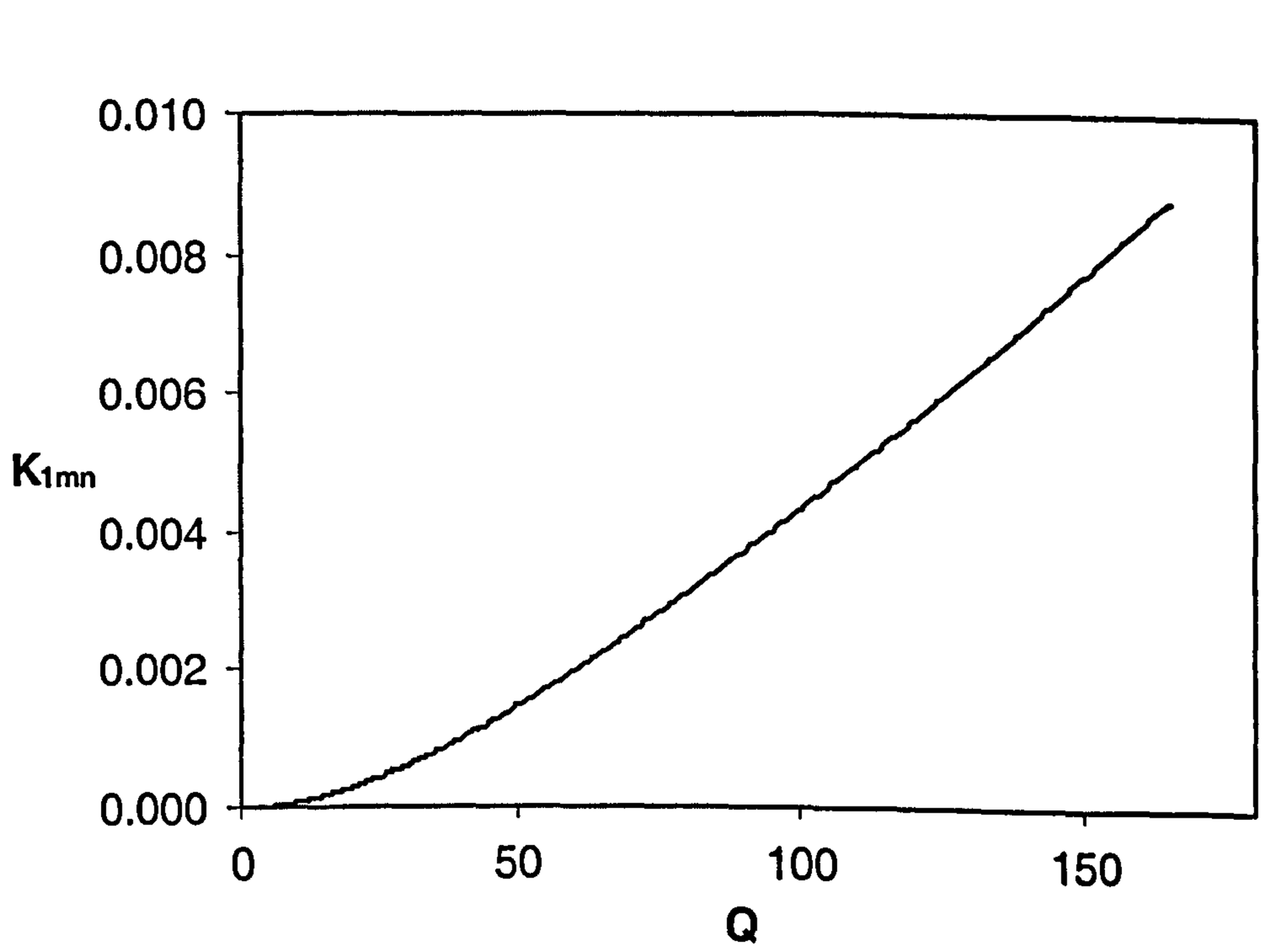

Figure 6-31: The normalized stress intensity factors in bending of the clamped cracked square plate ($2a = 0.4$).

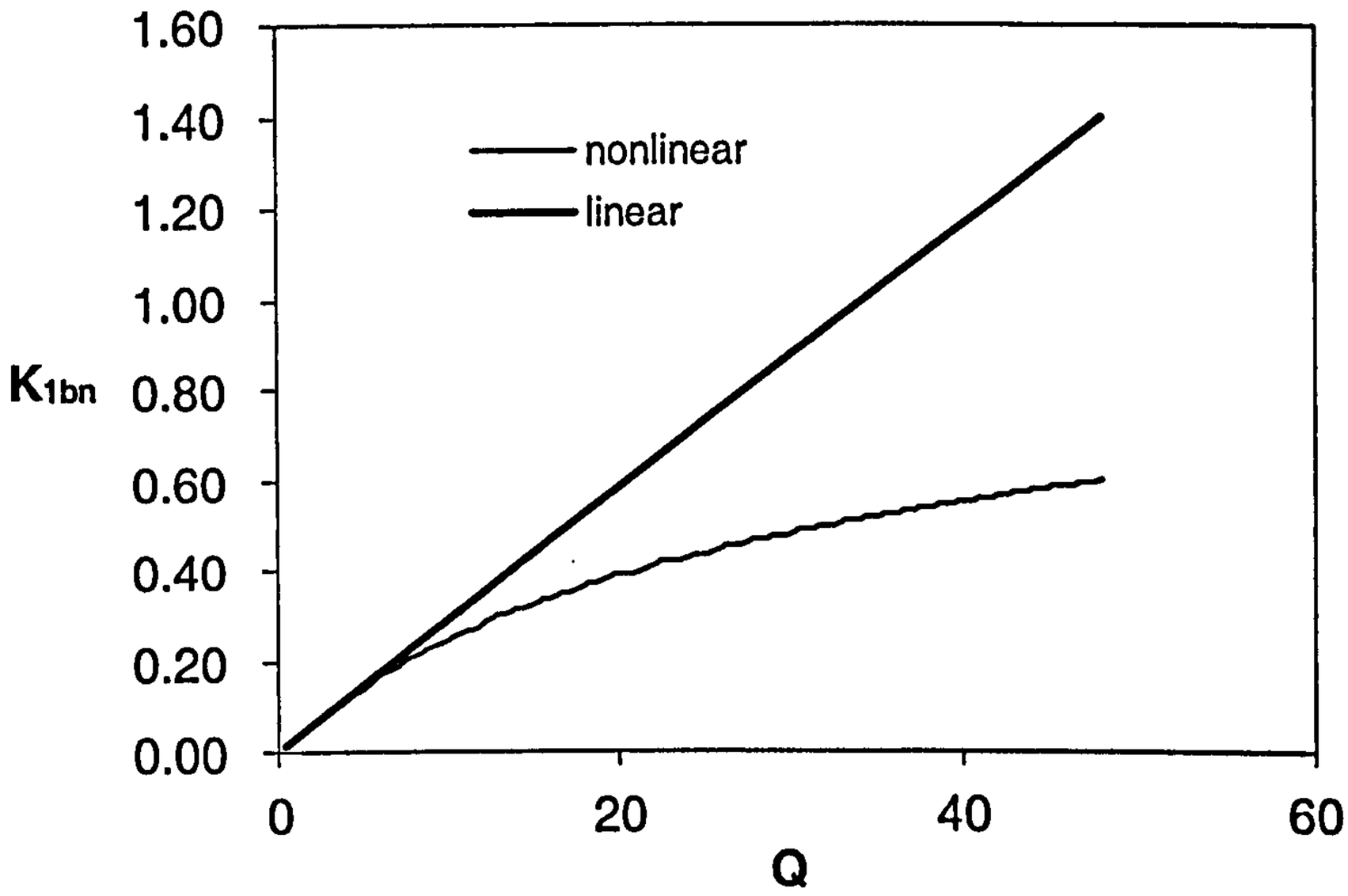

Figure 6-32: The normalized stress intensity factors in membrane of the simply supported cracked square plate ($2a = 0.4$).

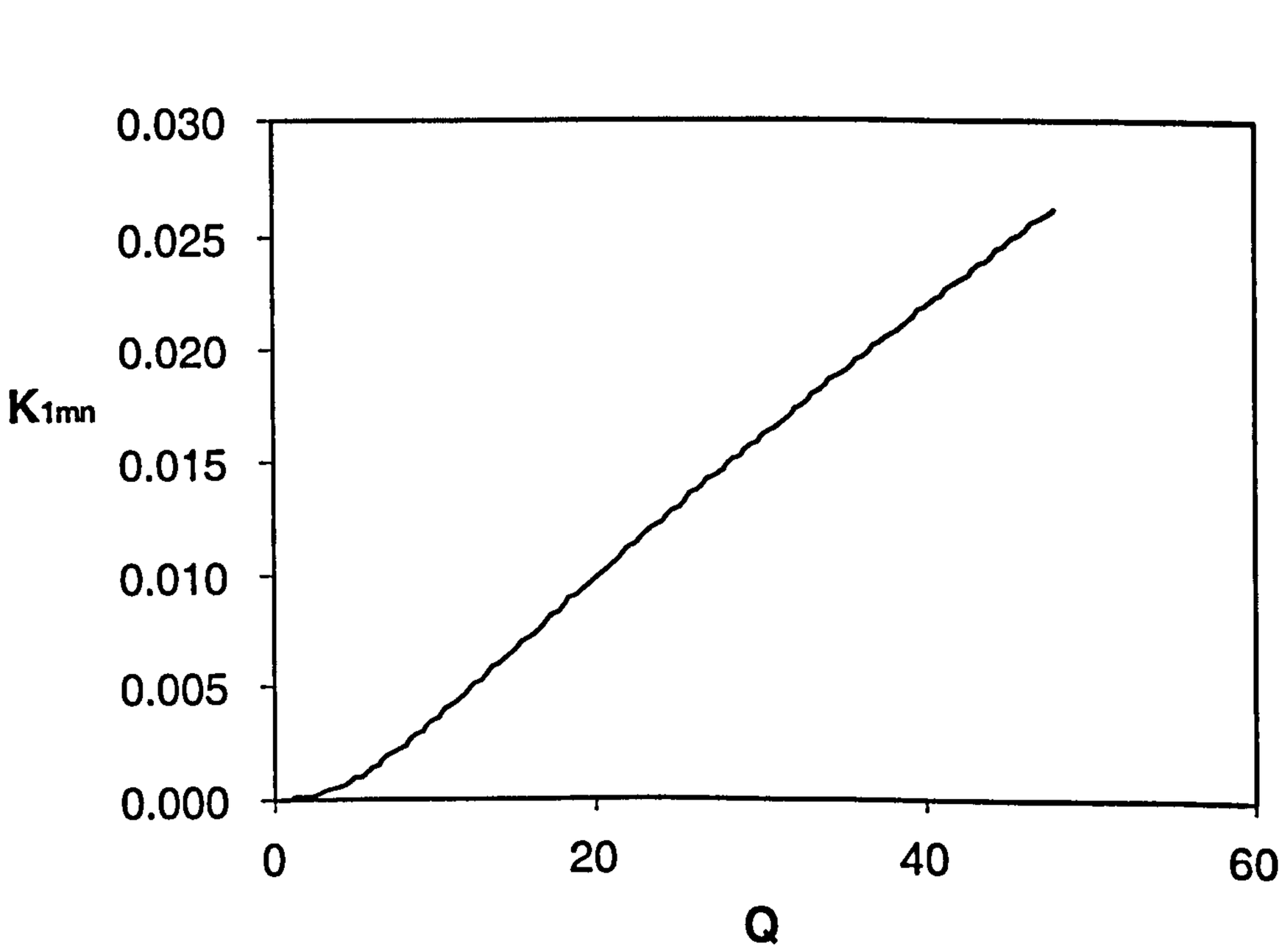

Figure 6-33: The normalized stress intensity factors in membrane of the simply supported cracked square plate ($2a = 0.4$).

6.11 Nonlinear Buckling Analysis of Cracked Plates

The dual boundary integral equations are extended to allow for nonlinear buckling analysis of cracked plates. The displacement equation (6.6) can be rewritten as

$$\begin{aligned}
&\frac{1}{2}u_\alpha(\mathbf{x}^+) + \frac{1}{2}u_\alpha(\mathbf{x}^-) + \int_\Gamma T^*_{\theta\alpha}(\mathbf{x}^+,\mathbf{x})u_\alpha(\mathbf{x})d\Gamma(\mathbf{x}) \\
= &\int_\Gamma U^*_{\theta\alpha}(\mathbf{x}^+,\mathbf{x})t_\alpha(\mathbf{x})d\Gamma(\mathbf{x}) - n_\gamma(\mathbf{x})\int_\Gamma U^*_{\theta\alpha}(\mathbf{x}^+,\mathbf{X})N^{nonlinear}_{\alpha\gamma}(\mathbf{X})d\Gamma(\mathbf{X}) \\
&+ \int_\Omega U^*_{\theta\alpha}(\mathbf{x}^+,\mathbf{X})N^{nonlinear}_{\alpha\gamma,\gamma}(\mathbf{X})d\Omega(\mathbf{X}) \qquad (6.86)
\end{aligned}$$

The in-plane stress resultants boundary integral equation can be expressed as

$$\begin{aligned}
&\frac{1}{2}N^{linear}_{\alpha\beta}(\mathbf{x}^-) + \frac{1}{2}N^{linear}_{\alpha\beta}(\mathbf{x}^+) + \int_\Gamma T^*_{\Delta\alpha\beta}(\mathbf{x}^+,\mathbf{x})u_\Delta(\mathbf{x})d\Gamma(x) \\
= &\int_\Gamma U^*_{\Delta\alpha\beta}(\mathbf{x}^+,\mathbf{x})t_\Delta(\mathbf{x})d\Gamma(\mathbf{x}) - n_\gamma(\mathbf{x})\int_\Gamma U^*_{\Delta\alpha\beta}(\mathbf{x}^+,\mathbf{x})N^{nonlinear}_{\Delta\gamma}(\mathbf{x})d\Gamma(\mathbf{x}) \\
&+ \int_\Omega U^*_{\Delta\alpha\beta}(\mathbf{x}^+,\mathbf{X})N^{nonlinear}_{\Delta\gamma,\gamma}(\mathbf{X})d\Omega(\mathbf{X}) \qquad (6.87)
\end{aligned}$$

The traction integral equations for a boundary source point at lower crack surface $\mathbf{x}^-$ is written as

$$\begin{aligned}
&\frac{1}{2}t^{linear}_\alpha(\mathbf{x}^-) - \frac{1}{2}t^{linear}_\alpha(\mathbf{x}^+) + n_\beta(\mathbf{x}^-)\int_\Gamma T^*_{\Delta\alpha\beta}(\mathbf{x}^-,\mathbf{x})u_\Delta(\mathbf{x})d\Gamma(\mathbf{x}) \\
= &\; n_\beta(\mathbf{x}^-)\int_\Gamma U^*_{\Delta\alpha\beta}(\mathbf{x}^-,\mathbf{x})t_\Delta(\mathbf{x})d\Gamma(\mathbf{x}) \\
&-n_\beta(\mathbf{x}^-)\int_\Gamma U^*_{\Delta\alpha\beta}(\mathbf{x}^-,\mathbf{x})N^{nonlinear}_{\Delta\gamma}(\mathbf{x})n_\gamma(\mathbf{x})d\Gamma(\mathbf{x}) \\
&+n_\beta(\mathbf{x}^-)\int_\Omega U^*_{\Delta\alpha\beta}(\mathbf{x}^-,\mathbf{X})N^{nonlinear}_{\Delta\gamma,\gamma}(X)d\Omega(\mathbf{X}) \qquad (6.88)
\end{aligned}$$

where traction boundary condition is denoted in equation 6.67.

Derivative of deflection $w_{3,\gamma}$ on the boundary can be approximated by considering a radial basis function $f(r)$ as described in section 4.2.3. Therefore terms $w_{3,\gamma}$ can be expressed as follows

$$w_3(x_1, x_2) = \sum_{m=1}^{M} f(r)^m \Psi^m \tag{6.89}$$

$$w_{3,\gamma}(x_1, x_2) = \mathbf{f}(r)_{,\gamma} \mathbf{F}^{-1}\{w_3\} \tag{6.90}$$

where M is selected points on the boundary and in the domain respectively

6.12 Numerical Examples

Here, the nonlinear buckling problem of a rectangular plate with a longitudinal central crack subjected to compression loads is studied. The model is similar to that shown in Figure 5-4 (i) but the aspect ratio of the plate is varied. Two configurations are considered: (a) the plate has aspect ratio $a/b = 1$ and (b) the plate has aspect ratio $a/b = 2$. Three different ratios of crack length to the length of plate are presented, i.e. $2c/a = 0.4, 0.5$ and 0.6. The normalized compression stresses K_{nl} and the normalized deflection Z are plotted as shown in Figures 6-34 and 6-35. Considering the origin point $(0.0, 0.0)$ as a center of the plate, the normalized deflection Z denotes deflection w_3 at point $(0.0, 0.25b)$ per thickness h. For aspect ratio $2c/a = 0.6$, the deformations are illustrated in Figure 6-36. The results presented are in agreement with the analytical critical values.

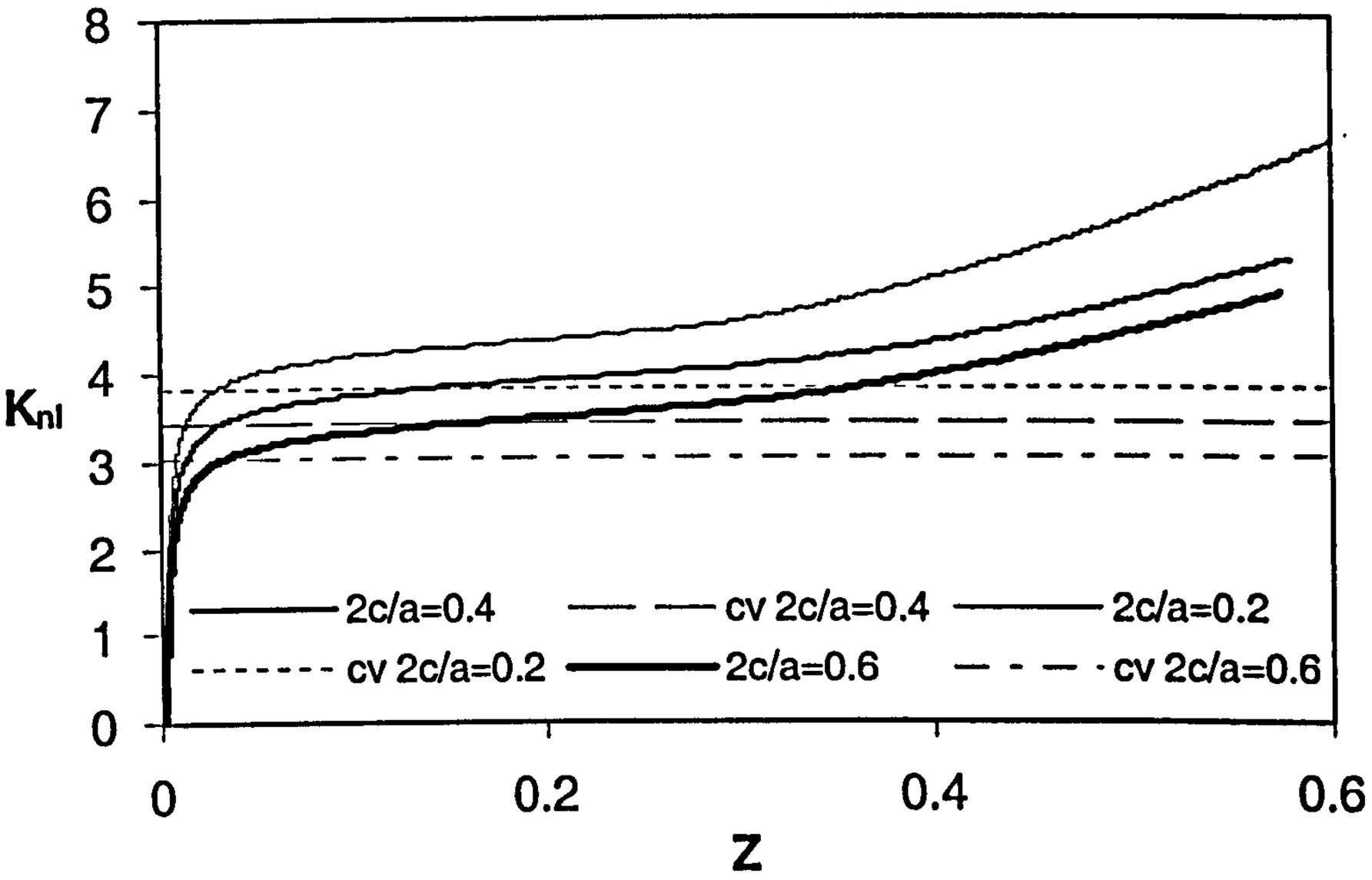

Figure 6-34: Nonlinear buckling of square plate with a longitudinal central crack.

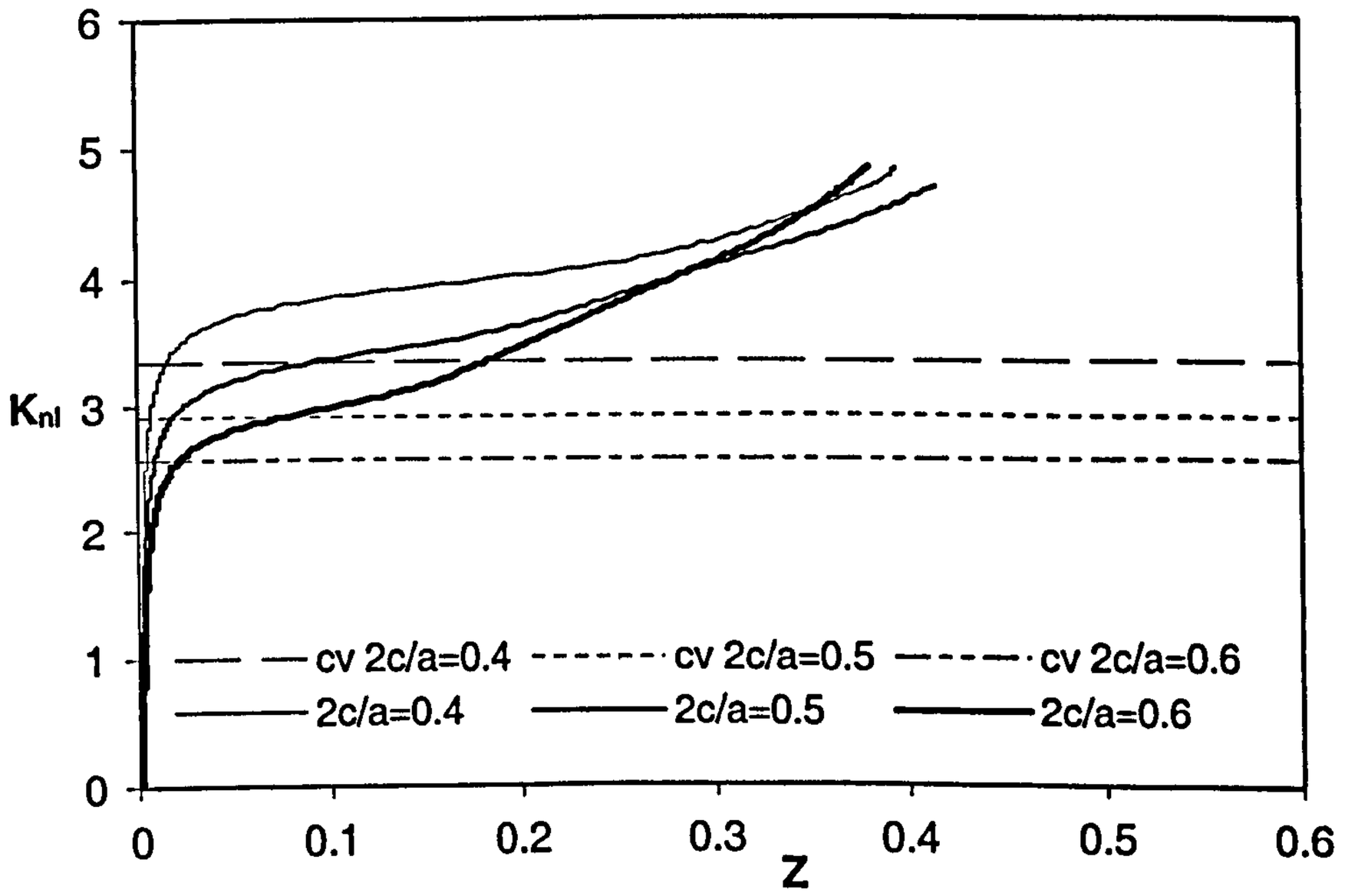

Figure 6-35: Nonlinear buckling of rectangular plate (a/b=2) with a longitudinal central crack.

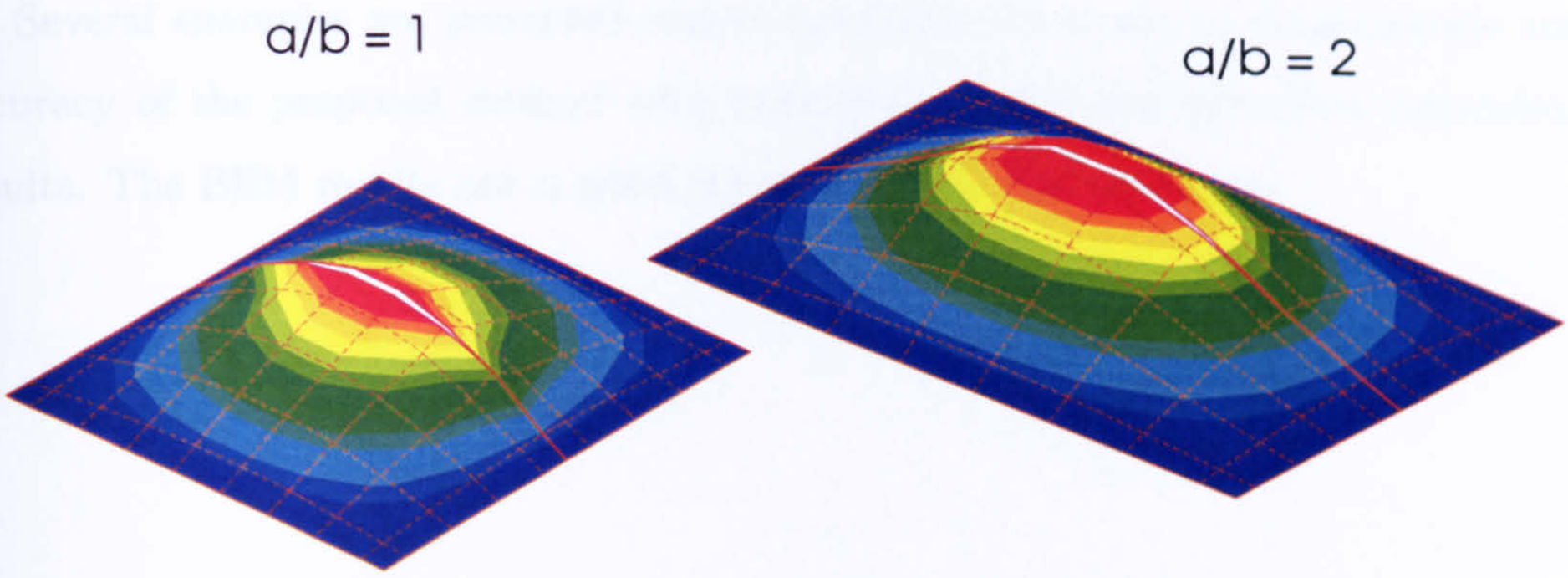

Figure 6-36: Nonlinear buckling deformations for simply supported rectangular plates with a longitudinal central crack.

6.13 Summary

In the analysis of the geometrically nonlinear plate bending problems, the domain integrals consist of coupling of the plate bending and membrane terms.

In the large deformation analysis, initially the domain is discretised using constant cells. Next, the domain integrals are transformed to the boundary integrals using the dual reciprocity technique. An approximation function is used to calculate the derivatives of the nonlinear terms in the domain integral.

The nonlinear buckling of thin plate is also presented. Two models of imperfection are introduced in the formulation, i.e. a small uniform transverse loads and distributed transverse loads based on eigenvectors. A simple numerical algorithms are presented to analyse the problems.

Next, large deformation analysis of cracked plates is also presented. The analysis is performed using the dual boundary element method. Five stress intensity factors are obtained, i.e. three SIFs from plate bending problem and two SIFs from membrane problem. The normalized stress intensity factors in membrane increase significantly after few increment of loads. While the normalized stress intensity factors in bending decrease if compared with the linear results.

The last analysis is the nonlinear buckling of cracked plates. The problem is analysed using the formulations for nonlinear buckling of thin plates and large deformation for cracked plates.

Several examples are presented and comparisons are made to demonstrate the accuracy of the proposed method with analytical results and the other numerical results. The BEM results are in good agreement with the references.

Chapter 7

Conclusions and Future Work

This chapter presents the final conclusions of the thesis and recommendations for extensions of the present work towards future research. These conclusions are based on the proposed methods described in the previous chapters, by which the main objectives outlined in Chapter 1 were achieved.

7.1 Summary and Conclusions

In the work presented in previous chapters, several new developments were reported. These include: normal boundary element formulations for linear and nonlinear buckling analysis of plates, dual boundary element methods for linear and nonlinear buckling analysis of plates.

The conclusions of the work are that the proposed boundary element methods are effective for buckling analysis of plates with different geometrics, loadings and boundary conditions. The method can also be applied reliably to solve buckling problems of cracked plates and geometrically nonlinear problems.

In chapter 4, the boundary integral equations for buckling analysis of shear deformable plates were derived. Plate buckling equations were written as a standard eigenvalue problem. The formulation was implemented in FORTRAN code using quadratic boundary elements. The domain integrals were evaluated using cell integration and the dual reciprocity technique. The eigenvalue problem of plate buckling yields a critical load factor and buckling modes. Several examples were analysed.

The results were compared to results of the analytical and the finite element method. The following conclusions can be made based on the results presented in chapter 4:

1. The boundary integral equation can be used as an effective tool to solve buckling problems of plates with different geometries, loadings and boundary conditions.

2. The evaluation of domain boundary integrals using the dual reciprocity technique were found to be more accurate than domain integration using constant cell discretisation. It is anticipated that higher order cells would provide more accurate solution. However, higher order cells would require more elaborate integration schemes to deal with strongly singular integrals. Preparing models of the problems using the dual reciprocity technique is much easier than the corresponding domain integration using constant cell.

3. The BEM results were shown to be in good agreement (most results are less than 2% difference) with analytical and finite element results.

Chapter 5 presented the dual boundary integral equations for the buckling analysis of the Reissner shear deformable cracked plates. The domain integrals which appear in this formulation were transferred to boundary integrals using the dual reciprocity method. The boundary integral equation for cracked plated buckling were presented as a standard eigenvalue problem, which would allow direct evaluation of critical load factor and buckling modes. Some examples were analysed. The results were compared with analytical and differential quadrature element results. The conclusions made from the results are:

1. The dual boundary element method can be used as an effective tool for modelling crack problems in presence of buckling.

2. The dual reciprocity method coupled with the dual boundary element method provided accurate solutions of buckling coefficients.

3. The BEM results are obtained in good agreement ($< 1.5\%$ difference) with analytical and differential quadrature element results.

In chapter 6, the boundary integral equations for geometrically nonlinear problems of shear deformable plates were presented. The domain integrals include coupling terms of the plate bending and membrane terms. In the large deformation analysis, initially the domain was discretised using constant cells. Later, the dual reciprocity technique is employed to transfer the domain integrals to the boundary. The nonlinear buckling analysis of thin plates and cracked plates was also presented. Two models of imperfection are introduced in the formulation, i.e. a small uniform transverse load and distributed transverse load evaluated based on eigenvectors. Next, large deformation of cracked plates were also presented. The analysis was performed using the dual boundary element method. Five stress intensity factors were obtained, i.e. three SIFs from plate bending problem and two SIFs from membrane problem. Several examples were presented and comparisons were made to show the agreement of the proposed method with analytical results, the other numerical results and the published results. The following conclusions can be made based on the proposed method and presented results in chapter 6:

1. Once the coefficient matrices have been formed, they can be used in each increment without any further change. Moreover, the system of equations can be carried out fast if the *LU*-decomposition method is adopted. Hence, computational time of the proposed method to solve the problems is faster than the finite element method which needs to update the stiffness matrices in each increment.

2. In large deformation, four different approximation functions to evaluate the derivative terms were presented. All approximations were shown to provide good agreement with finite element results.

3. The BEM large deformation results from different solution procedures show good agreement with analytical and other numerical results. The best method and solution procedure for solving large deformation is combination of approximation function method and total increment method.

4. Eigenvectors are very useful to introduce initial imperfections to the nonlinear buckling problems, especially for complex geometries.

5. The BEM nonlinear buckling result of square plate modelled using 20 quadratic boundary elements and 81 domain points are in a good agreement with analytical result. Other BEM results also show satisfactory agreements with buckling coefficients K from analytical and finite element results.

6. The nonlinear buckling formulation is also a robust method for analysis of cracked plates.

7. In large deformation, the normalized stress intensity factors in membrane increase significantly after few increments of the load. While the normalized stress intensity factors in bending decrease if compared with the linear results.

7.2 Future Research

The application of the boundary element method for buckling analysis of cracked plates and geometrically nonlinear problems presented in this work can be extended further to several area of researches, and are described as follows:

1. Buckling analysis of assembled plate-structures including in presence of crack.

2. To analyse buckling problems of shells with or without crack.

3. Buckling analysis of stiffened cracked plates and shells.

4. Nonlinear buckling analysis of assembled plate-structures, stiffened cracked plates and shells

Bibliography

[1] Abdel-Akher, A. and Hartley, G. A., Evaluation of boundary integrals for plate bending, *International Journal for Numerical Methods in Engineering*, 28, 75-93, 1989.

[2] Abdel-Akher, A. and Hartley, G. A., Boundary integration and interpolation procedures for plate bending, *International Journal for Numerical Methods in Engineering*, 28, 1389-1408, 1989.

[3] Abramowitz, M. and Stegun, I. A. (Eds.), *Handbook of mathematical functions*, Dover, New York, 1965.

[4] Ahmadi-Brooghani, S. Y. and Wearing, J. L., The application of the dual boundary element method in linear elastic crack problem in plate bending. in *Boundary Element Methods XVIII*, C. A. Brebbia, J. B. Martins, M. H. Aliabadi and N. Haie (Eds.), Portugal, 429-438, Computational Mechanics Publications, 1996.

[5] Aliabadi, M. H., Hall, W. S., and Phemister, T. G., Taylor expansion for singular kernels in the boundary element method, *International Journal for Numerical Methods in Engineering*, 21, 2221-2236, 1985.

[6] Aliabadi, M. H. and Rooke, D. P., *Numerical Fracture Mechanics*, Kluwer Academic Publisher, AA Dordrecht, The Netherlands, 1991.

[7] Aliabadi, M. H., Boundary element formulations in fracture mechanics, *Applied Mechanics Review*, 50(2), 83-96, 1997.

[8] Aliabadi, M. H., A new generation of boundary element methods in fracture mechanics, *International Journal of Fracture*, 86, 91-125, 1997.

[9] Aliabadi, M. H. (Ed.), *Plate Bending Analysis with Boundary Elements, Advanced in Boundary Element Series*, Computational Mechanics Publications, Southampton, 1998.

[10] Aliabadi, M. H., The boundary element method. Vol.2, Applications in solids and structures, Chichester ; New York : Wiley, 2002.

[11] Anderson, T. L., *Fracture Mechanics, Fundamentals and Applications*, CRC Press, Boca Raton, Florida, 1991.

[12] Atluri, S. N. and Pipkins, D. S., Large deformation analysis of plates and shells, *Boundary Element Analysis of Plates and Shells*, Beskos ed., Springer-Verlag, Berlin, 1942-165 (1991)

[13] Azizian, Z. G. and Dawe, D. J., Geometrical nonlinear analysis of rectangular Midlin plates using finite strip method, *Comput. Struct.*, **21** , 423-436 (1985)

[14] Bao, G., Jiang, W. and Robert, J.C., *Analytic and finite element solutions for bending and buckling of orthotropic rectangular plates,* International Journal of Solids Structures, **34** (14), 1797-1822, 1997

[15] Barcellos, C. A. and Silva, L. H. M., A boundary element formulation for the Mindlin's plate model, in *Boundary Element Technology*, C. A. Brebbia and W. S. Venturini (Eds.), Computational Mechanics Publications, 123-130, 1989..

[16] Bézine, G., Boundary integral formulation for plate flexure with arbitrary boundary conditions, *Mech. Res. Comm.*, **5**(4), 197-206, 1978.

[17] Berger, H. M., A new approach to the analysis of large deflections of plates, *J. Appl. Mech.*, **22**, 465-472, (1955)

[18] Blandford, G.E., Ingraffea, A. R. and Ligget, J. A., *Two-dimensional stress intensity factor computations using the boundary element method,* International Journal for Numerical Methods in Engineering, **17**, 387-406,1981

[19] Bleich, F., *Buckling Strength of Metal Structures*, 1st Eds., McGraw-Hill Book Co., Inc., 1952

[20] Brebbia, C. A., Telles, J. C. F. and Wrobel, L. C., *Boundary Element Techniques: Theory and Applications in Engineering*, Springer-Verlag, Berlin-Heidelberg, 1984.

[21] Brebbia, C. A. and Dominguez, J., *Boundary Elements, an Introductory Course*, 2nd edition, Computational Mechanics Publication, Southampton, McGraw-Hill Book Company, New York, 1992.

[22] Broek, D., *Elementary Engineering Fracture Mechanics*, 4th edition, Martinus Nijhoff Publishers, Dordrecht, 1987.

[23] Brush, D.O. and Almorth, B.O., *Buckling of Bars, Plates and Shells,* McGraw-Hill, New York (1975)

[24] Costa, J.A. and Brebbia, C.A., *Elastic buckling of plate using the boundary element method,* Boundary Element VII, Springer-Verlag, Berlin, 1985

[25] Cruse, T. A., *Boundary Element Analysis in Computational Fracture Mechanics,* Kluwer Academic Publishers, Netherland, 1988

[26] Delale, F. and Erdogan, F., Effect of transverse shear and material orthotrophy in a cracked spherical cap, *International Journal of Solids and Structures* , **15**, 907-926, 1979.

[27] Dirgantara, T. and Aliabadi, M. H., A new boundary element formulation for shear deformable shells analysis, *International Journal for Numerical Methods in Engineering,* **45**, 1257-1275, 1999.

[28] Dirgantara, T. and Aliabadi, M. H., Crack growth analysis of plate loaded by bending and tension using dual boundary element method, *International Journal of Fracture*, **105**, 27-47 (2000)

[29] El-Zafrany, A., Debbih, M. and Fadhil, S., Boundary element analysis of thick Reissner plates in bending. *Engineering Analysis with Boundary Elements*, **14**, 159-169, 1994.

[30] El-Zafrany, A., Debbih, M. and Fadhil, S., An efficient approach for boundary element bending analysis of thin and thick plates, *Computer and Structures*, **56**, 565-576, 1995.

[31] El-Zafrany, A., Debbih, M. and Fadhil, S., A modified Kirchhoff theory for boundary element bending analysis of thin plates, *Int. J. Solids Structures*, Vol. **31**, No. 21, 2885-2899 (1994)

[32] Fafard, M., Beaulieu, D. and Dhatt, G., *Buckling of thin-walled members by finite elements*, Computers & Structures, **25** (2), 183-190, 1987

[33] Forbes, D. J. and Robinson, A. R., *Numerical Analysis of Elastic Plates and Shallow Shells by an Integral Equation Method*, Structural research series report no. 345. University of Illinois, Urbana, 1969.

[34] Gerard, G. and Becker, H., *Handbook of Structural Stability Part I - Buckling of Flat Plates*, NACA TN 3781

[35] Greenberg, M. D., *Application of Green's Functions in Science and Engineering*, Prentice-Hall Inc., 1971.

[36] Griffith, A. A., The phenomena of rupture and flow in solids, *Philosophical Transactions of the Royal Society of London*, A221,163-197, 1920.

[37] Hartmann, F. and Zormantel, R., The direct boundary element method in plate bending, *International Journal for Numerical Methods in Engineering*, **23**, 2049-2069, 1986.

[38] Henwood, D. J., Whiteman, J. R. and Yettram, A. L., Finite difference solution of a system of first-order partial differential equations, *International Journal for Numerical Methods in Engineering*, **17**, 1385-1395, 1981.

[39] Hong, H. and Chen, J., Derivations of integral equations of elasticity, *Journal of Engineering Mechanics*, **114**(6), 1028-1044, 1988.

[40] Irwin, G. R., Fracture dynamics, *Fracturing of Metals*, American Society of Metals, Cleveland, 147-166, 1948.

[41] Jaswon, M. A. and Maiti, M., An integral equation formulation of plate bending problem, *J. Engng. Math.*, (2), 83-93 (1968)

[42] Kamiya, N., Sawaki, Y. and Nakamura, Y., *Postbuckling analysis by the boundary element method, Engineering Analysis,* 1 (3), 40-44, 1984

[43] Kamiya, N. and Sawaki, Y., An integral equation approach to finite deflection of elastic plates, *Int. J. Non-linear Mech.*, 17 (3), 187-194 (1982)

[44] Karam, V. J. and Telles, J. C. F., On boundary elements for Reissner's plate theory, *Engineering Analysis*, 5, 21-27, 1988.

[45] Karami, G., Zarrinchang, J. and Foroughi, B., Analytical treatment of boundary integrals in direct boundary element analysis of plate bending problems, *International Journal for Numerical Methods in Engineering*, 37, 2409-2427, 1994.

[46] Kawabe, H., *Plate buckling analysis by the boundary element method,* Theory and Application of Boundary Element Methods, eds. M. Tanaka and Q. Du, Pergamon, Oxford, 367-374, 1987

[47] Kirchhoff, G., Uber das gleichgewicht und die bewegung einer elastischen scheibe, *J. Reine Angew. Math.*, 40, 51-88, 1850.

[48] Lawry, M.H., *I-DEAS Master Series: Student Guide,* Structural Dynamics Research Corporation, Milford, Ohio (1998)

[49] Lei, X. Y., Huang, M. K. and Wang, X. X., Geometrically nonlinear analysis of a Reissner type by the boundary element method, *Comput. Struct.*, 37 (6), 911-916 (1990)

[50] Levy, S., Bending of rectangular plate with large deflections, *NACA TN-846,* (1942)

[51] Levy, S., Square plate with clamped edges under normal pressure producing large deflections, *NACA TN-847,* (1942)

[52] Lin, J., Duffield, R.C. and Shih, H., *Buckling Analysis of Elastic Plates by Boundary Element Method,* Engineering Analysis with Boundary Element, **23**, pp 131-137 (1999)

[53] Liu, Y., *Elastic stability analysis of thin plate by the boundary element method - new formulation,* Engineering Analysis, 4, 160-164, 1987

[54] Liu, F.L., *Differential Quadrature Element Method for Buckling Analysis of Rectangular Mindlin Plates Having Discontinuities,* Int. J. Solids Structures, Vol. **38**, pp 2305-2321 (2001)

[55] Manolis, G.D., Beskos, D.E. and Pineros, M.F., *Beam and plate stability by boundary element,* Computers & Structures, **22**, 971-923, 1986

[56] Mindlin, R. D., Influence of rotatory inertia and shear on flexural motions of isotropic, elastic plates, *Journal of Applied Mechanics*, **18**, 31-38, 1951.

[57] Mi, Y. and Aliabadi, M. H., Discontinuous crack-tip elements: application to 3-D boundary element method, *International Journal of Fracture*, **67**, R67-R71, 1994

[58] Nerantzaki, M.S. and Katsikadelis, J.T., *Buckling of Plates with Variable Thickness — An Analog Equation Solution,* Engineering Analysis with Boundary Element, **18**, pp 149-154 (1996).

[59] Okada, H., Rakiyah, H. and Atluri, S. N., A novel displacement gradient boundary element for elastic stress analysis with high accuracy, *Trans ASME Journal of Applied Mechanics*, **55**, 786-794, 1988.

[60] Palazotto, A.N. and Dennis, S.T., *Nonlinear Analysis of Shell Structures*, Americans Institute of Aeronautics and Astronautics, Inc., Washington DC (1992)

[61] Partridge, P. W., Brebbia, C. A. and Wrobel, L. C., *The Dual Reciprocity Boundary Element Method*, Computational Mechanics Publication, Southampton, 1992.

[62] Pica, R, Wood, R.D. and Hinton E., Finite element analysis of geometrically nonlinear plate behaviour using Mindlin formulation, *Comput. Struct.*, **11** , 203-215 (1980)

[63] Portela, A., Aliabadi, M. H. and Rooke, D. P., The dual boundary element method: effective implementation for crack problems, *International Journal for Numerical Methods in Engineering*, **33**, 1269-1287, 1992.

[64] Purbolaksono, J. and Aliabadi, M.H., *Buckling Analysis of Shear Deformable Plates by Boundary Element Method,* submitted for publication

[65] Purbolaksono, J. and Aliabadi, M.H., *Dual Boundary Element Analysis of Cracked Plates under Buckling Loads,* submitted for publication

[66] He, X. Q. and Qin, Q. H., Nonlinear analysis of Reissner's plate by the variational approaches and boundary element methods, *Appl. Math. Modelling*, **17**, 149-155 (1993)

[67] Qin, Q. and Huang Y., *BEM of postbuckling analysis of thin plates,* Applied Mathematical Modelling, **14**, 544-548, 1990

[68] Rashed, Y. F., Aliabadi, M. H., Brebbia, C. A., Hyper-singular boundary element formulation for Reissner plates, *International Journal of Solids and Structures,* **35**(18), 2229-2249, 1998.

[69] Rashed, Y. F., Aliabadi, M. H. and Brebbia, C. A., On the evaluation of the stresses in the BEM for Reissner plate-bending problems, *Appl. Math. Modelling*, **21**, 155-163 (1997)

[70] Rashed, Y.F. and Aliabadi, M.H., *Fundamental solutions for thick foundation plates,* Mechanics Research Communications, **24**, pp 331-340, 1997

[71] Reissner, E., On bending of elastic plates, *Quarterly of Applied Mathematics*, **5**, 55-68, 1947.

[72] Rhodes, J., *Buckling of thin plates and members - and early work on rectangular tubes,* Thin-Walled Structures, **40**, 87-108, 2002

[73] Salgado, N. K. and Aliabadi, M. H., Boundary element analysis of cracked stiffened sheets, reinforced by adhesively bonded patches, *International Journal for Numerical Methods in Engineering*, 42(2), 195-217, 1998.

[74] Sih, G. C. (Ed.) *Mechanics of Fracture Volume 3: Plate and Shells with Cracks*, Noordhoff International Publishing, Leyden, 1977a.

[75] Sokolnikoff, I.S., *Mathematical Theory of Elasticity*, 1st Eds., McGraw-Hill Book Co., Inc., 1946

[76] Sosa, H. A. and Eischen, J. W., Computation of stress intensity factors for plate bending via a path-independent integral, *Engineering Fracture Mechanics*, 25, 451-462, 1986.

[77] Sosa, H. A. and Herrmann, G., On invariant integrals in the analysis of cracked plates, *International Journal of Fracture*, 40, 111-126, 1989.

[78] Stahl, B. and Keer, L.M., *Vibration and Stability of Cracked Rectangular Plates*, Int. J. Solids Structures, Vol. 8, pp 69-91 (1972)

[79] Stern, M., A General boundary integral formulation for plate bending problems, *International Journal of Solids and Structures*, 15, 769-782, 1979.

[80] Stern, M., Boundary integral equations for bending of thin plates, in *Progress in Boundary Element Methods*, Prentech Press, London, 158-181, 1983.

[81] Stern, M. and Lin, T.-L., Thin elastic plates in bending, in *Development in Boundary Element Methods - 4*, Banarjee, P. K. and Watson, J. O. (Eds.), Elsevier Applied Science Publishers, London, 91-119, 1986.

[82] Syngellakis, S. and Elzein, A., *Plate Buckling Loads by the Boundary Element Method*, Int. J. Numer. Meth. Engng. 37, 1763-1778 (1994)

[83] Syngellakis, S., *Stability*, Plate Bending Analysis with Boundary Elements, Eds. M.H. Aliabadi, Advances in Boundary Element Series, Computational Mechanics Publications, Southampton UK and Boston USA, 1998

[84] Tanaka, M., Large deflection analysis of thin elastic plates, *Development in Boundary Element Methods, Elsevier Applied Science Publishers*, 3, 115-136 (1984)

[85] Tanaka, M., *Elastic buckling analysis of assembled plate structures by boundary element method,* Boundary Element VIII, Springer-Verlag, Berlin, 1986

[86] Tanaka, M., Matsumoto, T. and Zheng, Z., *Aplication of the domain-boundary element method to the pre/post-buckling problem of von Karman plates*, Engineering Analysis with Boundary Element, 23, 399-404, 1999

[87] Telles, J. C. F., A self-adaptive coordinate transformation for efficient numerical evaluation of general boundary element integrals, *International Journal for Numerical Methods in Engineering*, 24, 959-973, 1987.

[88] Timoshenko, S. and Goodier, J. N., *Theory of Elasticity*, 3rd edition, McGraw-Hill International Editions, Singapore, 1970.

[89] Timoshenko, S. P. and Woinowsky-Krieger, S., *Theory of Plates and Shells*, 2nd edition, McGraw-Hill International Editions, Singapore, 1959.

[90] Timoshenko, S. and Gere, J.M., *Theory of Elastic Stability,* second edition, McGraw-Hill, New York (1961)

[91] Tottenham, H., The boundary element method for plates and shells. In: *Development in Boundary Element Methods-I* (Edited by P. K. Banerjee and R. Butterfield), Applied Science, London (1979)

[92] Vafai, A.and Estekanchi, H.E., *Parametric Instability of Edge Cracked Plates,* Thin Walled Structures. 40, pp 29-44 (2002)

[93] Walker, A.C., *A Brief Review of Plate Buckling Research,* In: Rhodes J, Spence J, editors, Behaviour of Thin-walled Structures, Elsevier, London (1984)

[94] Vander Weeën, F., Application of the boundary integral equation method to Reissner's plate model, *International Journal for Numerical Methods in Engineering*, 18, 1-10, 1982.

[95] Vander Weeën, F., Application of the direct boundary element method to Reissner's plate model, in *Boundary Element Methods in Engineering*, C. A. Brebbia, (Ed.), Springer-Verlag, Berlin, 1982.

[96] Wearing, J. L. and Ahmadi-Brooghani, S. Y., Fracture analysis of plate bending problems using boundary element method, in *Plate Bending Analysis with Boundary Elements, Advanced in Boundary Element Series*, M. H. Aliabadi (Ed.), Computational Mechanics Publications, Southampton, 1998.

[97] Wen, P. H., Aliabadi, M. H. and Young, A., Plane stress and plate bending coupling in BEM analysis of shallow shells, *International Journal for Numerical Methods in Engineering*, 48, 1107-1125, 2000.

[98] Wen, P. H., Aliabadi, M. H. and Young, A., Application of dual reciprocity method to plates and shells, *Engineering Analysis with Boundary Element*, No. 24, 583-590 (2000)

[99] Wen, P.H., Aliabadi, M.H. and Young, A., *Boundary element analysis of shear deformable stiffened plates*, Engineering Analysis with Boundary Elements, 26, 511-520, 2002

[100] Weil, N. A. and Newmark, N. M., Large deflections of elliptical plates, *J. Appl. Mech.*, **23**, 21-26 (1956)

[101] Westphal, T. Jr. and Barcellos, C. A., Application of the boundary element method to Reissner's and Mindlin's plate model, in *Boundary Elements XII*, M. Tanaka, C. A. Brebbia and T. Honna (Eds.), Computational Mechanics Publication, 1, 467-477, 1990.

[102] Ye, T. Q., and Lin, Y. J., Finite deflection analysis of elastic plate by the boundary element method, *Appl. Math. Modelling*, 9, 183-188 (1985)

[103] Zhang, J. D. and Atluri, S. N., A boundary/ interior element method for quasi static and transient response analysis of shallow shells, *Computer and Structures*, 24, 213-223, 1986.

[104] Zienkiewicz, O. C. and Taylor, R.,*The Finite Element Method, Vol 1: Basic Formulation and Linear Problems,* 4^{th} edition, McGraw-Hill Publishing Company, London, 1994.

[105] Zienkiewicz, O. C. and Taylor, R., *The Finite Element Method, Vol 2: Non Linear Problems,* 4^{th} edition, McGraw-Hill Publishing Company, London, 1991.

Appendix A

Fundamental solutions

A.1 Plate Bending Problem

The expressions for the kernels W^*_{ij} and P^*_{ij} are given by Vander Weeën [94] as follows:

$$\begin{aligned} W^*_{\alpha\beta} &= \frac{1}{8\pi D(1-\nu)}\{[8B(z)-(1-\nu)(2\ln z-1)]\delta_{\alpha\beta} \\ &- [8A(z)+2(1-\nu)]r_{,\alpha}r_{,\beta}\} \\ W^*_{\alpha 3} &= -W^*_{3\alpha} = \frac{1}{8\pi D}(2\ln z-1)rr_{,\alpha} \\ W^*_{33} &= \frac{1}{8\pi D(1-\nu)\lambda^2}[(1-\nu)z^2(\ln z-1)-8\ln z] \end{aligned} \tag{A.1}$$

and

$$\begin{aligned} P^*_{\gamma\alpha} &= \frac{-1}{4\pi r}[(4A(z)+2zK_1(z)+1-\nu)(\delta_{\alpha\gamma}r_{,n}+r_{,\alpha}n_\gamma) \\ &+ (4A(z)+1+\nu)r_{,\gamma}n_\alpha-2(8A(z)+2zK_1(z)+1-\nu)r_{,\alpha}r_{,\gamma}r_{,n}] \\ P^*_{\gamma 3} &= \frac{\lambda^2}{2\pi}[B(z)n_\gamma-A(z)r_{,\gamma}r_{,n}] \\ P^*_{3\alpha} &= \frac{-(1-\nu)}{8\pi}\left[\left(2\frac{(1+\nu)}{(1-\nu)}\ln z-1\right)n_\alpha+2r_{,\alpha}r_{,n}\right] \\ P^*_{33} &= \frac{-1}{2\pi r}r_{,n} \end{aligned} \tag{A.2}$$

The expression for the kernels $W^*_{3j,\theta}$ and $W^*_{33,\theta\gamma}$ are written as

$$W^*_{3\alpha,\theta} = -\frac{1}{8\pi D}\left(2r_{,\theta}r_{,\alpha} + (2\ln z - 1)\delta_{\alpha\theta}\right)$$

$$W^*_{33,\theta} = \frac{1}{8\pi D\lambda}r_{,\theta}\left[(2\ln z - 1) - \frac{8}{z(1-\nu)}\right] \tag{A.3}$$

$$W^*_{33,\theta\gamma} = \frac{1}{8\pi D}\left[(2\ln z - 1) + 2r_{,\theta}r_{,\gamma} - \frac{8(\delta_{\theta\gamma} - 2r_{,\theta}r_{,\gamma})}{z^2(1-\nu)}\right] \tag{A.4}$$

The expression for the kernels $P^*_{3j,\theta}$ is written as

$$P^*_{3\alpha,\theta} = \frac{-(1-\nu)}{4\pi r}\left[\left(\frac{(1+\nu)r_{,\theta}}{(1-\nu)}\right)n_\alpha + r_{,\alpha}n_\theta - 3r_{,\theta}r_{,n}r_{,\alpha} + \delta_{\alpha\theta}r_{,n}\right]$$

$$P^*_{33,\theta} = \frac{-1}{2\pi r^2}\left[n_\theta - 2r_{,\theta}r_{,n}\right] \tag{A.5}$$

The expression of W^*_{ijk}, P^*_{ijk} and $Q^*_{i\beta}$ are [94]:

$$\begin{aligned}
W^*_{\alpha\beta\gamma} &= \frac{1}{4\pi r}[(4A(z) + 2zK_1(z) + 1 - \nu)(\delta_{\beta\gamma}r_{,\alpha} + \delta_{\alpha\gamma}r_{,\beta}) \\
&- 2(8A(z) + 2zK_1(z) + 1 - \nu)r_{,\alpha}r_{,\beta}r_{,\gamma} + (4A(z) + 1 + \nu)\delta_{\alpha\beta}r_{,\gamma}] \\
W^*_{\alpha\beta 3} &= \frac{-(1-\nu)}{8\pi}\left[\left(2\frac{(1+\nu)}{(1-\nu)}\ln z - 1\right)\delta_{\alpha\beta} + 2r_{,\alpha}r_{,\beta}\right] \\
W^*_{3\beta\gamma} &= \frac{\lambda^2}{2\pi}[B(z)\delta_{\gamma\beta} - A(z)r_{,\gamma}r_{,\beta}] \\
W^*_{3\beta 3} &= \frac{1}{2\pi r}r_{,\beta}
\end{aligned} \tag{A.6}$$

$$\begin{aligned}
P^*_{\alpha\beta\gamma} &= \frac{D(1-\nu)}{4\pi r^2}\{(4A(z) + 2zK_1(z) + 1 - \nu)(\delta_{\gamma\alpha}n_\beta + \delta_{\gamma\beta}n_\alpha) \\
&+ (4A(z) + 1 + 3\nu)\delta_{\alpha\beta}n_\gamma - (16A(z) + 6zK_1(z) + z^2K_0(z) + 2 - 2\nu) \\
&\times [(n_\alpha r_{,\beta} + n_\beta r_{,\alpha})r_{,\gamma} + (\delta_{\gamma\alpha}r_{,\beta} + \delta_{\gamma\beta}r_{,\alpha})r_{,n}] \\
&- 2(8A(z) + 2zK_1(z) + 1 + \nu)(\delta_{\alpha\beta}r_{,\gamma}r_{,n} + n_\gamma r_{,\alpha}r_{,\beta}) \\
&+ 4(24A(z) + 8zK_1(z) + z^2K_0(z) + 2 - 2\nu)r_{,\alpha}r_{,\beta}r_{,\gamma}r_{,n}\} \\
P^*_{\alpha\beta 3} &= \frac{D(1-\nu)\lambda^2}{4\pi r}[(2A(z) + zK_1(z))(r_{,\beta}n_\alpha + r_{,\alpha}n_\beta)
\end{aligned}$$

$$
\begin{aligned}
&- \quad 2(4A(z)+zK_1(z))r_{,\alpha}r_{,\beta}r_{,n}+2A(z)\delta_{\alpha\beta}r_{,n}] \\
P^*_{3\beta\gamma} &= \frac{-D(1-\nu)\lambda^2}{4\pi r}[(2A(z)+zK_1(z))(\delta_{\gamma\beta}r_{,n}+r_{,\gamma}n_\beta) \\
&+ \quad 2A(z)n_\gamma r_{,\beta}-2(4A(z)+zK_1(z))r_{,\gamma}r_{,\beta}r_{,n}] \\
P^*_{3\beta 3} &= \frac{D(1-\nu)\lambda^2}{4\pi r^2}[(z^2B(z)+1)n_\beta-(z^2A(z)+2)r_{,\beta}r_{,n}]
\end{aligned}
\tag{A.7}
$$

$$
\begin{aligned}
Q^*_{\alpha\beta} &= \frac{-r}{64\pi}\{(4\ln z-3)[(1-\nu)(r_{,\beta}n_\alpha+r_{,\alpha}n_\beta)+(1+3\nu)\delta_{\alpha\beta}r_{,n}] \\
&+ \quad 4[(1-\nu)r_{,\alpha}r_{,\beta}+\nu\delta_{\alpha\beta}]r_{,n}\} \\
Q^*_{3\beta} &= \frac{1}{8\pi}[(2\ln z-1)n_\beta+2r_{,\beta}r_{,n}]
\end{aligned}
\tag{A.8}
$$

where

$$
\begin{aligned}
A(z) &= K_0(z)+\frac{2}{z}\left[K_1(z)-\frac{1}{z}\right] \\
B(z) &= K_0(z)+\frac{1}{z}\left[K_1(z)-\frac{1}{z}\right]
\end{aligned}
\tag{A.9}
$$

in which $K_0(z)$ and $K_1(z)$ are modified Bessel functions of the second kind [3], $z=\lambda r$, λ is the shear factor defined in section 2.3.4, r is the absolute distance between the source and the field points, $r_{,\alpha}=r_\alpha/r$, where $r_\alpha=x_\alpha(\mathbf{x})-x_\alpha(\mathbf{x}')$ and $r_{,n}=r_{,\alpha}n_\alpha$.

Expanding the modified Bessel functions for small arguments:

$$
\begin{aligned}
K_0(z) &= \left[-\gamma-\ln(\tfrac{z}{2})\right]+\left[-\gamma+1-\ln(\tfrac{z}{2})\right]\frac{(z^2/4)}{(1!)^2} \\
&+\left[-\gamma+1+\frac{1}{2}-\ln(\tfrac{z}{2})\right]\frac{(z^2/4)^2}{(2!)^2} \\
&+\left[-\gamma+1+\frac{1}{2}+\frac{1}{3}-\ln(\tfrac{z}{2})\right]\frac{(z^2/4)^3}{(3!)^2}+\cdots
\end{aligned}
\tag{A.10}
$$

$$
\begin{aligned}
K_1(z) &= \frac{1}{z}-\left[-\gamma+\frac{1}{2}-\ln(\tfrac{z}{2})\right]\frac{(z^2/4)^{1/2}}{0!1!} \\
&-\left[-\gamma+1+\frac{1}{4}-\ln(\tfrac{z}{2})\right]\frac{(z^2/4)^{3/2}}{1!2!} \\
&-\left[-\gamma+1+\frac{1}{2}+\frac{1}{6}-\ln(\tfrac{z}{2})\right]\frac{(z^2/4)^{5/2}}{2!3!}+\cdots
\end{aligned}
\tag{A.11}
$$

where $\gamma = 0.5772156649$ is the Euler constant. Substitute equations (A.10 – A.11) into (A.9) and take the limit as $r \to 0$:

$$\lim_{r\to 0} A(z) = \frac{-1}{2},$$
$$\lim_{r\to 0} B(z) = -\frac{1}{2}\left[\lim_{r\to 0} \ln(\frac{z}{2}) + \gamma + \frac{1}{2}\right] \qquad (A.12)$$

As it can be seen, $A(z)$ is a smooth function, whereas, $B(z)$ is a weakly singular $O(\ln r)$. Therefore W^*_{ij} is weakly singular and P^*_{ij} has a strong (Cauchy principal value) singularity $O(1/r)$.

In this work, the modified Bessel functions are evaluated using polynomial approximations given by Abramowitz and Stegun [3] .

A.2 Two-dimensional Plane Stress Problem

The expressions for the kernels $U^*_{\theta\alpha}$ and $T^*_{\theta\alpha}$ are well known (Kelvin solution) for two-dimensional plane stress problems, and are given as [103] :

$$U^*_{\theta\alpha} = \frac{1}{4\pi B\,(1-\nu)}\left[(3-\nu)\ln\left(\frac{1}{r}\right)\delta_{\theta\alpha} + (1+\nu)\,r_{,\theta}r_{,\alpha}\right] \qquad (A.13)$$

$$\begin{aligned} T^*_{\theta\alpha} \;=\; & -\frac{1}{4\pi r}\left\{r_{,n}\left[(1-\nu)\,\delta_{\theta\alpha} + 2\,(1+\nu)\,r_{,\theta}r_{,\alpha}\right]\right. \\ & \left. +(1-\nu)\left[n_\theta r_{,\alpha} - n_\alpha r_{,\theta}\right]\right\} \end{aligned} \qquad (A.14)$$

where $U^*_{\theta\alpha}$ are weakly singular kernels of order $O(\ln\frac{1}{r})$ and $T^*_{\theta\alpha}$ are strongly singular in order $O(1/r)$.

The expressions for the kernels $U^*_{\alpha\beta\gamma}$ and $T^*_{\alpha\beta\gamma}$ are :

$$U^*_{\alpha\beta\gamma} = \frac{1}{4\pi r}\left[(1-\nu)\,(\delta_{\gamma\alpha}r_{,\beta} + \delta_{\gamma\beta}r_{,\alpha} - \delta_{\alpha\beta}r_{,\gamma}) + 2\,(1+\nu)\,r_{,\alpha}r_{,\beta}r_{,\gamma}\right] \qquad (A.15)$$

$$\begin{aligned} T^*_{\alpha\beta\gamma} \;=\; & \frac{B\,(1-\nu)}{4\pi r^2}\left\{2r_{,n}\left[(1-\nu)\,\delta_{\alpha\beta}r_{,\gamma} + \nu\,(\delta_{\gamma\alpha}r_{,\beta} + \delta_{\gamma\beta}r_{,\alpha}) - 4\,(1+\nu)\,r_{,\alpha}r_{,\beta}r_{,\gamma}\right]\right. \\ & +2\nu\,(n_\alpha r_{,\beta}r_{,\gamma} + n_\beta r_{,\alpha}r_{,\gamma}) + (1-\nu)\,(2n_\gamma r_{,\alpha}r_{,\beta} + n_\beta\delta_{\alpha\gamma} + n_\alpha\delta_{\beta\gamma}) \end{aligned}$$

$$-(1-3\nu)\,n_\gamma\delta_{\alpha\beta}\} \tag{A.16}$$

The expression for the Kelvin $U^*_{\theta\alpha,\beta}$ and $T^*_{\theta\alpha,\beta}$ are written as

$$U^*_{\theta\alpha,\beta} = \frac{1}{4\pi B\,(1-\nu)\,r}\left[(1+\nu)\,(\delta_{\theta\beta}+\delta_{\alpha\beta}-2r_{,\theta}r_{,\alpha}r_{,\beta})-(3-\nu)\,r_{,\beta}\delta_{\theta\alpha}\right] \tag{A.17}$$

$$\begin{aligned} T^*_{\theta\alpha,\beta} \;=\; & -\frac{1}{4\pi r^2}\{(n_\beta-2r_{,\beta}r_{,n})\left[(1-\nu)\,\delta_{\theta\alpha}+2\,(1+\nu)\,r_{,\theta}r_{,\alpha}\right] \\ & +r_{,\beta}r_{,n}\left[(1-\nu)\,\delta_{\theta\alpha}+2\,(1+\nu)\,r_{,\theta}r_{,\alpha}\right] \\ & +r_{,n}\left[2\,(1+\nu)\,((\delta_{\theta\beta}-r_{,\theta}r_{,\beta})r_{,\alpha}+(\delta_{\alpha\beta}-r_{,\alpha}r_{,\beta})r_{,\theta}\right)] \\ & +(1-\nu)\left[n_\theta(\delta_{\alpha\beta}-r_{,\alpha}r_{,\beta})-n_\alpha(\delta_{\theta\beta}-r_{,\theta}r_{,\beta})-r_{,\beta}(n_\theta r_{,\alpha}-n_\alpha r_{,\theta})\right]\} \end{aligned} \tag{A.18}$$

The expression for the kernel $U^*_{\alpha\beta\gamma,\theta}$ is written as

$$\begin{aligned} U^*_{\alpha\beta\gamma,\theta} \;=\; & \frac{1}{4\pi r^2}[(1-\nu)\,(\delta_{\gamma\alpha}(\delta_{\beta\theta}-2r_{,\beta}r_{,\theta})) \\ & +(1-\nu)\,(\delta_{\gamma\beta}(\delta_{\alpha\theta}-2r_{,\alpha}r_{,\theta})-\delta_{\alpha\beta}(\delta_{\gamma\theta}-2r_{,\gamma}r_{,\theta})) \\ & +2\,(1+\nu)\,(\delta_{\alpha\theta}+\delta_{\beta\theta}+\delta_{\gamma\theta}-3r_{,\alpha}r_{,\beta}r_{,\gamma}r_{,\theta})] \end{aligned} \tag{A.19}$$

Appendix B

Particular solutions

Particular solutions derived by Wen, Aliabadi and Young [97]are used for the dual reciprocity technique in the thesis and are given in the following sections.

B.1 Particular solutions for plate bending

Governing equation for shear deformable plate bending problem can be written as

$$\hat{\mathbf{w}} = \mathbf{II}\mathbf{c}\varphi \tag{B.1}$$

where particular solutions of displacement $\hat{\mathbf{w}} = \{\hat{w}_1, \hat{w}_2, \hat{w}_3\}^T$, $\mathbf{c} = \{c_1, c_2, c_3\}^T$ is arbitrary constant vector and components of matrix $\mathbf{II}$ are

$$H_{\alpha\beta} = 2\delta_{\alpha\beta}\nabla^4 - [(1+\nu)\nabla^2 + (1-\nu)\lambda^2)]\frac{\partial^2}{\partial x_\alpha \partial x_\beta}$$

$$H_{3\alpha} = -H_{\alpha 3} = -(1-\nu)(\nabla^2 - \lambda^2)\frac{\partial}{\partial x_\alpha}$$

$$H_{33} = (\nabla^2 - \lambda^2)[2\nabla^2 - (1-\nu)\lambda^2]/\lambda^2 \tag{B.2}$$

The function φ can be defined from equation (B.1) such that

$$D(1-\nu)(\nabla^2 - \lambda^2)\nabla^4\varphi + F(r) = 0 \tag{B.3}$$

If $e_1 = 0, e_2 = 0$ and $e_3 = 1$, the particular solution used in equation (3.55) can be written as

$$\hat{w}_{m\alpha} = -\frac{1}{D}\frac{\partial \psi}{\partial x_\alpha}$$

$$\hat{w}_{m3} = \frac{1}{(1-\nu)D\lambda^2}[2\nabla^2\psi - (1-\nu)\lambda^2\psi] \tag{B.4}$$

where

$$\nabla^4\psi(r) + F(r) = 0 \tag{B.5}$$

The particular solutions of moment and shear force can be determined from equations (2.20) and (2.21). The tractions on the boundary can be obtained by

$$\hat{p}_{m\alpha} = \hat{M}_{\alpha\beta}n_\beta, \;\; \hat{p}_{m3} = \hat{Q}_\alpha n_\alpha \tag{B.6}$$

If radial basis function $F(r) = 1 + r$, The function $\psi(r)$ can be solved from equation (B.5)

$$\psi(r) = -\left(\frac{r^4}{64} + \frac{r^5}{225}\right) \tag{B.7}$$

and the rotations and deflection can be deduced

$$\hat{w}^3_{m1} = -\left(\frac{1}{16} + \frac{r}{45}\right)\frac{x_1 r^2}{D}$$

$$\hat{w}^3_{m2} = -\left(\frac{1}{16} + \frac{r}{45}\right)\frac{x_2 r^2}{D} \tag{B.8}$$

$$\hat{w}^3_{m3} = -\left(\frac{1}{2} + \frac{2r}{9}\right)\frac{r^2}{(1-\nu)\lambda^2 D} + \left(\frac{1}{64} + \frac{r}{225}\right)\frac{1}{D}$$

The particular solutions of moments $\hat{M}_{\alpha\beta}$ and shear forces $\hat{Q}_\beta$ can be determined by equations (2.20) and (2.21) to give

$$\hat{M}^3_{m11} = -\left[\left(\frac{1}{8} + \frac{r}{15}\right)(x_1^2 + \nu x_2^2) + (1+\nu)\left(\frac{r^2}{16} + \frac{r^3}{45}\right)\right]$$

$$\hat{M}^3_{m12} = -(1+\nu)\left(\frac{1}{8} + \frac{r}{15}\right)(x_1 x_2)$$

$$\hat{M}^3_{m22} = -\left[\left(\frac{1}{8} + \frac{r}{15}\right)(\nu x_1^2 + x_2^2) + (1+\nu)\left(\frac{r^2}{16} + \frac{r^3}{45}\right)\right] \tag{B.9}$$

$$\hat{Q}^3_{m1} = -\frac{x_1}{2}\left(1+\frac{2r}{3}\right)$$

$$\hat{Q}^3_{m2} = -\frac{x_2}{2}\left(1+\frac{2r}{3}\right)$$

and the tractions on the boundary can be obtained from relationships in equation (B.6).

For the derivative of function $F_{,\alpha} = x_\alpha/r$, the solution $\psi^\alpha(r)$ can be found

$$\psi^\alpha(r) = -\frac{r^3 x_\alpha}{45} \tag{B.10}$$

and particular solutions $\hat{w}^\alpha_{mk}$ are

$$\hat{w}^1_{m1} = -(3x_1^2 + r^2)\frac{r}{45D}$$

$$\hat{w}^1_{m2} = -\frac{x_1 x_2 r}{15D} \tag{B.11}$$

$$\hat{w}^1_{m3} = -[30 - (1-\nu)\lambda^2 r^2]\frac{r x_1}{45(1-\nu)\lambda^2 D}$$

and the particular solutions of moments $\hat{M}_{\alpha\beta}$ and shear forces $\hat{Q}_\beta$ are

$$\hat{M}^1_{m11} = -\frac{x_1}{15}\left[\nu\left(\frac{x_1^2}{r}+3r\right)+\left(\frac{x_2^2}{r}+r\right)\right]$$

$$\hat{M}^1_{m12} = -(1-\nu)\frac{x_2}{15}\left(\frac{x_1^2}{r}+r\right)$$

$$\hat{M}^1_{m22} = -\frac{x_1}{15}\left[\nu\left(\frac{x_1^2}{r}+3r\right)+\left(\frac{x_2^2}{r}+r\right)\right] \tag{B.12}$$

$$\hat{Q}^1_{m1} = -\frac{1}{3}\left(\frac{x_1^2}{r}+r\right)$$

$$\hat{Q}^1_{m2} = -\frac{1}{3}\frac{x_1 x_2}{r}$$

for $\alpha = 1$, and

$$\hat{w}^2_{m1} = -\frac{x_1 x_2 r}{15D}$$

$$\hat{w}^2_{m1} = -(3x_2^2 + r^2)\frac{r}{45D} \tag{B.13}$$

$$\hat{w}^2_{m3} = -[30 - (1-\nu)\lambda^2 r^2]\frac{r x_2}{45(1-\nu)\lambda^2 D}$$

and the particular solutions of moments $\hat{M}_{\alpha\beta}$ and shear forces $\hat{Q}_{\beta}$ are

$$\hat{M}^2_{m11} = -\frac{x_2}{15}\left[\nu\left(\frac{x_1^2}{r}+r\right)+\left(\frac{x_2^2}{r}+3r\right)\right]$$

$$\hat{M}^2_{m12} = -(1-\nu)\frac{x_1}{15}\left(\frac{x_2^2}{r}+r\right)$$

$$\hat{M}^2_{m22} = -\frac{x_2}{15}\left[\nu\left(\frac{x_1^2}{r}+r\right)+\left(\frac{x_2^2}{r}+3r\right)\right] \tag{B.14}$$

$$\hat{Q}^2_{m1} = -\frac{1}{3}\frac{x_1 x_2}{r}$$

$$\hat{Q}^2_{m2} = -\frac{1}{3}\left(\frac{x_2^2}{r}+r\right)$$

for $\alpha = 2$.

B.2 Particular solutions for two-dimensional plane stress

An expression displacement particular solution $\hat{u}^{\gamma}_{m\alpha}$ can be found in polar coordinates with the use of the Galerkin vector $G_{\alpha\beta}$ as

$$\hat{u}^{\gamma}_{m\alpha}(r) = G^{\gamma}_{\beta\alpha,\gamma\gamma}(r) - \frac{1+\nu}{2}G^{\gamma}_{\gamma\alpha,\beta\gamma}(r) \tag{B.15}$$

where $G_{\alpha\beta}$ satisfies

$$\nabla^4 G^{\gamma}_{\beta\alpha} + \frac{2}{(1-\nu)B}\frac{x_{\gamma}}{r}\delta_{\gamma\beta} = 0 \tag{B.16}$$

and a solution is determined by

$$G^{\gamma}_{\beta\alpha} = -\frac{r^3 x_{\gamma}}{45\,(1-\upsilon)\,B}\delta_{\alpha\beta} \tag{B.17}$$

Substituting equation (B.17) into equation (B.15), then the displacement particular solutions can be arranged as

$$\hat{u}^1_{m1} = -\frac{2}{(1-\nu)B}\left[\frac{r x_1}{3}-\frac{1+\nu}{30}\left(\frac{x_1^3}{r}+3x_1 r\right)\right]$$

$$\hat{u}^1_{m2} = \frac{(1+\nu)}{15(1-\nu)B}\left(\frac{x_1^2 x_2}{r}+x_2 r\right) \tag{B.18}$$

and using strain displacement relationships in equation (2.9), the strain are obtained as

$$\hat{\varepsilon}^1_{m11} = -\frac{2}{(1-\nu)}\left[\left(\frac{x_1^2}{r}+\frac{r}{3}\right)-\frac{1+\nu}{30}\left(-\frac{x_1^4}{r^3}+\frac{6x_1^2}{r}+3r\right)\right]$$

$$\hat{\varepsilon}^1_{m12} = -\frac{2}{(1-\nu)}\left[\frac{x_1x_2}{6r}-\frac{1+\nu}{30}\left(-\frac{x_1^3x_2}{r^3}+\frac{3x_1x_2}{r}\right)\right]$$

$$\hat{\varepsilon}^1_{m22} = \frac{2}{(1-\nu)}\frac{1+\nu}{30}\left(-\frac{x_1^2x_2^2}{r^3}+2r\right) \tag{B.19}$$

The particular solution for membrane stress resultant can be derived by substituting equation (B.19) into the stress resultant-strain relationships in equation (2.19) to give:

$$\hat{N}^1_{m11} = B\left[(1-\nu)\hat{\varepsilon}^1_{m11}+\nu\hat{\varepsilon}^1_{m\alpha\alpha}\right]$$

$$\hat{N}^1_{m12} = B(1-\nu)\hat{\varepsilon}^1_{m12}$$

$$\hat{N}^1_{m22} = B\left[(1-\nu)\hat{\varepsilon}^1_{m22}+\nu\hat{\varepsilon}^1_{m\alpha\alpha}\right] \tag{B.20}$$

and the traction particular solutions are obtained from

$$\hat{t}^1_{m\alpha} = \hat{N}^1_{m\alpha\beta}n_\beta \tag{B.21}$$

In the same way, displacement particular solutions $\hat{u}^2_{m\alpha}$ can be obtained as follows:

$$\hat{u}^2_{m1} = \frac{(1+\nu)}{15(1-\nu)B}\left(\frac{x_2^2x_1}{r}+x_1r\right)$$

$$\hat{u}^2_{m2} = -\frac{2}{(1-\nu)B}\left[\frac{rx_2}{3}-\frac{1+\nu}{30}\left(\frac{x_2^3}{r}+3x_2r\right)\right] \tag{B.22}$$

and the strains are

$$\hat{\varepsilon}^2_{m11} = \frac{2}{(1-\nu)}\frac{1+\nu}{30}\left(-\frac{x_1^2x_2^2}{r^3}+2r\right)$$

$$\hat{\varepsilon}^2_{m12} = -\frac{2}{(1-\nu)}\left[\frac{x_1x_2}{6r}-\frac{1+\nu}{30}\left(-\frac{x_2^3x_1}{r^3}+\frac{3x_1x_2}{r}\right)\right]$$

$$\hat{\varepsilon}^2_{m22} = -\frac{2}{(1-\nu)}\left[\left(\frac{x_2^2}{r}+\frac{r}{3}\right)-\frac{1+\nu}{30}\left(-\frac{x_2^4}{r^3}+\frac{6x_2^2}{r}+3r\right)\right] \tag{B.23}$$

The particular solution for membrane stress resultant are

$$\hat{N}^2_{m11} = B\left[(1-\nu)\hat{\varepsilon}^2_{m11} + \nu\hat{\varepsilon}^2_{m\alpha\alpha}\right]$$

$$\hat{N}^2_{m12} = B(1-\nu)\hat{\varepsilon}^2_{m12}$$

$$\hat{N}^2_{m22} = B\left[(1-\nu)\hat{\varepsilon}^2_{m22} + \nu\hat{\varepsilon}^2_{m\alpha\alpha}\right] \tag{B.24}$$

and finally the traction particular solutions are obtained from

$$\hat{t}^2_{m\alpha} = \hat{N}^2_{m\alpha\beta}n_\beta \tag{B.25}$$

Appendix C

Treatment of Singularities

C.1 Bi-cubic Nonlinear Coordinate Transformation

This coordinate transformation was developed by Telles [87]. Consider the integral

$$I = \int_{-1}^{+1} f(\eta)\, d\eta \tag{C.1}$$

in which $f(\eta)$ is singular at a point η'. Using a third-degree non-linear transformation

$$\eta(\gamma) = a\gamma^3 + b\gamma^2 + c\gamma + d \tag{C.2}$$

such that the following requirement are met:

$$\begin{aligned} \frac{d\eta}{d\gamma}|_{\eta'} &= 0 \\ \frac{d^2\eta}{d\gamma^2}|_{\eta'} &= 0 \\ \eta(1) &= 1 \\ \eta(-1) &= -1 \end{aligned} \tag{C.3}$$

The following solution is obtained

$$\begin{aligned} a &= \frac{1}{Q} \\ b &= -\frac{3\gamma'}{Q} \end{aligned}$$

$$
\begin{aligned}
c &= \frac{3(\gamma')^2}{Q} \\
d &= -b \\
Q &= 1+3(\gamma')^2
\end{aligned} \tag{C.4}
$$

where γ' is the value of γ which satisfies $\eta\left(\gamma'\right) = \eta'$; this parameter can be calculated by

$$
\gamma' = \left(\eta'\eta^* + |\eta^*|\right)^{\frac{1}{3}} + \left(\eta'\eta^* - |\eta^*|\right)^{\frac{1}{3}} + \eta' \tag{C.5}
$$

where $\eta^* = (\eta')^2 - 1$. Therefore, equation (C.1) becomes

$$
I = \int_{-1}^{+1} f\left\{\frac{(\gamma-\gamma')^3 + \gamma'\left[(\gamma')^2+3\right]}{1+3(\gamma')^2}\right\}\frac{3(\gamma-\gamma')^2}{1+3(\gamma')^2}d\gamma \tag{C.6}
$$

The above transformation can be used to calculate integral with a logaritmic singularity for any position of the singularity. The main advantage of the transformation is that since the Jacobian cancels the singularity, standard Gaussian quadrature can be employed without the need to separate the regular part from the singular term in the numerical evaluation of the integrals.

C.2 Triangle to Square Transformation

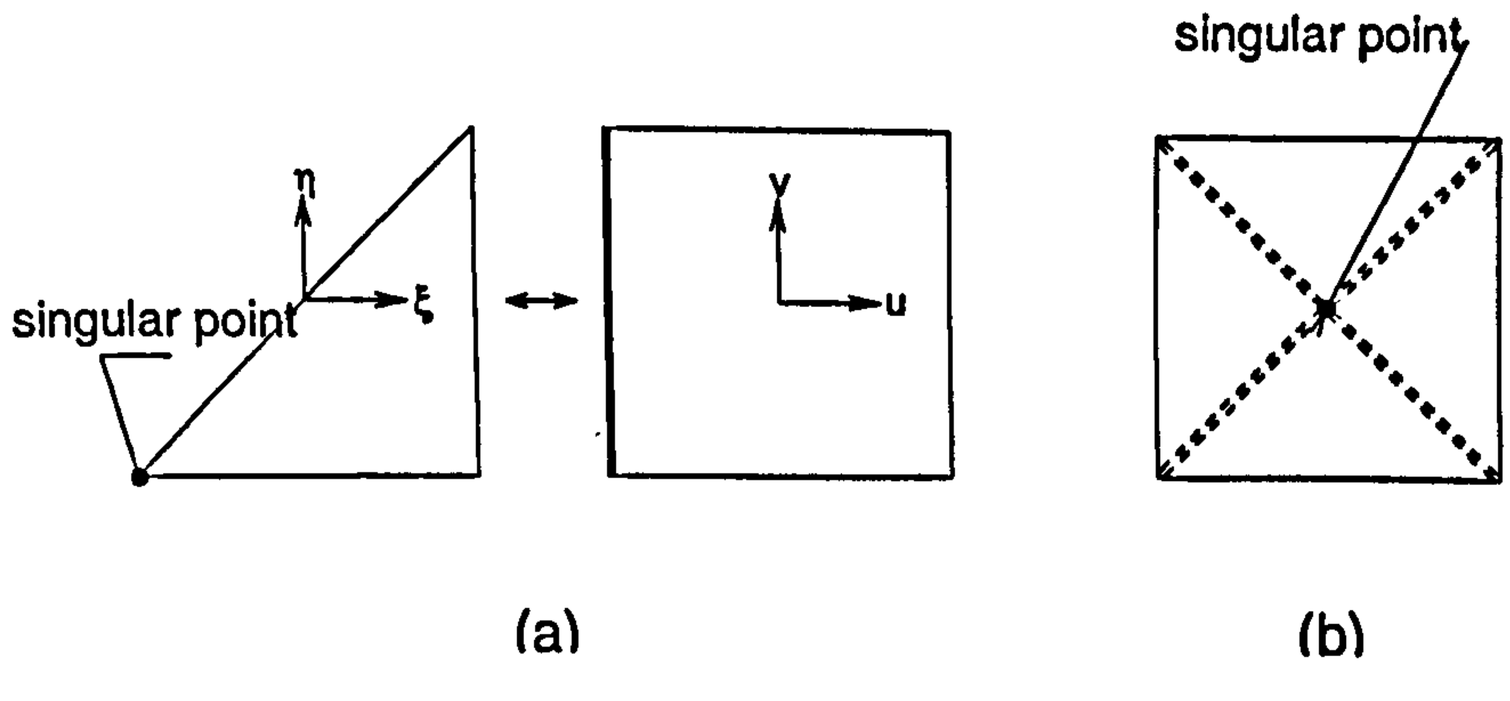

Figure C-1: (a) Transformation of triangle to square ; (b) Subdivision of quadrilateral element into four triangular sub element.

The procedure for the triangle to square transformation was presented by Aliabadi and Rooke [6]. This procedure is used to cancel weak singularity in an integral

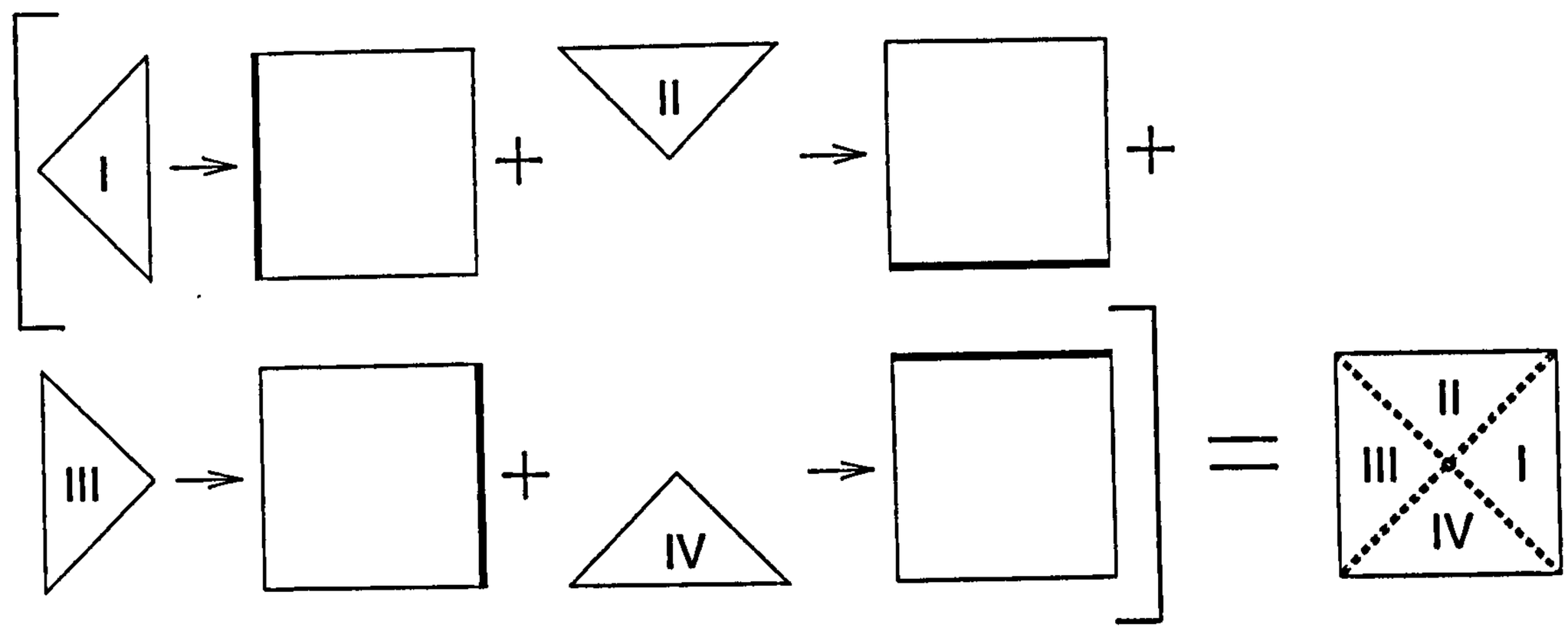

Figure C-2: Systematic use of transformation of variable technique.

over the domain. Consider a triangular element, shown in the Figure C-1(a), which has a singularity at $(\xi, \eta) = (-1, -1)$ in the local (ξ, η) plane. The singular integral is transformed in the following manner,

$$\int_{-1}^{1}\int_{-1}^{\xi} \frac{M(\xi,\eta)\,J(\xi,\eta)}{R} d\eta d\xi = \int_{-1}^{1}\int_{-1}^{1} \frac{M(\xi,\eta)\,J(\xi,\eta)\,J^c(\xi,\eta)}{R} du dv \qquad \text{(C.7)}$$

where $\xi = u$ and $\eta = \frac{1}{2}\,[(1+u)\,v - (1-u)]$. The Jacobian of this transformation $J^c(\xi,\eta) = \frac{1}{2}(1+\xi)$ exactly cancel out the singularity [6].

For constant cell element, where the singular point is at the centre of the quadrilateral element, as shown in Figure C-1(b), the element is divided into four triangular element and each triangular element is transformed to square, as shown in Figure C-2. The transformation are

triangle I : $\xi = \frac{1}{2}(1+u_1)$ and $\eta = \frac{1}{2}\,(1+u_1)\,v_1$; $J^c(u_1) = \frac{1}{4}(1+u_1)$

triangle II : $\xi = \frac{1}{2}(1+v_2)\,u_2$ and $\eta = \frac{1}{2}\,(1+v_2)$; $J^c(v_2) = \frac{1}{4}(1+v_2)$

triangle III : $\xi = \frac{1}{2}(u_3-1)$ and $\eta = \frac{1}{2}\,(1-u_3)\,v_3$; $J^c(u_3) = \frac{1}{4}(1-u_3)$

triangle IV : $\xi = \frac{1}{2}(1-v_4)\,u_4$ and $\eta = \frac{1}{2}\,(v_4-1)$; $J^c(v_4) = \frac{1}{4}(1-v_4)$

Hence,

$$\int_{-1}^{1}\int_{-1}^{1}\frac{M(\xi,\eta)\,J(\xi,\eta)}{R}d\eta d\xi = \int_{-1}^{1}\int_{-1}^{1}\frac{M(\xi,\eta)\,J(\xi,\eta)\,J^{c}(u_1)}{R}du_1dv_1 + \int_{-1}^{1}\int_{-1}^{1}\frac{M(\xi,\eta)\,J(\xi,\eta)\,J^{c}(v_2)}{R}du_2dv_2 + \int_{-1}^{1}\int_{-1}^{1}\frac{M(\xi,\eta)\,J(\xi,\eta)\,J^{c}(u_3)}{R}du_3dv_3 + \int_{-1}^{1}\int_{-1}^{1}\frac{M(\xi,\eta)\,J(\xi,\eta)\,J^{c}(v_4)}{R}du_4dv_4 \quad \text{(C.8)}$$

where the Jacobian factors cancel out the $\frac{1}{R}$ singularity.

C.3 Treatment of Singularities for The Traction Boundary Integral

In the traction integral equations, the singularity order is higher than the displacement integral equations. In the $[H]$ matrix, the kernels $P^*_{\alpha\beta 3}$ and $P^*_{3\beta\gamma}$ are strongly singular, whereas, the kernels $P^*_{\alpha\beta\gamma}$, $P^*_{3\beta 3}$ and $T^{(i)*}_{\alpha\beta\gamma}$ are hypersingular. In the off-diagonal sub-matrices, the shape functions will reduce the order of singularity by one. This means that, element entries in $[H]$ matrix corresponding to the kernels $P^*_{\alpha\beta 3}$ and $P^*_{3\beta\gamma}$ become smooth, whereas, elements of the kernels $P^*_{\alpha\beta\gamma}$, $P^*_{3\beta 3}$ and $T^{(i)*}_{\alpha\beta\gamma}$ still remain strongly singular.

In $[G]$ matrix, the off-diagonal sub-matrices are smooth again due to the shape functions reducing the order of singularity. The diagonal matrices, on the other hand, contain the kernels $W^*_{\alpha\beta 3}$ and $W^*_{3\beta\gamma}$ which are weakly singular and the $W^*_{\alpha\beta\gamma}$, $W^*_{3\beta 3}$ and $U^*_{\alpha\beta\gamma}$ which are strongly singular.

The singular integrals mentioned above are treated individually based on their order of singularity. The weak singularity is treated using a nonlinear coordinate transformation as in Telles [87]. The strong-singular and the hypersingular integrals are evaluated using a singularity subtraction method based on the Taylor series expansion around the singular point, as in Portela, Aliabadi and Rooke [63], and the singular terms are integrated analytically.

As an example, the integral which contains strongly singular kernel of $O(1/r)$

can be regularised as follows:

$$\int_{\Gamma_e} P^*_{ij}(\mathbf{x}',\mathbf{x}) w_j(\mathbf{x}) d\Gamma(\mathbf{x}) = w^n_j \int_{-1}^{+1} \frac{f^n_{ij}(\xi)}{\xi - \xi'} d\xi \tag{C.9}$$

where $f^n_{ij}(\xi) = P^*_{ij}(\xi',\xi)\Phi^n(\xi)J(\xi)(\xi - \xi')$; Γ_e denotes the boundary of the singular element, Φ^n is the element shape function corresponding to the node n in the element under consideration and J is the Jacobian of the transformation from x_α coordinate system to the local coordinate system ξ (i.e., $d\Gamma = J(\xi)d\xi$). The term $f^n_{ij}(\xi)$ is now a regular function. The integral in the right hand side of equation (C.9) can be regularised with the aid of a Taylor series expansion of the function $f^n_{ij}(\xi)$ about the singular point ξ' in the local coordinate system, as follows:

$$f^n_{ij}(\xi) = f^n_{ij}(\xi') + f^{n\prime}_{ij}(\xi')(\xi - \xi') + \frac{1}{2} f^{n\prime\prime}_{ij}(\xi')(\xi - \xi')^2 + ... \tag{C.10}$$

By substracting the first term of the Taylor expansion of the function $f^n_{ij}(\xi)$ and then adding it again, equation (C.9) can be written as

$$\int_{-1}^{+1} \frac{f^n_{ij}(\xi)}{\xi - \xi'} d\xi = \int_{-1}^{+1} \frac{f^n_{ij}(\xi) - f^n_{ij}(\xi')}{\xi - \xi'} d\xi + f^n_{ij}(\xi') \int_{-1}^{+1} \frac{d\xi}{\xi - \xi'} \tag{C.11}$$

The first integral in the right hand side is now regular and the second integral which is strongly singular can be integrated analytically to give,

$$\int_{-1}^{+1} \frac{d\xi}{\xi - \xi'} = \ln \left| \frac{1 - \xi'}{1 + \xi'} \right| \tag{C.12}$$

The hypersingular integrals of $O(1/r^2)$ can be treated in a similar way,

$$\int_{\Gamma_e} T^{(i)*}_{\alpha\beta\gamma}(\mathbf{x}',\mathbf{x}) u_\gamma(\mathbf{x}) d\Gamma(\mathbf{x}) = u^n_\gamma \int_{-1}^{+1} \frac{g^n_{\alpha\beta\gamma}(\xi)}{(\xi - \xi')^2} d\xi \tag{C.13}$$

where $g^n_{\alpha\beta\gamma}(\xi) = T^{(i)*}_{\alpha\beta\gamma}(\xi',\xi)\Phi^n(\xi)J(\xi)(\xi - \xi')^2$ is a regular function. The integral on the right hand side of equation can be regularised with the aid of the first and second term of a Taylor series expansion of the function $g^n_{\alpha\beta\gamma}(\xi)$ about the singular

point ξ' in the local coordinate system, as follows:

$$g^n_{\alpha\beta\gamma}(\xi) = g^n_{\alpha\beta\gamma}(\xi') + g^n_{\alpha\beta\gamma}{}'(\xi')\,(\xi-\xi') + \frac{1}{2}g^n_{\alpha\beta\gamma}{}''(\xi')\,(\xi-\xi')^2 + ... \qquad \text{(C.14)}$$

By substracting the first and the second terms of the Taylor expansion of the function $g^n_{\alpha\beta\gamma}(\xi)$ and then adding it again, equation (C.13) can be written as

$$\int_{-1}^{+1} \frac{g^n_{\alpha\beta\gamma}(\xi)}{(\xi-\xi')^2}d\xi = \int_{-1}^{+1} \frac{g^n_{\alpha\beta\gamma}(\xi) - g^n_{\alpha\beta\gamma}(\xi') - g^n_{\alpha\beta\gamma}{}'(\xi')\,(\xi-\xi')}{(\xi-\xi')^2}d\xi +$$

$$g^n_{\alpha\beta\gamma}(\xi')\int_{-1}^{+1}\frac{d\xi}{(\xi-\xi')^2} + g^n_{\alpha\beta\gamma}{}'(\xi')\int_{-1}^{+1}\frac{d\xi}{\xi-\xi'} \qquad \text{(C.15)}$$

where $g^n_{\alpha\beta\gamma}{}'$ denotes the first derivatives of $g^n_{\alpha\beta\gamma}$. At the collocation point the function $g^n_{\alpha\beta\gamma}$ is required to have continuity of its second derivatives. The requirement is automatically satisfied by the use of discontinuous elements, since the nodes are internal to the element. In equation (C.15) the first integral on the right hand side is now regular, and the third integral is identical with the one given in equation (C.11). The second integral on the right hand side is hypersingular and can be integrated analytically to give,

$$\int_{-1}^{+1}\frac{d\xi}{(\xi-\xi')^2} = -\frac{1}{(1+\xi')} - \frac{1}{(1-\xi')} \qquad \text{(C.16)}$$

The last type of singularity observed is hypersingular of $O\left(\frac{1}{r^2}+\ln(r)\right)$. This type of singularity can be treated in a similar way to the hypersingular integral of $O\left(1/r^2\right)$ except there is an additional weakly singular term to be treated. The integral is given as

$$\int_{\Gamma_e} P^*_{\alpha\beta\gamma}(\mathbf{x}',\mathbf{x})w_\gamma(\mathbf{x})d\Gamma(\mathbf{x}) = w^n_\gamma\int_{-1}^{+1} P^*_{\alpha\beta\gamma}(\xi',\xi)\Phi^n(\xi)J(\xi)d\xi \qquad \text{(C.17)}$$

The hypersingular integrals can be solved as follows

$$\int_{\Gamma_e} P^*_{\alpha\beta\gamma}(\xi',\xi)\Phi^n(\xi)J(\xi)d\xi =$$

$$\int_{-1}^{+1}\left[P^{*}_{\alpha\beta\gamma}(\xi',\xi)\Phi^{n}(\xi)J(\xi)-\frac{g^{n}_{\alpha\beta\gamma}(\xi')+g^{n}_{\alpha\beta\gamma}{}'(\xi')(\xi-\xi')}{(\xi-\xi')^{2}}-h^{n}_{\alpha\beta\gamma}(\xi')\ln|\xi-\xi'|\right]d\xi$$

$$+g^{n}_{\alpha\beta\gamma}(\xi')\int_{-1}^{+1}\frac{d\xi}{(\xi-\xi')^{2}}+g^{n}_{\alpha\beta\gamma}{}'(\xi')\int_{-1}^{+1}\frac{d\xi}{\xi-\xi'}+h^{n}_{\alpha\beta\gamma}(\xi')\int_{-1}^{+1}\ln|\xi-\xi'|\,d\xi \quad \text{(C.18)}$$

where $g^{n}_{\alpha\beta\gamma}(\xi)=P^{*1}_{\alpha\beta\gamma}(\xi',\xi)\Phi^{n}(\xi)J(\xi)(\xi-\xi')^{2}$ on which $P^{*1}_{\alpha\beta\gamma}(\xi',\xi)$ are part of the kernels which contain $1/r^{2}$. The term $h^{n}_{\alpha\beta\gamma}(\xi)=P^{*2}_{\alpha\beta\gamma}(\xi',\xi)\Phi^{n}(\xi)J(\xi)/\ln|\xi-\xi'|$, and $P^{*2}_{\alpha\beta\gamma}(\xi',\xi)$ are part of the kernels which contain $\ln|\xi-\xi'|$. The functions $g^{n}_{\alpha\beta\gamma}(\xi)$ and $h^{n}_{\alpha\beta\gamma}(\xi)$ are regular and can be expanded in terms of a Taylor series expansion about the singular point ξ' as before.

The first integral on the right hand side of equation (C.18) is now regular, the second integral on the right hand side which is hypersingular can be solved analytically using (C.16), the third integral is identical with the one given in equation (C.11). The last integral on the right hand side which is weakly singular can be integrated analytically to give,

$$\int_{-1}^{+1}\ln|\xi-\xi'|\,d\xi=\ln|(1-\xi')(1+\xi')|-\xi'\ln\left|\frac{1-\xi'}{1+\xi'}\right|-2 \qquad \text{(C.19)}$$